School of Earth and Planetary Sciences
Department of Applied Geology

The Use of Raman Spectroscopy and X-ray Diffraction for the Examination of Associated Clay and Silt Coatings of Forensically Important Sandy Soils from the Swan Coastal Plain, Western Australia

Kari Margaret Pitts
0000-0002-0329-3801

This thesis is presented for the Degree of
Master of Philosophy (Geology)
of
Curtin University

April 2022

Declaration

To the best of my knowledge and belief this thesis contains no material previously published by any other person except where due acknowledgment has been made.

This thesis contains no material which has been accepted for the award of any other degree or diploma in any university.

Kari Pitts

[27 July 2021]

Abstract

Soil is ubiquitous, complex and diverse in composition and hence, is a valuable evidential material in forensic investigations. It contains numerous components that can be analysed using a range of techniques allowing for the collection of large amounts of data related to its composition. When this data is interpreted correctly, soil is a valuable tool, for both reconstructing past events and drawing attention to new locations for further examination. However, even with its large potential, soil as a form of forensic trace evidence is underutilised, due to challenges associated with its interpretation. These challenges include questions regarding the commonality of soil characteristics and the ability to differentiate locations. Therefore, it is crucial to summarise its nature, formation and distribution in the Swan Coastal Plain, to allow greater confidence in its interpretation for forensic casework in Western Australia. As part of a greater soil examination protocol, this thesis looks to explore the application of a comparison technique to soils of forensic interest from the geomorphic units of the Pinjarra Plain, Bassendean, Spearwood and Quindalup dunes of the Swan Coastal Plain.

The project utilised the variability of the quartz fine fraction, present as variable coatings on the surface of quartz grains. These coatings were recovered from hand-picked grains and analysed using Raman micro-spectroscopy, lab-based X-ray diffraction (XRD) and synchrotron X-ray powder diffraction (PD). Raman spectroscopy was undertaken in an effort to utilise the 785 nm Renishaw Raman. Ideally, it was envisaged that Raman analysis would not only assist in the association of soils, but potentially allow for analyses of *in-situ* coatings from single quartz grains. Unfortunately, the 785 nm Raman produced spectra dominated by fluorescence and efforts to minimise this by photo-bleaching and substrate changes proved unsuccessful.

The examination of 202 soil samples from across the four geomorphic units of the Swan Coastal Plain using laboratory-collected, historical XRPD percentage intensity

data using multivariate statistics illustrated the ability of this approach to differentiate a large number of samples. Data illustrated the strength in using primary and secondary minerals for differentiation. The minerals quartz, microcline feldspar, chloritised vermiculite, mica, gibbsite and goethite all contributed to the differentiation of samples.

The Powder Diffraction beamline at the Australian Synchrotron was used to further examine 44 quartz fine fractions from Spearwood and Bassendean dune soils. The PD beamline demonstrated its benefits in a significant increase in count rates and far shorter analysis time. Preliminary data examination indicated the potential for further differentiation of similar samples.

Finally, the multivariate model developed from the laboratory-collected data was successfully applied to the re-examination of two case studies. The method allowed the comparison of recovered and control samples, as well as assisted in the interpretation of the results. The successful application to casework illustrated the benefit in the addition of this method into a standard soil analysis protocol for sandy soils. This work represents a novel combination of the recently published quartz fine fraction XRD data with the multivariate statistics and this methodology will continue to be utilised in casework, greatly assisting in the reporting of soil cases in Western Australia.

Table of Contents

List of Figures

List of Tables

Acknowledgements

Firstly, I'd like to express my thanks to my mentor and predominant supervisor, Richard, who has supported me throughout this research, as well as passed on just some of his vast and daunting knowledge about soil and mineralogy in general, as well as their use in forensics. I am extremely grateful that you agreed to be my teacher and mentor for my foray out of chemistry and into mineralogy. I thank you for our random and friendly chats in the lab, for chocolate in the afternoons, and for your support and encouragement in my academic endeavours.

Deep thanks also to my Curtin supervisor Mehrooz for agreeing to allow me to undertake this formal study into geology and minerals. I truly appreciate the chance you took on me, and I'm thankful of your continual patience with delays brought on by pregnancy, urgent and long case work and just everyday life.

I would like to say a special thank you to my supervisor, John for your support, time and overall edits in the drafting of this thesis. I would also like to acknowledge my Director at ChemCentre, Colin Priddis, and my Team Leader David DeTata for their continual support of my efforts in initially starting this journey into soils and finishing this thesis. Furthermore, I would like to thank the rest of the Physical Evidence Team at ChemCentre for their collaborative effort in keeping me sane during data collection, analysis and drafting. I would also like to acknowledge the Curtin University Department of Applied Geology for their support and resources throughout the project.

Finally, I would like to thank my family for supporting me during the compilation of this dissertation. My children, Lachlan and Zoe, have listened to me talk about dirt even though they really didn't care, and my wonderful husband has encouraged me, listened to me and supported me unendingly. I'm finally done…

Chapter 1. Introduction

1.1 Focus of the thesis

Soil can be important forensic trace evidence and may be recovered during a criminal investigation. It contains numerous components that can vary widely between locations, and that can be analysed using a range of techniques (1, 2). This suite of techniques allows for the collection of large amounts of data related to its composition. When this data is interpreted correctly, soil becomes a valuable tool in criminal investigations, for both reconstructing past events and drawing attention to new locations for further examination. However, even with its large potential, soil as a form of forensic trace evidence is underutilised, due to challenges associated with its interpretation. These challenges include questions regarding the commonality of soil characteristics and the ability to differentiate locations (3). Therefore, it is crucial to summarise its nature, formation and distribution within the Swan Coastal Plain, to allow greater confidence in its interpretation for forensic casework within Western Australia. As part of a greater soil examination protocol, this thesis explores the application of a comparison technique to soils of forensic interest from the Swan Coastal Plain.

1.2 Soil and its formation

In a geological sense, soil is defined as the biologically active, unconsolidated, regolithic material found above the bedrock in a given location, covering most of the land on earth (4). Soil comprises primary mineral and rock grains, secondary minerals and chemical precipitates, organic material including humus and decaying plant and animal matter, and microbes (5). It is by its very nature, a complex mixture of materials that may vary extensively within a small geographical area. Human activity influences the naturally-occurring soil, as it is adapted and altered to what is desired. Soil may also be extended to include any particulate materials capable of ‘soiling’ an item, such as dusts, mineral ores, mine tailings, and man-made mineral products such as concrete, bricks or plaster.

Soil is developed *in-situ* over long periods. From a geological time perspective, a human lifespan is minuscule, with the events of geology occurring over thousands to millions of years. The formation of *in-situ* soil is illustrated in Figure 1.

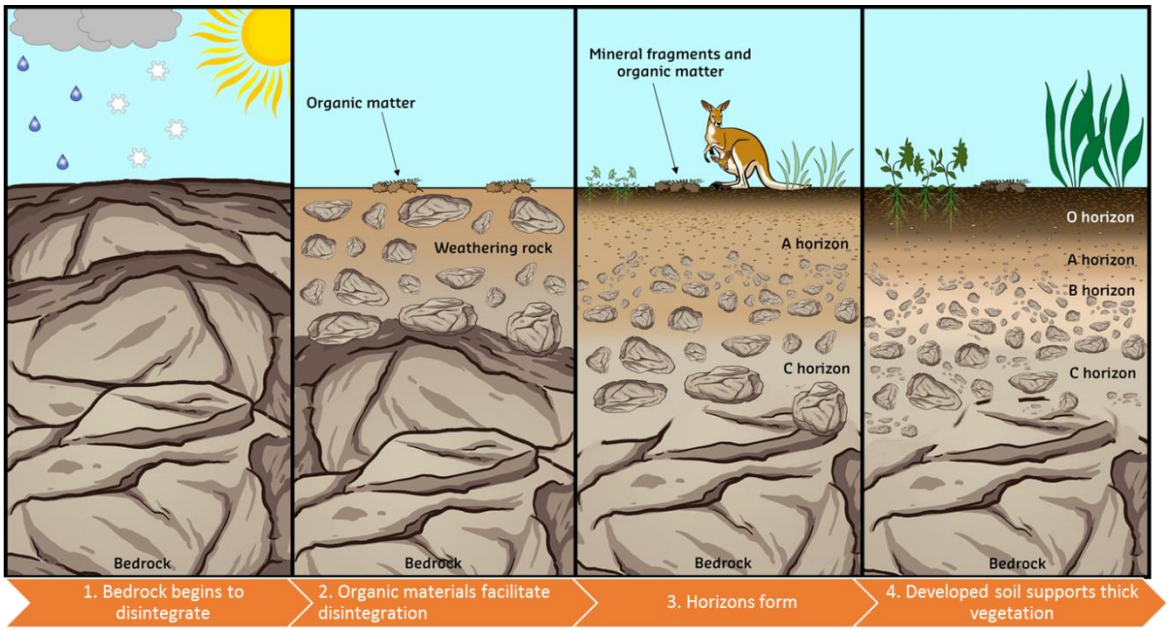

Figure 1: Schematic diagram detailing soil formation (from Pitts, Lewis and Newland 2018 [5])

Initially, the action of rain, heat and frost causes both physical and chemical weathering of the rocky lithosphere of a given area (Figure 1, panel 1). This disintegration of the bedrock creates a viable surface for the germination of windblown seeds and the establishment of plants, the roots of which burrow into the rock, assisting the influx of water, thus accelerating the breakdown of bedrock (Figure 1, panel 2). Over time and plant life cycles, animals may also be attracted, leading to the build-up of organic material at the surface and biomechanical dislocation and bio-chemical transformation of particles. In the meantime, the disintegration of the bedrock continues through the action of water, animal activity and plants (Figure 1, panel 3). Eventually, the formation of horizons occurs, with areas of differentiated texture and/or composition, and a layer of an unconsolidated mixture of organic and inorganic materials, adequate to support larger vegetation and more animal life. In addition to the *in-situ* formation, additional material may be deposited in the form of aeolian and fluviatile sediments and soil creep (solifluction).

1.2.1 Factors controlling natural soil formation

The factors that affect the characteristics of soil developed in this process include; bedrock type, climate, timeframe, relief (or topography), biological activity and parent material, often abbreviated to *clorpt* (climate, organisms, relief, parent material, time) (6). The combination of these factors, which will be detailed in further discussions, may create soils of differing characteristics within small geographical areas. Soils may be thought of as a stage in the rock cycle (7). A surficial process, whose genesis eventually results in the formation of clastic sediments and chemical ingredients for chemical sediments as shown in Figure 2.

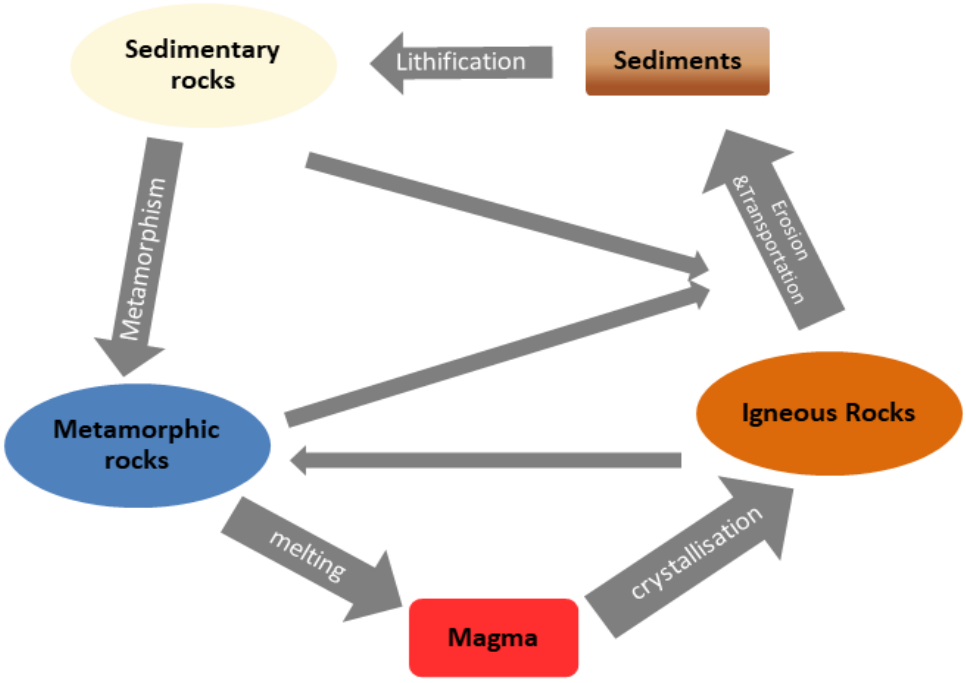

Figure 2: Stylised rock cycle, with reference to sediment formation (after Earth Science Australia, 2019- [7])

1.2.1.1 Bedrock type or parent material

The underlying rock type determines the mineralogy available and, hence, the overall composition of the soil formed. Mafic parent materials such as in basalt-rich rocks, provide minerals groups such as olivine, pyroxenes and plagioclase feldspars. These minerals will decompose on weathering to give abundant clay minerals such

as smectite, vermiculite and kaolinite, and good fertility for plant life. In contrast, more felsic parent materials such as exposed sandstones or granites lead to less fertile soils with lower clay contents and higher quartz contents. Quartz-rich rocks such as sandstones and quartzites are more resistant to chemical weathering and more stable for longer periods as quartz is the most resistant major primary rock-forming mineral (8). In addition, the underlying rock type will influence the resulting soil texture.

1.2.1.2 Time

Time is important to soil formation for several reasons. The amount of time a soil has to develop directly influences the soil characteristics. For example, Australia in most places has a thick covering of regolith material because many parts of the continent have been subaerially exposed for tens of millions of years (9). This is partly due to the stability of the continent in geological time and hence the time the soils have had to develop. A map of Australia, shown in Figure 3, illustrates the simplified ages of the geology of Australia (”Georegions”) (10). Overall, the land is ‘old’- Paleozoic belts, Precambrian shields and Phanerozoic basins, as well as the Archean area, the Yilgarn Craton, that dominates Western Australia. Also, there has been no large scale regional tectonic activity during the Cenozoic era and much of the continent escaped the erosive action of Quaternary glaciation that covered much of the Northern hemisphere (11). This has meant that the regolith has been exposed for far longer than much of the Northern hemisphere and had a far greater time to weather and alter.

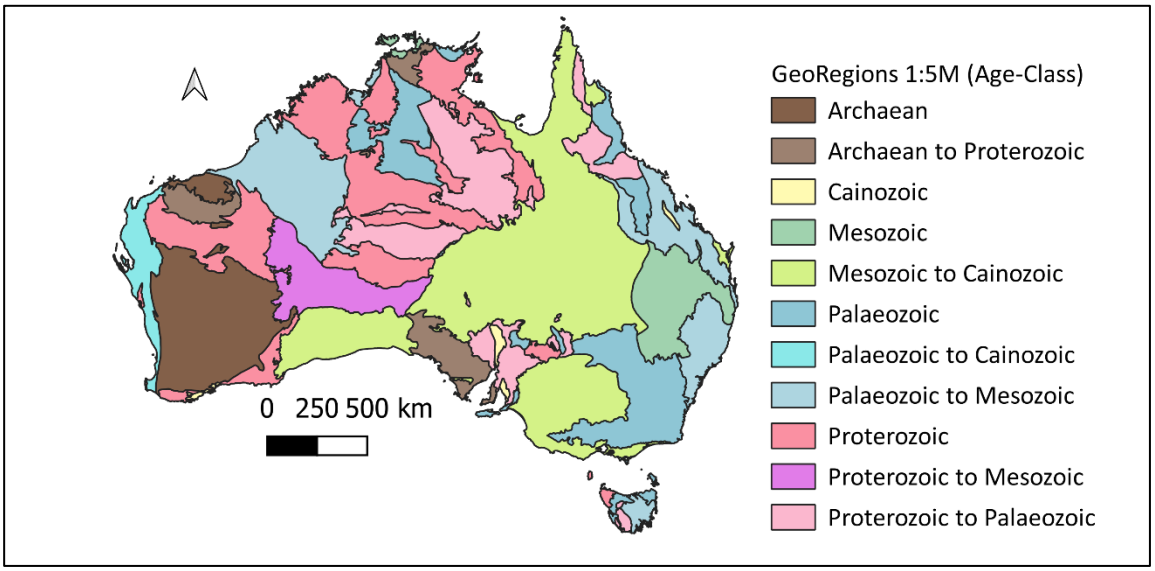

Figure 3: Geological Regions (1:5M) with simplified age classification in Australia (from Blake, D.H., Kilgour, B. 1998 [10])

1.2.1.3 Climate

In a general sense, the climate of a region has direct influence over the extremes of temperature, humidity, rainfall and snowfall that a developing soil experiences. The climate of a region can result in large areas of common soils, such as the tropical laterites, and the black earths (chernozem) of arid continental interiors as found in the Steppes of Russia. The climate affects the rate of weathering and the erosion of surface materials. Furthermore, the leaching nature of rainfall, the climate, and the climatic evolution, affects the formation of soils. For example, Australia was not exposed to the highly erosive forces experienced by the Northern Hemisphere during the Quaternary glaciation. This meant that soils from earlier periods remained *in-situ*, exposed to the climate of the region and time (9, 12, 13). In addition, the Neogene period brought an onset of aridity, with the reduction in surface water causing less erosion, and what little rainfall occurred causing more *in-situ* leaching. The hotter climate of an area like inland Australia compared with, for example, a colder area such as southern New Zealand leads to a difference in soil characteristics. Additionally, areas of high temperature and heavy rainfall commonly creates more saprolitic material, where weathering is dominated by chemical weathering. However in contrast to the generalisation, in Australia there

are certain areas that have deep weathering profiles, created in cooler weather over extended tectonically stable periods without glacial stripping (14).

Finally, the prevailing winds of a region influence the soils present, for example, aeolian sands and silty-clay loess are wind-blown sediments deposited in areas of accumulation. These wind-blown particulates can also act like sand-blasting agents causing erosion of exposed rock.

1.2.1.4 Relief (Topography)

On a regional scale, Australia has a lack of recent Orogeny, with no major Cenozoic tectonic activity producing a landscape of minimal high relief areas and hence, minimal exposure for erosion. The topography within a region also directly influences the formation of the soil on a more local scale. Moving water such as rivers, lake and ocean currents and wave actions will transport and deposit sediments (i.e. alluvial, lacustrine) into areas of accumulation, such as lakes and floodplains, changing the area's soils (9). Additionally, the transgression and regression of the ocean will alter the shoreline and associated areas. Hills, slopes, valleys and basins will also cause the redistribution of the regolith of an area, with upper hills being depleted and valleys and depressions accumulating downhill (i.e. colluvium) (8).

1.2.1.5 Biological activity

Biological activity not only includes the actions of larger mammals — such as elephants taking mud baths in shallow waters causing widening and deepening of the area— but also the action of microbes, plant roots and nematodes within the soil itself. The waste materials and decomposition products of the flora and fauna contribute directly to the organic content of an area, whereas the burrowing and foraging activity biomechanically mix the soil (i.e. bioturbation) (6). The biota hosted by an area can vary dramatically; hence the interactions of all of these with the soil can also lead to differentiation.

1.2.2 Soil Classifications

Whilst the forensic analysis of soils will be discussed subsequently, it is relevant to briefly introduce the Soil Classification System and specifically the Australian Soil Classification (ASC). It has been illustrated that soils vary both horizontally and vertically, and may be visualised and classified in the field as a soil profile. A soil profile is a vertical section extending from the surface through all of the horizons to the parent material, with a horizon being defined as a formed horizontal layer, differentiated morphologically to those layers above and/or below (15). These observable differences may be based on characteristics such as texture, structure, colour or composition. Minor variations within a comparable horizon may be referred to as sub-horizons and numbered accordingly, for example as an A1 horizon, A2 horizon etc. within an overall A horizon. The Australian Soil and Land Survey Field Handbook (16) contains the descriptions of the major soil types within Australia. Using these descriptions and appropriate fieldwork, soils may be assigned to one of 14 classifications according to the ASC system. Figure 4 represents the interpreted distribution of soil classifications across Australia (17), which can be seen to be partially related to the geological units visualised within Figure 3.

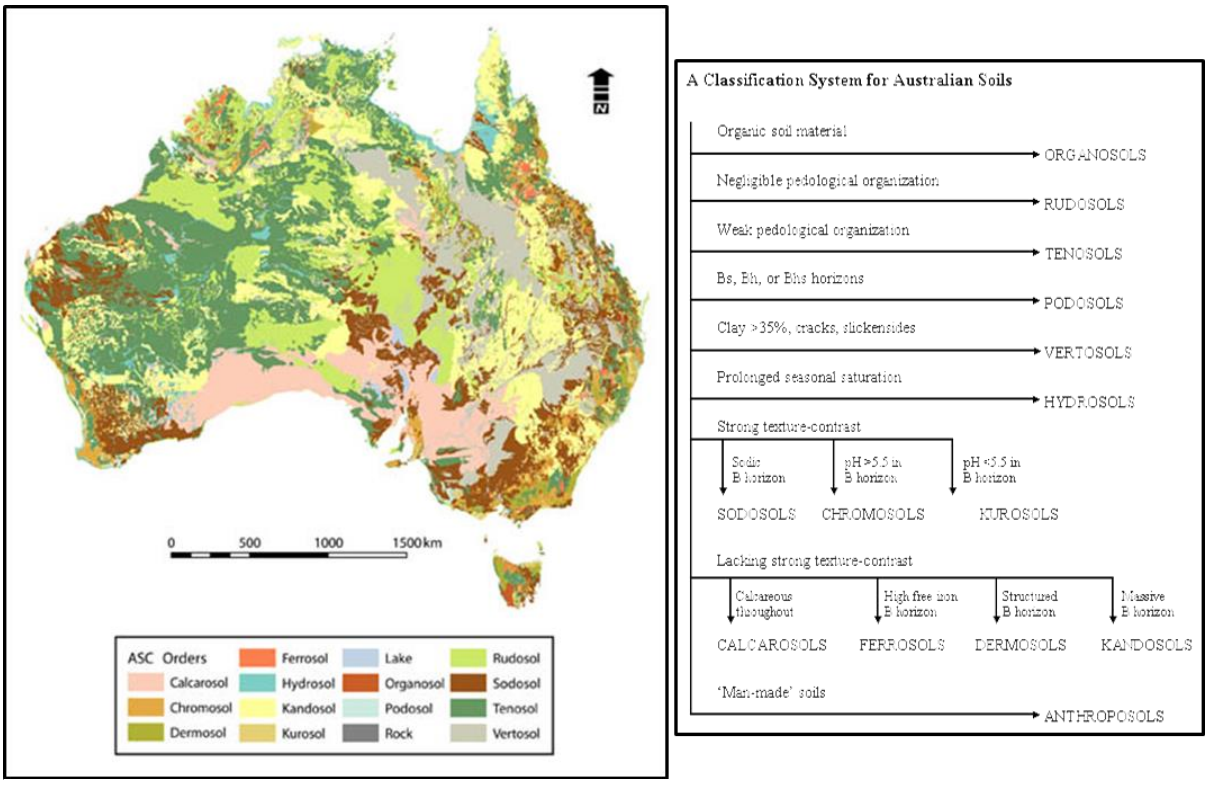

Figure 4: Australian Soil Classifications Atlas and a Schematic Summary of the orders NB: not a key (from Ashton and McKenzie 2001 [17])

1.3 Swan Coastal Plain

Australia is a large island continent of approximately 7,688,126 km^2, with the State of Western Australia accounting for approximately 32.9% of this area. Western Australia has a population of approximately 2.6 million people, with over 2.085 million of those living in the capital city of Perth (18). The majority of the Perth metropolitan area is located on the landform region known as the Swan Coastal Plain (19, 20). In geological terms, the region can be broadly described by the Perth Basin, a coastal plain abutting the Indian Ocean and the Darling Plateau to the east. For this study, the Swan Coastal Plain was used as an all-encompassing term for the area. A schematic outlining the location and extent of the area of interest is presented in Figure 5.

The Darling Plateau is topographically visible in the green boxed area of Figure 5. The marked change in elevation along the eastern edge of the plain is known as the Darling Scarp. This scarp is the visible remnant of the Darling Fault, one of the major fractures in the Earth's crust which developed about 1400 million years ago, due to a zone of deformation and mobilization in the western edge of the area. The fault extends from just east of Shark Bay, in the northwest, to Point D'Entrecasteaux on the State's south coast, a distance of approximately 1000 km. Pre-Cretaceous erosion of the rocks of the scarp has caused the retreat approximately 1–3 km inland (12). The area east of the fault is part of the Yilgarn Craton, an Archean-aged, stable craton that dominates the southwest of the state. The oldest rocks, originally muds and sands deposited between 3170 and 2830 million years ago (12), are found as metamorphic belts. These sedimentary rocks were metamorphosed approximately 2800 million years ago by tectonic movements. Approximately 2600 million years ago, intrusion by extensive granitoid masses occurred, most commonly by monzogranite, which is still visible today in the crystalline rocks of the plateau (21).

The coastal plain consists of sedimentary units, deposited in the Perth Basin, starting with the Paleozoic to Mesozoic bedrocks. This basin is part of the rift valley, between the west coast of Australia and the region of northern India, which

developed in the breakup of Gondwana (12, 22). Sedimentation by rivers in the Perth Basin of eroded continental rock continued from the Ordovician period (460 ma) through the Jurassic and earliest Cretaceous (140 ma), after which Greater India moved slowly away from Australia (23). During this time sea-floor spreading, a series of uplifts and erosion as well as subsidence and oceanic influxes further widened and deepened the basin. During the Paleogene, there was marine carbonate sedimentation, continental clastic sedimentation and heavy weathering of the Darling and Dandaragan plateaux to lateritic materials (12, 24).

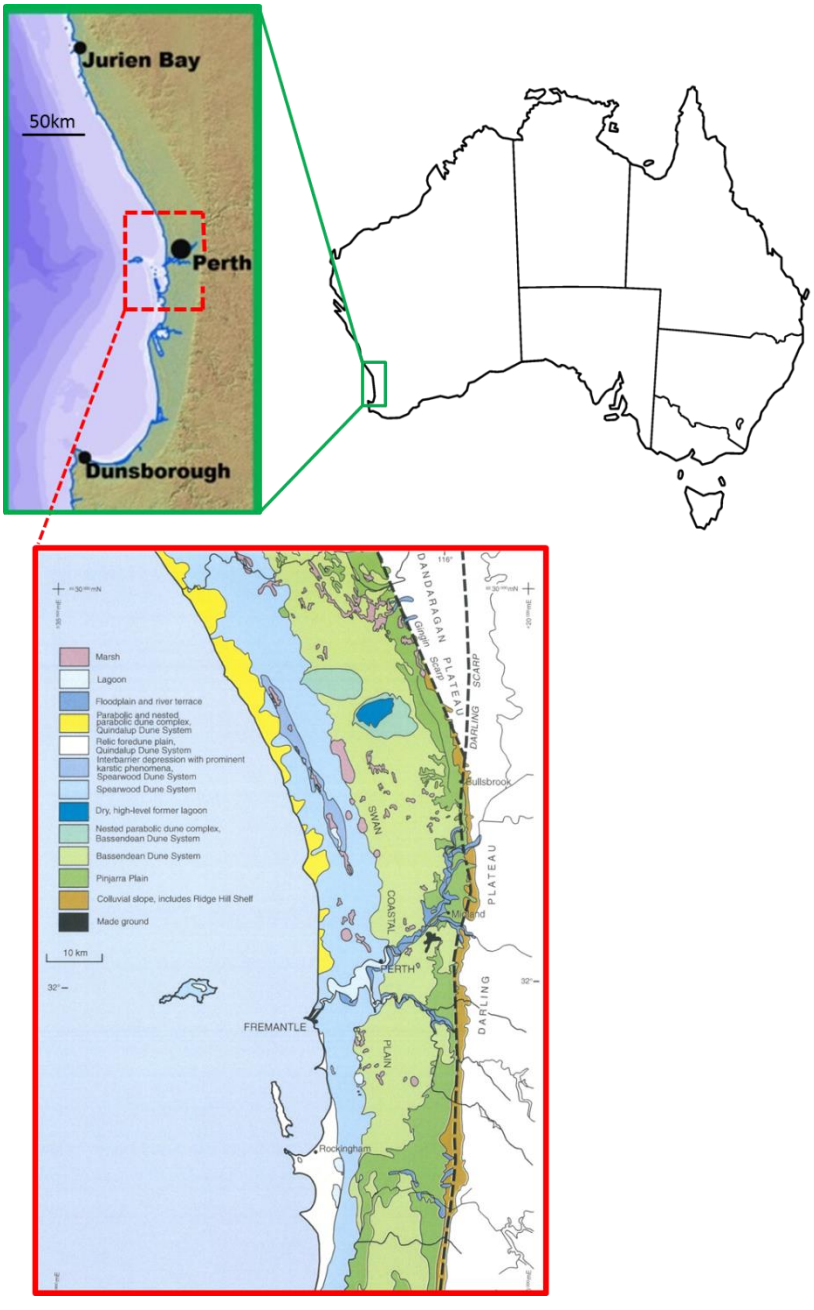

Figure 5: Schematic Diagram showing the location of Perth, the Swan Coastal Plain and Darling Plateau topography and geomorphology (from Pitts, Lewis and Newland, 2018 [5])

The Neogene and Quaternary times saw more lateritic weathering as well as the deposition of the youngest sedimentary rocks of the Perth Basin. These are generally unconsolidated or partially lithified and are generally believed to have been a combination of aeolian, fluvial and marine origins (12, 25, 26). Glassford (25) undertook extensive studies of the yellow sands within the Perth Basin, providing support for a Pleistocene-aged, aeolian component to the origin of many of the yellow sands around the south-west of the State, but researchers disagree about whether this constitutes evidence of a desert-origin aeolian contribution instead of an *in-situ* weathering (23).

The surface geomorphology of the Swan Coastal Plain can be divided into 4 main regions, the Pinjarra plain, and 3 north-south orientated dune systems; the Bassendean, Spearwood and Quindalup dunes. A diagrammatic interpretation of the geomorphology of the area is presented in Figure 5. Presented in Figure 6 are further details as to the underlying stratigraphy of the region (12). The general consensus is that the dunes represent a series of ancient shorelines, composed of aeolian, fluvial and marine materials (12, 25, 27). The distinction between the dunes is not hard-set but in places, there is more of a gradual shift in properties. The general soil characteristics of each dune system will be discussed individually.

The most easterly feature of the coastal plain is the Ridge Hill Shelf, a narrow (1.5 — 3 km) foothill area (piedmont zone), formed from remnants of the former shoreline deposits of the Ridge Hill Sandstone and the Yoganup formation, abutting the Darling Plateau. This shelf is not specifically shown in Figure 6, but is captured within the 'colluvium' and is presented as the narrow 'colluvial slope' in Figure 5. A series of alluvial fans from streams and colluvial fans from downslope transportation are also within the piedmont zone (12). The soils in this area are commonly classified as Ferric Tenosol, Ferric Kandosols or Ferric Chromosols (28, 29).

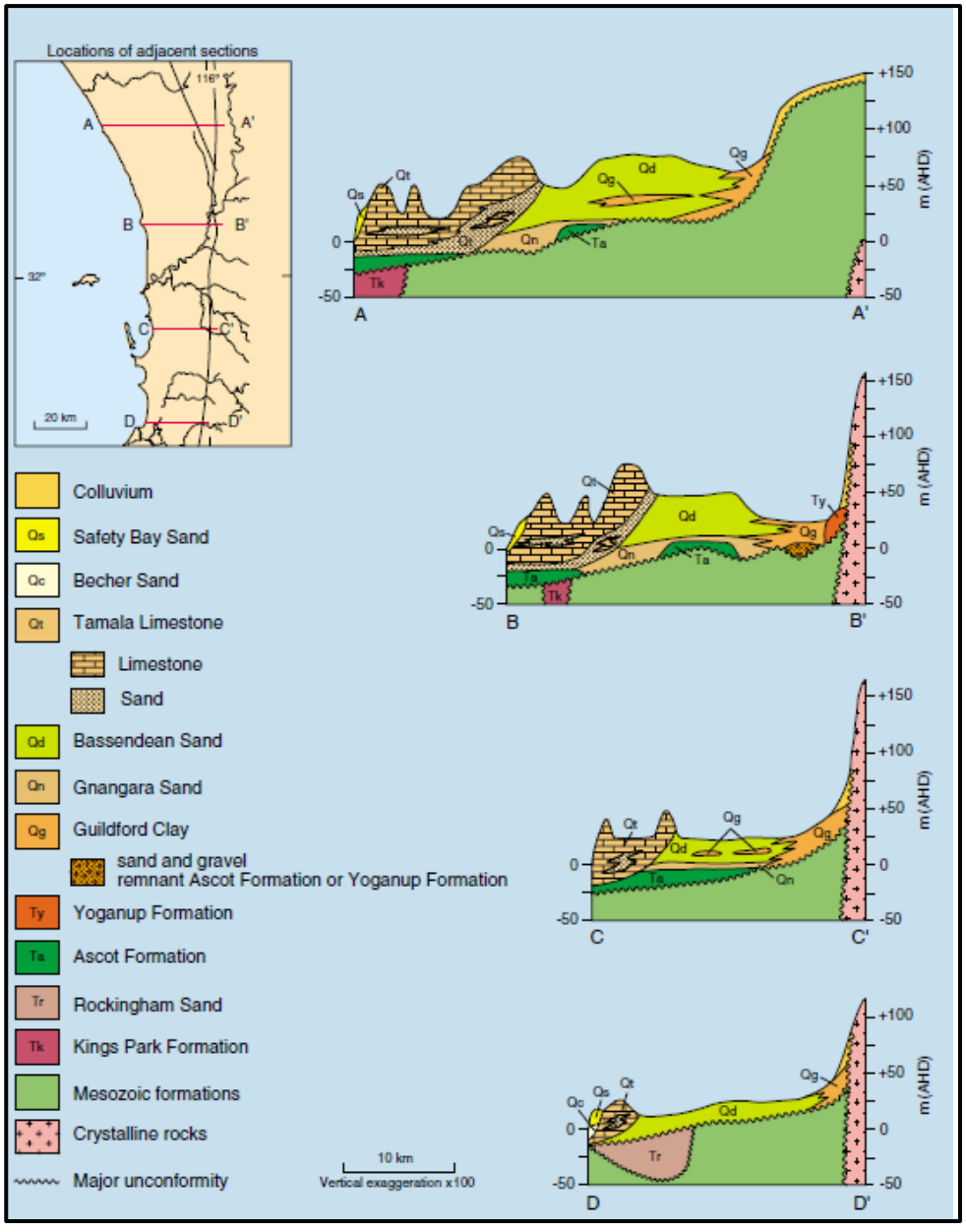

Figure 6: Geological sections showing the stratigraphy of Cenozoic formations within the Perth area (from Gozzard, 2007 [12] page9)

1.3.1 Pinjarra Plain

The Pinjarra Plain is predominantly unconsolidated clays and loams with minor limestone, formed as an alluvial tract to the west of the Ridge Hill Shelf. A mixture of alluvial fans near the scarp and material deposited in floodplains by the river makes this one of the most fertile areas within the Swan Coastal Plain. A large amount of this plain has been cleared and is used for agriculture, including wineries within the Swan Valley and farming and orchard areas within Serpentine-Jarrahdale.

1.3.2 Bassendean Dunes

The oldest of the 3 dune systems, the Bassendean dunes border the Pinjarra Plain and are the farthest from the current coast. The system forms a gently undulating aeolian sandplain about 20 km wide, with poorly-drained areas between low hills causing layers of iron and humus podzols to form underneath the surface (5, 24). Thought to have originally consisted of mostly calcareous sand with quartz sand and minor fine-grained heavy minerals (30), the Bassendean dunes formed over a period of 100,000 years beginning approximately 240,000 years ago (31). Except for a small area south of Perth, these dunes are now so heavily leached they are predominately quartz and are characterised by pale grey, white or pale yellow, water-repellent sands (32). Colloquially referred to as “Gutless” sand or “Banksia” sand, they are typically classified as Bleached-Orthic Tenosols or Aeric Podosols in ASC (31).

1.3.3 Spearwood Dunes

The next dune system west of the Bassendean is the Spearwood Dunes. These are the most variable in their characteristics due to a combination of a younger age and a higher relief, and were formed during the late Pleistocene interstadial period, around 40,000 years ago (12). Leaching of the underlying Pleistocene Tamala limestone has produced overall slightly calcareous aeolian sand (30), Yellow-Orthic/ Red-Orthic Tenosols, Leptic Tenosols or Aeric Podosols. The region is also referred to as the ‘coloured deep sands’ (33) as the sand grains are coated with layers of iron

and aluminium oxides, which gives colour to the sands (the more iron oxide the darker the red colour).

In addition to the large-scale, bare, dune sheets of the Spearwood system discontinuous lakes and marshes also occur throughout the Bassendean and Spearwood dunes (32). These areas contain peats and have commonly been cleared for vegetable production, such as the 'market gardens' that previously dominated the north-east area of metropolitan Perth (12). Overall, the fertility and nutrient retention capacity are greatest for Spearwood soils and least for the Bassendean soil type. However, the soils of the Swan Coastal Plain are some of the most infertile in the world (34).

1.3.4 Quindalup Dunes

The youngest and nearest to the coast are known as the Quindalup dunes. These unconsolidated, discontinuous dunes are predominantly quartz sand and shell fragments, creating an alkaline calcareous series of parabolic dunes, with blow-outs over the underlying Spearwood dunes in places. Leached calcite has caused limestone pipes (rhizoliths) throughout the dune, as well as contributing to the solid base of the dunes, known as the Tamala Limestone (35). These soils are characterised by pale sands of alkaline pH, the presence of calcite and aragonite as well as shell remnants closer to the current shoreline (31, 36).

1.3.5 Pedogenesis of the Swan Coastal Plain

Previous discussions surrounding the factors affecting soil formation have provided a generalist approach. In reality, there are more complex influences that have affected the retrogressive chronosequences (a set of ecological sites that share similar attributes but represent different ages) of the Swan Coastal Plain, and all these factors interact in a complex manner. Pedogenesis in the Swan Coastal Plain is believed to have involved decalcification and secondary carbonate precipitation in younger Holocene soils, the leaching of iron oxides from Mid-Pleistocene soils, which resulted in deep bleached quartz sands in the oldest soils (i.e. those of the Bassendean dunes, up to 2 million years old) (37).

Along the chronosequence, the chemistry of the soil indicates leaching conditions; soil pH, exchangeable cations and total phosphorous (P) decline. There is also the influence of the plant biomass; with a change from Nitrogen (N) to P limitations across the chronosequence, typical of that seen in aged arid ecosytems. Nitrogen availability increases in the early stages of ecosystem development, due to biological N fixation, whereas P leaches away (11).

However, the influence of the climate (including rainfall and average temperature) on the biomass can reduce N fixation, which in turn influences the soil formation. Climatically, two regimes have been particularly important in the soil development of the Swan Coastal Plain; the initial regime of humid, cool to warm climates during the Mesozoic and early Tertiary, followed by an arid regime that continues today (11).

There has been research into the chronosequences at multiple points across the south-western area of Western Australia, including at Jurien Bay and Guilderton to the north of Perth, and Yalgorup and Warren to the south (23, 37). There is a regional variation in the chemical composition of beach sands within the areas studied, believed to be due to differences in off-shore productivity, but this difference has not been confirmed to be present historically (37).

The Quindalup dunes as mentioned previously are the youngest in age- as demonstrated by the minimally-established plant biomass, high carbonate soil content and the immature soil profiles, typical of nearshore coastal dune environments. The Spearwood dunes are believed to represent the weathering results of the underlying Tamala limestone, deposits of a medium-to-coarse sand sized aeolian calcarenite (23). This parent material contained shell fragments and quartz, and minor amounts of feldspars and heavy minerals. The feldspars, garnets, amphiboles and epidote weathered rapidly, resulting in a quartz-dominated sand. The Bassendean sands may have originated similarly as calcarenites, however it is deemed more likely that the parent material contained less carbonates (23). The heavily weathered sand has made it very difficult to quantify the origins of the Bassendean sands. However, soils from each of the three dunes have similar sand-

dominated granulometry and ‘tumbled-like’ grain features, suggesting a common aeolian origin. As mentioned previously, some have proposed a ‘desert extension’ hypothesis where the sands originated from inland dunes (26) but this is not believed to be the major contributor of the sands by many researchers (23).

These observations are also made in another dune area, the Scott Coastal Plain, near Pemberton, which is believed to be a chronosequence of consistent age and formation to the Swan Coastal Plain (37). These results all provide evidence that the Swan Coastal plain soils resulted from *in-situ* soil development, with a long period of pedogenesis in an arid climate, from aeolian-calcarenite parent materials.

1.4 Forensic Analysis of Soil

Soil has been demonstrated in many forensic cases as a valuable source of evidential material (3, 5, 38). Soil is ubiquitous in most crime scenes and the contact with objects, persons and vehicles allow the opportunity for the transfer of soil to those substrates. Recognition of the evidential value of soil has been variable between jurisdictions over time, though soil as trace evidence is well-established.

1.4.1 The Forensic Approach

Soil scientists have several analytical techniques at their disposal for the analysis and characterisation of the soils in any given area. They may undertake fieldwork, where soil profiles are viewed to gain an understanding of the inter-relationships of the soil horizons and allow for classification and determination of the likely characteristics of the soil. These interpretations may then be used in agricultural applications, ‘trouble-shooting’ problem areas or undertaking risk assessments regarding development (39-41). The analysis of soil materials from a forensic perspective differs in some aspects, in that the characteristics are used for comparison purposes, most commonly in a “questioned versus known” situation. This may require an adjustment to the analytical approach, as well as an adaptation of methodology to suit the limitations of the exhibits (as forensic samples are often referred to) submitted for analysis. These limitations may include small sample

sizes, fractionated or non-representative samples and the complications of biological matter including blood and decomposition products.

In some situations, it is possible to also undertake a “forensic provenance” focus to soil analysis, where the identifying characteristics of a specific soil or place are determined to allow for identification based on a collection of soils. This requires vast numbers of samples, as a true database contains all representatives from the population and is considered too excessive for this thesis. Whilst it is hoped that the analysis of soils distinguishes soils with no provenance, the risks of misinterpretation based on ineffective or inadequate sampling means that the ‘questioned vs known’ approach is often more appropriate for case work.

1.4.1.1 The “Standard” Method

Whilst there are many analytical techniques available to soil scientists, there is no single ‘standard’ method in use for the analysis of soil in a forensic context. Efforts recently have initially focussed on; standardising the collection of soil materials (42), the refinement of the terminology used (43) and the research into developing new techniques for comparison and interpretation (44-50). Despite this, it is possible to establish a ‘typical’ method for soil analysis. Most forensic scientists are used to working within set guidelines but understand that, in each case, circumstances will impact upon the most appropriate suite of analyses.

In a forensic case, usually there is a sample with a documented history, commonly referred to as the ‘known’ (k). This sample, or sample/s in a case where multiple locations are possibly involved, is analysed and compared against a sample whose origin is to be determined, commonly referred to as the ‘questioned’ (q). The questioned sample may be collected in many ways. The sample may simply be ‘scooped’ or collected with a shovel, which is typical for scene samples and larger questioned samples. Additionally, samples may be collected by shaking, swabbing, vacuuming, hand-picking or washing. Each system of recovery has advantages and disadvantages, which are presented in Table 1. Hence, most forensic scientists use a combination of techniques, dependent on the case circumstances (5, 38).

Reference samples may also be included in a forensic case for elimination purposes or to assist in the interpretation of results. Several analytical techniques are utilised to characterise the questioned and known samples and, if there are no discernible differences the two samples may be reported as 'having a shared origin', a so-called "source-level" association. This may be followed by an interpretation that also utilises knowledge of transfer and persistence characteristics specific to case circumstances in so-called "activity-level" reporting (51-54). However, this is outside the focus of this project.

Any forensic scientist aims to be able to differentiate between samples that are not of the same origin (exclusion) and associate samples of a shared origin (55). The complications arise as to the interpretation of what a 'shared origin' is, which is related to the differentiating power of the analyst's protocol. This is best demonstrated by a comparison of the older 'ABO' serologic blood groupings to DNA typing for the association of a blood spot (q) to a possible offender (k). A 'shared origin' using blood grouping is not very strong evidence as depending on the blood group, the 'shared origin' may also include up to 40% of the Australian population, a discriminating power as poor as 1 in 4 (56). On the other hand, a 'shared origin' based on DNA typing, using a commercially-available STR-kit such as ProMega's PowerPlex® Fusion has a "probability of identity", which illustrates the far higher resolving power on the same DNA samples, of 6.58×10^{-29} (57). Soil protocols are not equivalent to the 'gold standard' that is DNA typing. However, the forensic scientist aims to minimise both false positives (incorrect associations) and false negatives (incorrect exclusions) by using a series of analytical tests.

Table 1: Common Collection Techniques for Soil Materials of Forensic Interest

Collection Technique	Brief Description	Advantage(s)	Disadvantage(s)
Scoop/Dig	Collection of a large sample into a bag or jar using a shovel, trowel or scoop.	A large sample is collected, with the ability to represent all characteristics of the soil.	Original sample must be larger. Any sample layers are lost as the sample is mixed.
Shaking	Item is shaken over paper and the debris collected. Common for clothing or shoes (possibly with initial microscopic inspection and some hand-picking).	Able to concentrate and collect a sample from a larger area. Relatively fast.	Potential for loss of smaller particles or incomplete collection of adhering material. Potential for the mixing of soils from more than one source and from different parts of the substrate, such as within pockets.
Vacuuming	Using a new or specially prepared vacuum system to collect a sample of loose debris from larger objects, such as car interiors or rugs.	Able to collect and concentrate a sample from a large surface area.	Contamination from previous uses of cleaner. Collection of historical exposures, rather than recent depositions, especially within carpets.
Hand-picking	Using tweezers to collect individual grains, usually with the aid of a stereo-microscope.	Allows for the visualisation and isolation of specific grains, *in-situ* and with context.	Time-consuming. The initial object may be size limited.
Swabbing	Wiping area to be sampled with a support, commonly a cotton swab or wipe.	Easy and familiar to crime scene officers. Dry swab/wet swab may aid recovery.	Isolation of the sample may be difficult for the analyst. Swab substrate may interfere in analyses.
Washing	Washing. the item for the removal of material using a liquid, such as water or a mild detergent solution.	Possible to collect from deeper within an item than shaking. Ability to concentrate sample from a large object.	Isolation of the sample may be difficult for the analyst The solvent may interfere with or alter materials, especially soluble salts.

Figure 7 illustrates a 'typical' analysis protocol for soil in a forensic context (5). This protocol is based on several different publications as well as the experience of soil analysts as to what allows for the best differentiation and associations (38, 58). This flowchart does not include crime scene examinations, which are covered within

other publications (59, 60), but rather is initiated once the samples are submitted to the analytical laboratory.

Most analysis schemes will follow a similar sequence; i.e. whole/bulk examinations of characteristics like colour, texture and estimated bulk mineralogy (61), followed by separation and more detailed examination using various techniques and an ultimate comparison between samples (62, 63). A short discussion of the examination techniques of particular relevance to soil analysis follows.

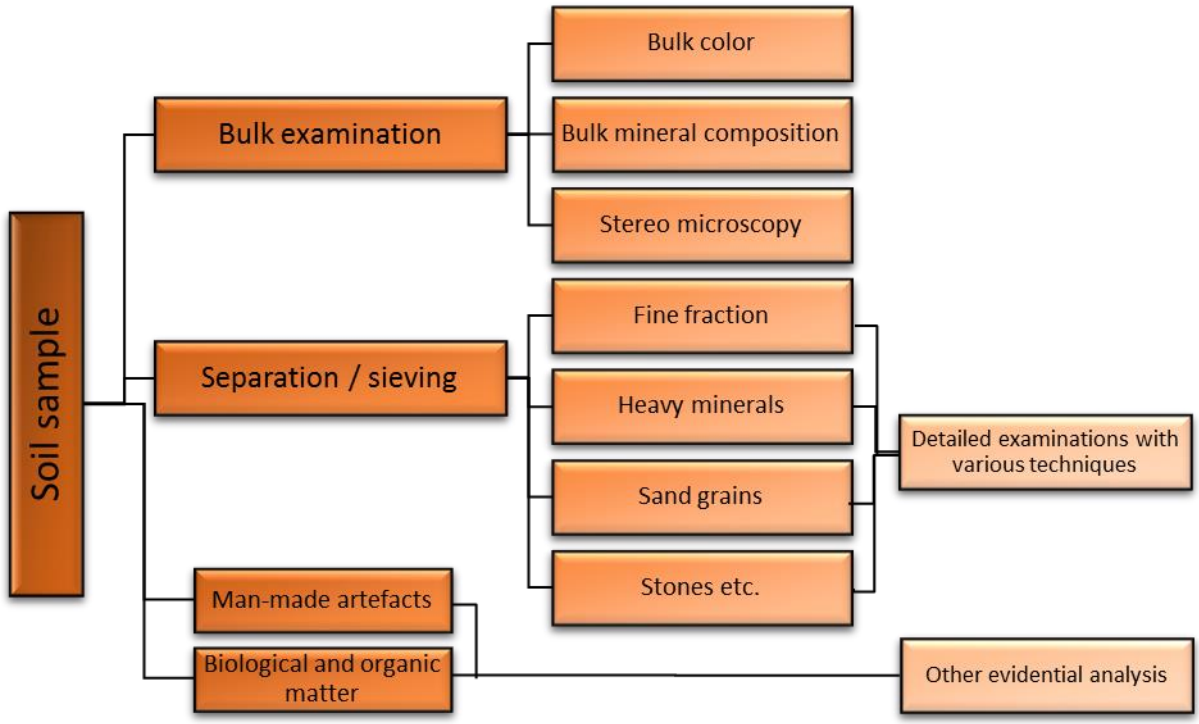

Figure 7: Simplified Flow-chart of a 'typical' forensic soil analysis (from Pitts, Lewis and Newland 2018 [5])

1.4.2 Inorganic Analysis

As mentioned previously, a large proportion of soil is the dominantly inorganic component comprising minerals and rock fragments. Many techniques have been utilised for analysing this component in any of the separated fractions or the sample as a whole. A selection of applicable techniques will be discussed, with the specific techniques of interest in this thesis discussed in subsequent chapters.

1.4.2.1 Optical Microscopy

A large amount of information may be obtained simply by the visual examination of the sample, with the aid of a stereomicroscope. Examination of visible physical characteristics includes an approximate colour, texture descriptions such as relative particle sizing, the presence or absence of peds or agglomerates, the relative homogeneity of the sample, and any visible layering or noticeable artefacts, biotubules or foraminifera, may all be used as characteristics for initial comparison between questioned and known samples(58).

Additionally, an examination may occur of separated fractions, such as the heavy minerals of the sand fraction, or the pebble/stones. Polarised light microscopy (PLM) can be used for identification of bulk minerals and individual grains (38, 64).

1.4.2.2 Microspectrophotometry

Colour is a very discriminating characteristic within soils, and bulk colour is commonly recorded according to the best match of the soil to 'standard' colour chips of the Munsell colour system (65). However the classification of a soil to a colour designation is still somewhat subjective. Woods et al (66) utilised objective colour determination in L*a*b space using microspectrophotometry (MSP). MSP allowed objective colour comparison of the <38μm fraction but is complicated by sample heterogeneity and does not eliminate the need for more advanced mineralogical examinations.

1.4.2.3 Particle size distribution

The distribution of the size of particles within a soil is another characteristic that can be used for forensic purposes. The Wentworth scale (67) details the classifications of particulates based on their physical size, regardless of mineralogy. The determination of amounts within established sizings, whether by weights of wet/dry sieved fractions, a Coulter counter, laser granulometry or a combination, can illustrate significant differences in soils (68). However, this characteristic is complicated by the fact that a forensic sample may be limited in size or not be a representative sample of the original soil distribution.

1.4.2.4 Grain characteristics

The surface morphology of grains, especially quartz sand grains, has been utilised for the comparison of soil samples recovered in a forensic context (44, 69). The theory is that environmental factors such as weathering, fluid movement and biota actions all impact on the surfaces of mineral grains within a location. By using a subjective classification system an area's 'types' may be compared to other sites (45, 70). The similar histories and ages of the Swan Coastal Plain dunes mean there is limited scope for differentiation of grains morphologically and significant overlap is likely of the 'types' present (69).

1.4.2.5 Infra-red and Raman Spectroscopy

Infra-red (most commonly as Fourier transform infra-red, FTIR) and Raman spectroscopy are complementary techniques that have long been utilised in the analysis of forensic trace evidence (71, 72). In FTIR, the interactions of an infra-red beam with the vibrational frequencies of molecules present within a sample create characteristic absorbances of bonds present, which undergoes Fourier transform resulting in spectra indicative of compositions. The most common modes of FTIR used in soils are attenuated total reflectance (ATR)-FTIR spectroscopy, and diffuse reflectance infrared Fourier transform (DRIFT) spectroscopy (66, 73-76).

Raman spectroscopy is generally considered complementary to FTIR, as a poor IR absorber may commonly exhibit a better Raman scatter. The incident laser wavelength within the Raman spectrometer is used in initial excitation and Raman scattering, again producing spectra of peaks characteristic of bonds within the sample. Whilst not as widely used as FTIR, Raman spectroscopy is becoming more routine, especially with the development of portable systems, and the utilisation of it for soil and mineralogy also expanding (77-80).

1.4.2.6 X-ray Fluorescence

The determination of elemental composition allows for comparison between samples since the elemental composition is directly related to mineralogical composition and, hence, may be used for soil analysis (81-83). X-ray fluorescence

spectroscopy (XRF) is one technique, utilising the characteristic photons produced by the excitement and relaxation of an element's electron shells by the incident X-ray beam. However, whilst XRF has detection limits in the parts per million (ppm) range for most metals, it is limited to the detection of heavier elements (usually sodium and above) and is complicated by overlaps such as those of titanium and barium. Additionally, it cannot differentiate between minerals of the same chemical composition (polymorph) and sample preparation may be semi-destructive.

1.4.2.7 Scanning Electron Microscopy

Scanning electron microscopy with energy dispersive X-ray spectroscopy (SEM-EDS) and the associated but more advanced technique of inferring mineral identities from quantitative elemental concentrations, known by a few trade names, such as Quantitative Evaluation of Materials by Scanning Electron Microscopy (QEMSCAN), Automatic Geological SEM (AutoGeoSEM), or TESCAN Integrated Mineral Analyser (TIMA), allow for the imaging and elemental analysis of mineralogical materials related to soils, especially heavy mineral separations. Studies utilising SEM-EDS for grain morphology characterisation or identification, as well as classification-mapping of prepared thin-sections or mounted grains, have illustrated its application for comparisons (84, 85). As with XRF, lighter elements may be problematic, and interferences or polymorphs may complicate analysis. However, the use of SEM, in any of its' forms, is an invaluable tool in a soil analysis protocol as it allows visualisation of materials at a higher magnification than possible with an optical microscope, coupled with the ability to determine elemental distributions within that image.

1.4.2.8 ICP-MS and LA-ICP-MS

Inductively coupled plasma mass spectrometry (ICP-MS) emerged as a technique for elemental analysis in the late 1980s, an improvement on the coupling of the ICP to an atomic emission spectrometer (86-88). It became used in forensic chemistry shortly thereafter (89). After suitable sample digestion, a solution is nebulised into a stable plasma of approximately 8000 K equivalence, where the molecules de-

solvate, atomise and ionise and are then introduced into a detector, most commonly a mass spectrometer. Alternatively, a laser may be used for the introduction of a small, ablated sample directly into the plasma, a technique known as laser ablation ICP-MS(90, 91). Both techniques have very low detection limits relative to other elemental techniques, with over 60 elements able to be detected routinely at levels as low as 0.1 $ng.L^{-1}$ and some even lower using more advanced detectors such as the magnetic-sector or high-resolution MS (92). Hence ICP-MS allows for trace elemental comparison of a wide range of materials, including soil fractions and mineral grains (91, 93-96). Complications from sample heterogeneity, fractionation arising from minerals such as quartz and other silicates resisting digestion unless dangerous HF is used, and the destruction of the sample during digestion are draw-backs. Therefore, this technique is commonly undertaken last in a sequence of soil analysis.

1.4.2.9 X-ray Diffraction

X-ray Diffraction (XRD) utilises *Braggs' Law*, where an incident X-ray beam will be scattered by the lattice planes of a crystalline material, in such a way that creates constructive and destructive interferences, known as diffraction. *Braggs' Law* stipulates that this diffraction only occurs in cases where 1) the spacing between lattice planes is roughly equivalent to the incident wavelength and 2) the scattering centres (atoms) are structured in an ordered three-dimensional pattern. As a consequence, only crystalline solid materials, such as minerals, will diffract predictably. Hence, diffraction (including XRD's related techniques of small-angle/ wide-angle X-ray diffraction SAXS/WAXS, electron and neutron diffraction) is the only technique to give crystallographic information rather than elemental information. One requirement of XRD is that most instruments require samples to be ground to a fine powder (ca.<20µm) to minimise single-crystal diffraction that will affect reproducibility of patterns and, hence, the interpretation of the mineralogy. Micro-XRD with automated stages has been developed to overcome this requirement and attempt in-situ XRD pattern 'maps'. XRD will be discussed in further detail in Chapter 3.

1.4.3 Organic Analysis

An emerging area of research and development has been the use of techniques that allow for the analysis and comparison of the organic fraction of soils, referred to as 'soil organic matter' or SOM. This fraction is dominated by contributions from biota in two groups, the decomposing material and the humus. The decomposing plant and animal residues, litter and detritus, comprise carbohydrates, proteins and plant fractions and account for approximately 10—15% of SOM, with a rapid (<10 years) turnover (97, 98). The other organic component is the humus, containing the more stable (>10 years) humic substances, lipids and plant waxes, which whilst highly variable are hard to quantify (99). A small selection of the most common techniques for the analysis of the SOM fraction will be discussed.

1.4.3.1 Chromatographic Techniques

In most organic analyses an initial sample preparation method is undertaken, followed by an instrumental technique designed to separate, detect and identify the many organic compounds contributing to the organic content of the soil. The most common of these techniques are the chromatographic techniques, gas-chromatography and liquid chromatography (GC and LC). These techniques are similar in that a small sub-sample of an appropriately prepared sample is injected onto a column, packed with a stationary phase. The mobile phase is used to 'push' the sample along the column, with the different interactions of the compounds with the mobile and stationary phases allowing for their separation based on polarity, functional groups and molecular weight. In GC, the samples are in the gaseous phase, whilst LC is better suited to thermally labile compounds. A wide range of detectors have been coupled to GC and LC columns, such as mass spectrometers (MS), ultra-violet (UV) detectors and time-of-flight mass spectrometers (TOF-MS).

Chromatographic techniques have been utilised by many authors to characterise and compare the organic fraction of soils (3, 97, 100, 101). Most have determined that a suitable work-up followed by analysis is appropriate for the analysis of organic 'markers'. The organic fraction may also be analysed to allow for the comparison of the ratios of C, N, O and H isotopes, known as isotope-ratio (IR)-MS

or GC-IR-MS (102, 103). Further research into the characterisation and identification of appropriate compounds and associated methodology, especially in areas of low organic content like the Swan Coastal Plain, is needed before the analysis of SOM becomes routine in forensic casework.

1.4.3.2 Microbiome and Proteome Analysis

One growing area of analysis with a large range of forensic applications is the exploitation of variations within the microbiome and associated expressed proteins (proteome) within a sample. Soil contains an abundance of microbiota, which can be 'rNA-typed', classified and compared in a similar manner to DNA-typing of a human sample (49, 104-106). In comparison, proteomic analysis characterises the long and short-chain proteins present within a sample (107). Both techniques show promise for soil comparison work, however, are still in developmental stages.

1.4.4 Use of the Fine Fraction from Quartz Grains

Given the heterogeneity of soils, transfer events inherent in criminal activity are unlikely to provide a representative sample, particularly if only a small amount is involved. Subsequent activity and variable persistence will further alter the sample. When the sample size is very small, the use of soil constituents least affected by sampling factors, such as the finer fractions, should be preferred (108).

As previously detailed, many protocols for soil comparison utilise fractions of specific sizes or characteristics, such as heavy minerals (64, 109) or <38 µm fines for FTIR/MSP (66). Asumadu et al (69) specifically studied quartz grains in an attempt discriminate between two soil materials and to give an indication of provenance for sandy soils in WA but proved unsuccessful. However, the potential for the discrimination of soils using clay mineralogy has been demonstrated by the work of Marumo et al. (110, 111). The authors found significant variation in clay mineralogy in soils developed on a single granitic parent material in a small area of Japan. Additionally, Corrêa et al. (112) used clay mineralogy to distinguish between 32 soil samples based on the colour and XRD pattern of wet-sieved clay and silt fine fractions.

The issue with many of these approaches is that they are difficult to apply to small samples of soils dominated by sand grains, with little organic matter and minimal heavy minerals, such as the soils found in the Bassendean dunes of the Swan Coastal Plain. These soils require an adaptation to the 'standard' protocol, one developed over many years with the Chemistry Centre of Western Australia (ChemCentre). The technique developed (108, 113, 114) is based on the characterisation of *in-situ* primary and secondary minerals found as coatings on the quartz sand grains. The analysis is performed in conjunction with the 'standard' protocol but is considered a 'next step' in the comparison process.

The methodology for the recovered coatings is discussed in detail in Chapter 2; in brief it involves the hand-picked quartz grains being ultrasonicated to remove the coatings, which are then separated further, concentrated and analysed by XRD (108).

1.4.5 Objectives for this Project

The objectives for this project were to expand and further validate the ChemCentre method developed for the utilisation of the fine coating recoverable from quartz grains (referred to as 'quartz fine fraction') (108). Initially, the potential to utilise Raman spectroscopy was investigated, which is detailed in Chapter 2. This chapter aimed to examine Raman spectroscopy firstly as a screening technique or complementary information from the quartz fine fraction. Secondly, if successful, Raman was to be used to examine single grains of quartz, to attempt *in-situ* analysis of the coating to assist with 'speeding up' the analysis.

The development of a multivariate approach to analyse the quartz fine fraction was the aim of Chapter 3. The data from the lab-based, XRD analysis of 202 samples was examined using multivariate statistics, expanding on the previous 'fuzzy-logic' based algorithm of comparisons. Structure within the dataset was examined by viewing scores and loading plots of percentage intensities to determine if structure exists that may allow for more objective comparisons of samples using the quartz fine fraction.

Chapter 4 aimed at exploring efforts into the use of the powder diffraction beamline at the Australian Synchrotron. The PD beamline was used for more extensive characterisation of the fine coatings. Finally, Chapter 5 aimed at illustrating the application of the quartz fine fraction, as well as the associated multivariate statistical models developed in Chapter 3, to two case studies submitted to ChemCentre. In all cases, the evaluation of the applicability of the technique to forensic casework was of most importance.

Chapter 2. Analysis of the Recovered Fine Fraction by Raman Spectroscopy

2.1 Introduction

The use of Raman spectroscopy for forensic analysis is well established (77, 115). Many studies have shown the value of this vibrational spectroscopic technique, especially when complemented with FTIR (72, 77, 79). In this chapter, the use of Raman spectroscopy for examination of the recovered quartz sand grain derived 'quartz fine fraction' is presented. The initial recovery of this previously discussed fraction will be detailed as well as its analysis using a Raman microscope. The aim was to explore whether the technique would enable the initial screening of samples, to further extend the technique to allow for *in-situ* analysis of the coatings on quartz grains.

2.1.1 Raman Spectroscopy

Based on the identification of specific chemical bonds inherent to a structure by the detection of characteristic scatterings of an incident radiation source (currently a monochromatic laser) as it interacts with the chemical bonds, Raman spectroscopy has become a useful part of any analytical protocol (116). During irradiation, the electrons of the sample undergo excitations to virtual energy states, as illustrated in Figure 8.

Over 99.999% of the excitation undergoes elastic (Rayleigh) scattering, where it is excited and relaxed to the ground state with no energy differential (117). It is the 0.001% inelastic (Raman) scattering that is of interest in the technique. Stokes Raman scattering occurs when the incident radiation induces a polarisation that couples with a vibrational change within the molecule, that is a relaxation of the excited electrons back to a level other than the ground state, whereas Anti-Stokes Raman scattering occurs when an electron from a vibrational state other than ground is excited and relaxed past its initial state to the ground state, giving a photon greater than the incident (117).

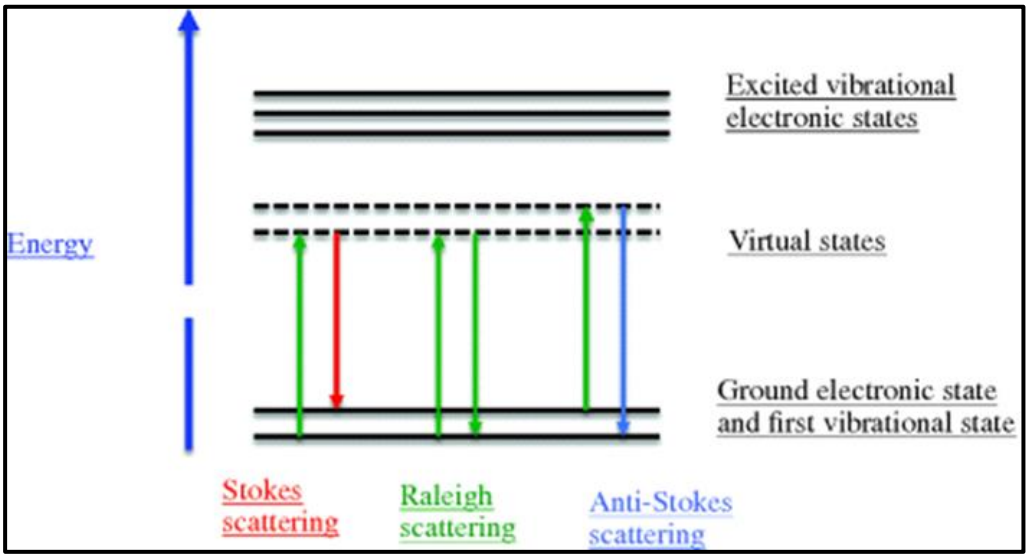

Figure 8: Rayleigh and Raman (Stokes and Anti-Stokes) Scattering (from Smith, 2017 [112])

The vibrations related to the bonds within a molecule are revealed by filtering the Rayleigh scattering and then detecting the 'shifted' radiation. A molecule will have multiple vibrations characteristic of the bonds present within. By obtaining all possible energies and their intensities, a Raman spectrum may be established, which can be examined and compared to standards for determination of a sample's composition. A mixed sample is likely to be more complex than a single analyte. However, characteristic peaks may occur that allow for resolution of mixtures. Additionally, it is most common to only record the Stokes shifts, as this is simpler experimentally and usually contains sufficient information (117).

Raman spectroscopy has been utilised for mineral analysis, and many reference spectra are available in commercial software such as WiRE [Renishaw Pty Ltd, United Kingdom] or online spectra collections (118). In addition, Raman spectroscopy has been utilised in forensic science for the comparison of forensic samples such as paint and fibres (72, 119). As such, it was envisaged that Raman spectroscopy may be a viable addition to the current analysis protocol of the quartz fine fraction, especially as it is already utilised for the identification of isolated grains. It was proposed that Raman spectroscopy could be utilised in 3 possible ways:

- As an additional characterisation technique in the analytical sequence, after XRD analysis of the fine fraction.
- As a 'screening' technique prior to the analysis of the quartz fine fraction using XRD
- As an *in-situ* method for the characterisation of coatings directly from the quartz grains, as a 'single grain' test.

Hence it was proposed to test the capability of Raman spectroscopy to successfully obtain spectra from the low background plates currently utilised for the XRD analysis, as well as the ability to distinguish between soils from different locations.

2.2 Experimental

2.2.1 Recovery of the fine fraction

This technique was developed within ChemCentre for the recovery of the <20 µm fraction (referred to as the quartz fine fraction) from quartz grains (108). This project utilised the established method to recover samples to analyse using Raman spectroscopy, as well as X-ray powder diffraction (XRPD, see Chapter 4). In simple terms, quartz grains were hand-picked from the samples, and the coating removed and isolated for analysis.

Generally, 100–300 quartz grains with a combined mass of 20–100 mg were collected, depending on particle size and amount of coating. The grains were added to de-ionized water in a 15 mL tapered tube and agitated in a low power (50 Watt) ultrasonic bath. The resulting suspension was allowed to settle, according to Stokes' Law following published guidelines on sedimentation rates (120, 121), then decanted to obtain the <20 µm fraction. For most samples, a volume of water approximately 1 cm above the grains, followed by a settling time of 30 seconds before decanting the supernatant was used. The decanted solution was concentrated using a centrifuge [3500 rpm for 10 minutes] and the supernatant carefully removed using a Pasteur pipette. The fraction was then re-suspended in a minimal amount of the liquid and drops of the suspension dried on a "low-

background" quartz, single crystal wafer (low-background plate, LBP) for analysis. A deposit with a typical areal concentration of approximately 1 $mg.cm^{-2}$ was produced, with an effort to keep the deposit infinitely thin and within the bounds of the expected X-ray footprint on the plate (108).

2.2.2 Sample Selection

The samples chosen for initial Raman analysis, as well as for characterisation using the Powder Diffraction beamline at the Australian Synchrotron, were selected to illustrate the diversity within the Spearwood and Bassendean dunes. The samples were chosen from previously collected samples held within the soil collection of the Forensic Science Laboratory of ChemCentre. These samples were collected with a view to stratigraphically sub-divide the dune systems of the Swan Coastal Plain by examination of the primary mineral assemblages (122, 123). This collection was enhanced and the work extended to the examining of secondary mineral coatings present in the quartz fine fraction during a National Institute of Forensic Science (NIFS) funded project (113), as detailed in Bastian (122). This project aimed to obtain the full or maximum possible age of the soil representative of the dune ridges. Samples of 1–2 kg each were collected along a series of east-west transects across the Perth area. The following criteria were applied to the selection of sampling sites along these transects:

- Lower slopes or inter-dune areas were avoided to minimise mixed residual sands.
- Samples were taken preferentially from thick soil profiles, from the upper parts.
- Areas of limestone outcrop were avoided, due to the likelihood that much of the residual sand had probably been already stripped.
- The bottom levels of deep trenches or sandpits were also rejected.
- Additionally, any site where evidence of significant disturbance could be seen was rejected.

- Soil was collected from below the plant-rich A_1 horizon, at the B-horizon or the A_2 horizon.

In practice, samples were collected from the higher levels of railway cuttings, roadside cuts, shallow trenches, shallow building excavations and isolated pockets of natural bushland left within urban areas. Whilst it is possible that some sites, especially pockets of natural bushland, may be likely crime scenes the sites were chosen to be representative of the soils overall.

A map showing the location and 'transect groups' for the samples chosen for the Raman spectroscopy analysis and the work on the Powder Diffraction beamline is presented in Figure 9, with sites projected onto physiographic regions of the Swan Coastal Plain (124).

2.2.3 Analysis using Raman Spectroscopy

The fine fractions separated from hand-picked quartz grains (quartz fine fraction) were initially mounted on low background XRD plates, to allow for XRD analysis. The plates were then presented to a Renishaw Raman microscope spectrometer, with a laser of 785 nm wavelength, using the 5× objective for initial experimentation. A scan of 1 or more accumulations, with at least 10 seconds exposure time, and an extended scan from 100 cm^{-1} to 3200 cm^{-1} was undertaken on each sample. The laser power was optimised for each sample with the exposure time/accumulations increasing where possible, to give the maximum signal output without overloading the detector or damaging the sample.

Recorded data was compared to the commercially available Renishaw database as well as selected spectra from the RRUFF project database (118) and publications for the inference of mineral identity. Identification was only confirmed by the presence of multiple corresponding peaks.

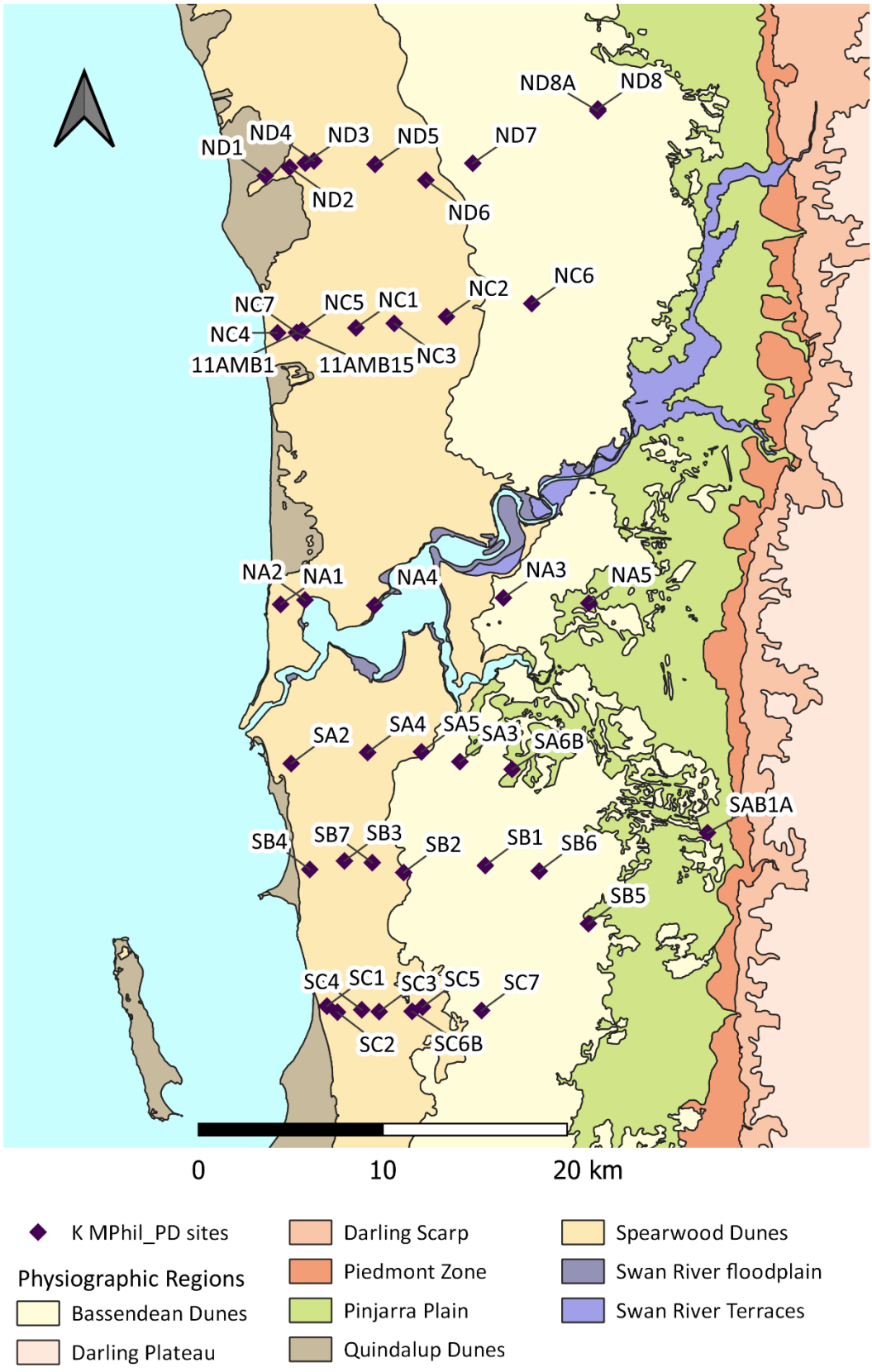

Figure 9: Map showing locations in 'transect groups' selected for the Raman spectroscopy and the PD Beamline work. The sites are overlaid onto the physiographic regions of the Swan Coastal Plain [124]

2.3 Results and Discussion

2.3.1 Initial Analysis

A small selection of samples was examined initially to determine the best conditions for the collection of Raman spectra from the low-background plates. It was decided to use the 5× objective, with the 'pin-out' to visualise the quality of the spectra from a greater area of the sample and minimise the possible effects of sample heterogeneity in initial experiments. If successful, higher magnification may then be used for further sample characterisation.

Additionally, research into the spectral bands of the suspected minerals present within the fine fraction showed that most bands should be present within the 100–3200 cm^{-1} shifts, with some phyllosilicates also showing peaks between 3600–3800 cm^{-1} (125, 126). The suspected minerals were; quartz, microcline feldspar, kaolinite, 'mica' (probably muscovite), vermiculite, goethite and gibbsite, with the possible presence of anatase, chlorite and calcite in some soils. The identification of these 10 minerals was based on previous work and are discussed in more detail in Chapter 3 (108). A diagram showing the expected peaks for the minerals is shown in Figure 10 and a diagram of some minerals unavailable as data files is presented in Figure 11 (118, 125, 127). Hematite was also contemplated, given its strong colour, so was monitored but the reference spectra is not presented here.

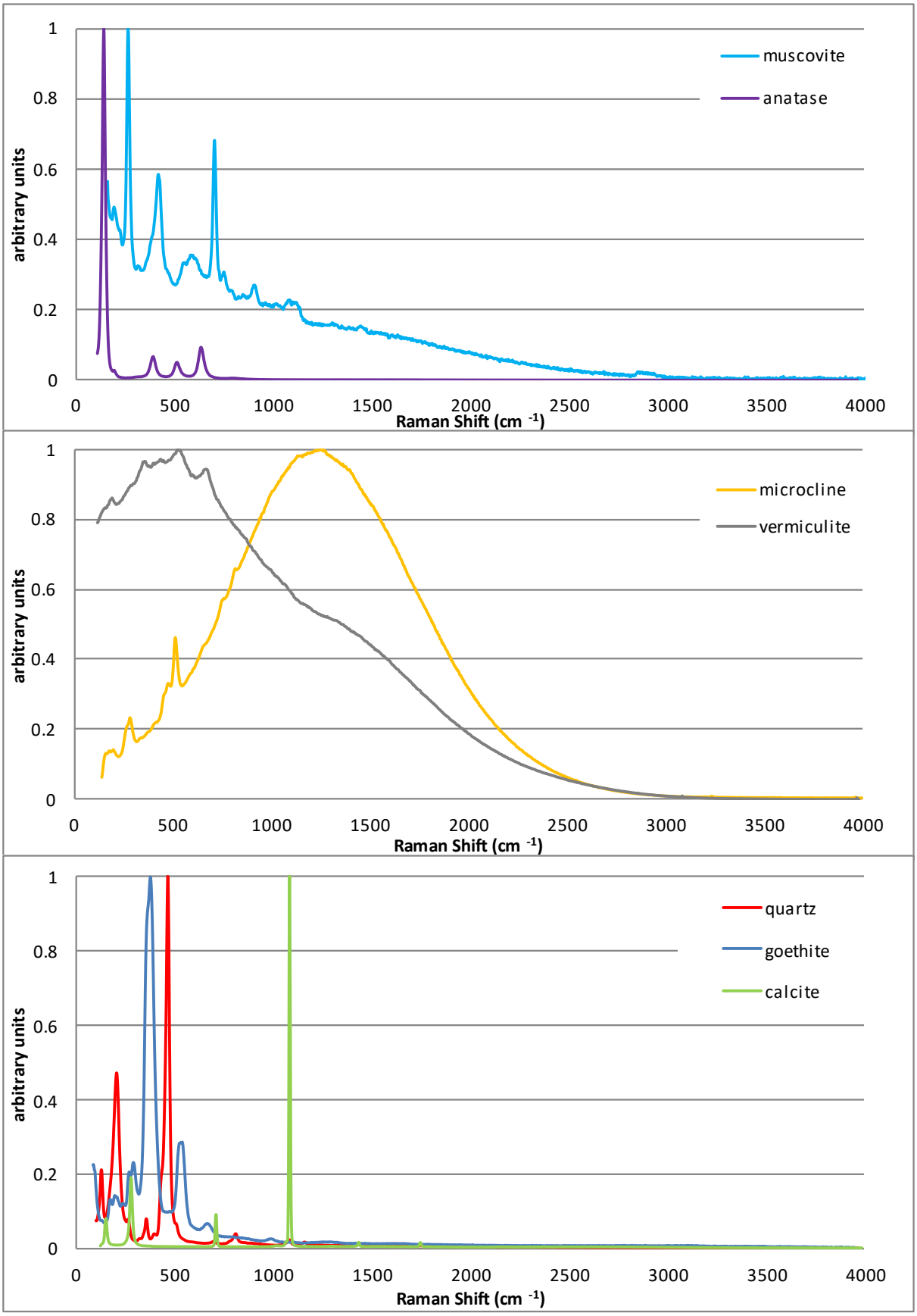

Figure 10: Raman Spectra of anatase, muscovite, microcline, vermiculite, quartz, goethite and calcite using 780-785nm laser, based on RUFF data, normalised to most intense peak

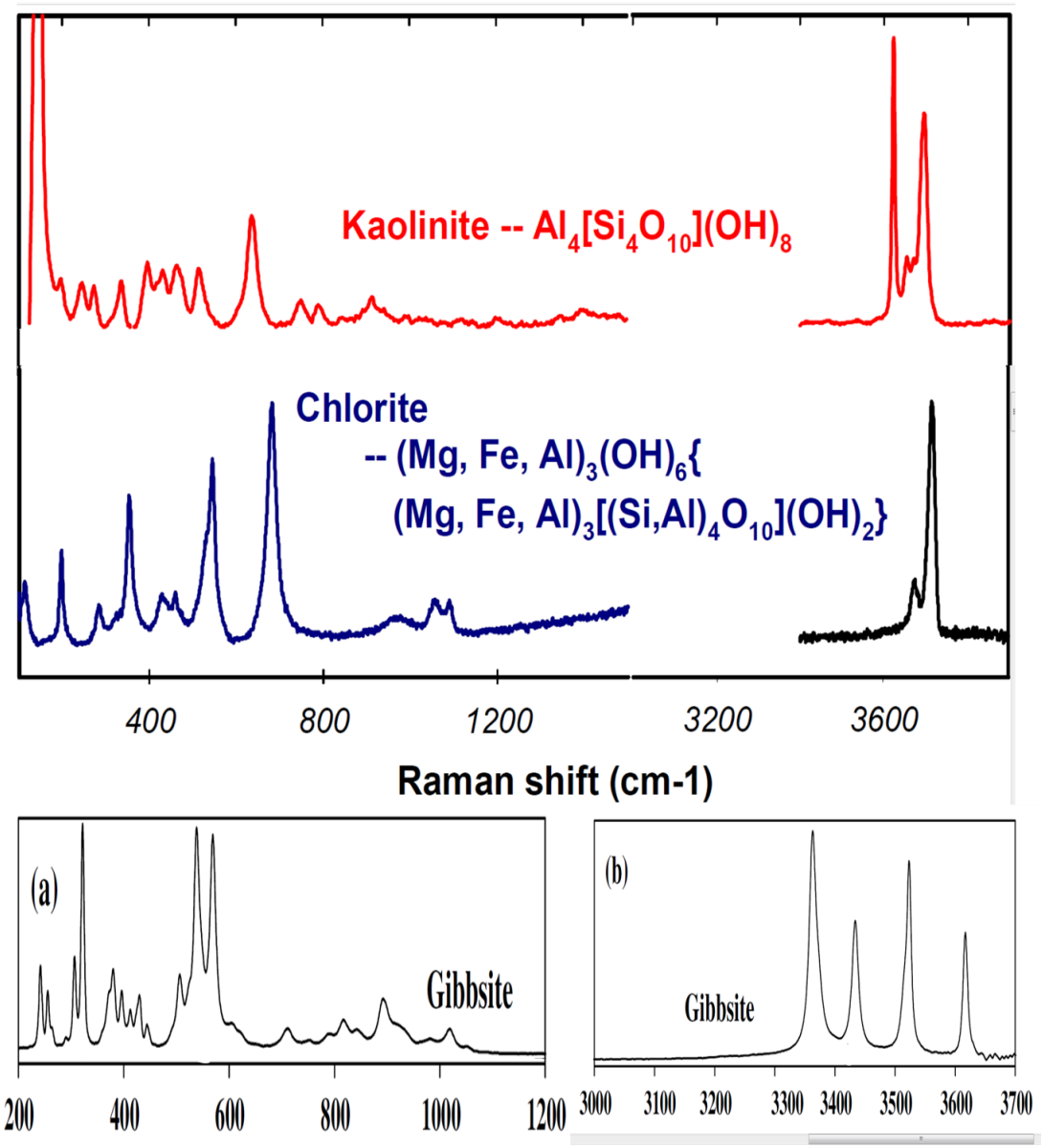

Figure 11: Published kaolinite and chlorite Raman spectra (from Wang et al. 2002 [125] and Ochando et al. 2018 [127])

The spectrum for the low background plate (LBP) is presented in Figure 12, which corresponds mostly to the quartz reference spectrum from within the WiRE software (128). The spectra for 3 of the samples analysed initially using the Raman spectrometer are presented in Figure 13. Visible are the high levels of fluorescence within the samples, and the strong peaks characteristic of the quartz LBP. Additionally, the broad shift seen in NA5 at approximately 1350 cm^{-1} was attributed to the LBP. Other broad shifts are seen around 500 cm^{-1} in ND8A and NE3 but were not reproducible and due to their poor shape and broad nature could not be assigned to a specific mineral.

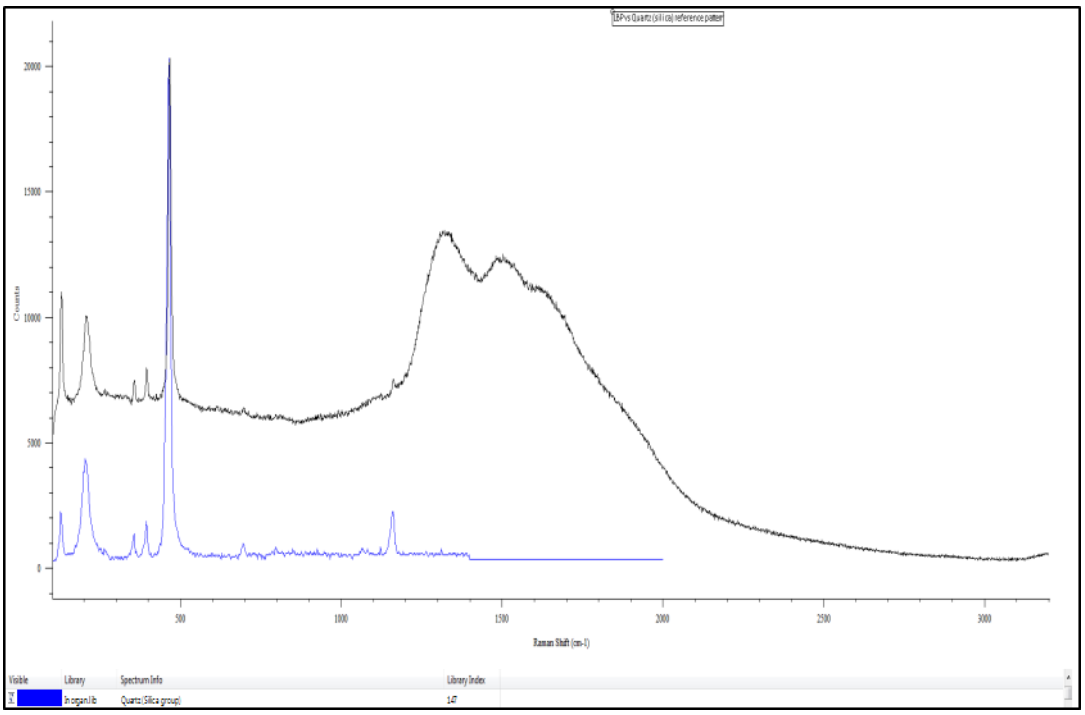

Figure 12: Raman Spectrum of quartz 'low background plate' (LBP) using 785nm laser, 10 second exposure, 5 accumulations vs the 'known' quartz reference spectrum (blue) from the WiRE software

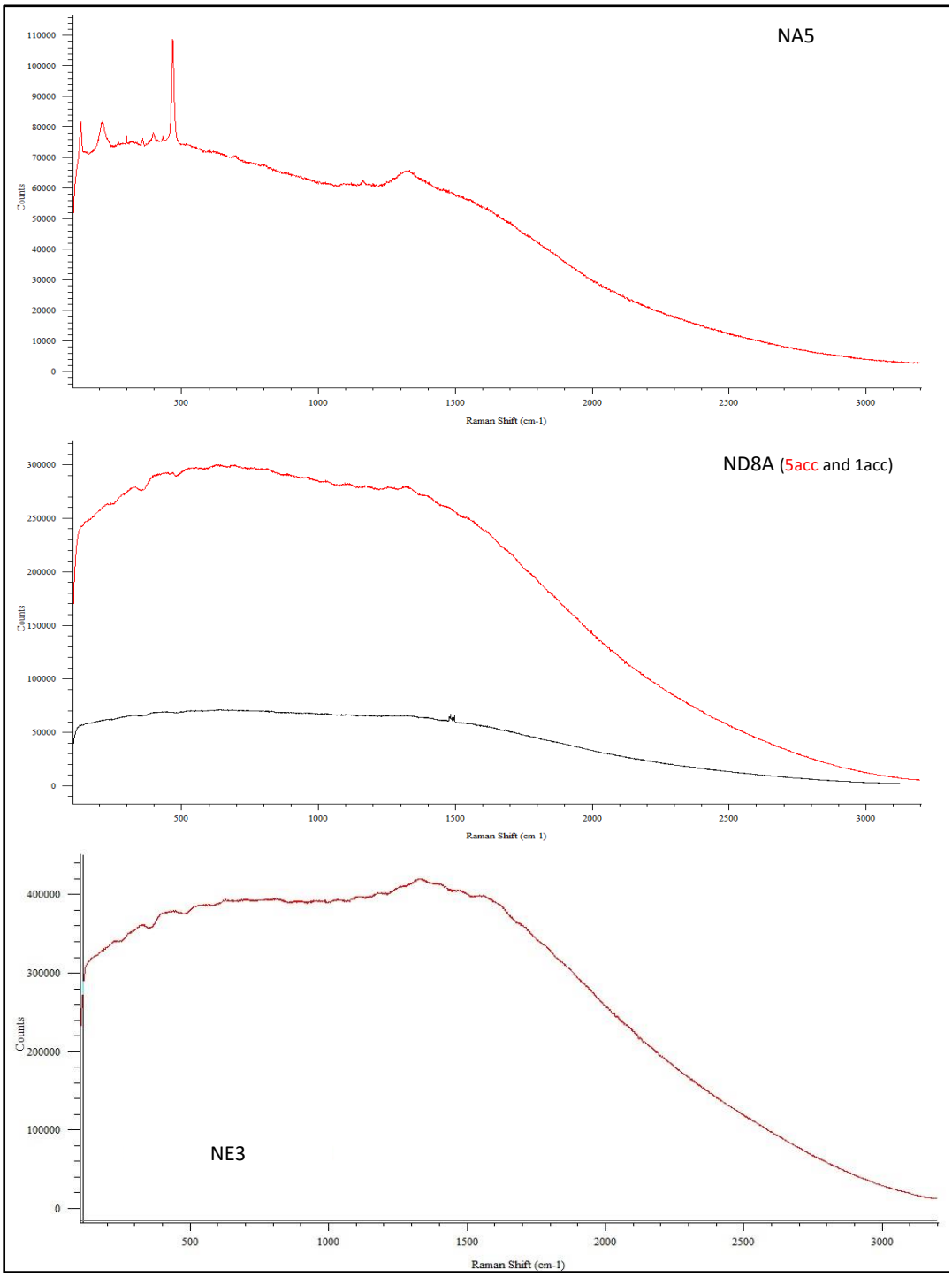

Figure 13: Spectra of NA5, ND8A NE3 analysed from LBP using 785nm, 100–3200 cm^{-1}, 10 sec exposure, 1 accumulation, also shown is ND8A with 5 accumulations

2.3.2 Background correction

The fluorescence within the spectra represents a 'swamping' signal, but in some cases, background correction may be able to provide a useable spectrum. However, background correction must be performed systematically and reproducibly to allow

for accurate and reliable spectra. Background correction may lead to erroneous peaks and cannot improve poor data. Presented in Figure 14 are the attempts at background correction using the baseline fitting options within the Renishaw Wire software, for the 11AMB05 sample that was used in subsequent optimisations. Even with a sextic-based polynomial function and multiple variations to the points used for the fitting, no adequate baseline was found that removed all of the interference from the spectrum. Hence for comparisons, all samples were left as collected for subsequent experiments.

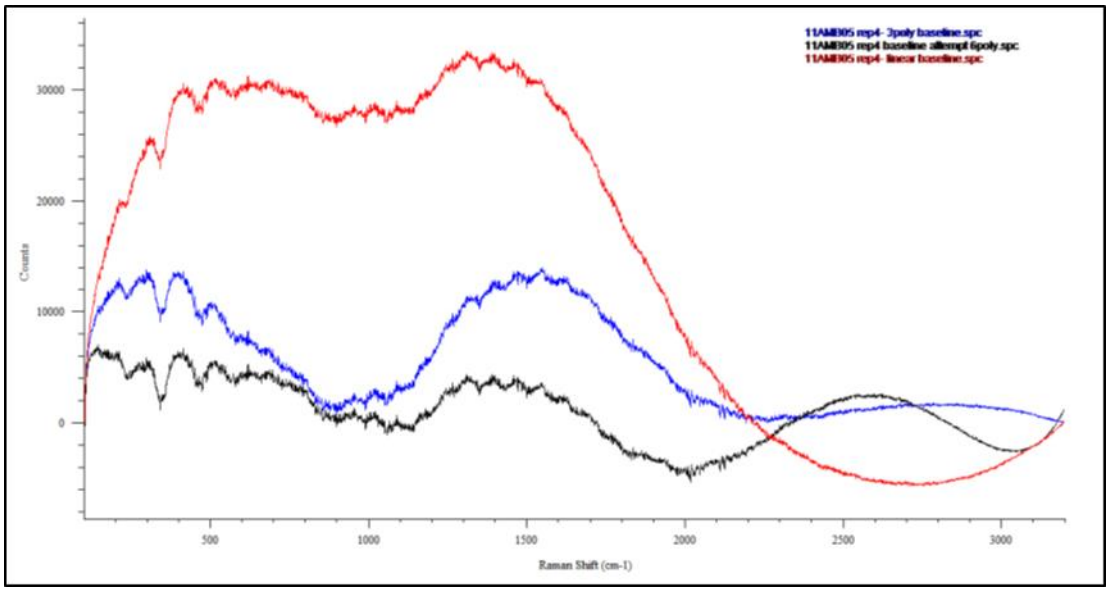

Figure 14: Baseline attempts using a linear baseline (red), cubic (blue) and sextic (black) fitting schedule

2.3.3 Attempts to overcome difficulties

In addition to previous increases to the accumulations (see ND8A in Figure 13) and creating a slightly thicker sample by concentrating the sample in a smaller area, some other options were investigated in an attempt to increase the quality of the Raman spectra. Photo-bleaching prior to signal collection and utilising alternative mounting substrates (glass slide and a mirrored slide) were attempted. Spectra representative of the results of each of these alterations on the spectra for the sample 11AMB05 are presented in Figure 15 to Figure 17.

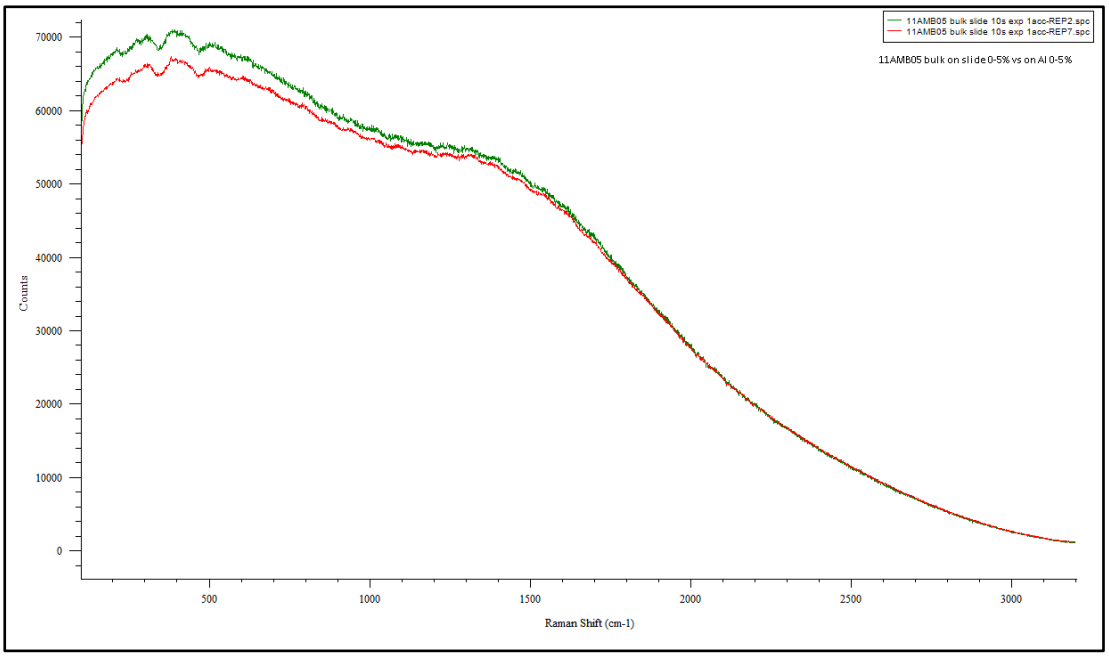

Figure 15: 11AMB05 bulk on glass slide vs same sample on mirrored slide (green)

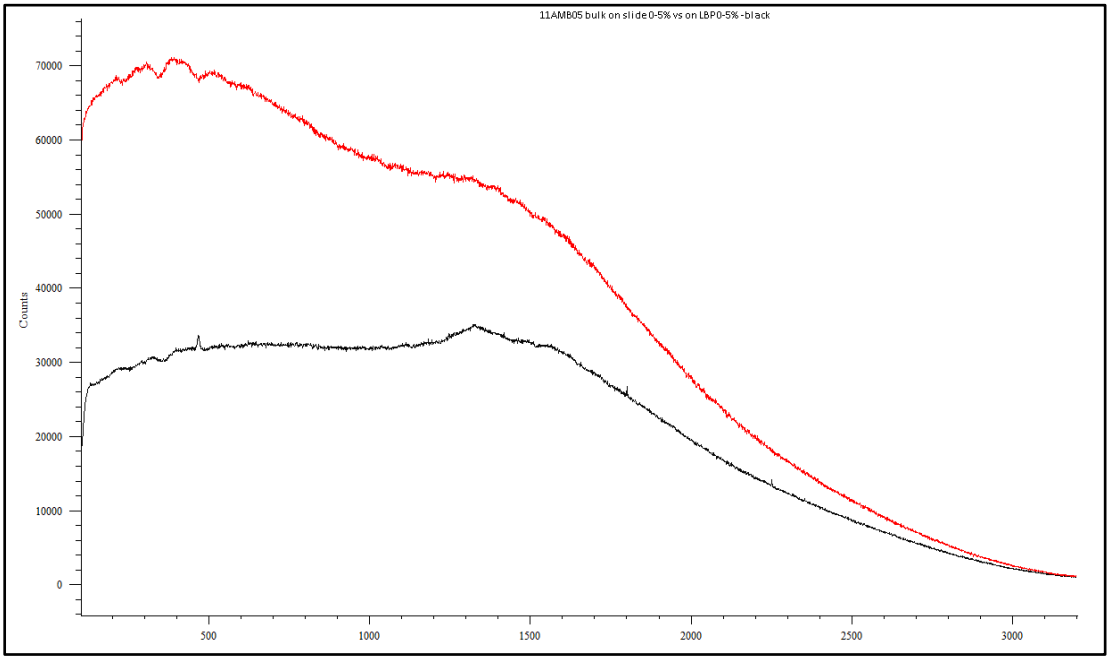

Figure 16: 11AMB05 bulk on a glass slide vs the same sample on the LBP (black) under the same Raman conditions

The move from the LBP to a standard laboratory glass slide again showed an increase in the signal (Figure 16), but only in the amount of fluorescence seen in the 100–1300 cm^{-1} region. It did remove the small peak due to the LBP however. It was theorised that the use of a 'bulk' sample on a mirrored surface may assist in maximising the interaction volume and possibly improve the quality of the spectra; however, as seen in Figure 15, it only resulted in slightly higher fluorescence in the

sample. It is possible that a sample showing no fluorescence would show improvement with the use of the mirrored surface. However, given that all the samples tested showed some level of fluorescence this was not explored further.

Experiments involving photo-bleaching are presented in Figure 17. Photo-bleaching is the exposure of the sample to the laser radiation for an initial time, prior to the start of the collection of the Raman-shifted radiation. The theory is that the fluorescence may be 'quenched' or bleached out, thereby reducing the impact of fluorescence on the quality of the resulting spectra (117). Photo-bleaching for 15 seconds and 20 seconds resulted in a reduction in fluorescence, hence allowing the use of increased laser power, from 0.5% through 1% to 5% for the same amount of exposure time and accumulations. However, the resulting spectra still only showed broad humps, unresolved peaks, with the detector maxing out on the 5% laser power as shown by the sudden drop in signal in the red line. Additionally, this photo-bleaching may cause alteration to those minerals, such as goethite, which are sensitive to laser radiation. Hence, the reduction in fluorescence may also be artificial caused by the unwanted mineral transformations.

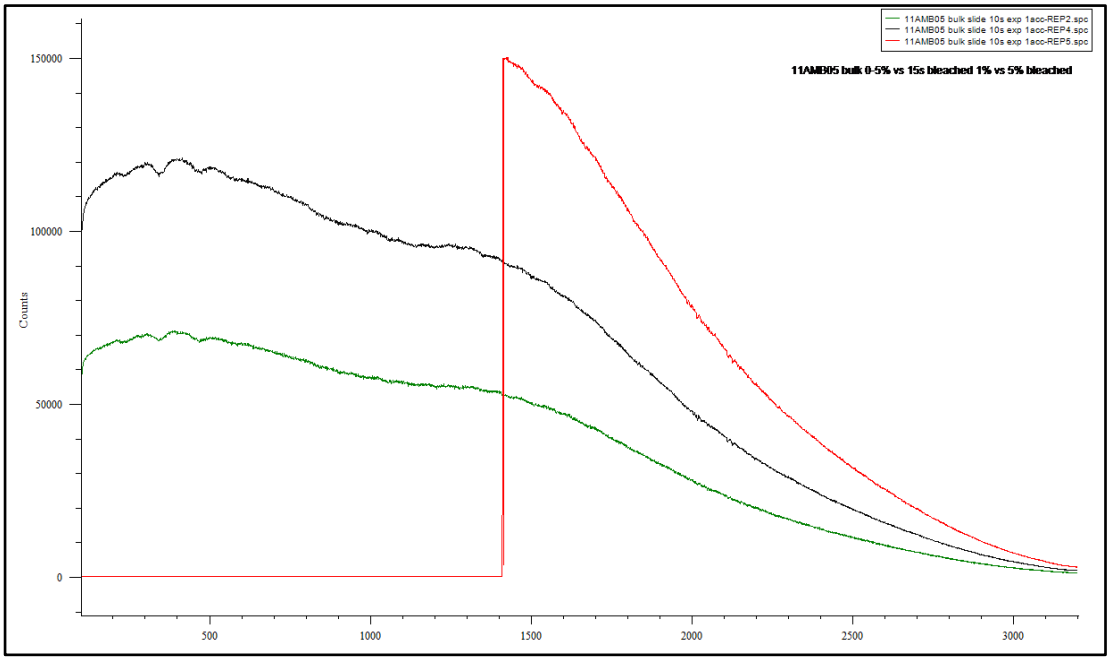

Figure 17: 11AMB05 Raman spectra with photo-bleaching and increasing laser power (green: 10sec exposure, 1 accumulation 0.5% laser, black: as previous but 1% and 15 sec photo-bleaching, red: as initial but 5% and 20 sec photo-bleaching)

Finally, further attempts to utilise the 785 nm Raman microscope focused on higher Raman wavenumber shifts, specifically for kaolinite around 3600 cm^{-1}. To investigate whether kaolinite could be detected a spectrum was collected from a sample with kaolinite in levels detectable by XRPD. This sample, SA5, was then mounted on a glass slide, pressed flat and analysed. The resulting spectrum (presented in Figure 18) again showed strong fluorescence but did not show any peaks characteristic of kaolinite, even at a scan of 3000–3800 cm^{-1}, with a 10-fold increase in laser power.

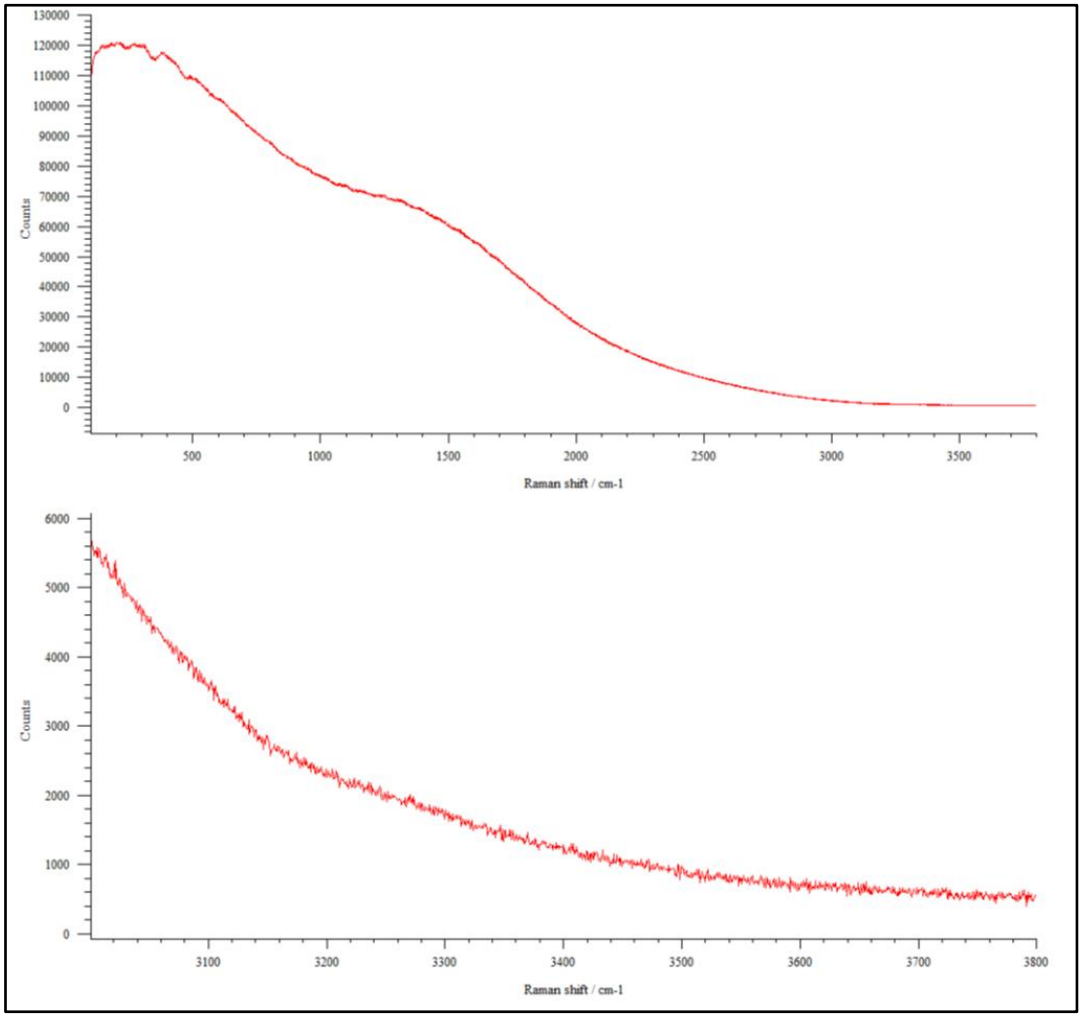

Figure 18 from top: SA5 extended scan 100-3800 cm^{-1}, [0.5% laser power, 10s exposure, 2 accumulations,15 seconds photo-bleaching] and repeated scan 3000-3800 cm^{-1} [5%, 10s exposure, 2 accumulations,15 seconds photo-bleaching]

2.4 Conclusion

The usefulness of Raman spectroscopy is complicated by the significant fluorescence of most samples. This severely affected the quality of the spectra, to a point where the use of the 785 nm wavelength Raman spectrometer for bulk screening and additional characterisation of the quartz fine fraction for forensic comparisons of sandy soils was ruled out. Work focussing on the use of different excitation laser wavelengths, which may reduce or remove the fluorescence problem, as well as the exploration of surface-enhanced Raman spectroscopy (SERS) is recommended. However, due to the limitations of the instrumentation at ChemCentre, the use of Raman spectroscopy to analyse the quartz fine fraction was discontinued and further project work focussed on the use and further characterisation of the quartz fine fraction using XRD and Synchrotron XRPD with a multivariate approach.

Chapter 3. Analysis of the Quartz Fine Fraction by Lab-based XRPD

3.1 Introduction

As introduced in Chapter 1, X-ray diffraction, specifically X-ray powder diffraction (XRD/XRPD), is a valuable technique for the characterisation of soils and minerals. The patterns created by the diffraction of an incident X-ray beam allow for the identification of the crystalline mineral form of a combination of elements, as compared to an inference of identity based on relative elemental concentrations as with SEM-EDS, for example. XRD has been used within ChemCentre for almost 3 decades, the data obtained from samples analysed during this time, therefore, represents a valuable resource (108). This chapter utilises the database of fine fraction coating mineralogy, the associated geological categories and multivariate statistics to explore structure within the data and identify whether mineralogical differences exist between the different geological categories, and whether these differences can be exploited for forensic purposes.

3.1.1 Theory of XRPD

When exposed to a monochromatic source, like an X-ray beam, a single crystal produces diffraction maxima according to the Bragg relationship:

$$n\lambda = 2d \sin\theta$$

where λ= incident wavelength, *d*= lattice spacing and θ is the resulting angle of diffraction (129) (which is also equal to the angle of incidence, hence the phenomenon is referred to as “reflection”).

If the crystal is rotated in all directions about the axis of the beam, a theoretical ‘cone’ of diffracted rays is generated. If the single crystal is then ground to a powder of randomly orientated grains, each grain acts as a diffraction source. With a fine enough powder, a sample in which all statistical increments of rotation relative to the incident beam is created. This theoretically then generates diffraction cones

representing all lattice orientations and rotations. These cones can subsequently be detected and recorded, and form the basis for all XRPD instruments (129).

As detailed, the diffractions are directly related to the lattice spacings and, as such, are characteristic of the organisation of the atoms within the minerals. This makes XRPD capable of polymorph differentiation, as the same atoms arranged differently will create different diffractions. Additionally, subtle differences within minerals, such as isomorphic elemental substitutions, will alter the diffractions, allowing for inference of compositional differences.

3.1.2 Use of XRPD for Differentiation in Swan Coastal Plain Soils

Developed in-house at ChemCentre, XRPD of the coating collected from quartz sand grains is used for the differentiation of soils with high quartz content, typical of the highly leached sands of the Swan Coastal Plain (108). The technique, discussed in the previous chapter, uses the primary and secondary minerals present as a coating on the quartz grains within a soil. These minerals, presented in Table 2, are likely formed *in-situ* on the heavily re-worked quartz grains and add another layer of differentiation in the soil comparison protocol discussed in The “Standard” Method in Chapter 1.4.1.1. The calculation of these percentage intensities is undertaken using the counts for each mineral, divided by either the ‘subtotal counts’ (the counts for that designated “sub” within the table) or the ‘total counts’ (the counts for all 8 mineral reflections used), expressed as a percentage. The final row within Table 2 shows the formula used for each.

In the method currently used (108), and detailed in Chapter 2 Section 2.2.1, the quartz grains are hand-picked from a sample that has already undergone bulk characterisation (i.e. colour, bulk mineralogy using optical microscopy and possibly particle size distributions). The coatings, hereafter referred to as the “quartz fine fraction” or “<20µm fraction”, are isolated and analysed using XRPD. Comparisons are made using on a screening software program [Automated Powder Diffraction for a Philips Analytical PW1820] to ‘narrow down’ those samples most similar, based on a ‘fuzzy-logic’ algorithm utilising the counts of the minerals as calculated percentage intensities (% intensity) (108). Once first pass comparisons have been

performed using this software, more detailed comparisons are performed using the entire XRD pattern of the sample. Illite is integrated within the 'mica' counts. Additional minerals such as calcite, aragonite, magnesian-calcite, hematite, chlorite, anatase and boehmite may also be present within the soils, but due to the possibility of contamination, low overall percentages or overlaps with other minerals, are not utilised as initial minerals.

Table 2: Angle and d-spacing for each of the minerals utilised for the characterisation of the quartz fine fraction using the Co Kα radiation source of the ChemCentre XRD.

Co Radiation [hkl]	vermiculite [002]	kaolinite (basal) [001]	gibbsite [002]	kaolinite2 (non-basal) [020]	goethite [110]	mica [001]	quartz [101]	microcline feldspar [220]
Reference	V1	K1	G1	K2	g1	M1	Q1	F1
angle (°2θ)	7.25	14.35	21.37	23.2	24.95	10.4	31.05	32.1
d-spacing (Å)	14.15	7.16	4.83	4.44	4.14	9.87	3.337	3.24
	Sub-total counts (Sub)					Total counts (*Total*)		
% intensity	$\frac{V1}{Sub}\%$	$\frac{K1}{Sub}\%$	$\frac{G1}{Sub}\%$	$\frac{K2}{Sub}\%$	$\frac{g1}{Sub}\%$	$\frac{M1}{Total}\%$	$\frac{Q1}{Total}\%$	$\frac{F1}{Total}\%$

3.1.3 Advancement of the technique using Multivariate Statistics

This project utilised decades of data, held as an in-house dataset, of the XRPD patterns of <20 µm fractions from 202 samples of soils from across the Swan Coastal Plain and other areas of forensic interest in Western Australia. These samples were grouped based on approximate geological origin (i.e. Spearwood, Bassendean, Quindalup, Alluvial/Lateritic, mixed origin or Coastal Limestone) and their percentage intensities calculated from the original XRPD patterns. Mixed origin soils showed visible mixing, such as urban modified soils. This created a 'database' of normalised percentages for examination using multivariate analysis. This part of the project aimed to examine the possibility of a more objective comparison method using more contemporary methodology and to examine the

ability to differentiate the origin of the samples according to its fine fraction mineralogy using a large number of samples.

3.1.3.1 Principal Component Analysis (PCA)

The use of multivariate statistics allows for the visualisation of relationships and patterns within large datasets with large numbers of variables. Principal Component Analysis (PCA) is probably the most widely used multivariate technique and is well suited to spectra or chromatograms (130). PCA reduces the dimensionality of data sets by transforming original variables into their related orthogonal variables, referred to as principal components (or PCs) (130, 131), such that the first PC aligns with the direction that captures the greatest variance of the dataset. Subsequent PC's are calculated to then describe the maximum remaining variance proportions. Finally, projection of the samples onto the components allows the dataset to be described using the PCs instead of the original variables. Hence, the number of PCs is fewer than the number of original variables, and the majority of the information regarding trends or relationships is retained within the first few PCs.

There are two common algorithms used in the calculation of PCs; the Singular Value Decomposition (SVD) and the non-linear iterative partial least squares (NIPALS) algorithms. The SVD algorithm is non-iterative and is faster than NIPALS where data contain a small number of variables or a large number of samples, (or vice-versa). In comparison, NIPALS is useful for datasets containing missing values or where both the number of samples and the number of variables are large. In this thesis, where possible both were tested, but other than minor appearance changes, both seemed appropriate for use, as neither variable or sample numbers were excessive.

PCA is considered an unsupervised technique, requiring no assignment of classes from the analyser, in contrast with some other multivariate techniques, such as discriminant analysis (DA). Visual examination of a PCA is most commonly undertaken by examining the scores plot (a graphical representation of the scores matrix of the samples relative to the new PCs). Plotting samples on a scores plot based on the first few PCs will illustrate relationships, as samples with similar characteristics will have similar scores and hence form clusters within the larger

data sets, differentiated from those with dissimilar scores related to the variables measured in that PCA. An example of this separation is shown in Figure 21.

Additional information may be obtained by examining the loadings plot. The factor loadings are plotted for each variable — in the case of this thesis that is the mineral reflection counts or percentage intensities. The cosines of the angle between the PC and variable are represented by the factor loadings. If positive, the correlation between the PC and the variable is positive and vice versa. If the cosine is near zero there is no correlation (132). Hence, by examining the factor loadings illustrating the weighting of a variable against a particular PC, the basis for the separations seen within the scores plot can be examined.

Finally, a scree plot visualises the cumulative percentage variation explained by each subsequent PC. This allows for the appropriate number of PCs to be retained. PCs that are important to the explanation of variance and hence the relationships within the dataset will have larger eigenvalues (sum of squares of each PC or score). Scree plots (or tables) present the eigenvalues related to the cumulative variance and hence illustrate the relative 'gain' for the use of that PC in modelling the data. Retaining extraneous PCs may result in the model examining the noise or random variance, whereas if too few PCs are retained information capable of further data differentiation may be lost.

3.2 Experimental

3.2.1 Data Acquisition

The data for this examination represent an 'in-house' database of the percentage intensities for each of the minerals detailed above (108). Some of the samples were collected in the course of this project and are marked with a double asterisk (**) where appropriate. The complete table of all raw counts and percentage intensities is presented in Appendix A

X-ray diffraction analysis of all samples was carried out under laboratory conditions using a Philips Analytical PW1820 automatic powder diffractometer (APD) with

Bragg-Brentano para-focusing geometry and Co Kα radiation. In most samples, a step size of 0.05° and a counting time of 16 seconds per step was used, with the long, fine focus X-ray tube operated at 40 kV and 30 mA. An irradiated length of 12 mm was maintained by an automatic divergence slit and X-rays were recorded using a sample spinner (2 rps), 0.2 mm receiving slit, 1° anti-scatter slit, post-diffraction graphite monochromator and a xenon gas proportional detector.

Each sample was classified, based on sampling location, into 1 of 7 groups, as detailed in Table 3. These classifications are noted to be broad (and are not all technically "dunes"), with some amount of intra-variability expected, especially for samples from within the Spearwood and Alluvial-Lateritic classes. However, to avoid the need for complicated colouring for visualisations these were deemed fit for purpose and appropriate for classifying a large group of samples from a natural system.

3.2.2 Data pre-treatment

The scans were all checked for angular offset, with either the major quartz diffraction position (31.05° 2θ and 3.337Å *d*-spacing) or LBP peak position (18.95° 2θ, 5.912Å *d*-spacing) used to correct the patterns. The patterns were semi-automatic background corrected and the net intensity of each mineral's representative peak recorded. In the case of kaolinite, both the basal (K1; 001) and non-basal (K2; 020) reflections were used to capture any preferred orientation effects, as well as the contribution from possible halloysite, which may preferentially enhance the observed kaolinite non-basal peak. It is acknowledged that halloysite is uncommon in Australian soils and it was not confirmed in any samples using XRD diagnostic tests. These results were entered into Microsoft Excel for calculating the percentage intensities as previously discussed.

Table 3: Dune Groups [based on Physiographic Regions as per Figure 9] and General Descriptions

Group Name	Brief Description
Quindalup System	Samples from sites within the Quindalup dune system
Quindalup-Spearwood	Samples from sites in 'older' Quindalup or 'younger' Spearwood, where the two are mixed, with expected 'typical' characteristics also showing intermingling.
Spearwood	Samples from sites within the Spearwood dune system
Bassendean	Samples from sites within the Bassendean dune system
Coastal Limestone	Samples from sites with noticeable coastal limestone outcroppings, some of which are outside the Perth metropolitan area.
Alluvial-Lateritic	Samples from sites that are noticeably dominated by alluvial deposits, such as river sediments, or the lateritic sites from the Darling scarp. These sites are limited in number and some are outside the Perth metropolitan area, so have been grouped even though they represent different deposition and geological events.
Mixed Origin	Samples from sites with a noticeable mixed appearance, predominantly urban in origin, and with strong bioturbation or human interference.

3.2.3 Multivariate Analysis

Multivariate analysis was undertaken on the percentage intensities calculated from the background-corrected counts for each of the minerals detailed. This was undertaken by importing the counts and the corresponding percentage intensities

data from 202 samples into Camo Unscrambler®. Investigation using principal component analysis (PCA) (see Section 3.1.3.1) was undertaken to reduce the dimensionality and examine the variance within the data.

3.3 Results and Discussion

3.3.1 Initial XRPD Pattern Observations

'Typical' XRPD patterns from the quartz fine fraction of soil samples of the Bassendean, Spearwood and Quindalup dunes show similar mineralogy (Figure 19). Whilst there is variation seen between the samples from within the one dune system, there are typical trends that are noticeable. Firstly, the heavily leached nature of the Bassendean sands (SA6B) is visible in the very low levels of minerals other than quartz. The Spearwood sample (SB4) has more varied mineralogy. Additionally, chlorite may be present as seen by its (002) reflection as a small shoulder to the lower angle kaolinite K2 peak. Finally, the sample representing the youngest soils, the Quindalup sample (SWB3), contains detectable levels of calcite, aragonite and magnesian-calcite typical of a diagenetically unaltered, limestone-based soil.

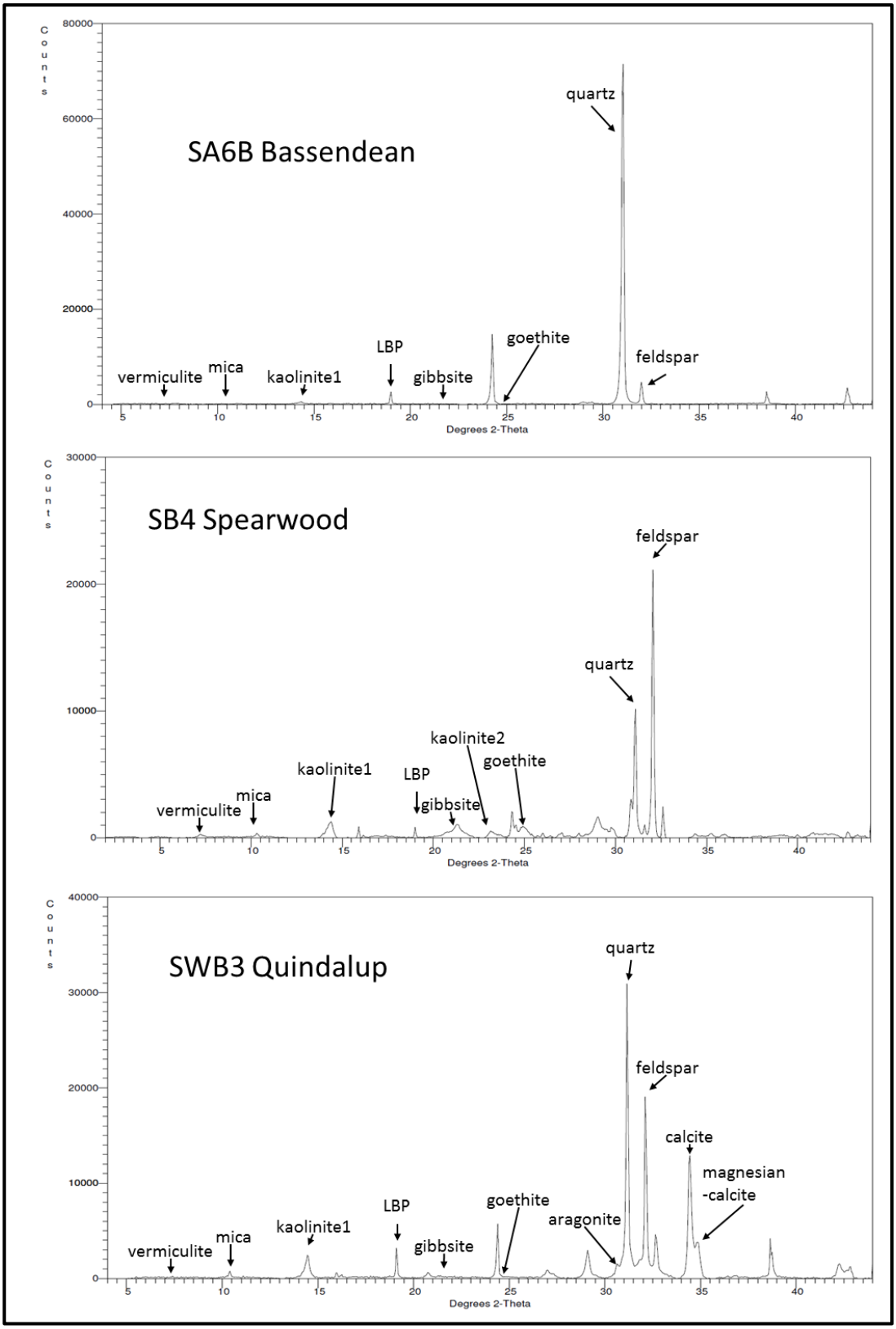

Figure 19 (from top): Examples of the quartz fine fraction XRPD patterns from Bassendean, Spearwood and Quindalup soils, with the mineral peaks marked.

3.3.2 Overall Multivariate Examinations

The background-corrected counts for each of the 8 reflections (representing 7 minerals) listed in Table 2, as well as the corresponding calculated percentage intensities, were imported into Camo Unscrambler® for the multivariate examination (see Appendix A for raw counts and calculated percentage intensities as imported). The zero values were retained in all cases, as they are considered significant since the absence (or presence below the detection limit) of a mineral is as important as its presence. The data were mean centred, as PCA can only be interpreted as the single value decomposition of a data matrix when columns have been mean centred. Additionally, the factor loadings and at least a 2-dimensional plot of the scores of the PCs were used, grouped by overall 'dune classifications' as presented in Table 3: Dune Groups [based on Physiographic Regions as per Figure 9] and General Descriptions

It is also acknowledged that a 'leave-one-out' cross-validation may lead to overestimations of the strength of the classification model (130, 133). However, the use of an external validation set was not possible as the database is made of predominantly samples representing single sites.

3.3.2.1 "Counts only" visualisation

As a first pass examination of the data, a principal component analysis was undertaken on the raw counts data, with 'random' cross-validation of 20 segments, mean-centred and using 0.000 for zero values. A singular value decomposition (SVD) algorithm was used for the analysis, with no rotation method and a maximum of 8 components allowed.

Presented in Figure 20 is a plot of the first 2 PCs, their associated loadings, and a scree table of the "counts only" data set. As shown on the scores and scree plots, the first 2 PCs account for 99% of the variance within the dataset. However, the data do not show significant clustering nor strong differentiation between the majority of the samples. Upon examination of the factor loadings, it was noted that the majority of the influence arises from the counts of quartz (Q1) and the

microcline feldspar (F1). This is unsurprising, as they are the dominant minerals present in all samples and have strong reflections at the points measured.

3.3.2.2 PCA modelling using the percentage intensities

It was obvious from the dominance of the model by the quartz and feldspar counts that some form of normalisation was required. Hence, the percentage intensities were subsequently used. A singular value decomposition (SVD) algorithm was used for the analysis, with no rotation method and a maximum of 8 components allowed.

Presented in Figure 21 are the 3-D plots of the first 3 PCs, and their associated loadings, for the percentage intensities of the 7 minerals within the data set. The loadings for each of the 8 reflections relative to the 8 PC's (the maximum number of possible PC's) and the cumulative percentages of total variance, (that are commonly presented in a scree plot) are presented in Table 4. As per the 'counts only' PCA, the first 3 PC's account for the majority of the total variance, 88% in total.

Upon examination the scores plot of the samples within Figure 21 (and presented in Appendix B), there are a few interpretations that may be made. Firstly, there are no distinct, far-separated clusters of points, with a large amount of overlap between dune classifications. This indicates that the database, as a whole, cannot be used to 'match' a sample to a particular dune system, suggesting that the variation is strongly dependent on local factors, such as topography. The variables used do not separate the dune systems sufficiently to allow for this. Additional minerals such as calcite and aragonite may be beneficial for separation. However, as mentioned in Chapter 1, Section 1.4.4, the minerals chosen are a mixture of primary and secondary minerals that form *in-situ* and, hence, are less likely to be due to contamination from larger grains. Calcite and aragonite commonly occur in limestone and, hence, are likely to be contaminated by larger fragments present within the soil. However, limestone pebbles are not characteristic of Spearwood or Bassendean soils. The overlaps visible are as expected for a natural system, where there is no hard 'edge' but more of a gradual shift of characteristics from one system to another.

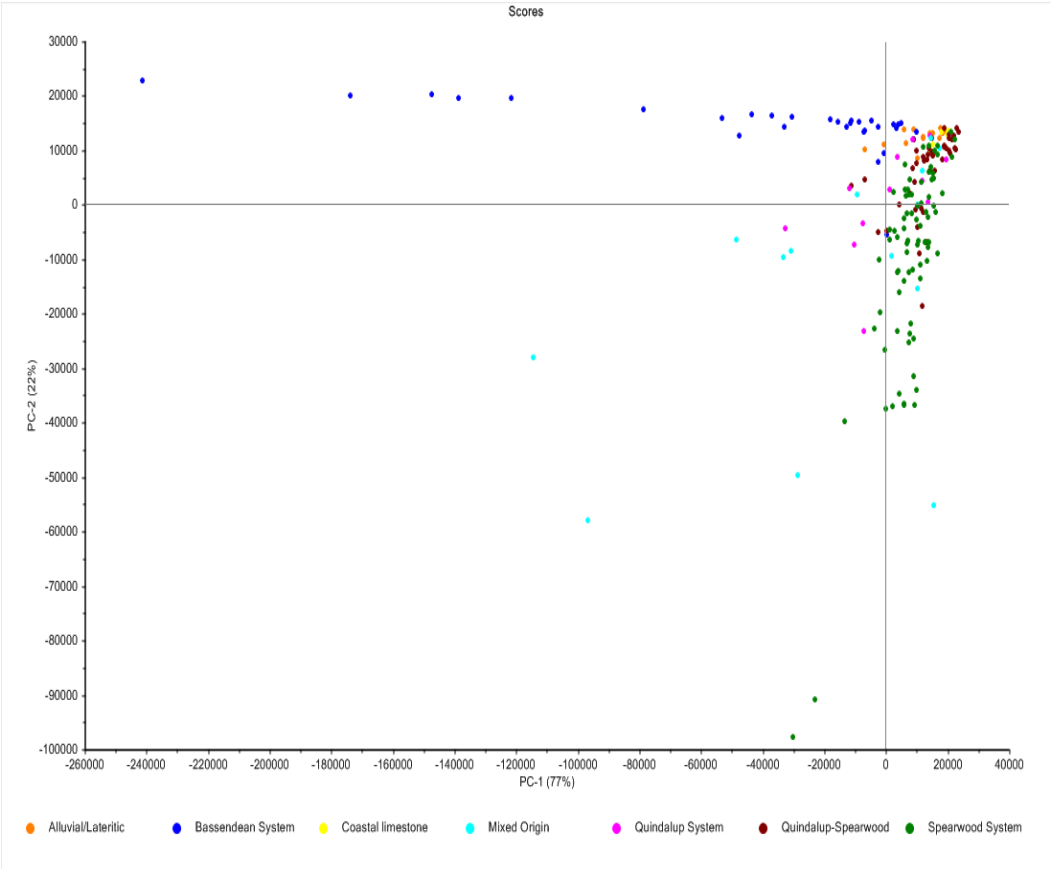

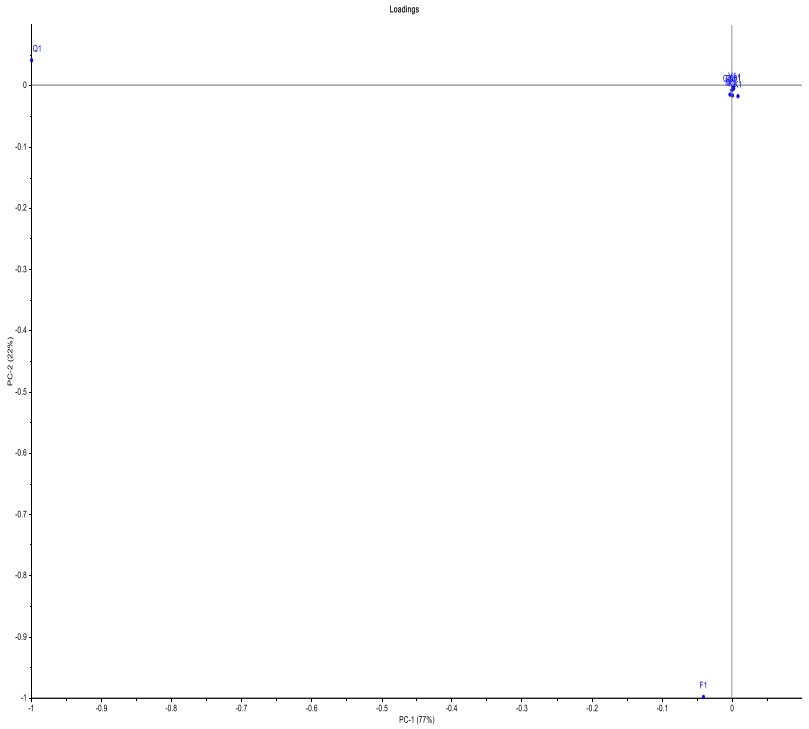

	PC1	PC2	PC3	PC4	PC5	PC6	PC7	PC8
Explained Total variance	76.503	98.745	99.844	99.916	99.961	99.991	99.997	100

Figure 20: PCA scores plot, loadings plot and scree table of the 'counts only' of the 8 reflections traditionally used for all 202 samples in the database

Table 4: Loadings and cumulative total variance percentages of the 8 PCs within the PCA of the full Lab XRD database.

	%V1	%K1	%Gibb1	%K2	%goe1	%M1	%Q1	%F1	Cumulative % total variance
PC-1	0.005	0.226	-0.011	-0.127	-0.145	-0.001	0.688	-0.663	55.5
PC-2	-0.008	0.843	-0.283	-0.115	-0.312	0.024	-0.306	0.064	79.7
PC-3	0.208	0.064	-0.153	-0.015	-0.161	-0.074	0.625	0.712	87.8
PC-4	-0.172	0.037	-0.739	0.330	0.548	-0.036	0.091	-0.064	93.9
PC-5	0.768	-0.284	-0.431	-0.217	-0.181	0.029	-0.173	-0.182	96.8
PC-6	-0.175	-0.221	-0.171	0.658	-0.667	0.079	-0.021	-0.076	98.7
PC-7	0.554	0.322	0.367	0.615	0.270	0.033	0.018	-0.050	99.7
PC-8	0.017	-0.001	0.017	0.053	-0.065	-0.992	-0.065	-0.062	100.0

However, closer examination shows some broad separation, such as between the Bassendean and Spearwood samples. By examining the loadings for PC1 and PC2 in Table 4, this separation is based on the strong positive association of the Bassendean samples in terms of the quartz percentages with PC1 and the strong negative association of the Spearwood samples with the feldspar percentages along PC1. Additional separation arises within PC1 and PC2 based on the influence of the K1 percentages, the basal kaolinite reflection. With the addition of PC3, there is also a pull away from the central mass by the alluvial/lateritic samples, visible as the shift downwards on PC3. Again, an examination of the loadings indicates the influence of quartz, vermiculite and feldspar (Q1, V1 and F1).

Upon viewing the cumulative percentage of total variance listed within Table 4, PC4 is noted to account for 6.1% of the variance within the dataset. Figure 22 presents the 3-dimensional plot of PC2, PC3 and PC4, as well as the associated loadings, from the PCA analysis of the Lab-XRD dataset. The Bassendean samples are even further separated from the rest of the dataset with the use of PC4. The alluvial-lateritic samples are also grouped to the right-hand side of the plot, with only a slight overlap with the coastal limestones. Upon examining Table 4 for PC4, gibbsite is positively associated with PC4 and goethite negatively, with both having the greatest loadings for this component.

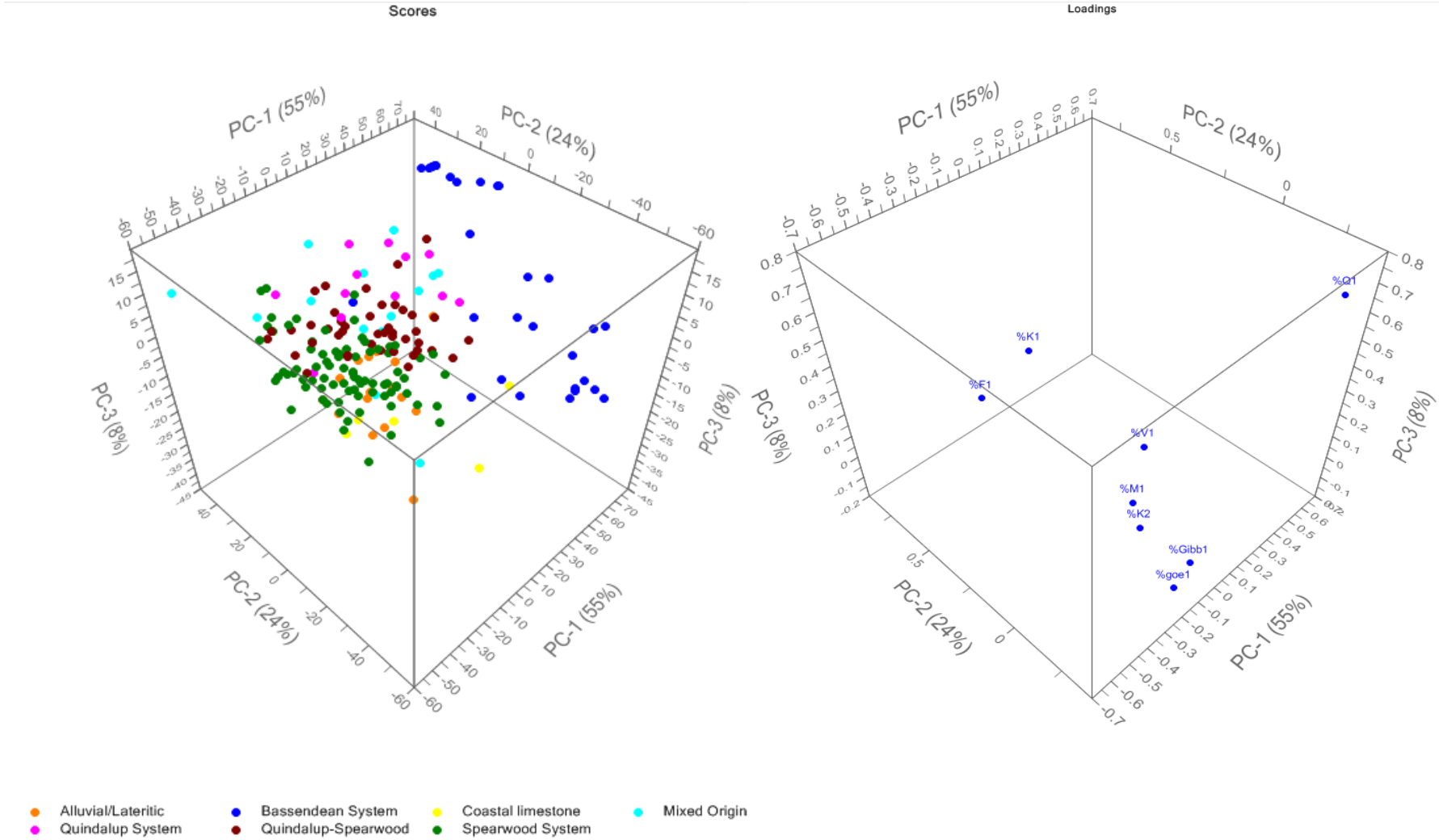

Figure 21: 3-D plots of first 3 PCs scores and loadings of the full database percentage intensities. Data is grouped according to dune classification.

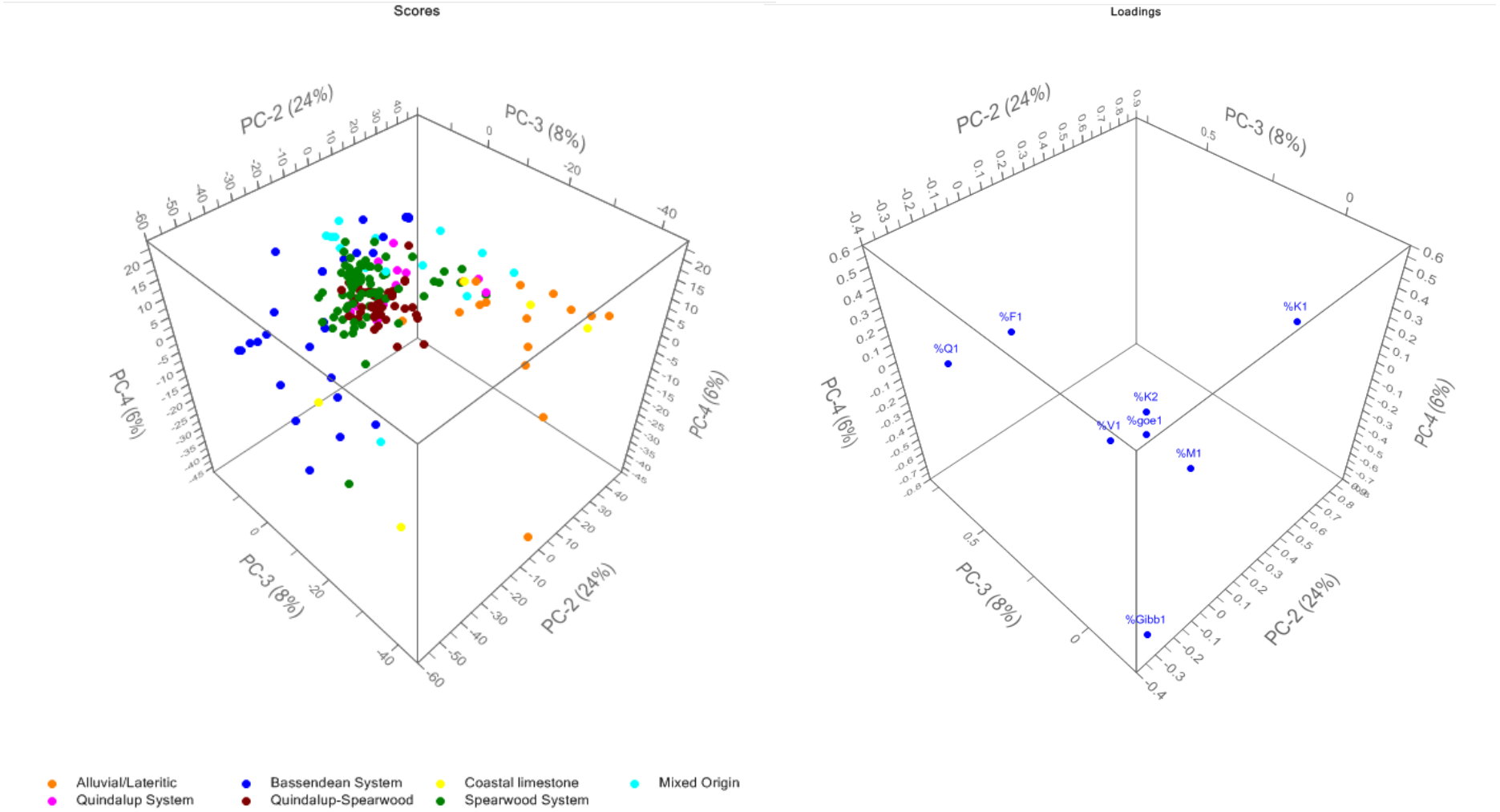

Figure 22: 3-D plot of PC2, PC3 and PC4 from the same dataset as Figure 21.

The combination of PCs 5, 6, 7 and 8 accounts for just over 6% of the explained variance of the dataset. Examination of the scores plots of these, presented in Figure 23, shows no groupings but the start of individualisation, with sites NE3, SB5, ND8 and WEMB100 being on the extremities of the scores plots. Examination of Table 4 shows the correlation of PC5 with vermiculite and gibbsite, PC6 with the non-basal kaolinite (K2) and goethite and PC7 with vermiculite, kaolinites and gibbsite.

Examination of the PC-8 scores table for the PCA analysis of this dataset (presented in Appendix B) shows just 1 sample with a high score against the highly negatively correlated mica loading (-0.992). This sample, 0F25084R, is noted to be highly abundant in mica, and is detailed as "D4 Donnybrook sandstone", included as an alluvial-lateritic sample due to its 'non-metro location' and nearness to the 'quartz-feldspar-biotite gneiss' of 0F25083R. An investigation into the provenance of this sample from case records (confidential), indicated that this sample was a pale greyish-brown loamy sand, taken from a site mid-way between a creek and the western area of a dam, on 'Donnybrook sandstone' geology.

It appears from the examination of the PCs 5–8, that these components are more influenced by intra-dune variability, with large overlaps between groups and individual sites being isolated in the scores plot. Whilst not useful for a 'database matching'-type situation, this shows that these minerals still prove useful for direct questioned versus known comparisons, where individual sites are being compared to determine if one site is more likely to be the source of a questioned sample than another.

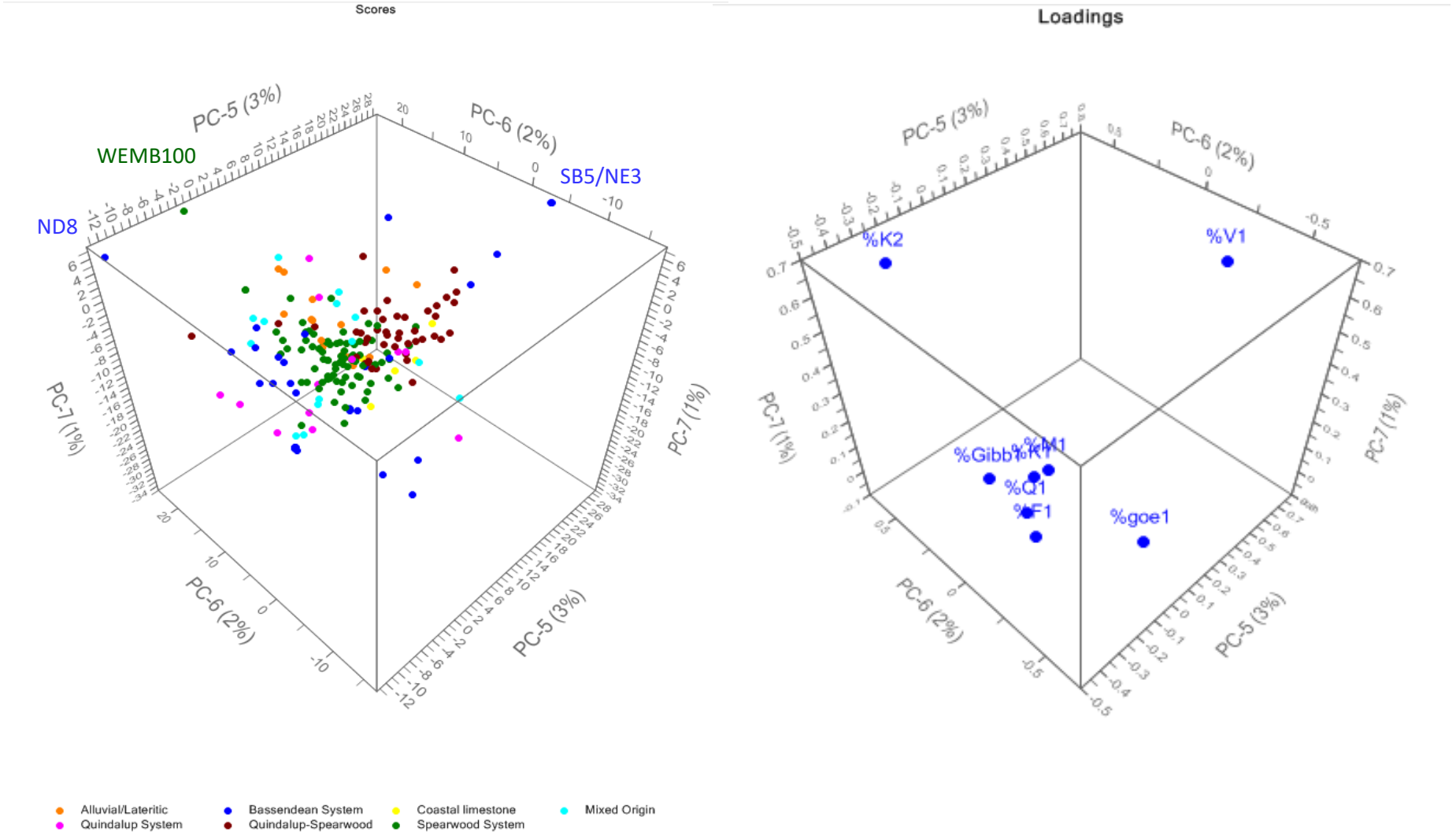

Figure 23: Scores and loadings of PCs 5, 6, and 7 from the same PCA as Figure 21, with samples ND8, WEMB100 and SB5/NE3 indicated

3.3.3 Within Classification Comparisons

Previously, the entire dataset was examined using PCA. This analysis, based on the 202 samples of recovered quartz fine fraction, showed some differentiation, but not strong clustering. To examine the relationships between samples from within the one classification, as well as determine the feasibility of 'site to site' questioned versus known comparisons, PCA visualisation was undertaken on the two largest groups– the Bassendean sands and the Spearwood samples.

3.3.3.1 Bassendean Sands

All samples designated as "Bassendean" within the original dataset were subjected to another PCA, and again the singular value decomposition (SVD) algorithm was used for the analysis, with no rotation method and a maximum of 8 components allowed. Figure 24 presents the scores and loadings plots of the first 3 PCs from this PCA, and Table 5 shows the loadings for each of the variables for each of the PCs as well as the cumulative variance percentages. The scores for the Bassendean dataset, with the additional 'site' classification, are detailed in Appendix C.

Table 5: Loadings for each variable, relative to the 8 PCs and the cumulative variance percentage, for the Bassendean Samples when analysed in isolation of the rest of the dataset.

	%V1	%K1	%Gibb1	%K2	%goe1	%M1	%Q1	%F1	Cumulative % total variance
PC-1	0.053	0.881	-0.315	-0.140	-0.295	0.000	0.120	-0.036	66.5
PC-2	-0.266	0.344	0.494	0.154	0.075	0.002	-0.625	0.384	79.1
PC-3	0.516	-0.246	-0.130	-0.124	-0.636	0.001	-0.372	0.313	87.9
PC-4	-0.391	-0.076	0.493	-0.046	-0.668	-0.002	0.235	-0.307	93.3
PC-5	0.712	0.199	0.579	0.095	0.151	-0.001	0.151	-0.253	97.8
PC-6	-0.028	-0.018	0.163	-0.962	0.184	-0.005	-0.107	-0.037	99.8
PC-7	0.002	0.005	0.186	-0.065	-0.001	-0.004	0.606	0.770	100.0
PC-8	0.000	0.000	-0.002	0.005	0.000	-1.000	-0.004	-0.001	100.0

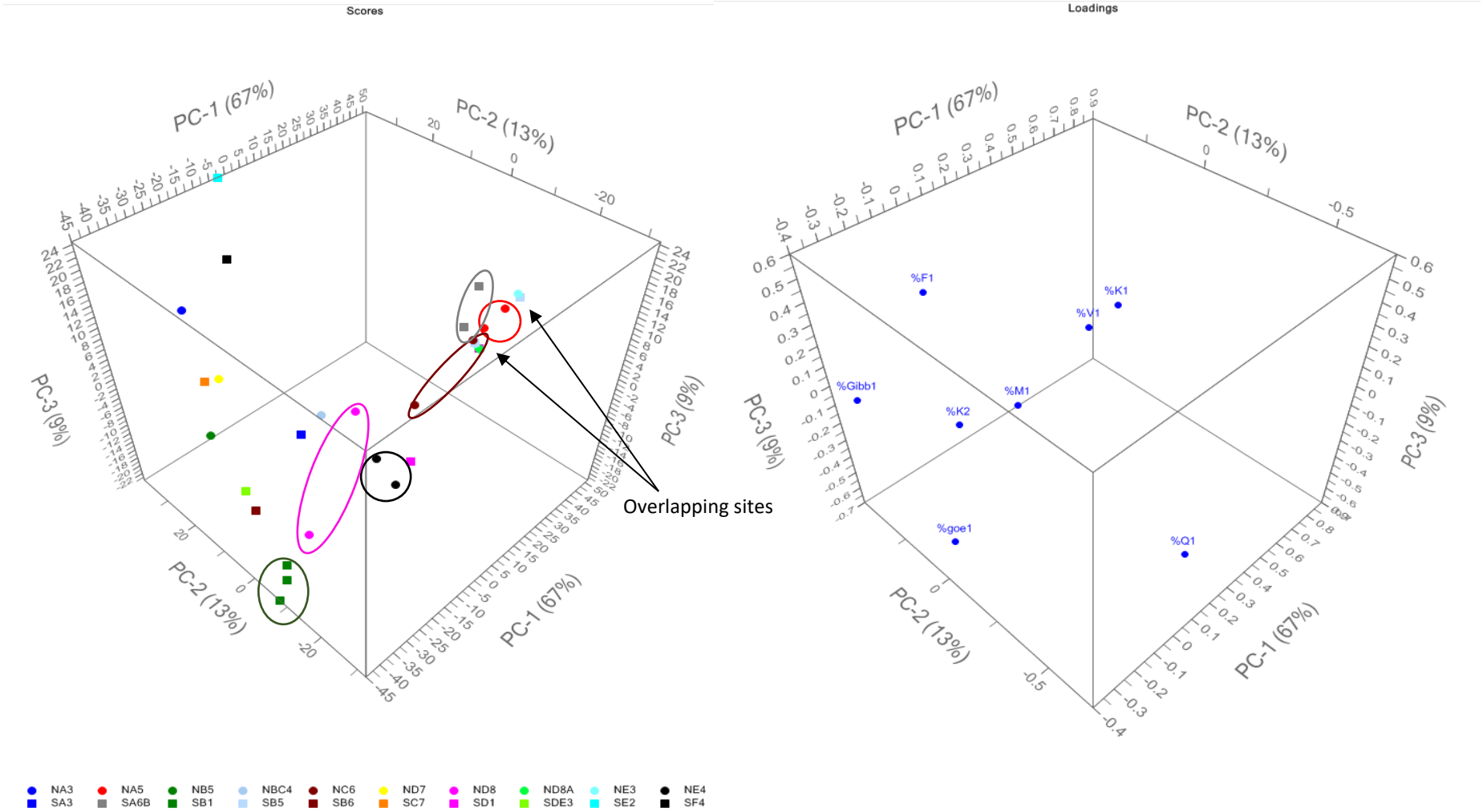

Figure 24: Scores and Loadings plots of PCs 1, 2, and 3 from the PCA analysis of only the sites designated as 'Bassendean' sands. Samples from the same site are marked the same colour and circled.

From within Table 5, it is notable that the first 3 PCs account for almost 88% of the variation within the dataset, and the first 5 PCs being influenced by the relative levels of all the minerals, except mica (M1). It is also noted that the inclusion of PC-6, PC-7 and PC-8 contribute negligibly to the model, with just under 2% attributable to PC-6 and only 0.2% explained variance between PC-7 and PC-8. It is worth mentioning that due to the decimal rounding chosen, PC-7 is presented as 100.0%, but is 99.9997% when the raw loadings data are viewed. Interestingly, it is only at PC-8 that mica (M1) shows any significant loadings, meaning that mica is not of any significance in samples from the Bassendean dune system. This is logical as there is very little present in any of the heavily weathered samples and, hence, most variation would be attributable to noise fluctuations within the very low counts of the muscovite 001 reflection.

When viewing Figure 24, there is a wide distribution of samples, with scores across 7 of the 8 quadrants of the 3D plot. In sites where multiple samples were present within the dataset, there is variable spreading of the replicates, with NE4, NA5 and SB1 showing good clustering, whereas ND8 and SAB6B show a spread that encompasses other sites between their replicates. There are also a small number of sites with almost overlapping loadings, as highlighted in the scores plot using black arrows; a group of samples comprising samples from sites ND8A, NE3, NC6, SB5 and SD1, and another that shows the overlap of the other samples from SB5 and NE3. Examination of the raw counts for each of these sites shows that the first group are those samples where quartz dominates the pattern, with low levels of feldspar, low counts at the kaolinite K1 reflections and all other minerals absent. The second group of 2 samples is similar to the first group, with additional counts for vermiculite. Upon examining the raw counts of these overlapping samples, sample SB520KR from SB5 contains additional mica in comparison to NE3's NE320URX and, hence, these two samples may be differentiated, though the duplicate sample SB520UM from SB5 contains no mica reflection. If this were to occur, additional replicates would be required to establish the significance of the mica.

3.3.3.2 Spearwood Sands

As per the previous examination of Bassendean sites, PCA was undertaken on samples that were designated as “Spearwood” within the original dataset. Presented in Figure 25 is the resulting 3-D plot of the first 3 PCs from this initial analysis (with data presented in Appendix D). One sample is distinctly different from others– it being the only sample in the upper half of the entire scores plot. This sample, from site SA2, shows very high levels of gibbsite when compared to the rest of the samples in the dataset. The original diffraction pattern was consulted, and gibbsite confirmed at levels resulting in a 58.3% percentage intensity for gibbsite. This sample is significantly different from the rest of the samples and easily differentiated.

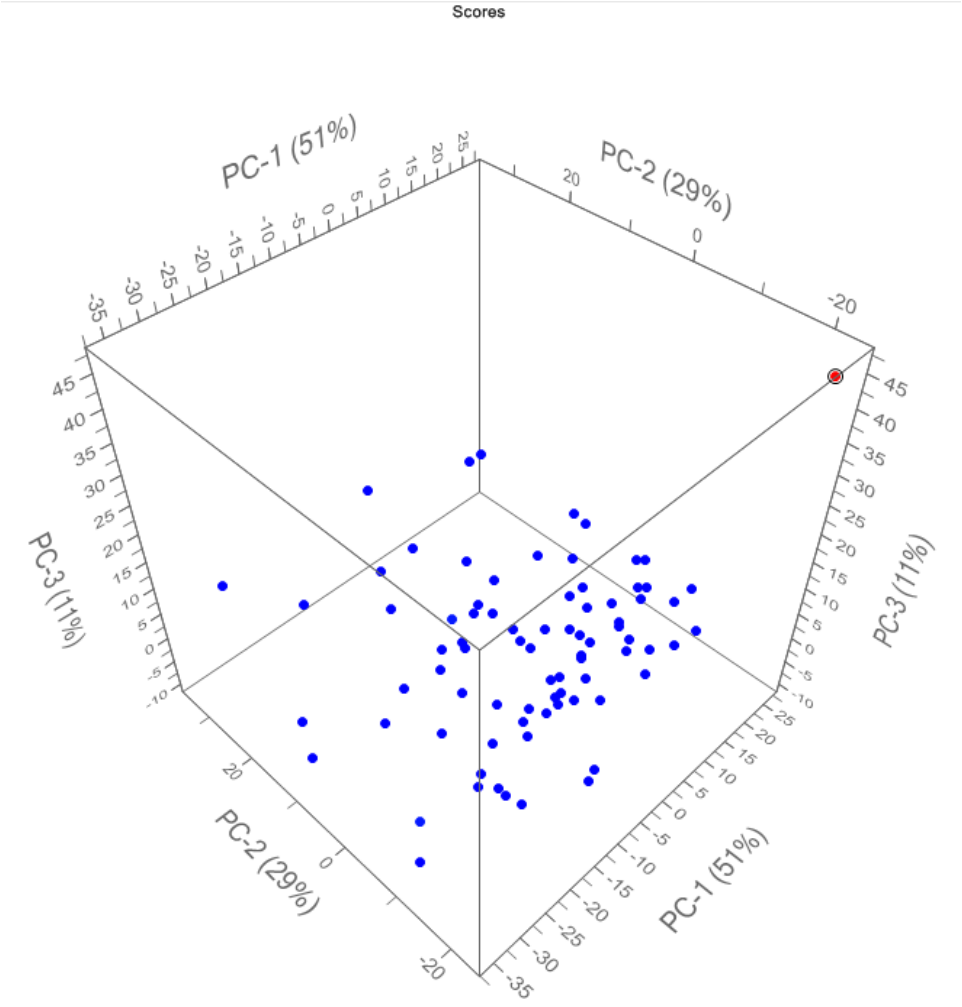

Figure 25: 3-D scores plot of PCs 1–3 of PCA analysis of all Spearwood dune classified samples. Outlier sample SA2 highlighted in red.

Due to SA2's strong influence on the model, it was removed and the PCA analysis repeated. The first 3 resulting PCs scores and loadings are presented in Figure 26. Again, there is one clear grouping of samples separate from the others, shown in red. These samples are 3 replicates from different depths of the same site, designated 'WEMB'. This site is detailed as the 6th Tee at the Wembley golf course, with the three samples from 0.1m, 0.925m and 1.85m depths. Given that this site is curated the sample may be adulterated (although it was believed to be undisturbed), or the location may have a different history such as a lake-bed remnant, explaining its separation from the rest of the dataset.

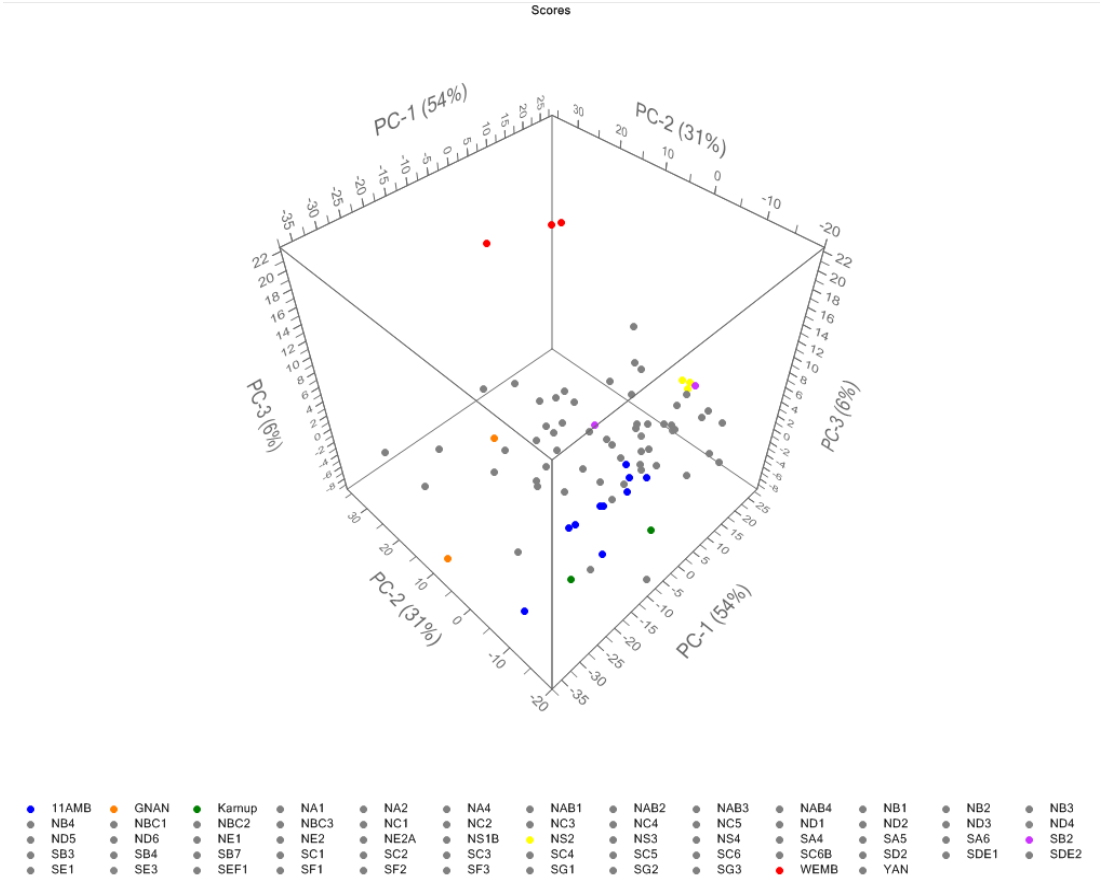

Figure 26: 3-D scores plot of first 3 PCs of repeated PCA analysis of Spearwood classified samples without site SA2. Samples with more than one replicate are coloured, the remaining ones are grey.

Finally, removing the 3 samples from Wembley and re-running the analysis resulted in the PCA scores plot and associated loadings as presented in Figure 27, Figure 28 and Table 6. Again, sites with multiple samples are presented in colours, with single-sample sites coloured grey to highlight the inter-variability of the Spearwood sites, as well as the intra-variability within sites. The replicates in these figures are joined

with lines of the same colour as their designated site, to highlight their spread in the 3-D plots without the need to overlay circles or foreign shapes. The lines only represent the distance between replicates. Whilst not extensively evaluated nor statistically tested, the sites with replicates show an acceptable level of differentiation, except NB2 and SB2 sites (shaded yellow and purple), which have close scores. Upon reviewing the specifics of these sites, one is a cultivated park (NB2), and the other is a natural lake reserve so it is possible that further examination of the samples with other techniques (3, 97) such as analysis of the soil organic matter content would lead to differentiation of these samples.

Site 11AMB comprises multiple replicates from the same soil sample as well as replicates from within the same site. Best illustrated in Figure 27, these samples show a spread of scores, typical of what may be expected with samples from varying depths but show clustering when compared to the rest of the dataset. 11AMB is a site of urban residence, typical of what may be encountered in a Perth backyard and potential crime scene. This clustering illustrates that the technique may be utilised with multiple samples from the same site to show the variation within a crime scene and the essential requirement for appropriate reference/control samples to be collected to allow for proper characterisation of the soil characteristics.

Viewing of the loadings for each of the minerals shows that 92.7% of the variance is explained by the first 3 PCs and, as with the Bassendean analysis, all of the minerals contribute to the variance, with the exception of mica (M1). Most of the influence within the first 2 PCs is dominated by the relative amounts of kaolinite, feldspar and quartz, with lower contributions within PC2 by goethite, gibbsite and the kaolinite K2 reflection.

Upon examination of the large number of sites with only a single sample, it is noted that they also show separation and differentiation from site to site. However, the individualisation of sites is not possible due to the large number of samples and a lack of distinct clustering.

Table 6: Loadings for each of the mineral intensities for each PC and the cumulative percentage of total variance for the PCA of the Spearwood samples after removal of SA2 and Wembley samples.

	%V1	%K1	%Gibb1	%K2	%goe1	%M1	%Q1	%F1	Cumulative % total variance
PC-1	0.041	-0.127	0.008	0.083	-0.005	0.000	-0.545	0.823	58.2
PC-2	-0.032	0.840	-0.224	-0.228	-0.356	0.009	-0.253	-0.013	87.6
PC-3	0.109	-0.032	0.743	-0.292	-0.527	-0.035	0.218	0.153	92.7
PC-4	-0.285	-0.123	0.374	0.002	0.032	0.023	-0.724	-0.488	96.6
PC-5	0.265	-0.005	0.031	-0.808	0.517	0.032	-0.078	0.018	98.5
PC-6	-0.796	0.249	0.238	-0.046	0.355	-0.022	0.244	0.244	99.9
PC-7	0.016	0.000	-0.024	-0.017	0.025	-0.998	-0.035	-0.022	100.0

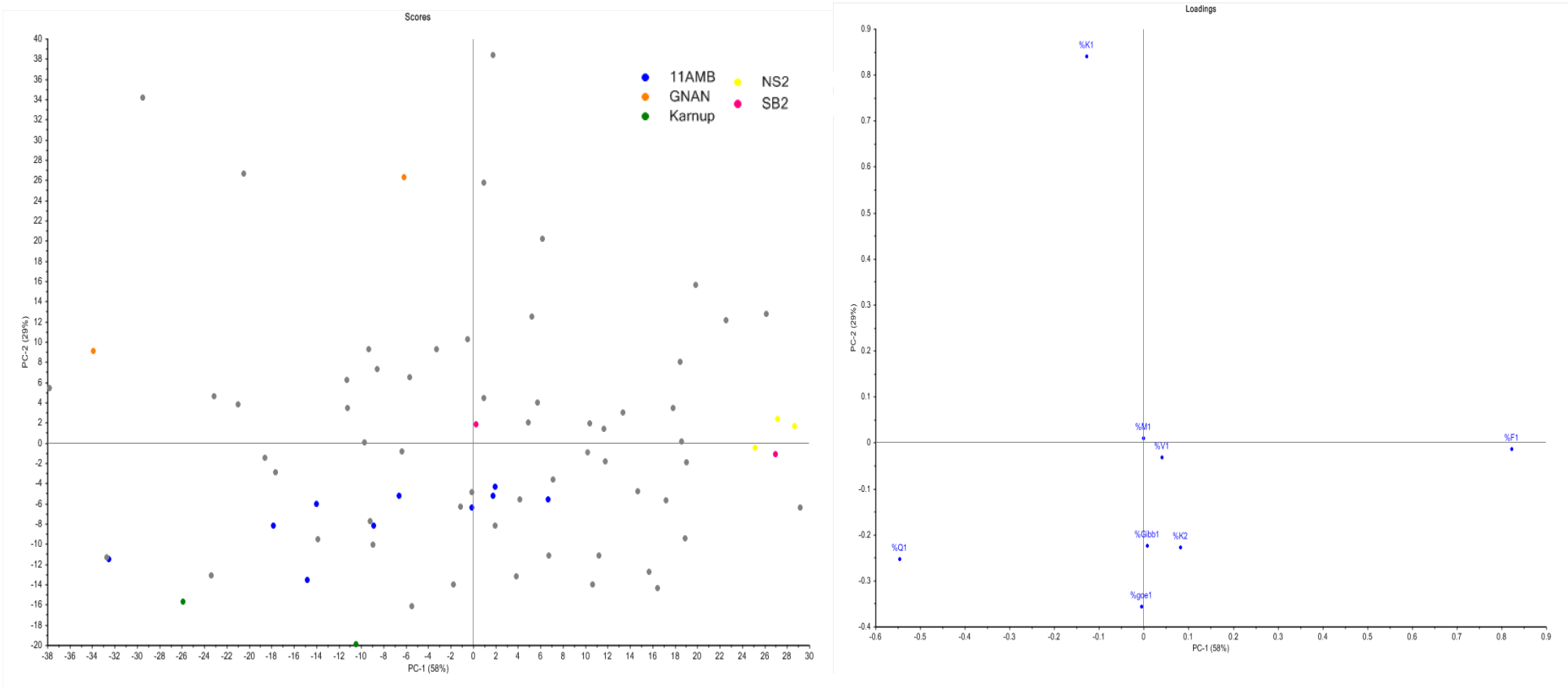

Figure 27: Scores and loadings plot of all Spearwood sample scores, after the removal of SA2 and WEMB samples. 3-D plot of the first 3 PCs and the associated loadings are presented in Figure 28.

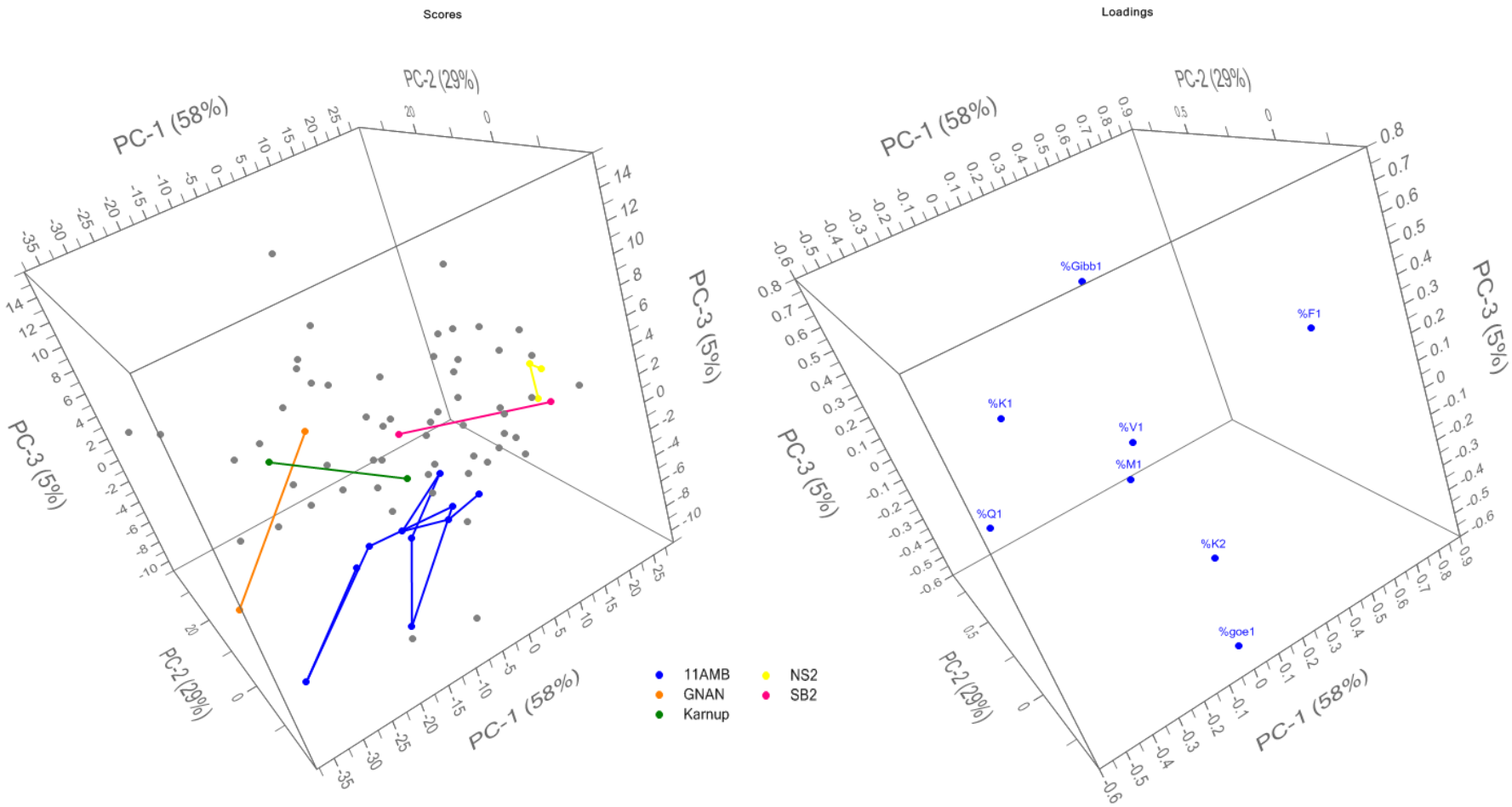

Figure 28: 3-D plot of the first 3 PCs from the analysis of the Spearwood samples, after the removal of SA2 and WEMB samples.

3.4 Conclusion

It has been demonstrated that the technique used traditionally by ChemCentre in the examination of the coatings recovered from quartz grains is amenable to chemometric analysis for the comparison and differentiation of sites from across the Swan Coastal Plain. The use of laboratory-based XRPD is shown to be applicable, appropriate and useful for the forensic comparison of sandy soils. Differentiation is possible within dune systems as leached as the Bassendean sands. However, some overlaps occur and complications may arise with mixed samples, as there are no clear 'clusters' within the data that allow for absolute classification to a particular site and a natural system has shown to be variable in its characteristics.

The 7 primary and secondary minerals have shown to be variable and able to be utilised in the chemometric differentiation of soils; however, further research to investigate the differentiation of sites based on soil mineralogy (mica, kaolinite, feldspar, goethite and gibbsite) is required. To explore the possibility of further differentiation based on varying compositions and effect on crystal lattice parameters of micas, kaolinite, aluminium-substituted goethite and feldspars a technique with more sensitivity and a faster analysis rate is required. Additionally, the examination of the data with the quartz removed may assist in differentiation of sites dominated by quartz, such as the Bassendean samples. Further examinations into the use of other minerals in addition to the 7 utilised in this chapter may also prove fruitful and, hence, techniques that allow for the use of the entire XRPD pattern also warrant investigation.

Chapter 4. Analysis of the Quartz Fine Fraction using Synchrotron Powder Diffraction

4.1 Introduction

In the previous chapters, the examination of the recovered quartz fine fraction was unsuccessful using Raman spectroscopy. However, examination using laboratory-based XRD, followed by multivariate analysis resulted in the differentiation of locations based on the percentage XRD peak intensity of a small number of minerals recovered from the quartz fine fraction. This chapter explores the potential of using the Powder Diffraction Beamline at the Australian Synchrotron to analyse the quartz fine fraction.

4.1.1 What is Synchrotron Radiation?

A synchrotron is a very large cyclic particle accelerator that generates intensely bright, highly collimated beams of electromagnetic radiation (134). These beams can be used as alternative light sources for a multitude of spectroscopic techniques. A schematic of the Australian Synchrotron is presented in Figure 29.

Synchrotrons produce intense beams of 'light' by directing high-energy electrons to travel in a circular orbit by the 'synchronised' application of strong magnetic fields at speeds just under the speed of light. This 'light' represents more than the visible spectrum, it covers all the electromagnetic spectrum. The electrons from the electron gun (1) are linearly accelerated (2) and move into the booster ring (3) for further acceleration before being moved to the storage ring (4). Electrons in the storage ring are deflected by bending magnets and insertion devices such as undulators and wigglers, causing the release of electromagnetic radiation. The intense radiation, in the form of X-rays and infrared light, is filtered using monochromators and channelled as a beamline, where it is used as a bright 'light' source for a suite of scientific instruments in the end station. There are currently 10 operational beamlines at the Australian Synchrotron, including infra-red (IR), X-ray fluorescence microscopy (XFM) and the Powder Diffraction (PD) beamlines (134).

Figure 29: Schematic diagram of the Australian Synchrotron (1) electron gun, (2) "linac" linear accelerator, (3) booster ring, (4) storage ring (5) beamline outlet (6) end station example (from ANSTO, 2020 [134])

Due to its high brightness, stability and highly collimated nature the synchrotron quite often allows for the collection of data not possible by standard laboratory-based instruments (134). This has been used in various applications in forensic science, including the characterisation of automotive paints and other substances (71, 135).

4.1.2 PD Beamline

Similar to standard laboratory based X-ray diffraction (XRD) discussed in Chapter 3, the PD beamline utilises the diffraction of incident X-rays to provide patterns that inform the analyst regarding the d-spacings and crystal lattice structures of crystalline material (136). This beamline allows the study of the crystallographic

structures of materials such as sodium-ion batteries (137), perovskites (138) and micrometeorites (139).

Laboratory-based XRDs are inherently resolution-limited in the d-space range, in the signal-to-noise ratio and the shape and width of observable reflections (136). Synchrotron-based instruments can overcome these issues and give the resolution required to accurate determine structures of complex materials from powder samples. Additionally, PD measurements are possible in 'real-time' for many reactions, allowing observation of chemical changes in these processes.

In the case of this project, the synchrotron was utilised to allow for the collection of rapid, high-quality patterns of the quartz fine fraction. The preliminary work was undertaken to investigate the potential for further discrimination to occur due to the far higher counts of observable patterns, and the possibility that additional minerals may be recognised at usable levels.

4.2 Experimental

4.2.1 Sample Preparation

A total of 44 samples, as listed in Table 7, from only the Bassendean and Spearwood Dune systems, were chosen for analysis on the PD beamline of the Australian Synchrotron. These samples were chosen to represent the 'typical' soils seen in these two dune systems in the Swan Coastal Plain, and as samples had already been analysed on the laboratory-based XRD as detailed in Chapter 3. The two dunes were the focus of the preliminary work as these dunes constitute the majority of the Perth region and are also similar in places and, therefore, represent the most challenging soils to discriminate.

Quartz grains were hand-picked from the samples, with the mass of grains recorded, and the quartz fine fraction recovered as per the method detailed in Chapter 2, Section 2.2.1. However, instead of being mounted on low background plates, the quartz fine fraction was isolated, deposited onto glass slides and allowed to air dry. The air-dried fractions were then lightly ground to break up any clumps

and mounted in 500 µm capillaries, creating a sample of at least 1 cm in length in the capillary tube. The differences in starting quartz grain weights were due to the need to increase the numbers of grains selected for those sites with very low coating levels, to ensure sufficient material was recovered for mounting in the capillaries. However, the mounting of samples to an approximate length, rather than as a measured weight, did not allow for quantitative analysis.

Table 7: Sample names, dune system and suburbs for PD beamline samples

Sample Name	Mass of sand (mg)	Suburb	Dune System
NA1	97	Cottesloe	S*
NA2	115	Peppermint Grove	S
NA3	122	Kensington	B
NA4	102	Dalkeith	S
NA5	516	Welshpool	B
NC1	106	Balcatta Rd	S
NC2	116	Mirrabooka	S
NC3	119	North Balga	S
NC4	104	North Beach	S
NC5	149	Carine	S
NC6	505	Ballajura East	B
NC7	504	Karrinyup	Mixed origin
ND1	119	Mullaloo	S
ND2	126	Eddystone Dr	S
ND3	109	Heathridge	S
ND4	116	Heathridge	S
ND5	139	Wanneroo South	S
ND6	137	Badgerup Rd	S
ND7	98	Gnangara (fine)	B
ND8	245	Gaskell Rd (fill)	B
ND8A	561	Gaskell Rd (silica sand)	B
SA2	53	Beaconsfield	S
SA3	215	Leeming	B
SA4	118	Kardinya	S
SA5	159	Murdoch	S
SA6B	504	Canning Vale	B
SAB1A	92	Westfield	Mixed origin
SB1	214	Jandakot	B
SB2	191	Yangebup	S

Sample Name	Mass of sand (mg)	Suburb	Dune System
SB3	237	Munster	S
SB4	209	Coogee	S
SB5	361	Forrestdale	B
SB6	257	Forrestdale 2	B
SB7	165	Bibra Lake	S
SC1	161	Hope Valley Road	S
SC2	147	Hope Valley Road, Hope Valley	S
SC3	169	Postans Rd Hope Valley	S
SC4	143	Hope Valley	S
SC5	138	Mandogalup	S
SC6B	139	Mandogalup 3	S
SC7	126	Wandi	B
Same site, Depth samples			
11AMB15m	103	Karrinyup 1.5m depth	S
11AMB1m	101	Karrinyup 1m depth	S
11AMB05m	105	Karrinyup 0.5m depth	S
* due to an oversight during the beamtime, sample NA1 was only analysed as a single grain S= Spearwood, B=Bassendean			

4.2.2 Sample Analysis

All samples were analysed in a single 24-hour beam allocation. Each sample was scanned from 2°–82° 2θ, with a wavelength of 0.954067 Å, 13keV, 0.004° step for a total of 5 minutes per position. Patterns were collected at standard room temperature and pressure. The horizontal slit was set at 3 mm for all capillary samples. The Mythen II microstrip detector was used for all samples.

Data was processed firstly using PDViper, normalised and spliced, due to the Synchrotron set-up recording as 2 positions. Wavelength adjustment from the synchrotron wavelength of 0.954067 ±0.000003 Å to the previously used Co Kα of 1.78901 Å, and subsequent pattern analysis of the resulting data was undertaken using PANalytical High Score Plus and ICDD powder diffraction files (140). Multivariate analysis was performed with Camo Unscrambler.

4.3 Results and Discussion

4.3.1 Laboratory versus Synchrotron PD

After collection, normalisation, splicing, wavelength correction and zero shift (0.0279°) correction, a preliminary comparison was made between a previous laboratory XRD pattern and the corresponding synchrotron PD pattern. Presented in Figure 30 is the comparison of the sample from Karrinyup, collected as per Chapter 3, compared to the same sample as collected at the Australian Synchrotron. Of note is the almost 10 hour acquisition time difference between the two techniques, although this is reduced with more modern laboratory instruments.

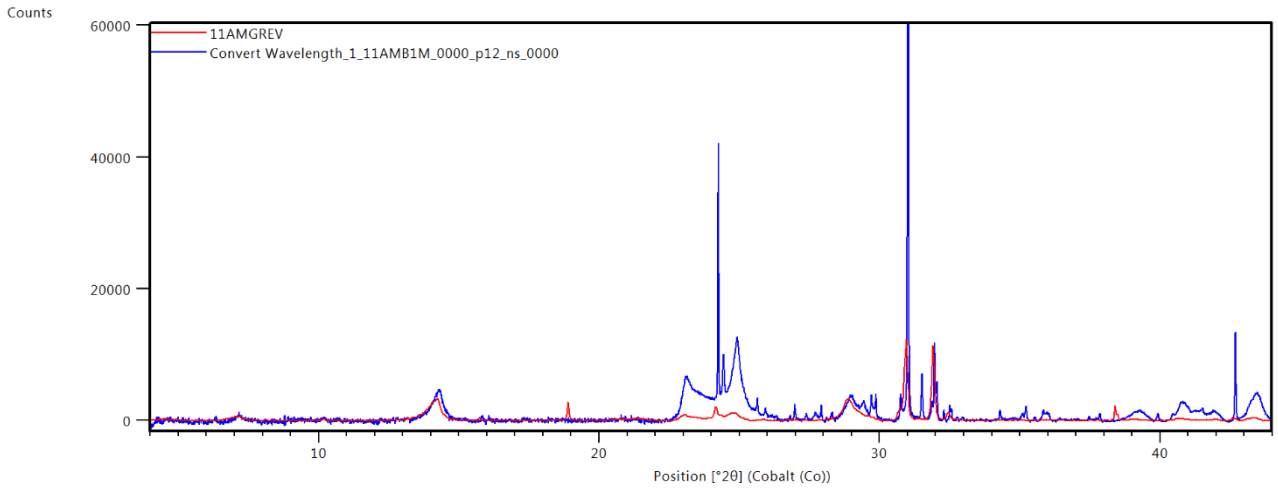

Figure 30: The sample (11AMGREV) analysed on the laboratory-based PW1820-APD 4-44, 0.05 step, 48sec/step [10 hours, red] compared to same sample analysed on the PD Beamline of the Australian Synchrotron in a capillary (blue), 2-80°, 0.004° step, approximately 10 minutes. Both scans are shown on the same scale.

By visually comparing the counts of the two patterns, it is evident that the synchrotron has a significant increase in overall counts. The peaks are sharper and there are peaks visible that were not detected above the background in the lab-based XRD, especially those between 25–44 degrees 2θ. These peaks may lead to further differentiation or may be just previously non-detected reflections of minerals already accounted for. It is of note that the peak at 18.95 degrees in the 11AMGREV sample is the peak from the low background plate. The peaks (doublet) at approximately 38.5 degrees in the lab XRPD pattern is a second-order LBP peak. There is a marked difference in the relative intensities of basal and non-basal peaks (e.g. kaolinite [001]: kaolinite [020]) due to the absence of preferred orientation in the capillary sample compared with the LBP sample.

4.3.2 Synchrotron PD data: visual examination of patterns

A selected number of the patterns were initially visually examined, to get an understanding of the response and appearance of the patterns. A few samples that previously showed very similar, very low count patterns were selected for visual

examination. These 2 groups of samples, 11AMB05/NC5 and SA3/SB1/SC7, were from Spearwood and Bassendean sites, respectively.

Presented in Figure 31 is the overlay of 11AMB05 and NC5 patterns, scaled so that the quartz peak at 31.05° 2θ are the same intensity in each. Mineral identification analyses of 11AMB05 and NC5 are presented in Figure 32 and Figure 33, respectively. From Figure 31 it is visible that the samples are still very similar, though with some subtle differences in peak heights and relative abundances of minerals.

Of interest in Figure 32, is the inferred presence of a small amount of muscovite mica, based on the relative proportions of the 001 (~10.4°) and 002 (~20.5°) reflections. Although goethite also has a peak at ~20.5°, relative proportion differences in micas are due to the shortening of the b lattice dimensions caused by distortion of the octahedral sheet related to vacancies in dioctahedral micas, and infer the presence of muscovite rather than the trioctahedral biotite or phlogopite (141). NC5 does not appear to contain mica, with only a very small, questionable peak near the 001 of muscovite, unable to be differentiated from the baseline of the surrounds.

Additional minerals inferred from peaks in the patterns, not easily detected with laboratory-based XRD, are anatase and the possibility of a spinel, though this is considered unlikely in consideration of the mineralogy and is only based on the presence of a small peak and cannot be confirmed, due to overlaps of the peaks with other more abundant minerals (see Figure 34).

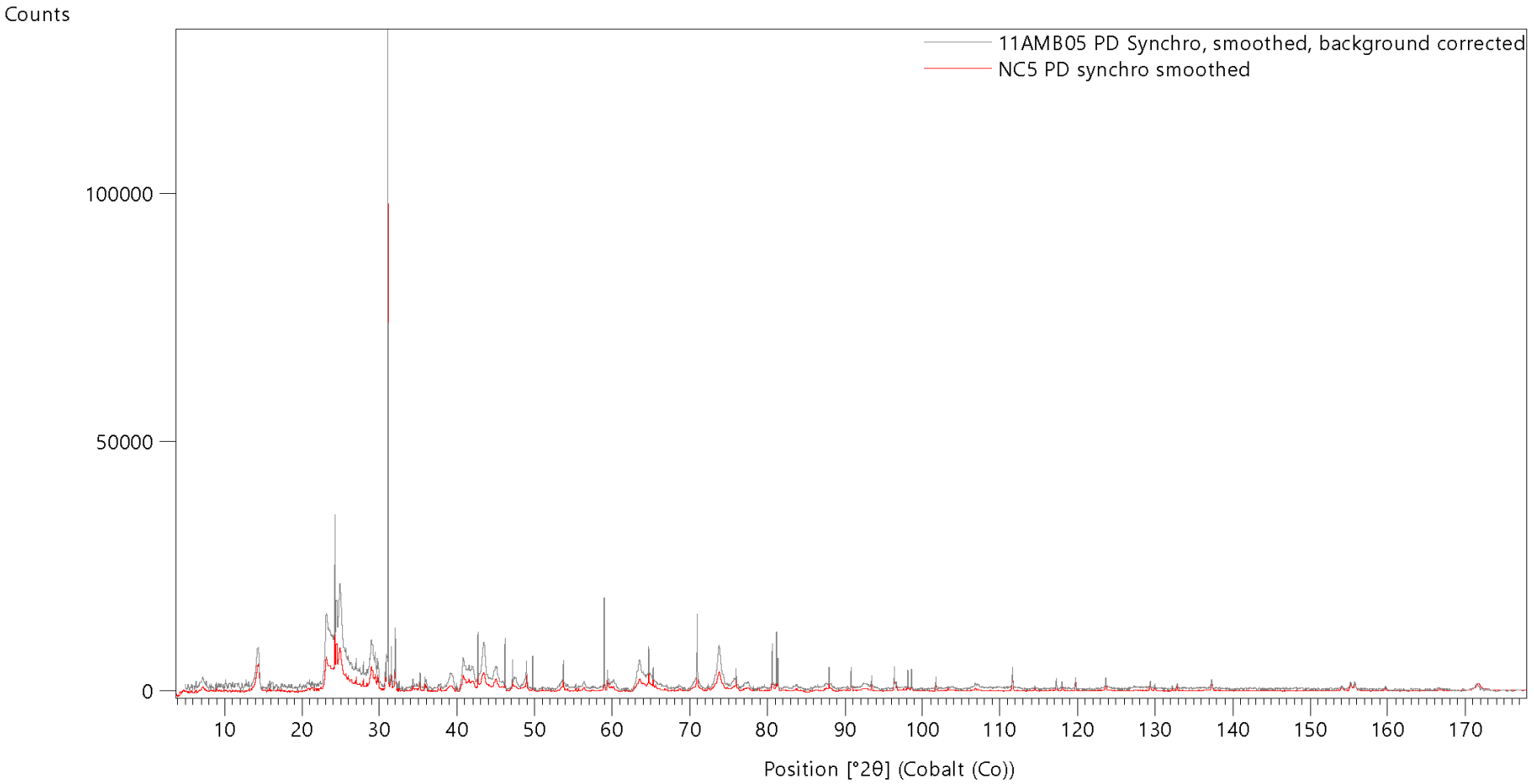

Figure 31: Overlaid PD patterns from 11AMB05 and NC5, scaled to equal (101) quartz reflections

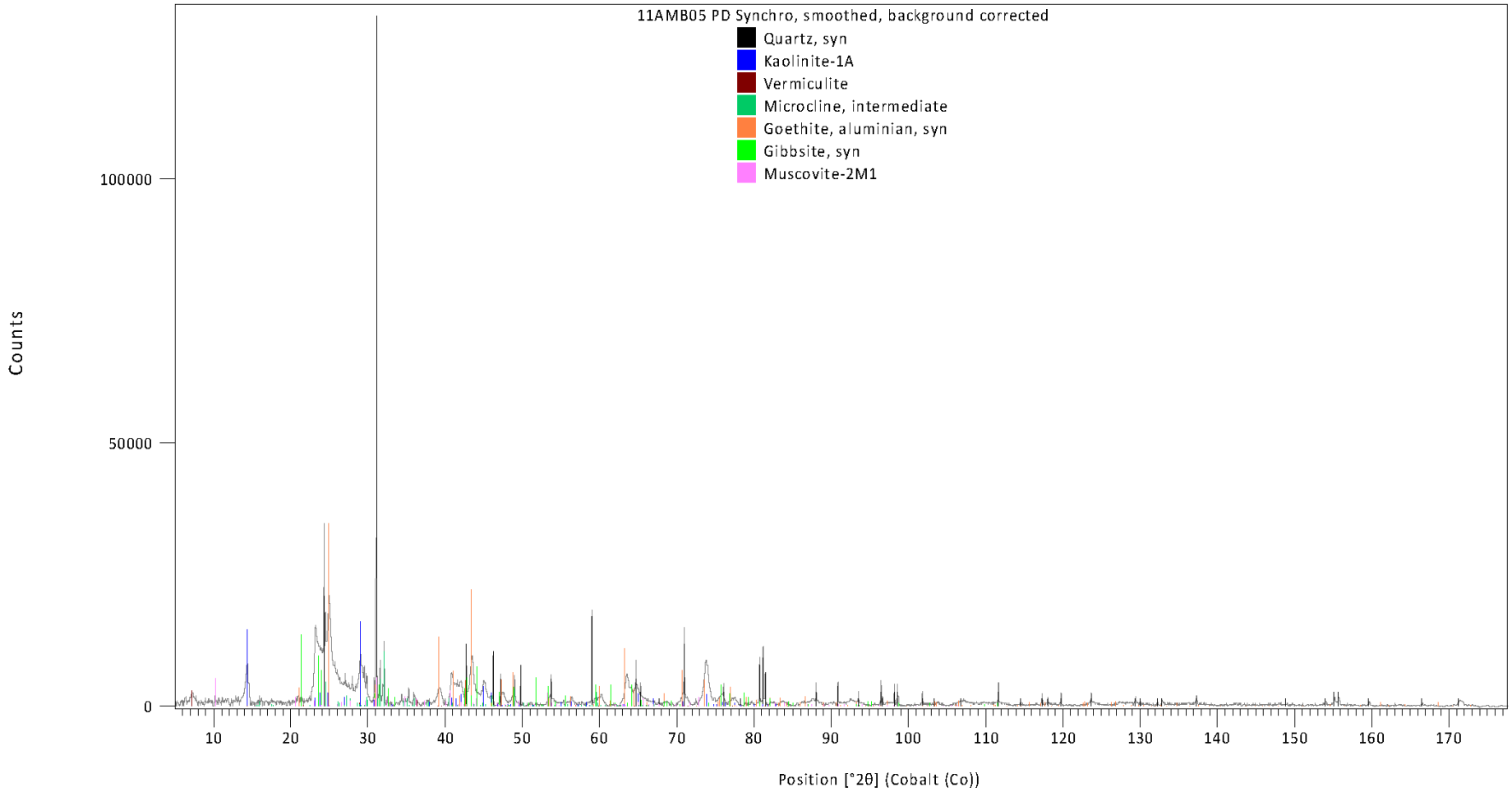

Figure 32: Mineralogy of 11AMB05 analysed on PD Beamline, Australian Synchrotron

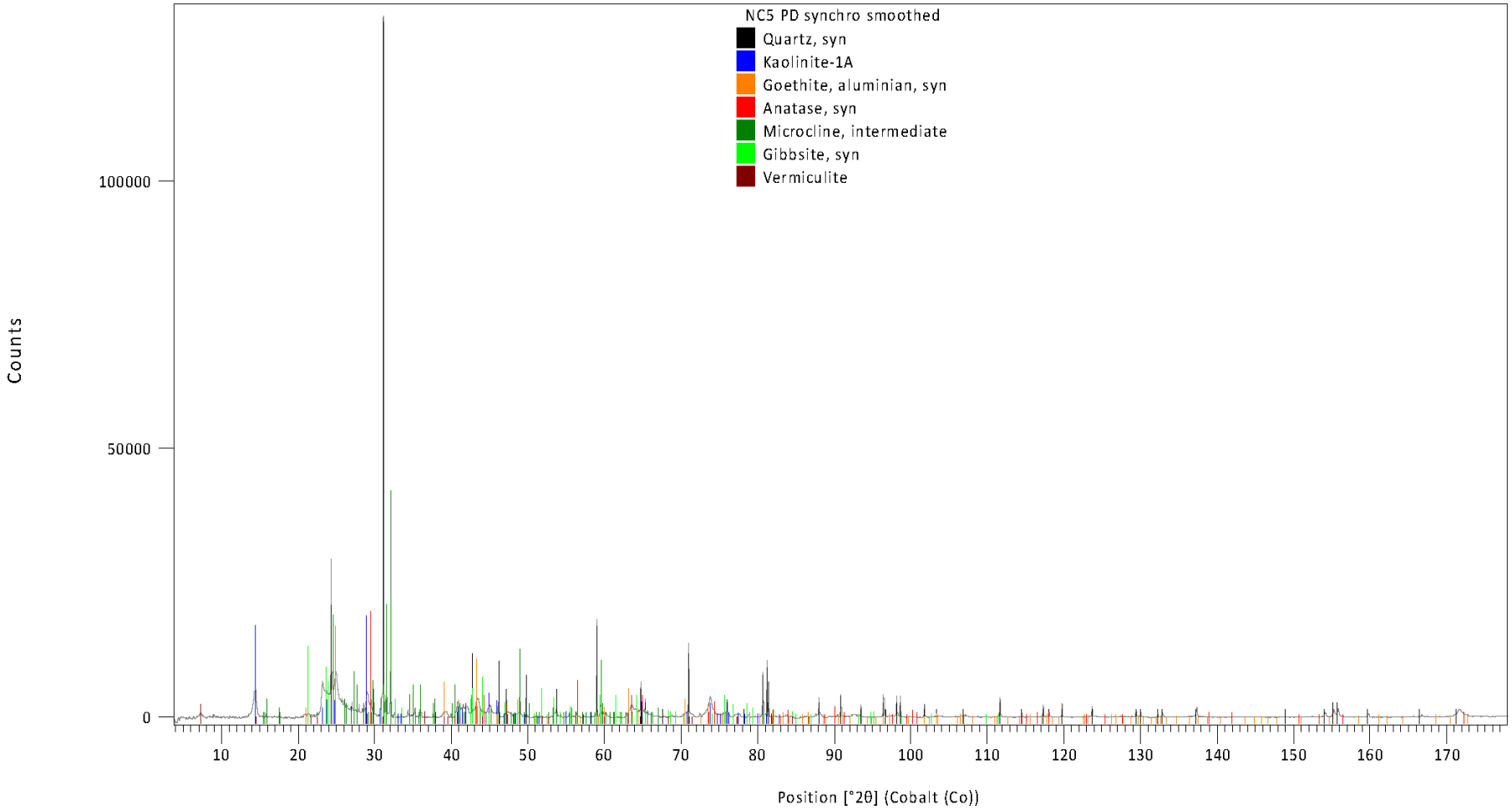

Figure 33: Mineralogy of NC5 analysed on PD Beamline, Australian Synchrotron

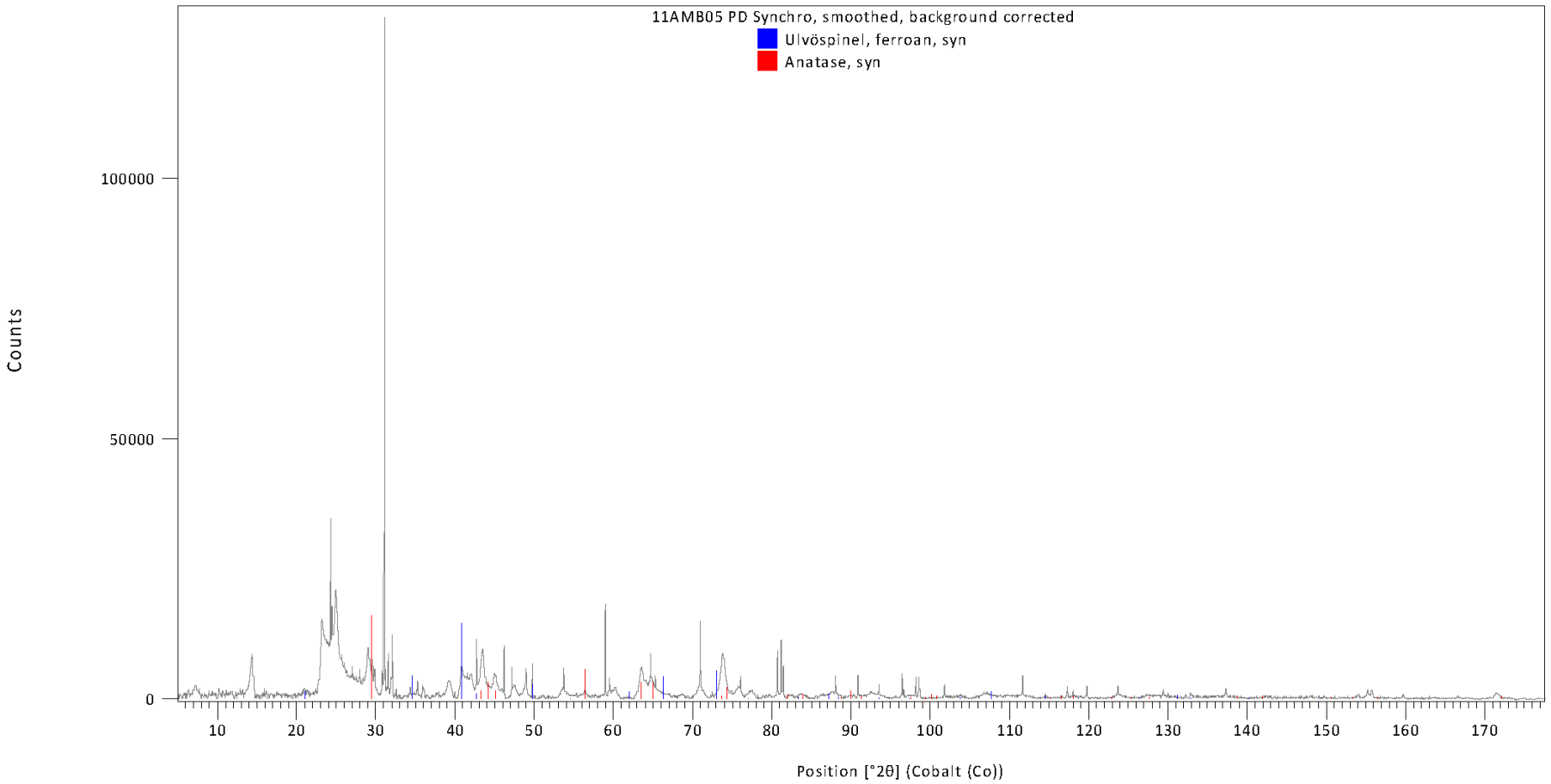

Figure 34: Sample 11AMB05 with positions of anatase and suspected spinel

Presented in Figure 35 is the overlay of SA3, SC7 and SB1 patterns, again scaled so that the (101) quartz peak at approximately 31.05° 2θ are the same intensity in each. Mineral identification analyses of SC7 is presented in Figure 36. In this case, all 3 samples have very similar mineral assemblages, with high levels of kaolinite, detectable amounts of anatase and vermiculite, with minimal microcline. Rietveld refinement and multivariate statistical analysis may be able to differentiate these samples but in a visual examination, only differences in the relative abundance of quartz to the other minerals are noted. SC7 seems to have a far higher response for the other detected minerals, though this may be due to smaller amounts of quartz grains in the recovered fine fraction. As was mentioned at the beginning of this chapter, the recovery was not a quantitative technique and small differences in the size of the grains originally hand-picked may account for differences in recovered quartz levels.

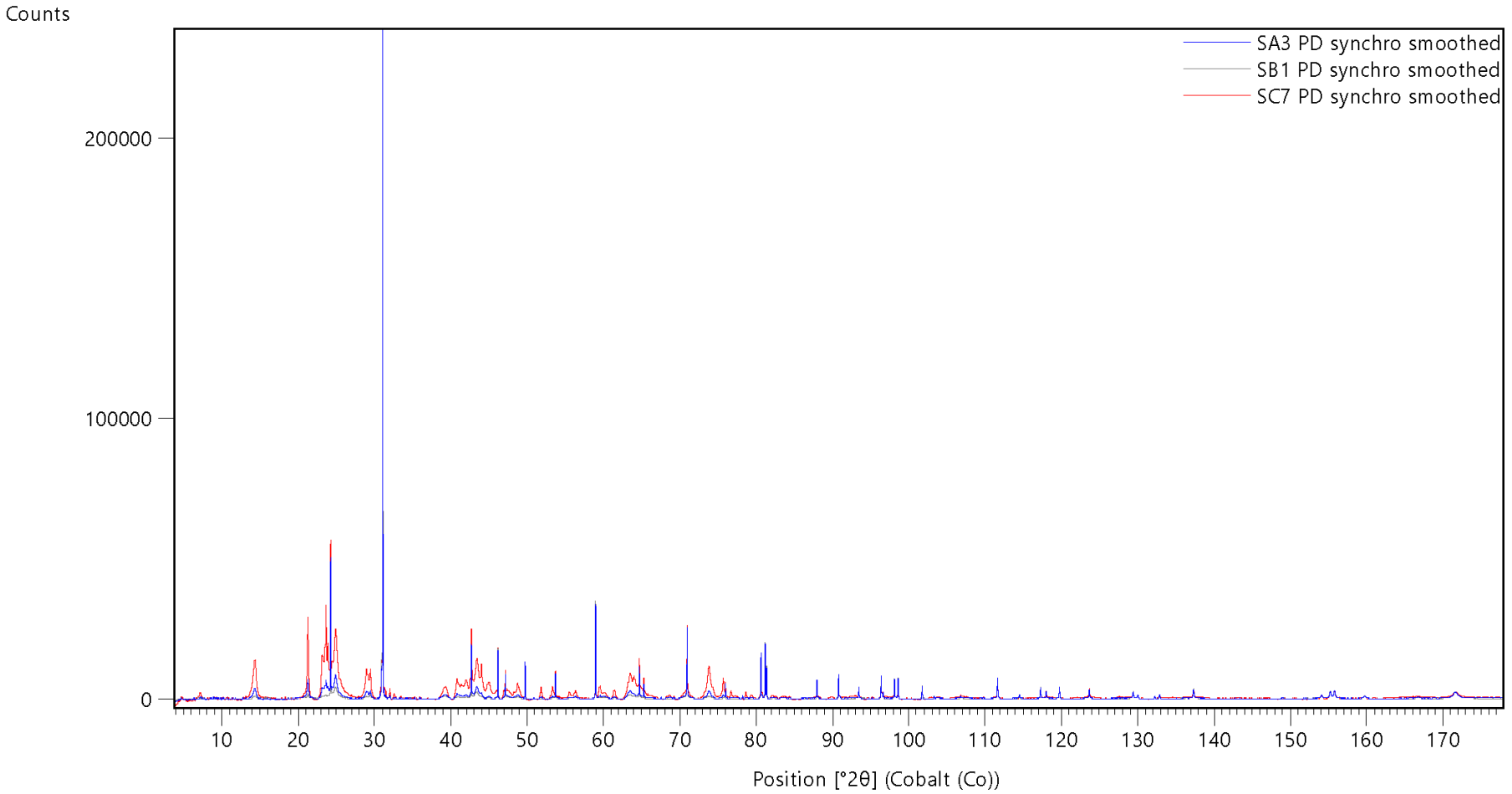

Figure 35: Overlaid PD patterns of SC7 (red), SA3 (blue) and SB1 (grey). scaled to equal (101) quartz reflections (most intense peak)

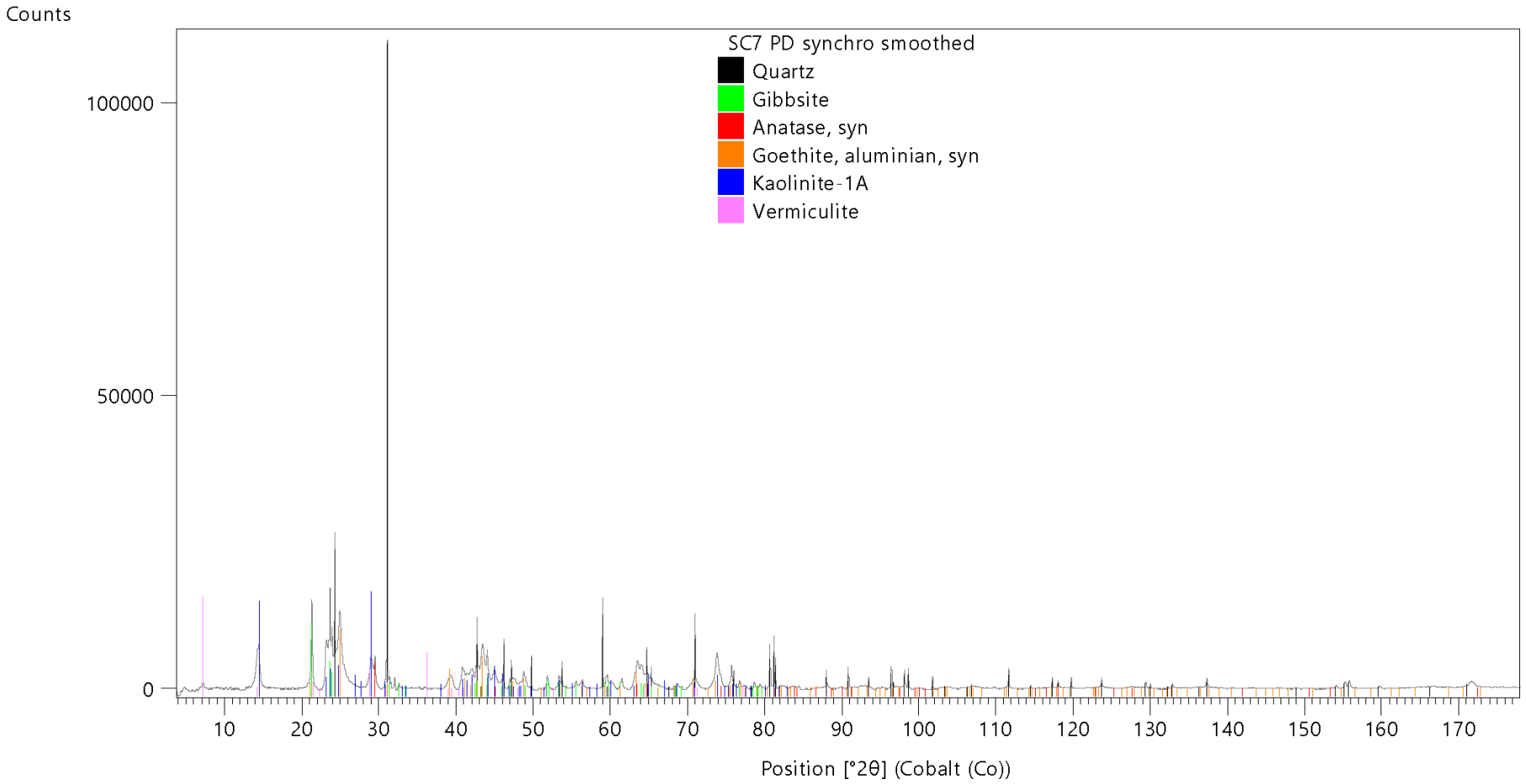

Figure 36: Mineralogy of SC7 analysed on PD Beamline, Australian Synchrotron

4.3.3 PD data: as percentage intensities

To compare to the work undertaken in Chapter 3, the data from the synchrotron samples were processed in a similar way. The peak intensity from the reflections for the 7 minerals were extracted, converted to percentage intensities in the same manner as in Chapter 3, and then a principal component analysis was undertaken. Appendix E presents the maximum counts and associated percentage intensities for the 38 samples. Presented in Figure 37 are the scores of the first 3 PCs for the 38 samples analysed, with these 3 PCs accounting for 94% of the variation in the dataset. The data are sorted by class- Spearwood/Bassendean and North/South of the Swan River as a first-pass visualisation. No duplicate samples were analysed, due to the limited allocated time and a desire to undertake an examination of inter-sample relationships. This means that reproducibility is not able to be examined in the PD beamline samples, this was examined in the laboratory based XRD analysis in Chapter 3. The 2 samples from mixed origins were also removed from the analysis, as they didn't have a distinct provenance.

As with the results of Chapter 3, some samples separate away from the majority of the samples, specifically in this case NC2 and SA2 as marked. By viewing the

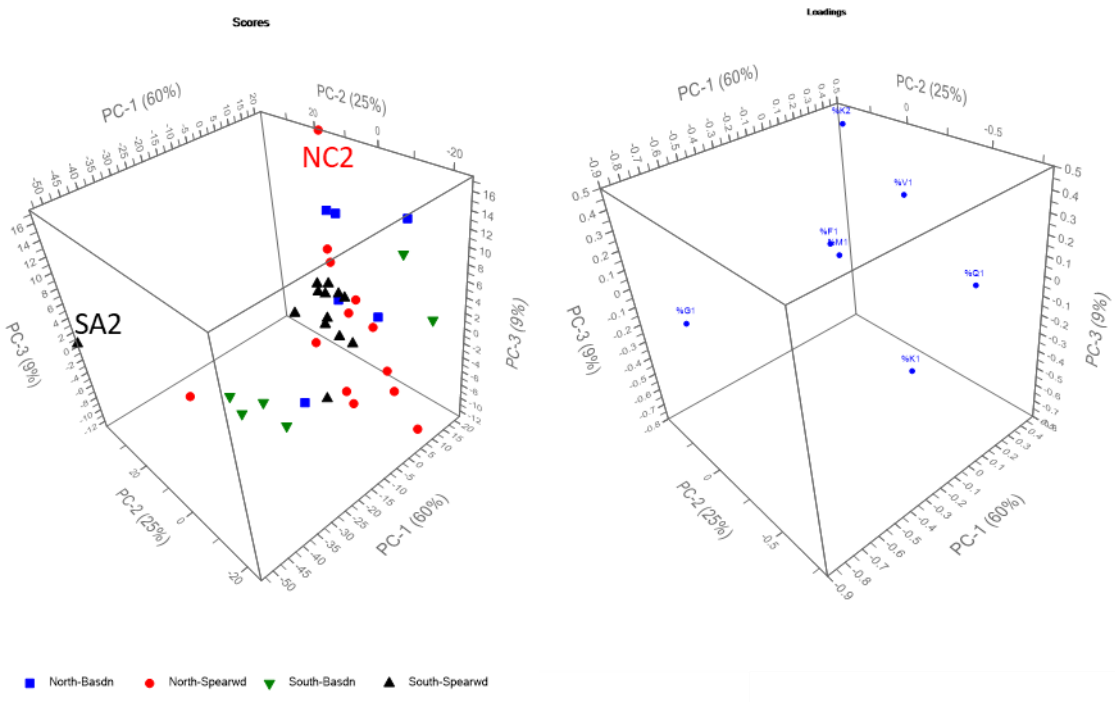

Figure 37: Scores and loadings plot of the first 3 PCs from the analysis of the percentage intensities of the 7 minerals, as per Chapter 3, for the 38 samples analysed at the Australian Synchrotron (Bassendean north (blue) and south (green), Spearwood- north (red) south (black))

loadings and associated scores for these samples, SA2 is separated based on its high relative abundance of gibbsite and kaolinite (K2), whilst NC2 shows high relative percentages of kaolinite (K1 and K2 reflections). SA2 interestingly was also easily separated from the others in Chapter 3 [Figure 25]. This leads to the conclusion that the sample itself is distinctive and that this is not due to inherent issues in the data analysis.

As with Chapter 3, the remaining samples showed some overlap between Spearwood and Bassendean sites and a distinction between north and south sites cannot be seen. However, most sites could be differentiated in space in a relative comparison. Future work would be to undertake Rietveld fitting on the 38 sample patterns and then a cluster analysis or multivariate assessment of fitted data, encompassing all minerals and reflections detected in the patterns. This is expected to be a time-consuming process and hence, is outside the limitations of time for this project.

4.4 Conclusion

Powder diffraction using synchrotron radiation is a powerful technique for the analysis of very small samples and very fast analyses. The signal to noise ratio is vastly improved even in very quick analysis timeframes. However, modern detectors in laboratory-based XRD systems are decreasing analysis time significantly. The multivariate analysis enabled further differentiation in some samples. However, the time and effort required for this analysis does not seem plausible for routine casework analyses. Hence, there appears to be need for synchrotron PD only when characterising very small samples, or those samples that may benefit from the altered incident radiation wavelength and shorter analysis time, such as those where the Co or Cu Kα incident X-ray wavelength causes issues or those unstable at room temperature or laboratory humidities.

4.4.1 Further work

It is acknowledged that there are still opportunities for further work involving this set of acquired data, not able to be completed in this project. Firstly, the analysis of

additional samples, with replicates, from areas other than Spearwood and Bassendean sites and then collation into a larger database of all minerals. Secondly, the use of Rietveld refinement for the examination of the XRD patterns to allow more robust comparisons of the percentage intensities developed herein. Finally, the use of multivariate statistics on the full Rietveld refined semi-quantitative date would be very interesting to determine if further differentiation is possible.

Chapter 5. The Use of Chemometrics for the Comparison of the Quartz Fine Fraction in Forensic Case Work

5.1 Introduction

In this chapter, the significance and use of the chemometric evaluation of the quartz fine fraction will be demonstrated by the use of the technique for the examination of evidence from redacted case studies. The significance of the chemometric evaluation and the quartz fine fraction technique is demonstrated.

5.2 Case 1- Comparison of Vehicle samples to Homicide Victim Recovery Site

5.2.1 Case Circumstances

The body of a deceased female was discovered in the Quindalup sand dunes located in a northern outer-metropolitan area of Perth (further outlined in Section 5.2.2). A small number of reference soil samples were collected from the scene at the time of the incident. Approximately eight years after the incident a greater number of samples were collected, from the crime scene, adjoining limestone tracks, parking areas, and throughout the broader dune area. At the initial time of the discovery of the victim, the area had minimal urbanisation, with large tracts of land undisturbed apart from the construction of limestone tracks and minimal housing.

Approximately six months after the discovery of the body of the victim, a vehicle was seized from a suspect. This vehicle was searched, and the interior car mats were seized. These mats were similar to small carpet squares and were positioned in the vehicle in such a way that the drivers' shoes would rest on them when the car was occupied. These mats were subject to multiple forensic examinations, by multiple personnel, creating multiple recovered samples of soil, shakings and washings (see Table 1 in section 1.4, page 37 for details as to sample collection). The car-mat examinations were focussed on the collection of evidence for DNA

examinations, fibres, soil and other trace evidence, and palynological examinations. All soil-related samples from the car mats were submitted for analysis and comparison to the location where the victim was discovered.

5.2.2 Crime Scene Location characteristics

The victim was recovered from light scrub in the dune systems of northern Perth. Based on regolith geology and geological maps, this region is an area of variably aged, mostly Quindalup soils, with Spearwood sand contributions. An image of the area with the body location, overlain with the designations (142), is presented in Figure 38. There were two limestone tracks in the immediate area (within 30 m) and a bituminised road a short distance away (approximately 40 m).

5.2.3 Samples Submitted and Complicating Factors

Several factors complicated the analysis and evaluation of the soil material located within the carpeted car mats. Firstly, there was a time gap between the event and the seizure of the mats during which the vehicle's movements and use were unknown. Secondly, the car mats were subjected to multiple examinations, including by biologists looking to recover DNA and/or blood, a palynologist and crime scene examiner for the recovery of pollens, and an international laboratory asked to assist in the investigation. All of these examinations resulted in fractionated soil samples, some of which were lacking in documentation outlining the processes undertaken and only identified by an exhibit reference and a brief description of origin. Upon submission, it was identified that some of the samples collected were washings, rather than shakings or vacuumings (see Table 1 in section 1.4, page 37), and were stored in water for a long period. Hence these were deemed unsuitable for mineralogical examination of the quartz fine fraction coatings. Finally, the suspect was known to reside in an area that was very close to a small Quindalup outcropping, with exposure to the soil likely and plausible.

Despite these complications, a mineralogical comparison of the recovered samples to the body recovery scene was requested by the investigators. Table 8 outlines the details of the four samples of soil that were recovered from the driver's side floor

mat of the suspect vehicle (analysed as nine XRD replicates) that were deemed appropriate to undergo mineralogical comparisons. Table 9 details the sample descriptions for the sites close to the suspects home, publicly accessible parks, and Quindalup sand dunes. Table 10 details the classification groups and sampling descriptions of the sites from the body disposal site and surrounds as well as sites within further areas of the Quindalup system and sites of coastal limestones. All sites were chosen based on their underlying geology and nearness to the body disposal site. A total of 71 samples were from Quindalup or near Quindalup locations, including seven from near the suspect's house, 43 from within the body disposal site and close surrounds, seven from other Quindalup system locations and five from areas of coastal limestones outside metropolitan Perth. The coastal limestones were included as the geology was expected to be potentially similar to Quindalup dunes.

Table 8: XRD sample identifiers for sub-samples from the four original samples of soil material recovered from the driver's side car mat of the suspect's vehicle (V stands for vehicle).

XRD Sample Identifier	Initial Exhibit Description
V1.1 V1.2 V1.3	Soil sample from driver's floor carpet from motor vehicle
V2.1	Soil sample from driver's floor carpet from motor vehicle
V3.1 V3.2	Soil sample from driver's floor carpet from motor vehicle
V4.1 V4.2 V4.3	Tapping's from motor vehicle carpet (recovered by international laboratory)

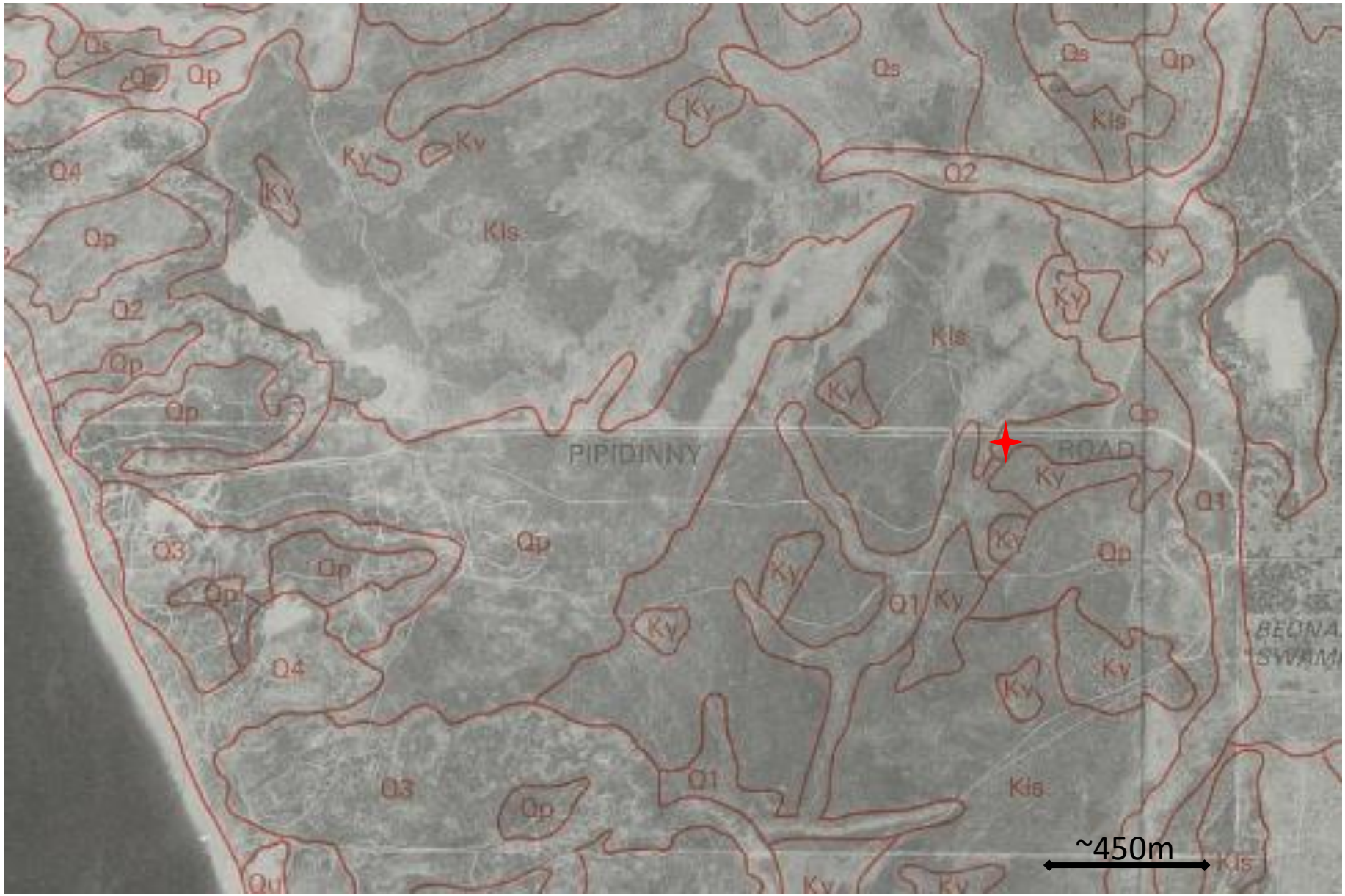

Figure 38: Map from McArthur (1979 [142]) showing location of body (red star) and regional soil classifications.
Ky- Karrakatta sand (yellow phase), Kls- shallow sands, Q1-oldest to Q4-youngest Quindalup, Qu- unstable sand, Qp- deep calcareous sandy soil over limestone.

Table 9: Sample names and brief location descriptions of seven samples from near the Suspects house

XRD Sample Identifier	Sample Description
LtMAR	Sample from soil in front of suspects house
MeH1 MeH2	Soils collected from Melon Hill, Quindalup location close to suspects house, named for Melon Hill in the publicly accessible Allen Park, in the suburb of Swanbourne, Perth
SwB1 SwB2 SwB3 SwB4	Soils collected from Swanbourne Quindalup Dunes, 4 publicly accessible locations bordering Swanbourne Reserve, Perth

Table 10: Group names for the 43 samples from the body disposal site and surrounds as well as seven samples from the Quindalup system and five samples from coastal limestone sites

XRD group Identifiers	Sample Description
body disposal site	Body disposal site samples, all within 2m of site
Near body disposal site	Samples of soils from areas 10m-2km from dump site
Quindalup System	Samples from areas in areas of underlying Quindalup geology, but not close to the suspects house or body disposal site
Coastal limestones	Samples of soil from coastal locations, outside the metropolitan area, underlying limestones

5.2.4 Experimental

5.2.4.1 Sample Analysis

All samples were initially visually inspected with the aid of a stereomicroscope, and the bulk colour and texture characteristics noted. All soils were predominantly

quartz-based, with the quartz fine fraction recovered and analysed using XRPD, as per the method detailed on page 49 in Section 2.2.1 Recovery of the fine fraction.

Additionally, heavy mineral grains were recovered using panning and hand-picking, and analysed using polarised light microscopy and SEM-EDS. Whilst not the focus of this chapter, and, hence, not extensively discussed, the heavy mineral assemblage was used for comparison purposes in the casework (see Figure 7 and section 1.4.2.1 in Introduction regarding heavy mineral assemblages) (113).

5.2.4.2 Chemometric Evaluation

As per previous chapters (Section 3.3.2.2, page 73), all XRD patterns were examined, shift corrected for the LBP (5.912 Å) or quartz line (3.337 Å), and the percentage intensities for the 8 mineral diffractions calculated. This data was imported to Camo Unscrambler®, along with appropriate groupings. PCA was undertaken in stages, with an evaluation of the explained variance and inter-relationships informing the removal and re-analysis where differentiations were observed.

5.2.5 Results and Discussion

5.2.5.1 Summary of the Analysis of Case Samples

5.2.5.1.1 Body Recovery Location

The majority of the samples from the body recovery site and surrounds were dominated by brownish-grey to pale yellow medium-coarse sands, with the quartz grains being mostly sub-angular to sub-rounded. This indicated a source not purely Quindalup in origin. Plant material, including fine humus, was visible in all samples, with minimal man-made artefacts noted.

The body disposal site and surrounding area are represented by four main soil types that approximately reflect the underlying the geology in terms of nature and age of the dune systems over which soils evolved (Figure 38). The levels of calcite, magnesian-calcite and aragonite varied, as would be expected with the various

classifications of the area as shown in Figure 38. Some samples, such as those closer to the coastal beaches, showed higher levels of shell and coral remnants.

5.2.5.1.2 Suspect's House Surrounds

The sample collected from the front verge area of the suspect's house (LtMar) was brownish-grey, medium-coarse sand, with the quartz grains being mostly sub-angular to sub-rounded. Plant material, including fine humus, was visible in all samples, with multiple man-made artefacts, such as blue metal (quarried, crushed aggregate rock) and paint noted. Additionally, XRPD analyses showed abnormally high levels of chlorite in the quartz fine fraction, suspected to be due to the blue metal.

The samples collected from Swanbourne and Melon Hill (grouped as House-Quindalup) were also brownish-grey to pale yellow, medium-coarse sands, with the quartz grains being mostly sub-angular to sub-rounded. Plant material, including fine humus, was visible in all samples, with minimal man-made artefacts noted. The colour and overall appearance of the samples from the immediate body disposal site and surrounds were consistent with those of the additional Quindalup sites of Swanbourne and Melon Hill.

5.2.5.1.3 Recovered Samples

The recovered soil samples contained artefacts including metal, road dust, blasting garnets, paint, fibres and hairs, indicative of a mixed source origin, i.e. representing more than a single transfer event. Also, the original samples from the carpet had been processed and fractionated by multiple samplings and subsequent analyses. For these reasons, comparisons based on overall colour, particle sizing and grain characteristics were not considered reliable and were not extensively undertaken.

The soil material recovered from within the mat [V1–V4], when combined and considered as a whole, indicated a Quindalup-dominated source. This was based on the lack of substantial coral and shell remnants, the relatively high levels of the heavy mineral ilmenite relative to leucoxene, the presence of amphibole with

various compositions and the presence of calcite, aragonite, and magnesian-calcite in the fine fraction. All these characteristics indicated a relatively young soil, rather than a more aged (higher degree of weathering) Spearwood or Bassendean-type soil, but not typical contemporary beach sands.

5.2.6 Significance of Chemometric work

Given the complications with multiple sub-samples, noted artefacts and likely mixed source, the fine fraction of the recovered soils was compared to the scene samples as well as the other samples in the database. This could not have been done without the chemometric work, as detailed in Chapter 3, establishing the comparison methodology and ability to differentiate samples.

As mentioned previously, based on preliminary visual observations of recovered samples, it was noted that the likely association would be to a Quindalup-based source. However, for completeness, the percentage intensities of the recovered samples (9) were calculated and multivariate analysis undertaken using the PCA analysis developed in Chapter 3. Given the numerous control and reference samples from the surrounding areas, the entire dataset underwent repeated full chemometric analysis, rather than using a projection in the data analysis software.

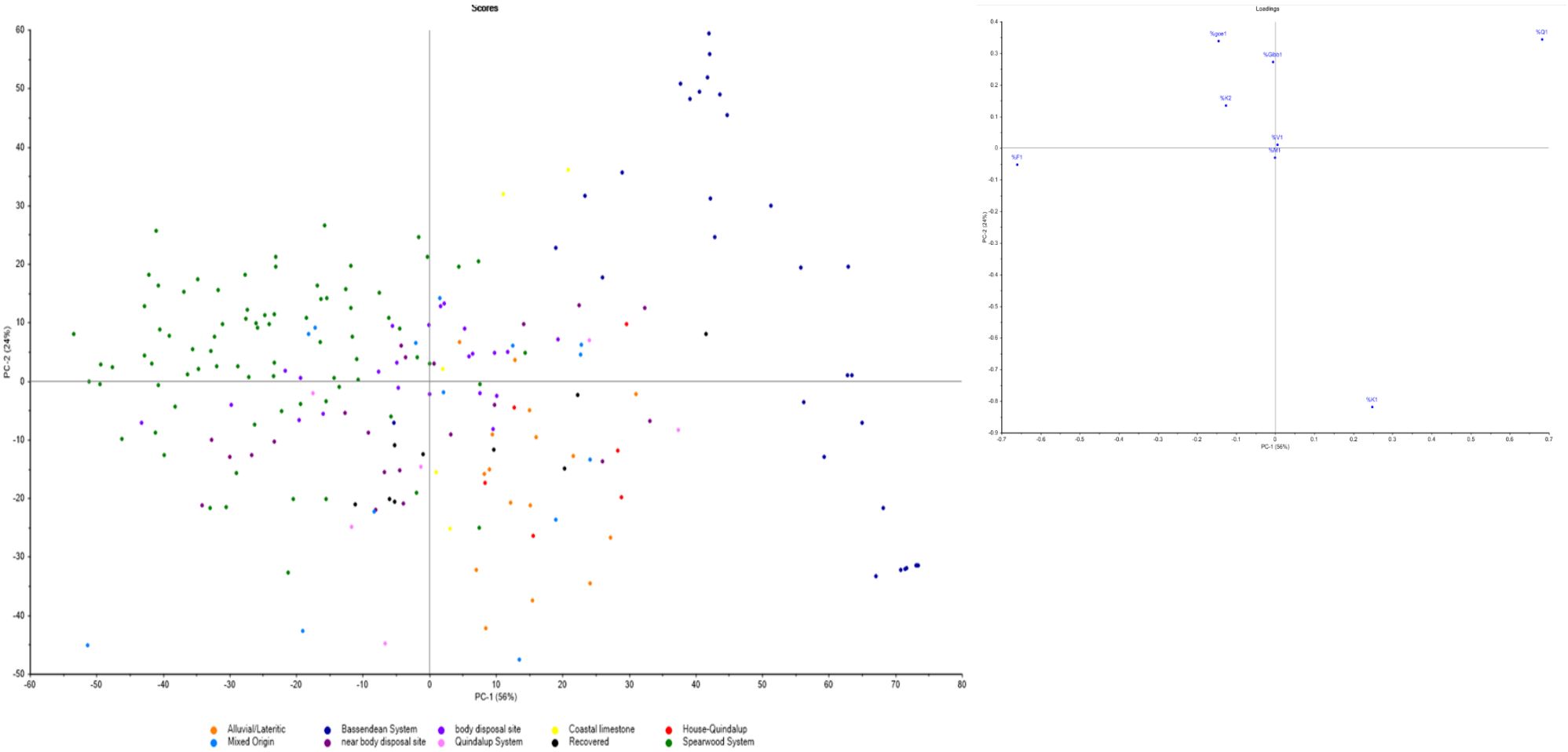

Figure 39: First two PCs of PCA analysis comparing recovered samples (V1–V4) to the samples from Bassendean, Spearwood, Quindalup, Alluvial/Lateritic locations. The samples from the body disposal site and surrounds are separated from the remaining 'unrelated' sites.

5.2.6.1 Full Database Comparison

This analysis used data for the recovered samples (V1–V4), as well as samples from the body disposal site and surrounding Quindalup sites, samples related to the Quindalup areas near the suspect's house, which include Swanbourne and Melon Hill, and all the other 'known' samples from sites across the Perth Metropolitan region and some Coastal limestones. The loadings plot and scores plot for the first 2 PCs from this PCA are presented in Figure 39. The first 2 PCs accounted for 56% and 24% of the variance in the model, respectively. PC1 was strongly influenced by quartz and feldspar, whilst PC2 was strongly influenced by kaolinite and goethite.

By examining Figure 39 and samples' scores (presented in Appendix G), the following interpretations can be made from the analysis:

1. The replicate samples from V4 and V1 showed some grouping, with those replicate analyses from V3 showing slightly more variation between replicates. This variation may be due to natural variation in the sample, noise in the patterns, slight background correction differences and pattern shifts causing a change in the overall counts of the mineral prior to the percentage intensity calculation. It is noted that sample V2 was a single analysis.
2. The quartz fine fraction recovered from sites in Swanbourne [MeH1-2, SwB1-4], overlapped the data of the fine fraction recovered from the body disposal site and surrounds. The quartz fine fractions recovered from these sites were differentiated from the quartz fine fraction of the soils collected from most of the sites in the Bassendean and Spearwood sands, especially when combined with the carbonate minerals observed in the full XRD pattern. Additionally, as mentioned previously, the sample from the suspect's house (LtMar) was differentiated from the vehicle samples based on the abundance of chlorite in the fine fraction.
3. Fine fraction samples recovered from quartz grains from in V1–V4 exhibited similarity with the body disposal site samples, as well as the additional Quindalup sites sampled.

5.2.6.2 Narrowing the comparisons

To further examine the possible relationship between the vehicle mat samples and the Quindalup-based samples, another PCA was undertaken after the removal of the Bassendean, Spearwood, and Alluvial/Lateritic samples from the dataset.

This analysis used data for all recovered samples, as well as samples from the body disposal site and surrounding Quindalup sites and the Quindalup-like samples near the suspect's house. The first 3 PCs accounted for 46%, 21% and 15% of the variance in the model, respectively. Similar information to Figure 39 was interpreted from the scores plot of PC1 and PC2, presented in Figure 40. The recovered samples from the vehicle mat, and the samples from the body disposal site and other Quindalup soils all show overlapping distributions.

However, additional information was revealed in plots of PC2 and PC3, as shown in Figure 41. Principal component 2 was again strongly influenced by kaolinite and goethite, whilst PC3 was strongly influenced by gibbsite, feldspar and quartz. Separation of the fine fraction recovered from quartz grains in the soil recovered from the carpet [V1–V4] from the control soils was based predominantly on gibbsite, kaolinite and goethite. This indicates that either the soil from the car mat originated from a location not represented by the body disposal site samples or other Quindalup controls, or alternatively, and decidedly more likely, had a mixed origin.

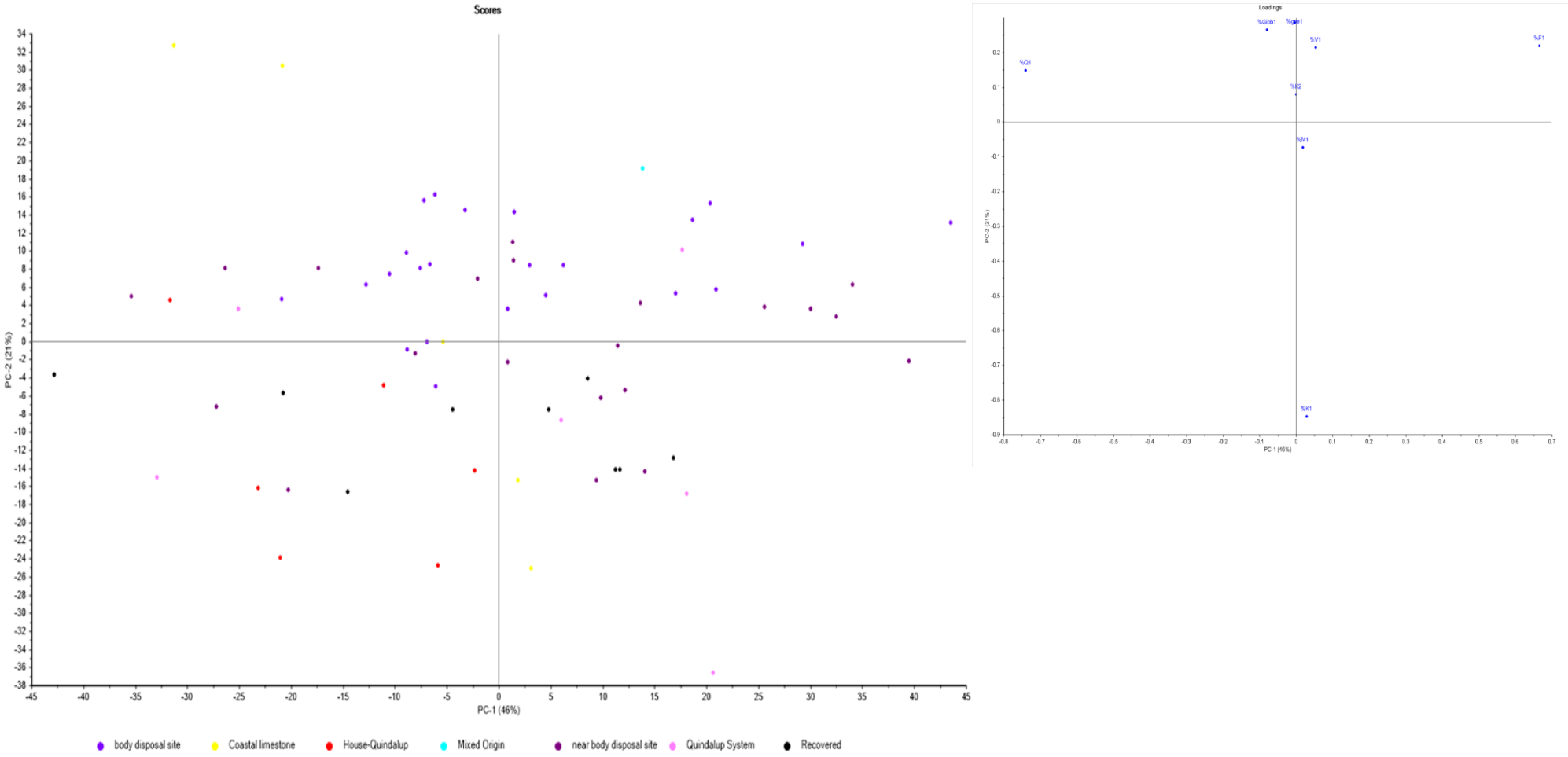

Figure 40: PC1 and PC2 of the second PCA, without the samples from Bassendean, Spearwood and Alluvial/Lateritic soil sites

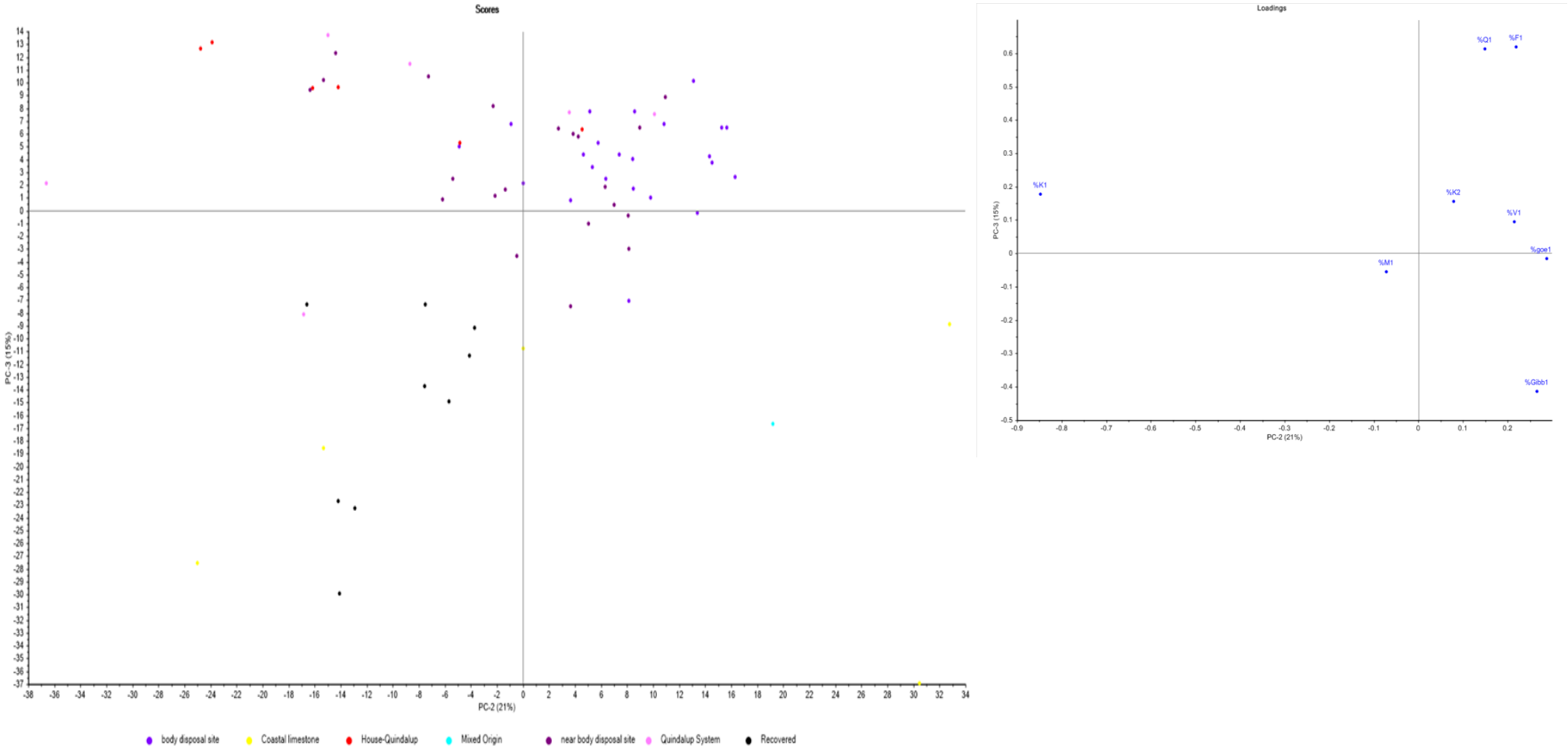

Figure 41: PC2 vs PC3 of the second PCA, with soils from only the body disposal site (purple) and surrounds, house sites (red), coastal limestones (yellow) and other Quindalup sites (pink) compared to the recovered vehicle mat samples (black).

5.2.7 Heavy Mineral Assemblages

An extensive analysis of the heavy minerals present in items V1–V4, with a specific focus on the ilmenite and amphibole populations, was undertaken outside of the scope of this thesis. However, to allow for an explanation of the fit of the methodology of quartz fine fraction analysis into standard soil analyses, a summary of the results is provided. Review of the individual, heavy mineral grain, elemental data indicated a range of amphibole compositions. There was considerable variability in the elemental concentrations of the ilmenites present, which was consistent with an ilmenite to pseudo-rutile population.

Analysis of the grain elemental compositions of the heavy mineral fractions isolated from the control samples at the body disposal site also indicated a comparable range of amphibole compositions, and a similar variability in the elemental concentrations of the ilmenites, consistent with an ilmenite to pseudo-rutile population.

Finally, separation of the heavy minerals from the additional Quindalup sites near the suspect's house indicated a population of heavy minerals consistent with the body disposal site controls. Analysis of the grain elemental data of a small selection of grains from each additional site also indicated a comparable range of amphibole compositions, and a similar variability in the elemental concentrations of the ilmenites, consistent with an ilmenite to pseudo-rutile population.

These heavy mineral results indicated that the scene and those near the suspect's house could not be easily distinguished, with extensive individual grain analyses required to characterise the heavy mineral population. This was time-consuming and complicated, showing the benefit for quartz fine fraction comparisons.

5.2.8 Case conclusions

Soil mineralogical controls from the body disposal site and surrounds, as well as other Quindalup-situated control soils such as the Swanbourne Dunes and Melon Hill, had overlapping fine fraction mineralogy and heavy mineral assemblages. The

fine fraction mineralogy and heavy mineral assemblages were considered typical for the relatively young, coastal dune system present in the Perth metropolitan area, specifically the Quindalup outcroppings.

The fine fraction mineralogy and heavy mineral assemblages of the soil recovered from the vehicle (V1–4) also had characteristics consistent with being a Quindalup-dominated soil. The range of compositions exhibited in the amphibole and ilmenite populations present in the recovered vehicle soils and the control soils from the body disposal site and the other Quindalup sites were found to be consistent.

Principal component analysis of the selected mineral percent-intensities from the fine fractions recovered from quartz grains grouped the soils recovered from the suspect's vehicle separately from the body disposal site soils and the other control soils. This indicates that the soil recovered from the vehicle originated from a location not represented by the body disposal site or other Quindalup controls, or had a mixed origin. Given the nature of the origin of the recovered samples, it is considered more likely that the samples had a mixed origin.

5.3 Case 2- Comparison of Recovered Illicit Material to Burial Site

5.3.1 Case Circumstances

As part of an ongoing investigation, Detectives from the WA Police Force conducted a vehicle stop, locating approximately 1.5 kg of alleged illicit drugs in the vehicle. Within the outer plastic bag containing the drugs was an amount of soil. Additionally, in a second vehicle stop in the same operation, another plastic bag containing illicit drugs with adhering soil was seized.

After investigation, it was alleged that the offenders were burying the material at the Floreat Athena Soccer Club grounds (Figure 42). A total of three (3) samples was taken from the garden bed of the soccer club and submitted to ChemCentre, along with the samples seized from the plastic bags containing the illicit material, for comparison.

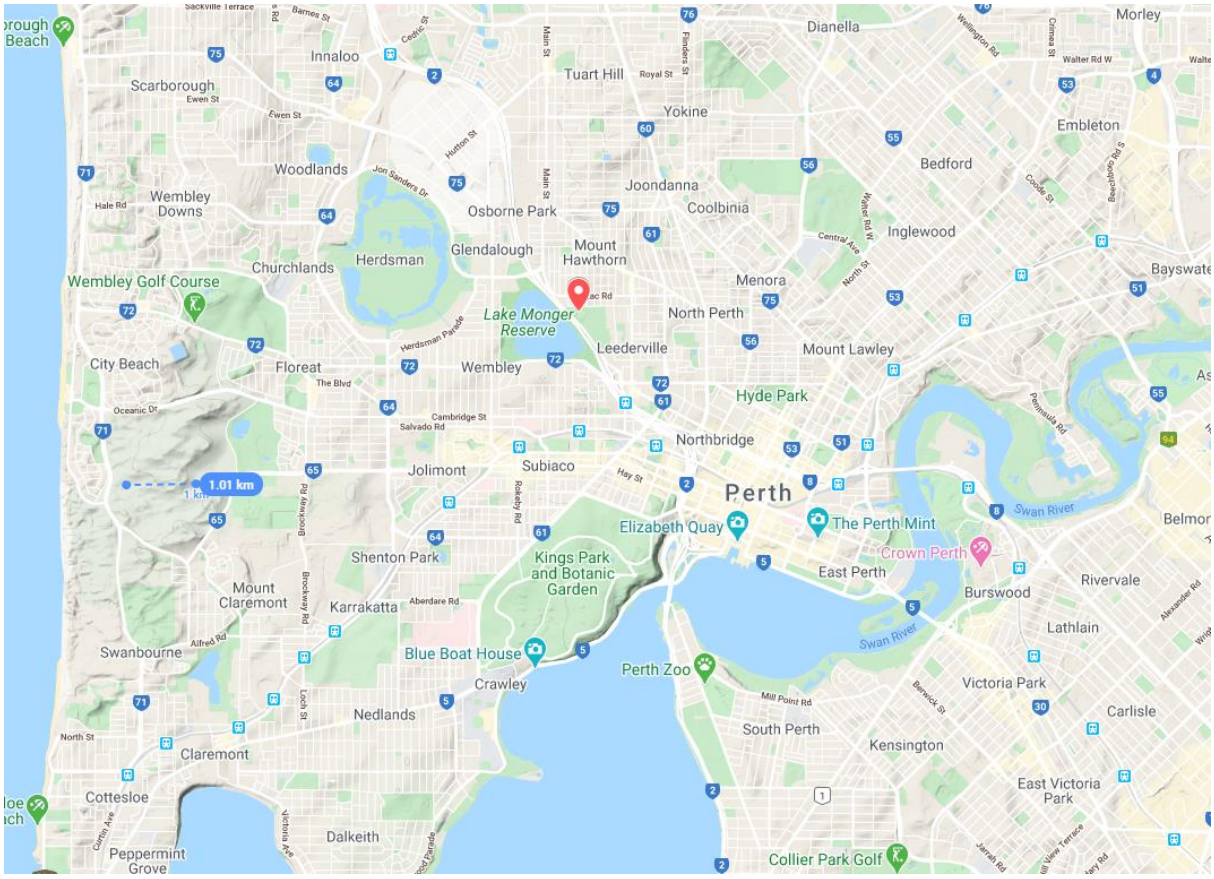

Figure 42: Map showing relative location of the Floreat Athena Soccer Club to the surrounding suburbs and landmarks such as the Swan River and Lake Monger

5.3.2 Experimental

5.3.2.1 Samples Received

Upon receipt, the samples were examined visually and using stereoscopic and polarised light microscopes to determine the general composition, physical and mineralogical characteristics (Figure 7). The texture (particle size distribution) was also determined used dry sieving and other characteristics of the soils noted (Table 11). A representative sub-sample of the quartz fine fraction (<20 µm) was obtained as per the method in Chapter 2 and analysed using XRD as per Chapter 3. This allowed the determination of the relative abundance of the mineral species in the soils.

Table 11: Samples received and preliminary results

Sample Name	Weight	General description, physical and mineralogical characteristics
Garden Bed1 (Case Control)	15.6 g	The sample was mostly medium-grained brownish-yellow sand, predominantly quartz, with abundant organic matter, feldspar, heavy minerals, and artificial materials such as glass, metal foils and building mortar. The quartz was mostly sub-angular to sub-rounded with yellowish clay coatings.
Garden Bed2 (Case Control)	16.8 g	As 001
Garden Bed3 (Case Control)	38.8 g	As 001
Plastic Bag1 (recovered sample)	3.4 g	The sample was mostly medium-grained brownish-yellow sand, predominantly quartz, with abundant organic matter, feldspar, heavy minerals, and artificial materials such as glass, metal foils and building mortar. The quartz was mostly sub-angular to sub-rounded with yellowish clay coatings.
Plastic Bag2 (recovered sample)	0.4 g	The small sample was mostly medium-grained brownish-yellow sand, predominantly quartz, with traces of organic matter, feldspar and heavy minerals. The quartz was mostly sub-angular to sub-rounded with yellowish clay coatings.

5.3.2.2 Chemometric Analysis

The original XRD data of the quartz fine fraction, converted to appropriate percentage intensities, was added to the Unscrambler files from Chapter 3. The data points were then projected onto the PCA plot of the samples in the lab-based XRD data. The model used was that presented in Figure 21, in Section 3.3.2.2; with the samples from mixed origins removed for Figure 43.

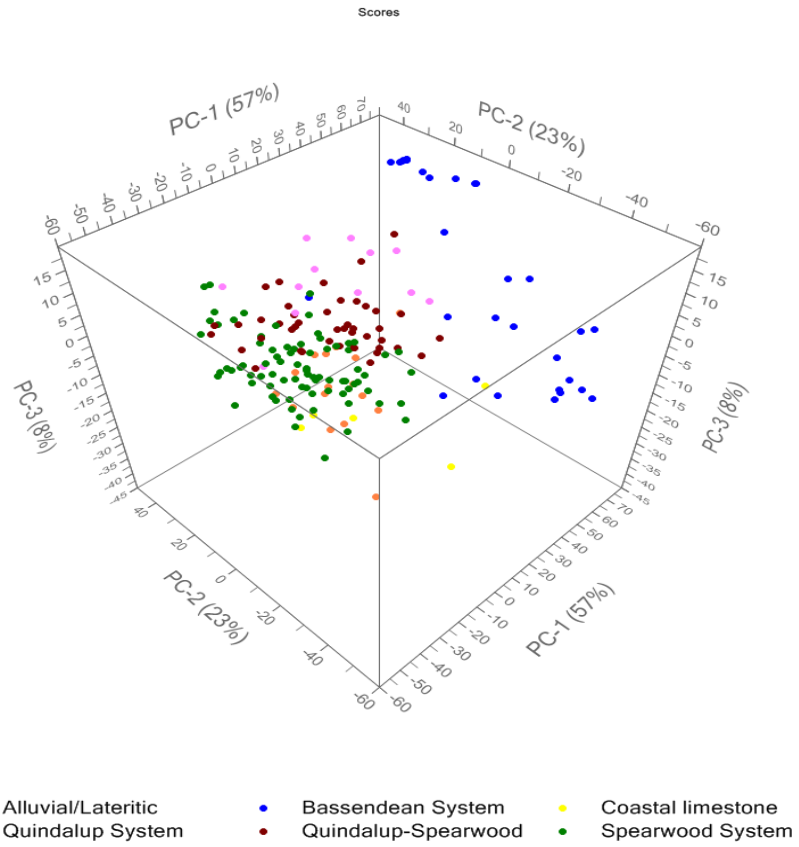

Figure 43: PCA of database as per Chapter 3, with mixed samples removed. Repeated here to show starting point for case analysis.

5.3.3 Results and Discussion

5.3.3.1 Alleged Burial Site Characteristics

The alleged burial site used by the offenders was garden beds in the Floreat Athena Soccer Club. Three samples were collected from the garden bed. These three samples all corresponded in appearance and composition. Figure 44 presents the projection of the 3 samples of the quartz fine fraction from the garden bed, as well as the two samples of soils from the plastic bags, onto the previous PCA model from

Chapter 3. There are immediate conclusions that can be made; the three control samples are close together in the model space, indicating shared characteristics. Additionally, the samples from the plastic bags are also close in the space to the samples from the garden bed. There are a few of the other samples in the database that are close to the group of the control samples; the first being NS1, which is from the Spearwood system at a similar longitudinal line to that of the control site, but on the other side of the river (Ardross). The next closest in the PCA projection are 2 samples of yellow-brown sand from a northern suburb of Perth (Eglinton) at the Quindalup-Spearwood boundary, but these are slightly separated along PC2 to the group from this case.

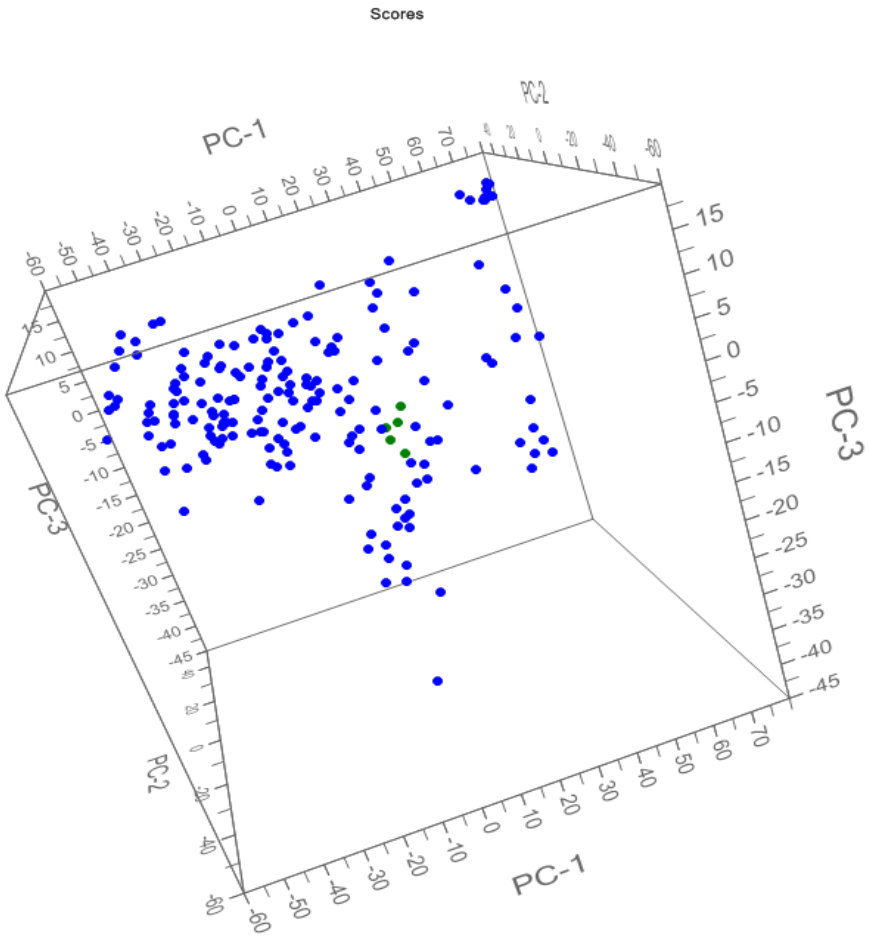

Figure 44: Projection of the 5 samples, 2 recovered and 3 control samples, (all coloured green due to software limitations for projections) onto the previous PCA from Figure 43 presented in monochrome (again due to software limitations).

5.3.4 Case Conclusions

These results indicate that the two recovered samples are consistent with originating from a site with quartz fine fraction characteristics corresponding to that of the garden bed samples. These results support the proposition that the soil found in the bags containing illicit materials originated from the garden bed of the Floreat Athena Soccer Club

5.4 Overall Conclusions

These 2 case studies demonstrate the applicability of the chemometric evaluation of the quartz fine fraction recovery and analysis to forensic soil analysis. The technique has demonstrated ability to distinguish locations and samples, though, issues with mixed source samples do complicate the analysis. The technique is appropriate for use in cases where sufficient quartz sands are recovered and if available, other fractions should also be utilised to complement the findings. Other fractions would include examination of the heavy minerals and soil organic matter. The possibility of utilising other analytical techniques, such as FTIR on this fine fraction should also be explored.

Chapter 6. Conclusions and Future Work

6.1 Summary and Conclusions

The thesis initially aimed to examine the quartz fine fraction using Raman spectroscopy and X-ray powder diffraction for the differentiation of soils from the Swan Coastal Plain, Western Australia.

The 785 nm wavelength laser used in the Raman spectroscopy caused strong fluorescence in the vast majority of samples, even when photo-bleaching and alternative substrates were used. Future work investigating alternative wavelengths and fluorescence suppression advancements are worth investigating. However, at this stage, the technique was deemed unsuitable for casework.

The examination of the laboratory-collected, historical XRPD percentage intensity data using multivariate statistics illustrated the ability to differentiate a large number of samples. It showed the strength in using primary and secondary minerals for differentiation. The specific minerals quartz, microcline feldspar, chloritised vermiculite, mica, gibbsite and goethite all contributed to the differentiation of samples, although issues with low counts and long analysis times hindered the results. The latest modern laboratory-based equipment is expected to highly increase the achievable counts as well as decrease the analysis speed.

The combination of the percentage intensity XRD data and PCA represents an advance in the application of XRD to sample discrimination. It has not been performed previously. Future work exploring the use of the full XRD pattern and multivariate statistics is recommended to remove the reliance on the initial percentage intensities, but optimisation of the normalisation process is needed.

The use of the powder diffraction beamline at the Australian Synchrotron further increased the achievable counts in very short analysis time. However, the complicated nature of the spectra, the need to obtain beam time and travel for analysis and the lack of quantification from the technique means that the benefits are outweighed by the drawbacks. Despite this, the dataset present an opportunity

for further work investigating differentiation using the whole pattern, fitted using Rietveld refinement and analysed using multivariate statistics.

Finally, the multivariate model developed from the laboratory-collected data presented in Chapter 3 was successfully applied to two case studies. The method allowed examination and comparison of recovered and control samples as well as assisted in the interpretation of the results. The successful application to casework illustrated the benefit in adding this method into a standard soil analysis protocol for sandy soils. This method will continue to be utilised in casework and will greatly assist in the reporting of soil cases in Western Australia.

References

1. Sangwan P, Nain T, Singal K, Hooda N, Sharma N. Soil as a tool of revelation in forensic science: a review. Analytical Methods. 2020;12(43):5150-9.

2. de Caritat P, Woods B, Simpson T, Nichols C, Hoogenboom L, Ilheo A, et al. Forensic soil provenancing in an urban/suburban setting: A sequential multivariate approach. Journal of Forensic Sciences. 2021;n/a(n/a).

3. Dawson LA, Mayes RW. Chapter 12 - Criminal and Environmental Soil Forensics: Soil as Physical Evidence in Forensic Investigations. Introduction to Environmental Forensics (Third Edition). San Diego: Academic Press; 2015. p. 457-86.

4. Skinner BJ. Dynamic earth / Brian J. Skinner, Stephen C. Porter, Jeffrey Park. 5th . ed. Porter SC, Park J, editors. Hoboken, New Jersey: Hoboken, New Jersey : Wiley; 2013.

5. Pitts K, Lewis S, Newland T. Forensic Analysis of Soil Evidence. Reference Module in Chemistry, Molecular Sciences and Chemical Engineering: Elsevier; 2018.

6. Johnson DL, Domier JEJ, Johnson DN. Reflections on the Nature of Soil and Its Biomantle. Annals of the Association of American Geographers. 2005;95(1):11-31.

7. Australia ESW. The Rock Cycle- Teachers Notes www.earthsciencewa.com.au: Earth Science Western Australia; 2019 [Available from: http://www.earthsciencewa.com.au/mod/resource/view.php?id=1435.

8. McQueen KG, Scott KM. Rock weathering and structure of the regolith. In: Scott KM, Pain CF, editors. Regolith Science. Victoria: CSIRO Publishing; 2009. p. 146-76.

9. Pillans B. Regolith through time. In: Scott K, Pain CF, editors. Regolith Science. Victoria: CSIRO PUBLISHING; 2009. p. 21-50.

10. Blake DH, Kilgour B. Geological Regions of Australia, 1:5 000 000 scale [Age-Class]. In: Australia G, editor. Canberra1998.

11. Taylor G, Butt CRM. The Australian regolith and mineral exploration. AGSO Journal of Australian Geology and Geophysics. 1998;17(4).

12. Gozzard JR. Geology and landforms of the Perth Region. Western Australia Geological Survey; 2007. p. 126.

13. Descourvieres C, Douglas G, Leyland L, Hartog N, Prommer H. Geochemical reconstruction of the provenance, weathering and deposition of detrital-dominated

sediments in the Perth Basin: The Cretaceous Leederville Formation, south-west Australia. Sedimentary Geology. 2011;236(1):62-76.

14. Taylor G, Eggleton RA, Holzhauer CC, Maconachie LA, Gordon M, Brown MC, et al. Cool Climate Lateritic and Bauxitic Weathering. The Journal of Geology. 1992;100(6):669-77.

15. Isbell RFa. The Australian soil classification / R.F. Isbell and the National Committee on Soil and Terrain. Second edition.. ed. National Committee on Soil and Terrain a, editor: Clayton South, VIC, Australia : CSIRO Publishing; 2016.

16. Publishing C. Australian soil and land survey field handbook / The National Committee on Soil and Terrain. 3rd ed.. ed. Collingwood, Vic.: Collingwood, Vic. : CSIRO Publishing; 2009.

17. Ashton LJ, McKenzie NJ. Conversion of the Atlas of Australian Soils to the Australian Soil Classification. In: mapping ASC, editor. https://www.asris.csiro.au/themes/Atlas.html: CSIRO Land and Water; 2001.

18. 3218.0 - Regional Population Growth, Australia, 2018-19. **Perth ERP at 30 June 2019**. accessed 13 June 2020 ed. https://www.abs.gov.au/AUSSTATS/abs@.nsf/mf/3218.0: Australian Bureau of Statistics; 2019.

19. Bioregional Assessment P. Interim Biogeographic Regionalisation for Australia (IBRA), Version 7 (Regions). data.gov.au; 2019.

20. Semeniuk V, Semeniuk CA. Human impacts on geoheritage features of the Swan Coastal Plain and coastal zone, southwestern Australia. In: Gostin V, editor. Gondwana to Greenhouse: Australian Environmental Geoscience. 21: Geological Society of Australia Special Publ. No. 21.; 2001. p. 181-99.

21. Kew GA, Gilkes RJ, Mathison CI. Nature and origins of granitic regolith in bauxite mine floors in the Darling Range, Western Australia. Australian Journal of Earth Sciences. 2008;55(4):473-92.

22. Veevers JJ, Powell CM, Johnson BD. Greater India's place in Gondwanaland and in Asia. Earth and Planetary Science Letters. 1975;27(3):383-7.

23. Turner BL, Lalibert, xe, Etienne. Soil Development and Nutrient Availability Along a 2 Million-Year Coastal Dune Chronosequence Under Species-Rich Mediterranean Shrubland in Southwestern Australia. Ecosystems. 2015;18(2):287-309.

24. McArthur WM. The development and distribution of the soils of the Swan Coastal Plain, Western Australia / by W.M. McArthur and E. Bettenay. 2nd printing.. ed. Bettenay E, Soils CDo, editors. Melbourne: Melbourne : Commonwealth Scientific and Industrial Research Organization, Australia; 1974.

25. Glassford DK. Late Cainozoic desert eolian sedimentation in Western Australia: Thesis (PhD)--University of Western Australia, 1980.; 1980.

26. Glassford DK, Semeniuk V. Desert-aeolian origin of late Cenozoic regolith in arid and semi-arid Southwestern Australia. Palaeogeography, Palaeoclimatology, Palaeoecology. 1995;114(2):131-66.

27. Davidson WA. Hydrogeology and groundwater resources of the Perth region, Western Australia / W. Angus Davidson. Perth: Thesis (Ph.D.)--Curtin University of Technology.; 1995.

28. MySoil: Ironstone gravels (Swan Coastal Plain) https://agric.wa.gov.au/n/4007: Government of Western Australia; 2015 [

29. Smolinski H. Soil assessment of the West Gingin area / by Henry Smolinski and Gottfried Scholz. Scholz G, Western Australia. Agriculture Western A, editors. South Perth, W.A.: South Perth, W.A. : Agriculture Western Australia; 1997.

30. McPherson A, Jones A. Appendix D: PERTH BASIN GEOLOGY REVIEW and SITE CLASS ASSESSMENT. In: Jones T, Middelmann M, Corby N, editors. Natural hazard risk in Perth, Western Australia : comprehensive report. Perth , W.A. : Geoscience Australia: Australia. Bureau of Meteorology.; Geoscience Australia.; Australia. Department of Industry, Tourism and Resources.; 2005.

31. Schoknecht NR. Soil groups of Western Australia : a simple guide to the main soils of Western Australia / compiled by Noel Schoknecht. Ed. 3. ed. Western Australia. Agriculture Western Australia. Natural Resources Assessment G, editor. South Perth [W.A.]: South Perth [W.A.] : Natural Resources Assessment Group, Dept. of Agriculture W.A.; 2002.

32. Salama RB, Silberstein R, Pollock D. Soils Characteristics of The Bassendean and Spearwood Sands of the Gnangara Mound (Western Australia) and their Controls On Recharge, Water Level Patterns and Solutes of The Superficial Aquifer. Water, Air, & Soil Pollution: Focus. 2005;5(1):3-26.

33. MySoil: Coloured deep sands (Swan Coastal Plain) https://agric.wa.gov.au/n/4006: Government of Western Australia; 2015 [

34. Vegetable crop nutrition on sandy soils of the Swan Coastal Plain https://www.agric.wa.gov.au/soil-productivity/vegetable-crop-nutrition-sandy-soils-swan-coastal-plain?page=0%2C1: Government of Western Australia; 2014 [

35. McArthur WM. Landforms and soils as an aid to urban planning in the Perth metropolitan northwest corridor, Western Australia / by W.M. McArthur and G.A. Bartle. Bartle GAja, Csiro, editors. Melbourne: Melbourne : Commonwealth Scientific and Industrial Research Organization; 1980.

36. Semeniuk V, Glassford DK. Significance of aeolian limestone lenses in quartz sand formations: an interdigitation of coastal and continental facies, Perth Basin, southwestern Australia. Sedimentary Geology. 1988;57(3):199-209.

37. Turner BL, Hayes PE, Laliberté E. A climosequence of chronosequences in southwestern Australia. European Journal of Soil Science. 2018;69(1):69-85.

38. Fitzpatrick RW. Soils. In: Siegel JA, Saukko PJ, Houck MM, editors. Encyclopedia of Forensic Sciences (Second Edition). Waltham: Academic Press; 2013. p. 206-12.

39. Jones T, Australia. Bureau of M, Geoscience A, Australia. Department of Industry TaR. Natural hazard risk in Perth, Western Australia : comprehensive report / compiled by T. Jones, M. Middelmann and N. Corby, Geoscience Australia. Perth, W.A.: Perth, W.A. : Geoscience Australia; 2005.

40. Allen DG, Mann S, Wilson IR. Managing Soil Nutrients in Residential Areas of the Swan Coastal Plain: A preliminary report. In: Natural Resources Chemistry Laboratory CCoW, editor.: Government of Western Australia; 2000. p. 35.

41. Prakongkep N, Gilkes RJ, Singh B, Wong S. Mineralogy and chemistry of sandy acid sulfate soils in the Perth metropolitan area of the Swan Coastal Plain. In: Conservation UoWADoEa, editor.: University of Western Australia; 2011.

42. Di Maggio RM, Donnelly L, Al Naimi KS, Barone P, Salvador F, Dawson L, et al. Global developments in forensic geology. Episodes. 2017;40(2):120-31.

43. Uniform Language for Testimony and Reports for the Forensic Geology Discipline. Adopted: 07/24/2018 ed. https://www.justice.gov/olp/uniform-language-testimony-and-reports: the United States Department of Justice; 2019. p. 4.

44. Bull PA, Morgan RM. Sediment Fingerprints: A forensic technique using quartz sand grains. Science & Justice. 2006;46(2):107-24.

45. Konopinski DI, Hudziak S, Morgan RM, Bull PA, Kenyon AJ. Investigation of quartz grain surface textures by atomic force microscopy for forensic analysis. Forensic Science International. 2012;223(1–3):245-55.

46. Cengiz S, Cengiz Karaca A, Çakır İ, Bülent Üner H, Sevindik A. SEM–EDS analysis and discrimination of forensic soil. Forensic Science International. 2004;141(1):33-7.

47. Demanèche S, Schauser L, Dawson L, Franqueville L, Simonet P. Microbial soil community analyses for forensic science: Application to a blind test. Forensic Science International. 2017;270:153-8.

48. Finley SJ, Benbow ME, Javan GT. Potential applications of soil microbial ecology and next-generation sequencing in criminal investigations. Applied Soil Ecology. 2015;88:69-78.

49. Habtom H, Demanèche S, Dawson L, Azulay C, Matan O, Robe P, et al. Soil characterisation by bacterial community analysis for forensic applications: A quantitative comparison of environmental technologies. Forensic Science International: Genetics. 2017;26:21-9.

50. Bruce RG, Dettmann ME. Palynological analyses of Australian surface soils and their potential in forensic science. Forensic Science International. 1996;81(2–3):77-94.

51. Stoney DA, Bowen AM, Stoney PL. Loss and replacement of small particles on the contact surfaces of footwear during successive exposures. Forensic Science International. 2016;269:78-88.

52. Stoney DA, Bowen AM, Ausdemore M, Stoney PL, Neumann C, Stoney FP. Differential analysis of very small particles (VSP) from the contact surfaces and recessed areas of footwear. Forensic Science International. 2019;298:106-14.

53. Murray KR, Fitzpatrick RW, Bottrill RS, Berry R, Kobus H. Soil transference patterns on bras: Image processing and laboratory dragging experiments. Forensic Science International. 2016;258:88-100.

54. Murray KR, Fitzpatrick RW, Bottrill R, Kobus H. Patterns produced when soil is transferred to bras by placing and dragging actions: The application of digital photography and image processing to support visible observations. Forensic Science International. 2017;276:24-40.

55. Committee AFSA. American Statistical Association Position on Statistical Statements for Forensic Evidence. American Statistical Association; 2019.

56. Cross AR. About Blood Types: Australian Red Cross Blood Service; 2019 [Available from: https://www.donateblood.com.au/learn/about-blood.

57. Promega. Probability of identity for various sets of STR loci, which illustrates the resolving power of different STR typing kits on the same DNA samples: Promega Australia; 2019 [Total N=1036, PowerPlex Fusion]. Available from: https://www.promega.com.au/products/pm/genetic-identity/population-statistics/power-of-discrimination/.

58. Palenik CS, Palenik S, Groves E. Microscopy Applications: Forensic Microscopy☆. Reference Module in Chemistry, Molecular Sciences and Chemical Engineering: Elsevier; 2018.

59. Robertson J. Crime Scene Considerations. In: Siegel JA, Saukko PJ, Houck MM, editors. Encyclopedia of Forensic Sciences (Second Edition). Waltham: Academic Press; 2013. p. 202-5.

60. Fitzpatrick RW, Raven MD. Guidelines for Conducting Criminal and Environmental Soil Forensic Investigations: Version 10.1. CAFSS_076 (Version 101): Centre for Australian Forensic Soil Science, CSIRO Land and Water Flagship; 2016.

61. Woods B. An examination procedure for forensic soil analysis in trace evidence laboratories: University of Canberra; 2014.

62. Woods B, Lennard C, Kirkbride KP, Robertson J. Soil examination for a forensic trace evidence laboratory–Part 3: A proposed protocol for the effective triage and management of soil examinations. Forensic Science International. 2016;262:46-55.

63. Ruffell A. Forensic Geoscience. In: Siegel JA, Saukko PJ, Houck MM, editors. Encyclopedia of Forensic Sciences (Second Edition). Waltham: Academic Press; 2013. p. 213-6.

64. Palenik S. Chapter 37 Heavy Minerals in Forensic Science. In: Mange MA, Wright DT, editors. Developments in Sedimentology. 58: Elsevier; 2007. p. 937-61.

65. Color M. Munsell Soil-Colour Charts. M50215B. Grand Rapids, MI: x-rite; 2009.

66. Woods B, Lennard C, Kirkbride KP, Robertson J. Soil examination for a forensic trace evidence laboratory—Part 1: Spectroscopic techniques. Forensic Science International. 2014;245:187-94.

67. Wentworth CK. A Scale of Grade and Class Terms for Clastic Sediments. The Journal of Geology. 1922;30(5):377-92.

68. Pye K, Blott SJ. Particle size analysis of sediments, soils and related particulate materials for forensic purposes using laser granulometry. Forensic Science International. 2004;144(1):19-27.

69. Asumadu K, Gilkes RJ, Churchward HM, Armitage TM. Detailed characterization of quartz grains in two sandy soils, Western Australia. Geoderma. 1987;41(1):29-47.

70. Vos K, Vandenberghe N, Elsen J. Surface textural analysis of quartz grains by scanning electron microscopy (SEM): From sample preparation to environmental interpretation. Earth-Science Reviews. 2014;128:93-104.

71. Maric M, van Bronswijk W, Lewis SW, Pitts K. Synchrotron FTIR characterisation of automotive primer surfacer paint coatings for forensic purposes. Talanta. 2014;118:156-61.

72. Maric M, van Bronswijk W, Pitts K, Lewis SW. Characterisation and classification of automotive clear coats with Raman spectroscopy and chemometrics for forensic purposes. Journal of Raman Spectroscopy. 2016;47(8):948-55.

73. Chauhan R, Kumar R, Sharma V. Soil forensics: A spectroscopic examination of trace evidence. Microchemical Journal. 2018;139:74-84.

74. Cox RJ, Peterson HL, Young J, Cusik C, Espinoza EO. The forensic analysis of soil organic by FTIR. Forensic Science International. 2000;108(2):107-16.

75. Post JL, Crawford SM. Uses of near-infared spectra for the identification of clay minerals. Applied Clay Science. 2014;95(0):383-7.

76. Štyriaková I, Mockovčiaková A, Štyriak I, Kraus I, Uhlík P, Madejová J, et al. Bioleaching of clays and iron oxide coatings from quartz sands. Applied Clay Science. 2012;61:1-7.

77. Armenta S, de la Guardia M. Vibrational spectroscopy in soil and sediment analysis. Trends in Environmental Analytical Chemistry. 2014;2:43-52.

78. Frost RL, Fredericks PM, Bartlett JR. Fourier transform Raman spectroscopy of kandite clays. Spectrochimica Acta Part A: Molecular Spectroscopy. 1993;49(5):667-74.

79. Kammrath BW, Koutrakos A, Castillo J, Langley C, Huck-Jones D. Morphologically-directed Raman spectroscopy for forensic soil analysis. Forensic Science International. 2018;285:e25-e33.

80. Kloprogge JT. Chapter 6 - Raman Spectroscopy of Clay Minerals. In: Gates WP, Kloprogge JT, Madejová J, Bergaya F, editors. Developments in Clay Science. 8: Elsevier; 2017. p. 150-99.

81. Bong WSK, Nakai I, Furuya S, Suzuki H, Abe Y, Osaka K, et al. Development of heavy mineral and heavy element database of soil sediments in Japan using synchrotron radiation X-ray powder diffraction and high-energy (116 keV) X-ray fluorescence analysis: 1. Case study of Kofu and Chiba region. Forensic Science International. 2012;220(1–3):33-49.

82. Woods B, Paul Kirkbride K, Lennard C, Robertson J. Soil examination for a forensic trace evidence laboratory – Part 2: Elemental analysis. Forensic Science International. 2014;245:195-201.

83. Uitdehaag S, Wiarda W, Donders T, Kuiper I. Forensic Comparison of Soil Samples Using Nondestructive Elemental Analysis. Journal of forensic sciences. 2017;62(4):861-8.

84. Pirrie D, Rollinson GK, Andersen JC, Wootton D, Moorhead S. Soil forensics as a tool to test reported artefact find sites. Journal of Archaeological Science. 2014;41:461-73.

85. Rollinson G. Automated Mineralogy by SEM-EDS. Reference Module in Earth Systems and Environmental Sciences: Elsevier; 2019.

86. Catterick T, Hickman DA. Sequential multi-element analysis of small fragments of glass by atomic-emission spectrometry using an inductively coupled radiofrequency argon plasma source. The Analyst. 1979;104(1239):516-24.

87. Catterick T, Hickman DA. The quantitative analysis of glass by inductively coupled plasma-atomic-emission spectrometry: A five-element survey. Forensic Science International. 1981;17(3):253-63.

88. Locke J. The application of plasma source atomic emission spectrometry in forensic science. Analytica Chimica Acta. 1980;113(1):3-12.

89. Tanaka T, Hara K, Tanimoto A, Kasai K, Kita T, Tanaka N, et al. Determination of arsenic in blood and stomach contents by inductively coupled plasma/mass spectrometry (ICP/MS). Forensic Science International. 1996;81(1):43-50.

90. Waring PM, Watling RJ. Rare earth deposits in a deceased movie projectionist: A new case of rare earth pneumoconiosis? Medical Journal of Australia. 1990;153(11-12):726-30.

91. Watling RJ, Herbert HK, Delev D, Abell ID. Gold fingerprinting by laser ablation inductively coupled plasma mass spectrometry. Spectrochimica Acta Part B: Atomic Spectroscopy. 1994;49(2):205-19.

92. PerkinElmer. The 30-Minute Guide to ICP-MS. In: Inc. P, editor. https://wwwperkinelmercom/CMSResources/Images/44-74849tch_icpmsthirtyminuteguidepdf. accessed 13 June 2020 ed. Waltham, MA 02451 USA2004.

93. Houck MM, Siegel JA. Chapter 17 - Soil and Glass. Fundamentals of Forensic Science (Third Edition). San Diego: Academic Press; 2015. p. 427-50.

94. Pye K, Blott SJ, Wray DS. Elemental analysis of soil samples for forensic purposes by inductively coupled plasma spectrometry — precision considerations. Forensic Science International. 2006;160(2–3):178-92.

95. Pye K, Blott SJ. Development of a searchable major and trace element database for use in forensic soil comparisons. Science & Justice. 2009;49(3):170-81.

96. Reidy L, Bu K, Godfrey M, Cizdziel JV. Elemental fingerprinting of soils using ICP-MS and multivariate statistics: A study for and by forensic chemistry majors. Forensic Science International. 2013;233(1–3):37-44.

97. Mayes RW, Macdonald LM, Ross JM, Dawson LA. Discrimination of Domestic Garden Soils Using Plant Wax Compounds as Markers. In: Ritz K, Dawson L, Miller D, editors. Criminal and Environmental Soil Forensics. Dordrecht: Springer Netherlands; 2009. p. 463-76.

98. Kononova MM. CHAPTER 8 - METHODS OF INVESTIGATING SOIL ORGANIC MATTER. In: Kononova MM, editor. Soil Organic Matter (Second Edition): Pergamon; 1966. p. 377-426.

99. Semenov VM, Tulina AS, Semenova NA, Ivannikova LA. Humification and nonhumification pathways of the organic matter stabilization in soil: A review. Eurasian Soil Science. 2013;46(4):355-68.

100. Dawson LA, Hillier S. Measurement of soil characteristics for forensic applications. Surface and Interface Analysis. 2010;42(5):363-77.

101. McCulloch G, Dawson LA, Brewer MJ, Morgan RM. The identification of markers for Geoforensic HPLC profiling at close proximity sites. Forensic Science International. 2017;272:127-41.

102. Pye K, Blott SJ, Croft DJ, Carter JF. Forensic comparison of soil samples: Assessment of small-scale spatial variability in elemental composition, carbon and nitrogen isotope ratios, colour, and particle size distribution. Forensic Science International. 2006;163(1–2):59-80.

103. Santoiemma G. Recent methodologies for studying the soil organic matter. Applied Soil Ecology. 2018;123:546-50.

104. Habtom H, Pasternak Z, Matan O, Azulay C, Gafny R, Jurkevitch E. Applying microbial biogeography in soil forensics. Forensic Science International: Genetics. 2019;38:195-203.

105. Khodakova AS, Burgoyne L, Abarno D, Linacre A. Forensic analysis of soils using single arbitrarily primed amplification and high throughput sequencing. Forensic Science International: Genetics Supplement Series. 2013;4(1):e39-e40.

106. Khodakova AS, Burgoyne L, Abarno D, Linacre A. Robust and reliable DNA typing of soils. Forensic Science International: Genetics Supplement Series. 2015;5:e330-e1.

107. Yu L-R, Stewart NA, Veenstra TD. Chapter 8 - Proteomics: The Deciphering of the Functional Genome. In: Ginsburg GS, Willard HF, editors. Essentials of Genomic and Personalized Medicine. San Diego: Academic Press; 2010. p. 89-96.

108. Pitts KM, Clarke RM. The forensic discrimination of quartz sands from the Swan Coastal Plain, Western Australia. Forensic Science International: Reports. 2020;2:100130.

109. Isphording WC. Chapter 38 Forensic Use of Heavy Minerals in Civil and Criminal Investigations. In: Mange MA, Wright DT, editors. Developments in Sedimentology. 58: Elsevier; 2007. p. 963-82.

110. Marumo Y, Nagatsuka S, Oba Y. Clay Mineralogical Analysis Using the <0.05-mm Fraction for Forensic Science Investigation—Its Application to Volcanic Ash Soils and Yellow-Brown Forest Soils. 1986.

111. Marumo Y, Nagatsuka S, Oba Y. Rapid Clay Mineralogical Analysis for Forensic Science Investigation—Clay Mineralogy Over the Short Distances. 1988.

112. Corrêa RS, Melo VF, Abreu GGF, Sousa MH, Chaker JA, Gomes JA. Soil forensics: How far can soil clay analysis distinguish between soil vestiges? Science & Justice. 2018;58(2):138-44.

113. Clarke R, Bastian L. The Forensic Comparison of Sandy Soils Using Associated Clay and Heavy Mineral Assemblages as Indicators of Provenance. Perth, Western Australia: Chemistry Centre of Western Australia for the National Institute of Forensic Science; 2004.

114. Clarke R, Allen D. Soil and Related Substances. In: Freckelton I, Selby H, editors. Expert Evidence. Pyrmont, N.S.W.: Thomson Reuters; 2010.

115. Hussain CM, Rawtani D, Pandey G, Tharmavaram M. Chapter 7 - Raman spectroscopy in forensic science. In: Hussain CM, Rawtani D, Pandey G, Tharmavaram M, editors. Handbook of Analytical Techniques for Forensic Samples: Elsevier; 2021. p. 109-28.

116. Pasteris JD, Beyssac O. Welcome to Raman Spectroscopy: Successes, Challenges, and Pitfalls. Elements. 2020;16(2):87-92.

117. Smith WE. Raman Scattering. Kirk-Othmer Encyclopedia of Chemical Technology. 2017.

118. Lafuente B, Downs R T, Yang H, N S. The power of databases: the RRUFF project. In: Armbruster TaD, R. M., editor. Highlights in Mineralogical Crystallography. Berlin, Germany: W. De Gruyter; 2015. p. 1-30.

119. Kavkler K, Demšar A. Examination of cellulose textile fibres in historical objects by micro-Raman spectroscopy. Spectrochimica Acta Part A: Molecular and Biomolecular Spectroscopy. 2011;78(2):740-6.

120. Moore DM, Reynolds RC. X-ray diffraction and the identification and analysis of clay minerals. 2nd ed.. ed. Oxford ; New York: Oxford ; New York : Oxford University Press ©1989; 1989.

121. Brindley GW, Brown G. Crystal structures of clay minerals and their X-ray identification. Brindley GW, Brown G, editors. London: Mineralogical Society; 1980.

122. Bastian LV. The dune systems of the Swan Coastal Plain: Subdivision based on mineral trends in the surface soils. Chemistry Centre of WA; 1994.

123. Bastian LV. Residual soil mineralogy and dune subdivision, Swan Coastal Plain, Western Australia. Australian Journal of Earth Sciences. 1996;43(1):31-44.

124. Gozzard JR. Sea to scarp — geology, landscape, and land use planning in the southern Swan Coastal Plain. Geological Survey of Western Australia; 2010. p. 72.

125. Wang A, Freeman J, Kuebler KE. Raman Spectroscopic Characterization of Phyllosilicates. Lunar and Planetary Science XXXIII2002.

126. Wang A, J. Freeman J, Jolliff B. Understanding the Raman spectral features of phyllosilicates2015.

127. Ochando J, Munuera M, Carrión JS, Fernández S, Amorós G, Recalde J. Forensic palynology revisited: Case studies from semi-arid Spain. Review of Palaeobotany and Palynology. 2018;259:29-38.

128. Ltd RP. "WiRE" software for Raman Spectroscopy. Quartz. United Kingdom2012.

129. Kaelble EF. Handbook of x-rays : for diffraction, emission, absorption and microscopy / edited by Emmett f. Kaelble. New York: New York : McGraw-Hill; 1967.

130. Mendlein A, Szkudlarek C, Goodpaster JV. Chemometrics. In: Siegel JA, Saukko PJ, Houck MM, editors. Encyclopedia of Forensic Sciences (Second Edition). Waltham: Academic Press; 2013. p. 646-51.

131. Sauzier GY. Applications of chemometrics to the analysis and interpretation of forensic physical evidence 2016.

132. Massart DL, Vandeginste BGM, Deming SN, Michotte Y, Kaufman L. Chemometrics : a textbook. Vandeginste BGM, Kaufman L, editors. Amsterdam: Amsterdam : Elsevier; 1988.

133. Miller JNa. Statistics and chemometrics for analytical chemistry / James N. Miller, Jane C. Miller, Robert D. Miller. Seventh edition. ed. Miller JCa, Miller RDa, editors: Harlow, United Kingdom : Pearson Education Limited; 2018.

134. ANSTO. The Australian Synchrotron https://www.ansto.gov.au/research/facilities/australian-synchrotron/overview: ANSTO; 2020 [

135. Kempson IM, Paul Kirkbride K, Skinner WM, Coumbaros J. Applications of synchrotron radiation in forensic trace evidence analysis. Talanta. 2005;67(2):286-303.

136. ANSTO. AUSTRALIAN SYNCHROTRON BEAMLINES: Powder Diffraction https://www.ansto.gov.au/user-access/instruments/australian-synchrotron-beamlines/powder-diffraction: ANSTO; 2020 [

137. Tapia-Ruiz N, Dose WM, Sharma N, Chen H, Heath J, Somerville JW, et al. High voltage structural evolution and enhanced Na-ion diffusion in P2-Na2/3Ni1/3−xMgxMn2/3O2 (0 ≤ x ≤ 0.2) cathodes from diffraction, electrochemical and ab initio studies. Energy & Environmental Science. 2018;11(6):1470-9.

138. Reynolds E, Avdeev M, Thorogood GJ, Poineau F, Czerwinski KR, Kimpton JA, et al. Structure and magnetism in Sr1-x Ax TcO3 perovskites: Importance of the A-site cation. Physical Review B. 2017;95(5):054430.

139. Tomkins AG, Bowlt L, Genge M, Wilson SA, Brand HEA, Wykes JL. Ancient micrometeorites suggestive of an oxygen-rich Archaean upper atmosphere. Nature. 2016;533(7602):235-8.

140. Gates-Rector S, Blanton T. The Powder Diffraction File: a quality materials characterization database. Powder Diffraction. 2019;34(4):352-60.

141. Brindley GW, Brown G, Mineralogical S, Clay Minerals G. The X-ray identification and crystal structures of clay minerals. London: Mineralogical Society, Clay Minerals Group; 1961.

142. McArthur WM, Bartle GA, cartographers. Landforms and Soils of the Perth Metropolitan North-West Corridor- Western Australia: CSIRO Division of Land Resources Management, Printed by the Government Printer, Western Australia; 1979.

APPENDICES

Appendix A XRPD raw counts and percentage intensities for XRPD from Chapter 3 in Section 3.3.2 [page 145 to 155]

XRD FILE	Description	Group for ALL	V1	K1	Gibb1	K2	goe1	SUB TOTAL	M1	Q1	F1	Trad. TOTAL	% V1	% K1	% Gibb1	% K2	% goe1	%M1	% Q1	% F1
2F135406	45K SW SOUTHERN CROSS	Alluvial/ Lateritic	144	15779	0	2438	1988	20349	103	18250	935	39637	0.7	77.5	0.0	12.0	9.8	0.3	46.0	2.4
2F135409	66K NNW WUBIN	Alluvial/ Lateritic	117	19701	0	2023	1971	23812	191	15326	786	40115	0.5	82.7	0.0	8.5	8.3	0.5	38.2	2.0
2F135412	7.2K NNE WONGAN HILLS	Alluvial/ Lateritic	0	10736	0	2039	1640	14415	0	4031	952	19398	0.0	74.5	0.0	14.1	11.4	0.0	20.8	4.9
2F135403	7.5K NNE WONGAN HILLS	Alluvial/ Lateritic	0	23674	0	2176	2498	28348	0	6677	1907	36932	0.0	83.5	0.0	7.7	8.8	0.0	18.1	5.2
HELENA1	All1	Alluvial/ Lateritic	88	2192	202	1236	877	4595	510	5012	840	10957	1.9	47.7	4.4	26.9	19.1	4.7	45.7	7.7
HELENA2	All2	Alluvial/ Lateritic	207	5401	270	2416	1505	9799	949	9622	1456	21826	2.1	55.1	2.8	24.7	15.4	4.3	44.1	6.7
HELENA3	All3	Alluvial/ Lateritic	133	6053	230	1881	1165	9462	2245	13543	6176	31426	1.4	64.0	2.4	19.9	12.3	7.1	43.1	19.7
HELENA4	All4	Alluvial/ Lateritic	128	7485	429	2299	2055	12396	642	11957	2192	27187	1.0	60.4	3.5	18.5	16.6	2.4	44.0	8.1
HELENA5	All5	Alluvial/ Lateritic	165	12324	260	2964	3086	18799	2062	24800	4043	49704	0.9	65.6	1.4	15.8	16.4	4.1	49.9	8.1
HELENA6	All6	Alluvial/ Lateritic	452	19975	3222	2212	2998	28859	463	17550	3341	50213	1.6	69.2	11.2	7.7	10.4	0.9	35.0	6.7
HELENA7	All7	Alluvial/ Lateritic	0	21173	489	2238	1846	25746	1387	12034	2296	41463	0.0	82.2	1.9	8.7	7.2	3.3	29.0	5.5
HELENA8	All8	Alluvial/ Lateritic	0	8409	338	3184	2859	14790	1436	8881	1275	26382	0.0	56.9	2.3	21.5	19.3	5.4	33.7	4.8
0F25082R	D2 AUGEN GNEISS	Alluvial/ Lateritic	586	4715	1109	986	561	7957	2096	30637	5267	45957	7.4	59.3	13.9	12.4	7.1	4.6	66.7	11.5

0F25083R	D3 QTZ-FELD-BIOTITE GNEISS	Alluvial/ Lateritic	446	6870	8006	870	1028	17220	2653	6254	326	26453	2.6	39.9	46.5	5.1	6.0	10.0	23.6	1.2
0F25084R	D4 DONNYBROOK SST	Alluvial/ Lateritic	554	3148	501	425	270	4898	5518	5628	1330	17374	11.3	64.3	10.2	8.7	5.5	31.8	32.4	7.7
0F25085R	D5 DONNYBROOK SST	Alluvial/ Lateritic	2090	9557	3086	983	749	16465	320	5403	664	22852	12.7	58.0	18.7	6.0	4.5	1.4	23.6	2.9
NA320UM	NA3	Bassendean System	103	3411	3544	1081	1153	9292	87	24469	5865	39713	1.1	36.7	38.1	11.6	12.4	0.2	61.6	14.8
NA520UM	NA5	Bassendean System	45	308	0	0	0	353	0	19251	245	19849	12.7	87.3	0.0	0.0	0.0	0.0	97.0	1.2
NA520UMX	NA5 rep	Bassendean System	198	464	0	0	0	662	0	102781	1139	104582	29.9	70.1	0.0	0.0	0.0	0.0	98.3	1.1
NB520UM	NB5	Bassendean System	112	660	1576	449	405	3202	0	21590	522	25314	3.5	20.6	49.2	14.0	12.6	0.0	85.3	2.1
NBC420UM	NBC4	Bassendean System	164	1024	458	376	418	2440	87	30775	1946	35248	6.7	42.0	18.8	15.4	17.1	0.2	87.3	5.5
NC620UM	NC6	Bassendean System	0	380	0	74	76	530	129	36706	1694	39059	0.0	71.7	0.0	14.0	14.3	0.3	94.0	4.3
NC620UMX	NC6 rep	Bassendean System	0	626	0	0	0	626	0	77236	1632	79494	0.0	100.0	0.0	0.0	0.0	0.0	97.2	2.1
ND720UM	ND7	Bassendean System	87	867	784	450	574	2762	0	14860	2962	20584	3.1	31.4	28.4	16.3	20.8	0.0	72.2	14.4
ND820UM	ND8	Bassendean System	0	196	85	117	0	398	0	35155	291	35844	0.0	49.2	21.4	29.4	0.0	0.0	98.1	0.8
ND820UMR	ND8 rep	Bassendean System	0	393	243	352	455	1443	0	42095	428	43966	0.0	27.2	16.8	24.4	31.5	0.0	95.7	1.0
ND8A20UM	ND8A	Bassendean System	0	87	0	0	0	87	0	67790	494	68371	0.0	100.0	0.0	0.0	0.0	0.0	99.2	0.7
ND8A20UR	ND8A rep	Bassendean System	0	146	0	0	0	146	0	145733	728	146607	0.0	100.0	0.0	0.0	0.0	0.0	99.4	0.5
NE320UM	NE3	Bassendean System	0	93	0	0	0	93	0	39530	678	40301	0.0	100.0	0.0	0.0	0.0	0.0	98.1	1.7
NE320URX	NE3 rep	Bassendean System	132	203	0	0	0	335	0	197995	2414	200744	39.4	60.6	0.0	0.0	0.0	0.0	98.6	1.2
NE420UM	NE4	Bassendean System	0	0	0	0	0	0	0	56986	2510	59496	0.0	0.0	0.0	0.0	0.0	0.0	95.8	4.2
NE420URR	NE4 rep	Bassendean System	0	0	0	0	0	0	0	61122	430	61552	0.0	0.0	0.0	0.0	0.0	0.0	99.3	0.7

SA320UM	SA3	Bassendean System	51	456	298	190	226	1221	77	31313	2353	34964	4.2	37.3	24.4	15.6	18.5	0.2	89.6	6.7
SA6B20UM	SA6B	Bassendean System	0	114	0	0	0	114	0	20704	1088	21906	0.0	100.0	0.0	0.0	0.0	0.0	94.5	5.0
SA6B20UX	SA6B rep	Bassendean System	170	503	0	0	0	673	0	71480	4651	76804	25.3	74.7	0.0	0.0	0.0	0.0	93.1	6.1
SB120UM	SB1	Bassendean System	0	313	404	178	894	1789	0	54657	358	56804	0.0	17.5	22.6	9.9	50.0	0.0	96.2	0.6
SB120UMR	SB1 rep	Bassendean System	0	276	255	129	524	1184	0	35560	919	37663	0.0	23.3	21.5	10.9	44.3	0.0	94.4	2.4
SB120UKX	SB1 rep2	Bassendean System	202	1432	1567	759	3421	7381	0	162706	1265	171352	2.7	19.4	21.2	10.3	46.3	0.0	95.0	0.7
SB520UM	SB5	Bassendean System	0	81	0	0	0	81	0	20029	372	20482	0.0	100.0	0.0	0.0	0.0	0.0	97.8	1.8
SB520KR	SB5 rep	Bassendean System	183	282	0	0	0	465	134	171615	1085	173299	39.4	60.6	0.0	0.0	0.0	0.1	99.0	0.6
SB620UM	SB6	Bassendean System	88	427	616	241	692	2064	0	26509	1222	29795	4.3	20.7	29.8	11.7	33.5	0.0	89.0	4.1
SC720UM	SC7	Bassendean System	130	977	1386	350	558	3401	0	14097	1625	19123	3.8	28.7	40.8	10.3	16.4	0.0	73.7	8.5
CASU20UM	SD1	Bassendean System	0	57	0	0	0	57	0	28755	177	28989	0.0	100.0	0.0	0.0	0.0	0.0	99.2	0.6
SD120KR	SD1 rep	Bassendean System	185	339	0	204	187	915	246	265344	2358	268863	20.2	37.0	0.0	22.3	20.4	0.1	98.7	0.9
WELL20UM	SDE3	Bassendean System	99	777	1340	457	905	3578	0	32913	550	37041	2.8	21.7	37.5	12.8	25.3	0.0	88.9	1.5
SE220UM	SE2	Bassendean System	312	2205	130	524	708	3879	93	22857	20830	47659	8.0	56.8	3.4	13.5	18.3	0.2	48.0	43.7
SF420UM	SF4	Bassendean System	169	787	704	211	0	1871	58	26140	7561	35630	9.0	42.1	37.6	11.3	0.0	0.2	73.4	21.2
91M5781	CORONATION 0-10CM	Coastal limestone	0	4931	0	1967	3221	10119	158	8707	3556	22540	0.0	48.7	0.0	19.4	31.8	0.7	38.6	15.8
91M5788	CORONATION 160-195CM	Coastal limestone	339	11618	225	1479	3406	17067	138	4308	1302	22815	2.0	68.1	1.3	8.7	20.0	0.6	18.9	5.7
91M5785	CORONATION 60-90CM	Coastal limestone	227	12693	206	2494	5009	20629	110	9357	4573	34669	1.1	61.5	1.0	12.1	24.3	0.3	27.0	13.2
9KARRDGB	GOODE BEACH, Albany -9 Karrakatta Rd	Coastal limestone	233	764	1736	0	411	3144	0	3762	824	7730	7.4	24.3	55.2	0.0	13.1	0.0	48.7	10.7
SHELLY01	WEST CAPE HOWE -cliff	Coastal limestone	233	331	403	111	289	1367	0	6087	1273	8727	17.0	24.2	29.5	8.1	21.1	0.0	69.7	14.6

	above Shelly Beach																		
3116043R	21m elevation carpark end Pipidinny Road	Quindalup-Spearwood	62	587	0	147	80	876	1041	5581	6253	13751	7.1	67.0	0.0	16.8	9.1	7.6	40.6	45.5
116007SS	E 10M W body -30cm-slow scan	Quindalup-Spearwood	680	2407	441	185	299	4012	0	7936	8525	20473	16.9	60.0	11.0	4.6	7.5	0.0	38.8	41.6
116006SS	E 10M W of body - slow scan	Quindalup-Spearwood	415	2099	586	618	875	4593	0	13857	5004	23454	9.0	45.7	12.8	13.5	19.1	0.0	59.1	21.3
116008SS	E 20M W of body - slow scan	Quindalup-Spearwood	242	1020	210	161	261	1894	0	2393	2530	6817	12.8	53.9	11.1	8.5	13.8	0.0	35.1	37.1
116004SS	E 2M E of body - slow scan	Quindalup-Spearwood	551	2236	444	559	570	4360	300	13814	15837	34311	12.6	51.3	10.2	12.8	13.1	0.9	40.3	46.2
116002SS	E 2M N of body - slow scan	Quindalup-Spearwood	574	2514	717	852	1032	5689	0	15105	3009	23803	10.1	44.2	12.6	15.0	18.1	0.0	63.5	12.6
116003SS	E 2M S of body - slow scan	Quindalup-Spearwood	300	1617	343	541	730	3531	0	25745	20416	49692	8.5	45.8	9.7	15.3	20.7	0.0	51.8	41.1
116005SS	E 2M W of body - slow scan	Quindalup-Spearwood	465	2421	488	536	572	4482	0	9799	21607	35888	10.4	54.0	10.9	12.0	12.8	0.0	27.3	60.2
116009SS	E 30M W body - slow scan	Quindalup-Spearwood	523	1717	282	137	295	2954	115	14425	10762	28256	17.7	58.1	9.5	4.6	10.0	0.4	51.1	38.1
3F116022	E grid A4	Quindalup-Spearwood	521	1535	294	332	529	3211	0	9989	4347	17547	16.2	47.8	9.2	10.3	16.5	0.0	56.9	24.8
C1VSLOW	E grid C1 v slow	Quindalup-Spearwood	507	2931	804	549	1000	5791	247	34746	12257	53041	8.8	50.6	13.9	9.5	17.3	0.5	65.5	23.1
3F116024	E grid C2	Quindalup-Spearwood	369	1975	444	451	608	3847	195	23014	20012	47068	9.6	51.3	11.5	11.7	15.8	0.4	48.9	42.5
3F116025	E grid C2F	Quindalup-Spearwood	167	606	146	133	242	1294	490	10764	33347	45895	12.9	46.8	11.3	10.3	18.7	1.1	23.5	72.7
3F116026	E grid C3	Quindalup-Spearwood	600	2267	531	413	630	4441	114	13057	19092	36704	13.5	51.0	12.0	9.3	14.2	0.3	35.6	52.0
3F116027	E grid C4	Quindalup-Spearwood	468	2103	311	427	632	3941	209	10331	5528	20009	11.9	53.4	7.9	10.8	16.0	1.0	51.6	27.6
3F116028	E grid D1	Quindalup-Spearwood	302	1015	319	158	288	2082	0	11616	6114	19812	14.5	48.8	15.3	7.6	13.8	0.0	58.6	30.9
3F116029	E grid D2	Quindalup-Spearwood	559	2238	559	375	651	4382	303	12050	15594	32329	12.8	51.1	12.8	8.6	14.9	0.9	37.3	48.2

3F116030	E grid D2F	Quindalup-Spearwood	363	923	314	229	315	2144	0	11400	16261	29805	16.9	43.1	14.6	10.7	14.7	0.0	38.2	54.6
3F116031	E grid D3	Quindalup-Spearwood	560	2715	729	806	1014	5824	0	15857	12847	34528	9.6	46.6	12.5	13.8	17.4	0.0	45.9	37.2
3F116032	E grid D4	Quindalup-Spearwood	403	1519	282	490	573	3267	211	9405	8388	21271	12.3	46.5	8.6	15.0	17.5	1.0	44.2	39.4
3F116033	E grid D5	Quindalup-Spearwood	393	2036	513	734	919	4595	147	13762	7161	25665	8.6	44.3	11.2	16.0	20.0	0.6	53.6	27.9
3F116034	E grid D5A	Quindalup-Spearwood	447	1858	530	732	904	4471	371	19172	15041	39055	10.0	41.6	11.9	16.4	20.2	0.9	49.1	38.5
3F116018	E grid Z5	Quindalup-Spearwood	265	1569	300	250	411	2795	166	14981	8213	26155	9.5	56.1	10.7	8.9	14.7	0.6	57.3	31.4
3F116006	E scene 10M W of body	Quindalup-Spearwood	148	598	157	152	205	1260	61	3368	2244	6933	11.7	47.5	12.5	12.1	16.3	0.9	48.6	32.4
3F116008	E scene 20M W of body	Quindalup-Spearwood	107	288	0	66	85	546	0	960	428	1934	19.6	52.7	0.0	12.1	15.6	0.0	49.6	22.1
3F116004	E scene 2M E of body	Quindalup-Spearwood	164	602	123	121	135	1145	74	3001	5137	9357	14.3	52.6	10.7	10.6	11.8	0.8	32.1	54.9
3F116002	E scene 2M N of body	Quindalup-Spearwood	181	763	181	213	282	1620	0	5170	507	7297	11.2	47.1	11.2	13.1	17.4	0.0	70.9	6.9
3F116003	E scene 2M S of body	Quindalup-Spearwood	89	478	109	134	199	1009	0	4941	3885	9835	8.8	47.4	10.8	13.3	19.7	0.0	50.2	39.5
3F116005	E scene 2M W of body	Quindalup-Spearwood	163	649	150	152	188	1302	0	1650	4120	7072	12.5	49.8	11.5	11.7	14.4	0.0	23.3	58.3
3F116010	E scene Pipidinny Rd cutting	Quindalup-Spearwood	109	258	72	37	43	519	101	393	938	1951	21.0	49.7	13.9	7.1	8.3	5.2	20.1	48.1
116010SS	E scene Pipidinny Rd cutting - slow scan	Quindalup-Spearwood	290	871	163	251	0	1575	158	1238	4212	7183	18.4	55.3	10.3	15.9	0.0	2.2	17.2	58.6
3F116007	E scene sc. 10M W of body (30 cm)	Quindalup-Spearwood	189	653	99	47	101	1089	51	1899	1854	4893	17.4	60.0	9.1	4.3	9.3	1.0	38.8	37.9
3F116009	E scene scene 30M W of body (track)	Quindalup-Spearwood	163	427	93	0	0	683	0	9102	2572	12357	23.9	62.5	13.6	0.0	0.0	0.0	73.7	20.8
3F116039	Grid square B2, E scene	Quindalup-Spearwood	172	616	138	235	357	1518	0	8371	4948	14837	11.3	40.6	9.1	15.5	23.5	0.0	56.4	33.3
3F116038	Grid square B3, E scene	Quindalup-Spearwood	277	916	235	173	207	1808	196	4929	3614	10547	15.3	50.7	13.0	9.6	11.4	1.9	46.7	34.3

3F116037	Grid square B4, 14m NW body location Egl	Quindalup-Spearwood	323	717	246	167	224	1677	47	3273	4519	9516	19.3	42.8	14.7	10.0	13.4	0.5	34.4	47.5
3F116042	Grid square B6, E scene	Quindalup-Spearwood	367	892	290	163	279	1991	65	3379	1629	7064	18.4	44.8	14.6	8.2	14.0	0.9	47.8	23.1
3F116040	Grid square C6, E scene	Quindalup-Spearwood	351	981	320	347	487	2486	199	10607	6366	19658	14.1	39.5	12.9	14.0	19.6	1.0	54.0	32.4
3F116041	Grid square D6, E scene	Quindalup-Spearwood	319	848	275	298	319	2059	20	8684	5791	16554	15.5	41.2	13.4	14.5	15.5	0.1	52.5	35.0
3116044R	Pipidinny Road toward carpark	Quindalup-Spearwood	0	555	91	169	0	815	198	4203	4227	9443	0.0	68.1	11.2	20.7	0.0	2.1	44.5	44.8
3116048X	QP ref soil from Gibson Park Pinnaroo Valley	Quindalup-Spearwood	299	2860	475	534	0	4168	949	30665	10840	46622	7.2	68.6	11.4	12.8	0.0	2.0	65.8	23.3
RH71SLOW	RH71 E scene track - slow scan	Quindalup-Spearwood	372	1506	208	166	303	2555	277	8884	5025	16741	14.6	58.9	8.1	6.5	11.9	1.7	53.1	30.0
RH72SLOW	RH72 E scene track - slow scan	Quindalup-Spearwood	352	930	181	186	307	1956	0	11276	6672	19904	18.0	47.5	9.3	9.5	15.7	0.0	56.7	33.5
RH73SLOW	RH73 E scene body location - slow scan	Quindalup-Spearwood	519	1975	428	598	729	4249	144	12225	23699	40317	12.2	46.5	10.1	14.1	17.2	0.4	30.3	58.8
MEH1	MelonHill1	Quindalup System	0	1223	337	180	0	1740	395	35321	12770	50226	0.0	70.3	19.4	10.3	0.0	0.8	70.3	25.4
MEH2	MelonHill2	Quindalup System	182	665	178	260	95	1380	152	9855	2049	13436	13.2	48.2	12.9	18.8	6.9	1.1	73.3	15.3
SWB1	Swanbourne1	Quindalup System	0	1177	428	225	126	1956	542	22495	12380	37373	0.0	60.2	21.9	11.5	6.4	1.5	60.2	33.1
SWB2	Swanbourne2	Quindalup System	0	2659	371	209	172	3411	727	56057	21011	81206	0.0	78.0	10.9	6.1	5.0	0.9	69.0	25.9
SWB3	Swanbourne3	Quindalup System	121	2440	311	151	66	3089	770	30925	19053	53837	3.9	79.0	10.1	4.9	2.1	1.4	57.4	35.4
SWB4	Swanbourne4	Quindalup System	244	2943	485	358	255	4285	1494	33495	23068	62342	5.7	68.7	11.3	8.4	6.0	2.4	53.7	37.0
11AMB50S	50m 11AMB	Mixed Origin	62	248	0	142	159	611	63	13299	14872	28845	10.1	40.6	0.0	23.2	26.0	0.2	46.1	51.6
11AMB50SC	50m 11AMB rep	Mixed Origin	269	1327	0	557	517	2670	221	56236	26324	85451	10.1	49.7	0.0	20.9	19.4	0.3	65.8	30.8
RC130403	97F-038	Mixed Origin	179	801	71	141	0	1192	63	32933	13790	47978	15.0	67.2	6.0	11.8	0.0	0.1	68.6	28.7

RC130404	97F-039	Mixed Origin	0	209	0	120	108	437	71	11996	8545	21049	0.0	47.8	0.0	27.5	24.7	0.3	57.0	40.6
RC13044R	97F-039 rep	Mixed Origin	205	1071	0	548	265	2089	0	71677	23742	97508	9.8	51.3	0.0	26.2	12.7	0.0	73.5	24.3
HWYC20UM	HWYC	Mixed Origin	0	8123	0	1275	994	10392	642	5627	69691	86352	0.0	78.2	0.0	12.3	9.6	0.7	6.5	80.7
HWYCRPT	HWYC rep	Mixed Origin	0	14959	0	1852	1414	18225	939	12613	29897	61674	0.0	82.1	0.0	10.2	7.8	1.5	20.5	48.5
LtMAR	Little Marine	Mixed Origin	863	7482	9259	505	953	19062	4657	50104	65914	139737	4.5	39.3	48.6	2.6	5.0	3.3	35.9	47.2
11AMB501	NC7 rep	Mixed Origin	112	519	0	52	79	762	104	21162	24714	46742	14.7	68.1	0.0	6.8	10.4	0.2	45.3	52.9
NC720KR	NC7 rep2	Mixed Origin	327	1942	119	531	651	3570	170	136729	48050	188519	9.2	54.4	3.3	14.9	18.2	0.1	72.5	25.5
RC021204	SAB1	Mixed Origin	0	6766	151	339	0	7256	0	6523	4080	17859	0.0	93.2	2.1	4.7	0.0	0.0	36.5	22.8
RC021205	SAB1A	Mixed Origin	205	4912	0	1823	5720	12660	0	9284	2467	24411	1.6	38.8	0.0	14.4	45.2	0.0	38.0	10.1
SE420UM	SE4	Mixed Origin	618	12097	752	2670	0	16137	861	53851	24717	95566	3.8	75.0	4.7	16.5	0.0	0.9	56.3	25.9
SE4B0213	SE4B	Mixed Origin	758	15193	1705	6502	4320	28478	7724	117839	76658	230699	2.7	53.3	6.0	22.8	15.2	3.3	51.1	33.2
3F116045	1m elevation, Pinnaroo Point	Quindalup System	0	2409	197	105	46	2757	1151	4210	6220	14338	0.0	87.4	7.1	3.8	1.7	8.0	29.4	43.4
3F116036	E - 20m S of Pipidinny Rd at E end of long straight where it veers S	Quindalup System	669	2174	642	415	632	4532	231	29720	38819	73302	14.8	48.0	14.2	9.2	13.9	0.3	40.5	53.0
3F116035	E - ca 100m W of Pipidinny Rd/ Beonaddy Rd intersection	Quindalup System	155	873	248	168	232	1676	75	20114	6484	28349	9.2	52.1	14.8	10.0	13.8	0.3	71.0	22.9
PINNACLE	PINNACLE	Quindalup System	1329	12210	458	1833	2640	18470	244	9920	14006	42640	7.2	66.1	2.5	9.9	14.3	0.6	23.3	32.8
3F116047	QP ref soil from Burns Beach-Quinns blow	Quindalup System	148	937	50	199	70	1404	491	15373	2947	20215	10.5	66.7	3.6	14.2	5.0	2.4	76.0	14.6
3F116046	QP ref soil from Yanchep-Two Rocks	Quindalup System	221	1643	21	67	575	2527	240	11904	10373	25044	8.7	65.0	0.8	2.7	22.8	1.0	47.5	41.4
11AMBER	11AMB	Spearwood System	212	828	138	455	648	2281	169	7129	5331	14910	9.3	36.3	6.0	19.9	28.4	1.1	47.8	35.8
11AMBERR	11AMB rep	Spearwood System	314	1785	277	1091	1622	5089	172	9991	3942	19194	6.2	35.1	5.4	21.4	31.9	0.9	52.1	20.5

11AMB01	11AMB-1	Spearwood System	420	2112	435	1082	1603	5652	294	12054	10567	28567	7.4	37.4	7.7	19.1	28.4	1.0	42.2	37.0
11AMB02	11AMB-2	Spearwood System	254	1900	343	1078	1474	5049	1847	24626	35007	66529	5.0	37.6	6.8	21.4	29.2	2.8	37.0	52.6
11AMB03	11AMB-3	Spearwood System	203	1526	265	1128	1548	4670	282	16170	13113	34235	4.3	32.7	5.7	24.2	33.1	0.8	47.2	38.3
11AMB04	11AMB-4	Spearwood System	229	2090	376	1119	1616	5430	933	17444	19432	43239	4.2	38.5	6.9	20.6	29.8	2.2	40.3	44.9
11AMB05	11AMB-5	Spearwood System	326	1778	376	939	1282	4701	776	18945	27202	51624	6.9	37.8	8.0	20.0	27.3	1.5	36.7	52.7
11AMB06	11AMB-6	Spearwood System	380	1850	408	1073	1497	5208	494	16503	16689	38894	7.3	35.5	7.8	20.6	28.7	1.3	42.4	42.9
11AMB07	11AMB-7	Spearwood System	333	1859	342	1063	1527	5124	418	16075	21754	43371	6.5	36.3	6.7	20.7	29.8	1.0	37.1	50.2
11AMB08	11AMB-8	Spearwood System	319	1800	346	996	1495	4956	1013	18468	31092	55529	6.4	36.3	7.0	20.1	30.2	1.8	33.3	56.0
RC130401	97F-036	Spearwood System	237	1086	765	433	1091	3612	0	7124	3853	14589	6.6	30.1	21.2	12.0	30.2	0.0	48.8	26.4
RC130402	97F-037	Spearwood System	99	531	347	387	641	2005	46	9621	8765	20437	4.9	26.5	17.3	19.3	32.0	0.2	47.1	42.9
GNAN20UM	GNAN	Spearwood System	45	945	53	161	268	1472	51	1588	2347	5458	3.1	64.2	3.6	10.9	18.2	0.9	29.1	43.0
GN20UMR	GNAN rep	Spearwood System	0	1222	85	399	587	2293	0	2973	1188	6454	0.0	53.3	3.7	17.4	25.6	0.0	46.1	18.4
NA120UM	NA1	Spearwood System	383	1852	1153	1427	1413	6228	232	13048	22261	41769	6.1	29.7	18.5	22.9	22.7	0.6	31.2	53.3
NA220UM	NA2	Spearwood System	295	3564	503	1286	1609	7257	684	8289	9870	26100	4.1	49.1	6.9	17.7	22.2	2.6	31.8	37.8
NA420UM	NA4	Spearwood System	431	3212	499	1173	1222	6537	487	10396	16040	33460	6.6	49.1	7.6	17.9	18.7	1.5	31.1	47.9
NAB120UM	NAB1	Spearwood System	287	4084	208	887	953	6419	205	12690	21366	40680	4.5	63.6	3.2	13.8	14.8	0.5	31.2	52.5
NAB220UM	NAB2	Spearwood System	409	2667	276	992	1150	5494	162	20405	20040	46101	7.4	48.5	5.0	18.1	20.9	0.4	44.3	43.5
NAB320UM	NAB3	Spearwood System	258	1893	472	1163	1365	5151	68	7903	14819	27941	5.0	36.8	9.2	22.6	26.5	0.2	28.3	53.0
NAB420UM	NAB4	Spearwood System	127	952	66	350	566	2061	95	35272	55628	93056	6.2	46.2	3.2	17.0	27.5	0.1	37.9	59.8
NB120UM	NB1	Spearwood System	204	1141	765	945	830	3885	272	19329	27556	51042	5.3	29.4	19.7	24.3	21.4	0.5	37.9	54.0

NB220UM	NB2	Spearwood System	132	1502	429	673	770	3506	146	22652	42059	68363	3.8	42.8	12.2	19.2	22.0	0.2	33.1	61.5
NB320UM	NB3	Spearwood System	148	1110	103	502	702	2565	0	19389	21172	43126	5.8	43.3	4.0	19.6	27.4	0.0	45.0	49.1
NB420UM	NB4	Spearwood System	226	814	336	847	706	2929	201	16961	29164	49255	7.7	27.8	11.5	28.9	24.1	0.4	34.4	59.2
NBC120UM	NBC1	Spearwood System	236	1985	489	1211	1347	5268	207	16405	22149	44029	4.5	37.7	9.3	23.0	25.6	0.5	37.3	50.3
NBC220UM	NBC2	Spearwood System	215	2836	647	1127	1128	5953	0	17386	12327	35666	3.6	47.6	10.9	18.9	18.9	0.0	48.7	34.6
NBC320UM	NBC3	Spearwood System	233	2577	240	1127	1098	5275	74	15895	10408	31652	4.4	48.9	4.5	21.4	20.8	0.2	50.2	32.9
NC120UM	NC1	Spearwood System	75	5561	320	628	958	7542	1190	7176	15935	31843	1.0	73.7	4.2	8.3	12.7	3.7	22.5	50.0
NC220UM	NC2	Spearwood System	103	2263	893	942	1208	5409	0	17076	13323	35808	1.9	41.8	16.5	17.4	22.3	0.0	47.7	37.2
NC320UM	NC3	Spearwood System	244	2793	1030	1547	2008	7622	0	25272	25333	58227	3.2	36.6	13.5	20.3	26.3	0.0	43.4	43.5
NC420UM	NC4	Spearwood System	280	1293	549	880	843	3845	435	11887	28281	44448	7.3	33.6	14.3	22.9	21.9	1.0	26.7	63.6
NC520UM	NC5	Spearwood System	106	1158	201	473	678	2616	219	16313	12298	31446	4.1	44.3	7.7	18.1	25.9	0.7	51.9	39.1
ND120UM	ND1	Spearwood System	371	2591	284	1318	1561	6125	405	14720	38699	59949	6.1	42.3	4.6	21.5	25.5	0.7	24.6	64.6
ND220UM	ND2	Spearwood System	323	2654	359	1443	1588	6367	119	18798	38291	63575	5.1	41.7	5.6	22.7	24.9	0.2	29.6	60.2
ND320UM	ND3	Spearwood System	347	3771	745	1469	1893	8225	110	26146	38242	72723	4.2	45.8	9.1	17.9	23.0	0.2	36.0	52.6
ND420UM	ND4	Spearwood System	349	2530	455	1636	1792	6762	265	14928	40172	62127	5.2	37.4	6.7	24.2	26.5	0.4	24.0	64.7
ND520UM	ND5	Spearwood System	239	2303	98	763	911	4314	137	17699	49714	71864	5.5	53.4	2.3	17.7	21.1	0.2	24.6	69.2
ND620UM	ND6	Spearwood System	239	3173	775	1341	1021	6549	0	15047	16554	38150	3.6	48.5	11.8	20.5	15.6	0.0	39.4	43.4
NE120UM	NE1	Spearwood System	221	1780	128	442	614	3185	68	2260	5602	11115	6.9	55.9	4.0	13.9	19.3	0.6	20.3	50.4
NE220UM	NE2	Spearwood System	217	5784	342	1194	1291	8828	187	9178	7706	25899	2.5	65.5	3.9	13.5	14.6	0.7	35.4	29.8
NE2A20UM	NE2A	Spearwood System	275	6535	441	748	1031	9030	0	8100	4673	21803	3.0	72.4	4.9	8.3	11.4	0.0	37.2	21.4

NS1B20UM	NS1B	Spearwood System	217	2617	749	708	900	5191	0	11954	4222	21367	4.2	50.4	14.4	13.6	17.3	0.0	55.9	19.8
NS220UM	NS2	Spearwood System	295	1882	393	1239	1155	4964	84	16230	51668	72946	5.9	37.9	7.9	25.0	23.3	0.1	22.2	70.8
NS220UMY	NS2 rep	Spearwood System	231	1193	277	677	657	3035	179	6241	23651	33106	7.6	39.3	9.1	22.3	21.6	0.5	18.9	71.4
NS220UMZ	NS2 rep2	Spearwood System	453	2431	573	1440	1403	6300	266	12055	48940	67561	7.2	38.6	9.1	22.9	22.3	0.4	17.8	72.4
NS320UM	NS3	Spearwood System	164	1767	163	966	1753	4813	0	15117	13084	33014	3.4	36.7	3.4	20.1	36.4	0.0	45.8	39.6
NS420UM	NS4	Spearwood System	321	3459	199	1299	1600	6878	124	16128	21510	44640	4.7	50.3	2.9	18.9	23.3	0.3	36.1	48.2
SA220UM	SA2	Spearwood System	360	1020	3143	326	546	5395	691	9697	25065	40848	6.7	18.9	58.3	6.0	10.1	1.7	23.7	61.4
SA420UM	SA4	Spearwood System	405	3038	438	866	1150	5897	202	15428	27335	48862	6.9	51.5	7.4	14.7	19.5	0.4	31.6	55.9
SA520UM	SA5	Spearwood System	562	3191	922	1039	1324	7038	66	21986	21628	50718	8.0	45.3	13.1	14.8	18.8	0.1	43.3	42.6
SA620UM	SA6	Spearwood System	135	613	148	138	242	1276	182	13306	15217	29981	10.6	48.0	11.6	10.8	19.0	0.6	44.4	50.8
SB220UM	SB2	Spearwood System	95	1125	243	778	715	2956	78	15923	51832	70789	3.2	38.1	8.2	26.3	24.2	0.1	22.5	73.2
SB220UMR	SB2 rep	Spearwood System	103	1567	346	825	771	3612	0	9440	13403	26455	2.9	43.4	9.6	22.8	21.3	0.0	35.7	50.7
SB320UM	SB3	Spearwood System	238	1489	450	1142	1983	5302	94	8717	10094	24207	4.5	28.1	8.5	21.5	37.4	0.4	36.0	41.7
SB420UM	SB4	Spearwood System	265	1636	900	1008	1629	5438	264	10511	21538	37751	4.9	30.1	16.6	18.5	30.0	0.7	27.8	57.1
SB720UM	SB7	Spearwood System	120	1180	346	471	674	2791	46	5388	12589	20814	4.3	42.3	12.4	16.9	24.1	0.2	25.9	60.5
SC120UM	SC1	Spearwood System	136	1094	838	757	1229	4054	184	9117	21616	34971	3.4	27.0	20.7	18.7	30.3	0.5	26.1	61.8
SC220UM	SC2	Spearwood System	295	1373	612	795	1107	4182	83	8602	8824	21691	7.1	32.8	14.6	19.0	26.5	0.4	39.7	40.7
SC320UM	SC3	Spearwood System	247	1482	258	793	1061	3841	133	10601	21691	36266	6.4	38.6	6.7	20.6	27.6	0.4	29.2	59.8
SC420UM	SC4	Spearwood System	142	1092	616	810	1121	3781	0	11768	25873	41422	3.8	28.9	16.3	21.4	29.6	0.0	28.4	62.5
SC520UM	SC5	Spearwood System	161	1299	630	402	521	3013	58	17562	17605	38238	5.3	43.1	20.9	13.3	17.3	0.2	45.9	46.0

SC620UM	SC6	Spearwood System	307	1883	552	1406	1290	5438	207	9577	22462	37684	5.6	34.6	10.2	25.9	23.7	0.5	25.4	59.6
SC6B20UM	SC6B	Spearwood System	252	2404	549	1142	1355	5702	0	9693	17035	32430	4.4	42.2	9.6	20.0	23.8	0.0	29.9	52.5
SD220UM	SD2	Spearwood System	246	1453	340	786	1143	3968	228	13505	17595	35296	6.2	36.6	8.6	19.8	28.8	0.6	38.3	49.8
LEDA20UM	SDE1	Spearwood System	165	857	468	628	764	2882	146	11902	14485	29415	5.7	29.7	16.2	21.8	26.5	0.5	40.5	49.2
PARM20UM	SDE2	Spearwood System	191	739	268	432	547	2177	0	21082	12839	36098	8.8	33.9	12.3	19.8	25.1	0.0	58.4	35.6
BALD20UM	SE1	Spearwood System	303	2972	689	1548	1966	7478	146	19891	52194	79709	4.1	39.7	9.2	20.7	26.3	0.2	25.0	65.5
SE320UM	SE3	Spearwood System	486	1487	253	633	990	3849	149	14332	26999	45329	12.6	38.6	6.6	16.4	25.7	0.3	31.6	59.6
SEF120UM	SEF1	Spearwood System	310	2181	866	1495	1914	6766	210	12760	51587	71323	4.6	32.2	12.8	22.1	28.3	0.3	17.9	72.3
KARN20UM	SF1	Spearwood System	235	1661	583	812	1249	4540	0	17728	7666	29934	5.2	36.6	12.8	17.9	27.5	0.0	59.2	25.6
SF220UM	SF2	Spearwood System	167	1661	281	510	707	3326	0	13065	46499	62890	5.0	49.9	8.4	15.3	21.3	0.0	20.8	73.9
SF320UM	SF3	Spearwood System	270	939	292	427	695	2623	367	12294	18651	33935	10.3	35.8	11.1	16.3	26.5	1.1	36.2	55.0
SG120UM	SG1	Spearwood System	334	1582	918	1096	1286	5216	145	14633	36678	56672	6.4	30.3	17.6	21.0	24.7	0.3	25.8	64.7
SG220UM	SG2	Spearwood System	231	845	132	282	358	1848	0	22033	52864	76745	12.5	45.7	7.1	15.3	19.4	0.0	28.7	68.9
SG320UM	SG3	Spearwood System	379	1014	170	278	311	2152	146	13607	39435	55340	17.6	47.1	7.9	12.9	14.5	0.3	24.6	71.3
WEMB100	WEMB100	Spearwood System	249	1668	163	1105	0	3185	282	22166	19783	45416	7.8	52.4	5.1	34.7	0.0	0.6	48.8	43.6
WEMB1850	WEMB1850	Spearwood System	703	5080	736	1967	0	8486	1932	42693	107067	160178	8.3	59.9	8.7	23.2	0.0	1.2	26.7	66.8
WEMB925	WEMB925	Spearwood System	836	6175	845	2371	0	10227	1100	49649	114152	175128	8.2	60.4	8.3	23.2	0.0	0.6	28.4	65.2
XTALCAVE	XTALCAVE	Spearwood System	649	2543	484	2024	1988	7688	274	16185	23606	47753	8.4	33.1	6.3	26.3	25.9	0.6	33.9	49.4

Appendix B Scores for individual samples for PC1-PC8, in the PCA performed in Section 3.3.2.2:PCA modelling using the percentage intensities [page 157 to 164]

Sample ref	Group for ALL##1	PC-1	PC-2	PC-3	PC-4	PC-5	PC-6	PC-7	PC-8
2F135406	Alluvial/ Lateritic	27.11189	27.41183	-21.23872	7.008759	-0.3669209	2.595074	-0.440619	2.8847
2F135409	Alluvial/ Lateritic	23.8154	35.03903	-25.85648	4.580482	0.4526176	0.4003589	-1.550817	3.104126
2F135412	Alluvial/ Lateritic	6.849552	31.97754	-35.81965	6.166561	3.093398	4.066471	-0.6582932	4.616359
2F135403	Alluvial/ Lateritic	8.052417	41.98281	-36.23786	2.703521	2.81706	-0.4375224	-2.480919	4.590519
HELENA1	Alluvial/ Lateritic	13.36637	-3.081661	-22.02204	11.93662	1.425129	11.77221	3.787424	-1.473702
HELENA2	Alluvial/ Lateritic	15.40263	5.489353	-22.34536	10.53464	1.799265	11.47907	3.307448	-0.9105095
HELENA3	Alluvial/ Lateritic	9.161257	15.75669	-12.89433	6.957594	-1.642195	7.848134	1.310488	-4.501878
HELENA4	Alluvial/ Lateritic	16.18452	10.13167	-21.3713	9.021198	-0.01624346	5.288632	1.099405	0.5687201
HELENA5	Alluvial/ Lateritic	21.76903	13.68964	-17.07379	10.23874	-1.059235	2.818048	0.3292077	-1.769772
HELENA6	Alluvial/ Lateritic	15.0935	21.22079	-27.25288	-4.091295	-0.1784382	-0.9235487	-1.437824	2.623848
HELENA7	Alluvial/ Lateritic	15.12586	37.52104	-29.50626	1.536007	0.5736079	1.287905	-1.720291	0.7356561
HELENA8	Alluvial/ Lateritic	9.662419	9.323867	-31.09407	11.59047	2.014661	7.28091	1.60854	-1.679308
0F25082R	Alluvial/ Lateritic	31.3434	3.178102	-3.676579	-5.347016	-0.7674847	4.379169	2.052398	-2.706698
0F25083R	Alluvial/ Lateritic	4.852463	-8.478361	-45.16995	-35.75759	-1.725873	1.917023	0.2039518	-4.553213
0F25084R	Alluvial/ Lateritic	12.1503	20.2449	-27.80601	-9.00054	10.92784	4.954804	2.239459	-27.34551
0F25085R	Alluvial/ Lateritic	8.304358	14.8253	-35.61726	-16.58625	12.34559	1.641985	1.286447	3.729364
NA320UM	Bassendean System	19.61194	-22.5582	-11.44509	-20.82805	-10.26504	1.743324	0.7790606	1.663183
NA520UM	Bassendean System	68.07028	24.25252	14.6806	0.6908236	1.881705	-4.032064	0.3445597	0.1223931
NA520UMX	Bassendean System	65.26206	9.245625	17.8559	-2.780895	19.73494	-3.259908	4.357164	0.3604028
NB520UM	Bassendean System	40.22609	-47.70183	-7.990824	-26.13882	-10.9819	4.841974	3.583539	1.492124
NBC420UM	Bassendean System	43.68177	-23.06376	1.66754	-0.5268927	-3.526742	2.41466	3.014764	0.2034512

NC620UM	Bassendean System	56.52912	6.284334	8.82515	14.28472	-9.150927	1.106744	0.524451	-0.596738
NC620UMX	Bassendean System	70.46307	35.09919	13.53482	3.326458	-11.70499	-4.683467	-2.650899	-0.1711645
ND720UM	Bassendean System	24.25614	-30.71974	-4.92976	-7.052825	-7.273434	1.498305	1.95038	0.8003268
ND820UM	Bassendean System	56.49126	-17.47101	6.270983	-4.494835	-12.81674	22.29346	6.989321	1.81037
ND820UMR	Bassendean System	45.93984	-43.29744	-0.7774067	13.42766	-8.864448	3.624255	3.622709	-0.4066648
ND8A20UM	Bassendean System	72.71357	34.40408	13.83072	3.59248	-11.80667	-4.624501	-2.547294	-0.2176201
ND8A20UR	Bassendean System	73.0377	34.31189	13.8282	3.630005	-11.80933	-4.612702	-2.531258	-0.2200603
NE320UM	Bassendean System	71.34638	34.79137	13.85014	3.434355	-11.79774	-4.674909	-2.615151	-0.2081563
NE320URX	Bassendean System	63.33173	1.067005	19.52477	-4.746638	29.63838	-2.839837	6.560502	0.5034391
NE420UM	Bassendean System	45.51659	-48.6259	7.846428	-0.678692	16.5546	17.25666	-34.9928	-0.1153485
NE420URR	Bassendean System	50.26979	-49.93006	7.538008	-0.1331646	16.5875	17.44955	-34.75093	-0.1255646
SA320UM	Bassendean System	43.0891	-29.59238	2.024996	-3.494264	-7.490003	1.952701	2.628291	-0.01414275
SA6B20UM	Bassendean System	66.71246	36.09686	13.95695	2.899125	-11.77838	-4.848765	-2.846159	-0.1799387
SA6B20UX	Bassendean System	59.41587	15.11615	17.46926	-2.597852	14.84056	-3.740509	2.932782	0.3058953
SB120UM	Bassendean System	43.39704	-57.39719	-4.969393	14.226	-8.795555	-17.01082	-1.28796	-2.263087
SB120UMR	Bassendean System	42.9878	-49.85435	-3.371904	12.11584	-9.185083	-13.77775	-0.8831933	-1.862349
SB120UKX	Bassendean System	43.39467	-53.94196	-4.208639	12.82784	-5.869838	-15.02195	-0.4551437	-1.914001
SB520UM	Bassendean System	71.05233	34.89142	13.75898	3.398677	-11.77053	-4.678769	-2.627392	-0.1971419
SB520KR	Bassendean System	63.99769	0.9510422	19.3499	-4.666181	29.62627	-2.800592	6.588156	0.4357016
SB620UM	Bassendean System	38.92818	-49.41278	-4.42951	-1.079146	-6.338449	-7.702659	1.082743	-0.6612208
SC720UM	Bassendean System	29.86396	-35.25653	-9.302042	-20.26813	-8.428848	-0.7657455	1.45464	1.25581
CASU20UM	Bassendean System	72.81702	34.38385	13.77756	3.603541	-11.79363	-4.616901	-2.540883	-0.2134688
SD120KR	Bassendean System	52.40232	-27.6198	10.20926	16.25484	13.10777	6.782308	7.58919	-0.02325535
WELL20UM	Bassendean System	41.77179	-48.37248	-6.468174	-10.3968	-9.310501	-2.552554	1.956032	0.200228
SE220UM	Bassendean System	-5.061365	8.199678	7.721456	5.162693	-0.03498638	-2.531878	-0.6293193	0.01367152
SF420UM	Bassendean System	26.50771	-17.23067	4.563692	-27.87917	-6.365188	6.568802	3.030043	1.469205

91M5781	Coastal limestone	2.482104	-1.477558	-21.99045	19.05245	0.5094831	-1.562011	-0.3714946	1.082019
91M5788	Coastal limestone	3.017435	24.78759	-37.97457	7.259923	5.705982	-4.399188	-2.246907	3.308641
91M5785	Coastal limestone	1.097647	15.61499	-28.8575	11.16716	2.722664	-4.13903	-1.926008	2.496671
9KARRDGB	Coastal limestone	11.84526	-33.07051	-24.46833	-39.37224	-3.879543	-7.078618	-0.4767442	2.723556
SHELLY01	Coastal limestone	21.86355	-35.59966	-3.986144	-13.25734	7.056342	-5.118079	2.756288	0.7563035
3116043R	Quindalup-Spearwood	-8.08049	22.747	6.2028	3.221825	-0.1114914	4.8111	0.4471897	-6.258767
116007SS	Quindalup-Spearwood	-6.660657	15.70076	3.273537	-11.44709	8.460087	-4.407729	-0.334622	1.436856
116006SS	Quindalup-Spearwood	14.68386	-8.954691	-3.323368	0.4972082	1.849971	-0.9763833	1.286618	1.001759
116008SS	Quindalup-Spearwood	-8.992357	8.935864	-4.587674	-6.318517	6.427165	-3.580657	-0.3305133	1.683864
116004SS	Quindalup-Spearwood	-12.45527	5.772335	5.005307	-4.830308	4.115683	-0.2439747	0.5680395	0.184732
116002SS	Quindalup-Spearwood	23.05919	-11.98098	-6.512439	1.332744	3.816895	1.375802	2.534803	1.411152
116003SS	Quindalup-Spearwood	-3.821195	-5.235966	6.272309	2.419067	-0.3182045	-1.581831	0.3604865	0.1864425
116005SS	Quindalup-Spearwood	-29.92131	12.93928	6.643167	-7.360936	1.196814	-1.79389	-1.135222	0.9675345
116009SS	Quindalup-Spearwood	3.371148	9.750829	8.240297	-7.853767	8.265721	-5.510558	0.07009326	0.2870286
3F116022	Quindalup-Spearwood	12.24169	-4.174431	0.421381	-0.856288	9.2149	-2.628571	1.803712	0.9914849
C1VSLOW	Quindalup-Spearwood	19.78391	-5.957572	2.349719	-1.938581	-0.4802322	-3.865672	0.2459293	-0.06911981
3F116024	Quindalup-Spearwood	-4.378656	1.842021	6.580664	-3.139395	0.07784319	-2.443848	-0.2147707	0.04460925
3F116025	Quindalup-Spearwood	-43.08126	7.094329	12.10667	-6.845202	2.727932	-6.568455	-1.995039	-1.025895
3F116026	Quindalup-Spearwood	-19.34399	6.919702	6.062066	-7.633514	4.378288	-4.0992	-0.6387211	0.4732534
3F116027	Quindalup-Spearwood	7.956476	2.81291	-1.224535	0.2579398	5.23911	-2.282348	0.6987368	0.07343632
3F116028	Quindalup-Spearwood	10.24646	-4.09585	5.047477	-7.673457	4.638577	-4.138692	0.7385042	0.6065868
3F116029	Quindalup-Spearwood	-15.6808	5.848948	4.009957	-7.596519	3.900486	-4.745397	-0.788398	-0.1070606
3F116030	Quindalup-Spearwood	-21.25597	-1.589509	9.253805	-9.685834	6.790082	-3.094596	0.5644535	0.6049154
3F116031	Quindalup-Spearwood	-4.479454	-2.600821	0.2375592	-2.375677	1.734466	-0.8186004	0.5681822	1.003886
3F116032	Quindalup-Spearwood	-7.267781	-1.109027	1.795609	0.1415923	5.176746	0.02115715	1.247259	0.02647316
3F116033	Quindalup-Spearwood	5.822958	-8.151145	-2.235369	2.119735	1.6071	0.3748235	1.379129	0.4185646

3F116034	Quindalup-Spearwood	-5.028906	-8.71362	2.441636	0.4026698	1.93569	0.047609	1.245854	-0.2708753
3F116018	Quindalup-Spearwood	10.35365	3.503076	4.508501	-2.396048	0.3640931	-3.756659	-0.3122003	-0.1258682
3F116006	Quindalup-Spearwood	1.143082	-2.432575	-0.9019655	-3.359629	4.196204	-1.394417	0.9205505	0.2728365
3F116008	Quindalup-Spearwood	10.12577	4.700079	-3.478584	5.103526	15.87377	-0.6301135	2.734484	1.672825
3F116004	Quindalup-Spearwood	-23.11505	10.41766	6.711411	-8.233487	5.343525	-2.044317	-0.2018241	0.2585313
3F116002	Quindalup-Spearwood	32.93075	-11.32368	-5.174361	2.343701	4.728545	0.3509579	2.647838	1.227365
3F116003	Quindalup-Spearwood	-3.109982	-3.303835	4.34911	0.3824367	0.188139	-2.729054	-0.01287051	0.3616897
3F116005	Quindalup-Spearwood	-32.50656	9.828867	2.590571	-7.763331	4.554482	-2.431594	-0.755949	1.272264
3F116010	Quindalup-Spearwood	-26.51118	11.87663	-4.583918	-15.65891	14.7481	-1.924571	0.9293344	-2.687151
116010SS	Quindalup-Spearwood	-34.13448	20.67729	2.898514	-14.87152	10.77123	8.251009	2.501883	0.6940868
3F116007	Quindalup-Spearwood	-4.354601	15.44346	0.6398172	-9.003993	10.04027	-5.190766	-0.2838184	0.471929
3F116009	Quindalup-Spearwood	33.36958	7.865247	12.70346	-15.58622	12.03497	-3.841154	2.117488	0.8685057
3F116039	Quindalup-Spearwood	2.887598	-12.29355	3.534284	4.722856	3.67084	-2.122566	1.362063	0.2335214
3F116038	Quindalup-Spearwood	0.3615975	2.591663	0.9030333	-8.042075	7.215019	-1.271852	1.197903	-0.4484073
3F116037	Quindalup-Spearwood	-18.99385	-0.6250999	2.461013	-10.99768	11.01938	-2.368599	1.264274	0.8880246
3F116042	Quindalup-Spearwood	7.022388	-4.539312	-6.679772	-8.152514	12.25318	-2.65794	2.004034	0.9492278
3F116040	Quindalup-Spearwood	2.311377	-12.20912	1.817606	-1.4459	6.171257	-1.186493	1.973424	-0.2655436
3F116041	Quindalup-Spearwood	0.476695	-9.078713	3.770763	-4.322146	6.917244	0.9471861	2.491457	0.8778078
3116044R	Quindalup-Spearwood	-4.002109	21.57994	6.85208	-6.873002	-10.58309	12.13466	0.8692898	-0.1710079
3116048X	Quindalup-Spearwood	26.02861	14.91297	6.426455	-7.560188	-3.359534	6.68802	1.695276	-0.447806
RH71SLOW	Quindalup-Spearwood	9.783625	8.958831	2.941888	-3.945724	6.640055	-4.257931	0.2074835	-0.6855046
RH72SLOW	Quindalup-Spearwood	6.423286	-3.448763	6.955114	-2.531709	9.380776	-3.58244	1.571921	0.509262
RH73SLOW	Quindalup-Spearwood	-29.48816	4.180433	6.774579	-3.898785	3.594306	-1.780658	-0.2164009	0.3589414
MEH1	Quindalup System	28.28353	13.12167	8.343803	-12.64973	-13.46187	4.224459	-0.4011867	0.2443676
MEH2	Quindalup System	30.18048	-8.481092	4.044691	-3.475687	3.979731	9.640244	5.075306	0.475931
SWB1	Quindalup System	12.82261	5.353794	5.366095	-12.41093	-12.72313	2.17166	-0.8390167	-0.5375524

SWB2	Quindalup System	28.7295	21.32393	8.889242	-4.865594	-11.82932	-2.154263	-2.321849	-0.5083231
SWB3	Quindalup System	15.29279	27.61899	9.878808	-8.586919	-7.687781	-2.241165	-2.334674	-0.7026901
SWB4	Quindalup System	8.345999	18.2353	7.489657	-7.443884	-5.001888	-0.7215664	-1.169162	-1.522792
11AMB50S	Mixed Origin	-17.51723	-7.046896	10.6704	13.46376	3.012922	1.929045	1.724185	-0.3672973
11AMB50SC	Mixed Origin	13.10464	-4.378428	9.868325	12.50231	2.467794	3.971014	2.766853	-0.1051122
RC130403	Mixed Origin	24.2679	14.73377	14.65867	-5.293574	4.073267	5.287282	2.699111	0.9101806
RC130404	Mixed Origin	-1.528265	-4.978066	8.151737	17.84453	-7.39327	6.368801	1.429482	-0.3867147
RC13044R	Mixed Origin	23.31407	-4.365281	11.13441	11.84061	1.702213	11.97117	5.086095	0.761745
HWYC20UM	Mixed Origin	-51.852	45.12286	9.762928	-1.503419	-8.540816	-2.16731	-5.160091	0.1433866
HWYCRPT	Mixed Origin	-19.50334	42.91033	-3.976021	0.2665753	-5.381841	-0.999295	-3.780638	0.4589198
LtMAR	Mixed Origin	-16.89341	-9.999207	-4.08338	-40.58653	-10.92948	-3.843032	-2.206986	-1.521865
11AMB501	Mixed Origin	-8.382462	23.23616	16.55583	-0.4456552	4.993649	-5.384094	-1.289166	-0.2015094
NC720KR	Mixed Origin	23.18776	-2.715444	10.16087	8.735966	0.3010001	-0.4176623	1.395071	-0.2503036
RC021204	Mixed Origin	12.84901	48.18535	-10.35385	-3.75619	-5.007272	-0.7712622	-3.354441	2.748088
RC021205	Mixed Origin	2.305046	-13.6505	-28.71704	24.39202	4.366828	-11.49311	-1.918228	1.074141
SE420UM	Mixed Origin	18.8377	24.79119	3.168384	-1.518533	-4.515466	9.394904	1.369549	1.143485
SE4B0213	Mixed Origin	2.441799	2.888874	0.581261	6.241316	-4.316408	7.902793	1.817419	-2.023653
3F116045	Quindalup System	-7.207214	45.091	-2.200846	-9.346396	-7.909144	-2.799696	-4.370767	-6.08167
3F116036	Quindalup System	-17.21038	2.320867	9.604352	-9.385929	4.304193	-4.126273	-0.2342824	0.1602511
3F116035	Quindalup System	24.43536	-5.655899	6.196185	-3.825737	-1.316064	-1.902551	0.8453169	0.06654662
PINNACLE	Quindalup System	-11.72533	24.78525	-14.23045	1.394536	4.811732	-2.621797	-1.605627	1.930008
3F116047	Quindalup System	37.62704	10.10954	7.594578	2.236328	1.756166	5.897762	2.902896	-1.29056
3F116046	Quindalup System	-1.237875	15.64285	6.263189	6.176993	1.325322	-13.93789	-3.861343	-1.477794
11AMBER	Spearwood System	-6.840156	-14.24931	-1.298082	10.33921	3.861012	-0.5358788	1.562889	-0.6472366
11AMBERR	Spearwood System	5.184017	-18.62005	-10.68587	15.04199	3.153807	0.1010248	1.901476	0.04414082
11AMB01	Spearwood System	-11.20011	-11.89589	-4.471148	8.607538	2.3433	-1.209049	0.8020766	-0.3019107

11AMB02	Spearwood System	-25.46186	-9.280437	2.78476	9.344822	-1.7164	-0.73457	-0.01638484	-2.658433
11AMB03	Spearwood System	-10.98334	-18.78892	-1.850769	15.11266	-0.8905398	0.5943822	1.23337	-0.6318404
11AMB04	Spearwood System	-17.88433	-10.20607	-0.7740359	10.30337	-1.776736	-1.207995	-0.01935148	-1.874858
11AMB05	Spearwood System	-25.2364	-8.645542	3.286947	6.63769	-0.176748	-1.037731	0.1257389	-1.274525
11AMB06	Spearwood System	-15.61937	-13.46266	-0.3764677	8.782863	1.206538	-0.5316033	0.8990957	-0.8667325
11AMB07	Spearwood System	-24.10308	-10.73418	1.345261	9.489894	0.2547472	-1.433368	0.1754636	-0.7581702
11AMB08	Spearwood System	-30.5524	-9.265388	2.953848	8.50995	-0.2418778	-2.448825	-0.3696015	-1.779593
RC130401	Spearwood System	-0.7898731	-24.34604	-10.68293	-1.511421	-0.09391522	-7.114295	-0.3683742	0.6679533
RC130402	Spearwood System	-14.86974	-26.05013	-0.4268899	3.649031	-3.253041	-2.934777	0.278123	-0.2759532
GNAN20UM	Spearwood System	-15.60172	20.42808	-5.179909	3.548562	-2.082173	-4.478659	-2.814269	0.3190986
GN20UMR	Spearwood System	7.999561	1.376004	-14.66277	12.92601	-2.599068	-0.7987424	-0.4944414	1.489696
NA120UM	Spearwood System	-31.04749	-15.64794	-1.21989	-3.342273	-2.019817	4.071584	1.351162	0.6055709
NA220UM	Spearwood System	-15.20799	3.632572	-9.337859	5.274484	-0.1173664	0.3954312	-0.2883117	-1.016031
NA420UM	Spearwood System	-21.90285	5.328034	-1.496091	1.81652	0.3361971	1.45044	0.01761526	-0.1469959
NAB120UM	Spearwood System	-20.4644	20.71015	3.754721	2.251754	-2.805426	-1.198977	-1.936725	0.4121299
NAB220UM	Spearwood System	-10.30706	0.4946342	3.82123	6.362634	0.355763	0.4327444	0.4464236	0.2047547
NAB320UM	Spearwood System	-31.73154	-7.353869	-2.192993	5.765088	-0.9244013	1.617098	0.3198752	0.6719917
NAB420UM	Spearwood System	-26.80921	0.1086622	10.3144	9.449528	-2.003736	-4.700883	-1.533283	-0.6721737
NB120UM	Spearwood System	-27.03433	-18.01944	3.217222	-3.774212	-4.452999	5.726692	1.764783	0.3225706
NB220UM	Spearwood System	-31.6006	-2.2133	7.32507	0.2285256	-5.763628	0.01601458	-0.9222592	0.005556345
NB320UM	Spearwood System	-15.86132	-5.694732	6.70121	10.94009	-1.648008	-1.70626	-0.1611462	-0.2150209
NB420UM	Spearwood System	-34.0858	-17.04497	5.961376	4.190392	-0.4228654	7.913993	2.841252	0.3154658
NBC120UM	Spearwood System	-23.46168	-9.274405	1.525889	6.409296	-2.613644	2.410142	0.6814528	0.1100129
NBC220UM	Spearwood System	-1.433285	-3.325811	-1.139064	2.86359	-3.844368	2.75543	0.6972238	1.021658
NBC320UM	Spearwood System	0.4624045	-1.938201	-0.5591627	9.498631	-1.653571	3.900053	1.335855	0.7111009
NC120UM	Spearwood System	-21.51971	32.85005	-3.464183	-1.239681	-5.155446	-4.553459	-4.124284	-2.288282

NC220UM	Spearwood System	-5.592604	-10.18765	-2.026292	-0.1395479	-6.522042	-0.06699727	-0.2202505	0.7005548
NC320UM	Spearwood System	-14.79123	-13.59652	-0.5071807	4.012002	-4.518234	0.1976488	0.1849426	0.4579313
NC420UM	Spearwood System	-39.93928	-8.886831	4.555098	-1.776179	-1.378644	3.576269	0.8688343	-0.169356
NC520UM	Spearwood System	-3.916803	-8.001078	3.258893	8.520167	-3.600229	-1.598792	-0.1042214	-0.6900425
ND120UM	Spearwood System	-40.33765	0.9296734	5.091993	7.13758	-0.7714348	0.2010496	-0.529738	-0.2805392
ND220UM	Spearwood System	-34.24641	-1.654021	4.853623	7.373115	-2.026593	1.639485	-0.0555855	0.2433089
ND320UM	Spearwood System	-23.00669	-0.3965353	3.347484	3.580828	-3.659807	-1.150842	-0.9059732	0.2484637
ND420UM	Spearwood System	-42.38764	-4.237909	3.836653	6.956379	-1.674287	2.145582	0.06289923	0.09434843
ND520UM	Spearwood System	-39.70729	13.01305	10.19076	5.457542	-2.542597	-1.748205	-1.895563	-0.06890702
ND620UM	Spearwood System	-13.22093	1.371933	-0.2343173	-0.5683217	-4.189756	5.18928	0.7615609	1.392842
NE120UM	Spearwood System	-28.91934	15.75046	-5.36333	2.55822	2.402788	-2.575465	-1.634306	0.9165743
NE220UM	Spearwood System	-1.980434	19.49137	-10.18362	3.823991	-1.637515	0.2374475	-1.220314	1.297968
NE2A20UM	Spearwood System	7.377854	25.50482	-13.98739	0.4631143	-0.6501439	-2.32319	-1.979798	2.367844
NS1B20UM	Spearwood System	14.81814	-4.041778	-7.096285	-0.7854719	-2.837557	-0.004265189	0.3994551	1.361778
NS220UM	Spearwood System	-47.22549	-2.304984	7.663733	3.895769	-2.134588	3.902447	0.3376141	0.4205906
NS220UMY	Spearwood System	-49.08698	0.4172981	6.495293	0.6409757	-0.4136314	2.488894	0.007076979	0.1926944
NS220UMZ	Spearwood System	-50.76566	-0.0664897	6.350111	1.082254	-0.7623525	2.608124	-0.03679597	0.3238349
NS320UM	Spearwood System	-11.87778	-14.77743	-1.796271	17.37689	-1.494101	-4.750053	-0.5738165	-0.2895294
NS420UM	Spearwood System	-19.06085	4.559851	1.578164	8.99408	-1.411914	-0.3034497	-0.5613812	0.3192667
SA220UM	Spearwood System	-40.48933	-27.31344	-4.630663	-46.9009	-9.883193	-3.519924	-1.541109	0.0834651
SA420UM	Spearwood System	-26.02122	7.849078	4.759462	0.9462988	-1.055111	-2.473302	-1.350987	0.1358982
SA520UM	Spearwood System	-10.47517	-3.233124	1.742319	-2.088825	-0.401301	-1.026748	0.09667858	0.6472297
SA620UM	Spearwood System	-14.02359	0.07118726	9.106815	-2.988649	0.6583498	-5.12098	-0.9051969	-0.5940672
SB220UM	Spearwood System	-48.93015	-2.612422	8.746023	4.968485	-5.341595	4.389326	-0.04772651	0.2327735
SB220UMR	Spearwood System	-22.87698	-2.707349	1.492239	4.171288	-4.621225	4.076218	0.4322716	0.8928429
SB320UM	Spearwood System	-22.30112	-20.84061	-7.748087	13.08588	0.4163008	-3.513955	0.01185179	-0.04316485

SB420UM	Spearwood System	-36.27303	-15.27124	-1.719925	0.3260756	-2.710799	-3.380347	-0.9408426	-0.3061024
SB720UM	Spearwood System	-36.04432	-0.9995396	1.790035	-0.1606834	-3.712468	-2.735325	-1.666039	0.2785909
SC120UM	Spearwood System	-41.46773	-18.32096	-0.6288109	-2.79192	-5.43377	-3.624132	-1.365296	-0.2821079
SC220UM	Spearwood System	-16.20443	-16.07431	-4.503708	1.850855	0.4694463	-0.4332944	0.8309226	0.507215
SC320UM	Spearwood System	-35.03814	-5.107828	3.850375	7.020281	-0.4764042	-1.163833	-0.4028769	-0.1223768
SC420UM	Spearwood System	-40.06185	-16.28327	2.275419	1.176412	-4.790618	-1.246872	-0.6344422	0.1676551
SC520UM	Spearwood System	-11.1568	-7.230481	4.151282	-8.775566	-5.644889	-1.64196	-0.6261494	0.3631431
SC620UM	Spearwood System	-38.56036	-7.629241	0.9130573	3.711089	-1.159004	5.402994	1.243295	0.5311947
SC6B20UM	Spearwood System	-28.35931	-2.301437	-0.9044609	3.571529	-2.256637	0.5787098	-0.352383	0.8760639
SD220UM	Spearwood System	-22.75864	-10.95853	1.741714	7.439436	-0.6641712	-1.759507	-0.004405499	-0.4594822
LEDA20UM	Spearwood System	-22.4059	-19.15273	1.323052	1.23458	-2.670526	1.354158	0.9946883	-0.03349078
PARM20UM	Spearwood System	0.4494184	-20.24568	4.580257	4.893516	0.2179325	0.8264109	2.031073	0.1124614
BALD20UM	Spearwood System	-41.32808	-2.738389	4.64193	4.170337	-3.778512	-0.8604991	-1.127242	0.07578695
SE320UM	Spearwood System	-32.38262	-4.744296	6.849853	3.86705	5.216609	-3.763645	-0.04669297	-0.2177396
SEF120UM	Spearwood System	-52.92215	-8.265126	3.838684	1.618743	-3.473479	-0.6865542	-1.011064	0.02115393
KARN20UM	Spearwood System	8.088499	-19.55246	-3.013699	6.595546	-1.856951	-1.360958	1.037565	0.359981
SF220UM	Spearwood System	-46.08283	10.07501	9.927792	-0.4951408	-4.347216	-3.892112	-2.752749	0.04208684
SF320UM	Spearwood System	-26.95797	-10.31724	4.910801	1.850502	2.223557	-3.826822	-0.1328684	-0.9973048
SG120UM	Spearwood System	-42.24052	-12.90162	3.498652	-3.452955	-2.69646	0.7122388	0.02619576	0.3092928
SG220UM	Spearwood System	-37.89632	4.674752	13.07414	-0.9888885	3.061422	-2.620353	-0.5986081	0.07018113
SG320UM	Spearwood System	-40.96734	8.823255	14.03522	-6.381409	7.949728	-2.281462	0.005871177	0.2219307
WEMB100	Spearwood System	-5.461043	6.9347	10.12374	0.7855105	-1.103439	24.34998	6.591267	1.873821
WEMB1850	Spearwood System	-33.01027	21.86128	13.03216	-8.967052	-2.301949	13.17058	1.9272	0.7414926
WEMB925	Spearwood System	-30.62251	21.77253	13.02508	-8.342624	-2.364174	13.19371	1.98059	1.298732
XTALCAVE	Spearwood System	-26.65022	-11.83803	-0.3162527	8.76916	2.989661	5.396104	2.414667	0.4574547

Appendix C Scores for individual samples for PC1-PC8, in the PCA performed in Section 3.3.3.1 Bassendean Sands

Sample ref	Site	PC-1	PC-2	PC-3	PC-4	PC-5	PC-6	PC-7	PC-8
NA320UM	NA3	-26.658	30.621	11.003	5.804	0.575	3.940	-5.853	-0.088
NA520UM	NA5	40.523	-3.973	1.422	-0.074	2.613	2.114	-0.893	0.025
NA520UMX	NA5	26.483	-15.297	13.983	-5.139	11.639	1.821	-0.271	0.023
NB520UM	NB5	-41.300	10.653	1.529	20.742	12.539	1.648	0.539	0.023
NBC420UM	NBC4	-14.120	2.692	-0.816	-0.790	1.686	-4.636	-1.218	-0.163
NC620UM	NC6	19.492	0.365	-10.078	-5.801	-7.302	-7.837	-1.354	-0.240
NC620UMX	NC6	51.062	4.004	-8.107	3.735	-4.101	2.185	-0.121	0.021
ND720UM	ND7	-29.993	18.017	4.676	-2.609	-1.284	-1.664	-1.878	0.124
ND820UM	ND8	-4.325	0.596	-2.743	17.342	1.418	-21.752	1.278	0.106
ND820UMR	ND8	-31.167	-6.093	-15.236	-4.659	-1.697	-11.224	-0.651	0.086
ND8A20UM	ND8A	51.350	2.250	-9.264	4.612	-3.464	2.021	0.060	0.013
ND8A20UR	ND8A	51.388	2.005	-9.430	4.740	-3.368	2.002	0.040	0.012
NE320UM	NE3	51.187	3.283	-8.568	4.067	-3.867	2.099	0.155	0.017
NE320URX	NE3	18.666	-21.262	21.127	-8.085	16.529	1.690	0.004	0.023
NE420UM	NE4	-37.241	-28.664	17.734	10.326	-24.764	4.085	0.221	0.007
NE420URR	NE4	-36.691	-32.214	15.321	12.234	-23.341	3.837	-0.357	-0.007
SA320UM	SA3	-20.303	3.753	-3.073	2.562	2.474	-3.742	2.085	-0.160
SA6B20UM	SA6B	50.639	6.776	-6.209	2.219	-5.238	2.362	0.519	0.030
SA6B20UX	SA6B	29.525	-7.303	13.933	-6.421	7.213	2.240	0.411	0.041
SB120UM	SB1	-44.901	-7.872	-23.793	-12.532	1.251	7.140	1.330	-0.005
SB120UMR	SB1	-38.180	-4.851	-20.337	-10.690	0.302	5.029	1.406	0.012
SB120UKX	SB1	-41.786	-8.001	-19.908	-12.337	2.062	5.953	0.389	0.008
SB520UM	SB5	51.146	3.521	-8.415	3.956	-3.946	2.126	0.077	0.018
SB520KR	SB5	18.775	-21.702	20.762	-7.800	16.710	1.669	-0.200	-0.055
SB620UM	SB6	-40.543	0.578	-9.296	-2.719	4.840	4.106	0.882	0.026
SC720UM	SC7	-33.677	18.574	5.189	8.794	6.318	5.398	-2.809	0.069
CASU20UM	SD1	51.359	2.181	-9.315	4.656	-3.429	2.020	0.000	0.013
SD120KR	SD1	-12.217	-19.455	1.148	-13.376	3.487	-15.035	-1.838	0.020
WELL20UM	SDE3	-39.760	3.712	-6.987	7.766	7.894	2.903	0.146	0.021
SE220UM	SE2	-2.261	38.853	24.327	-31.661	-18.961	-2.603	1.681	0.060
SF420UM	SF4	-16.473	24.252	19.420	11.139	5.214	0.106	6.219	-0.079

Appendix D Scores for individual samples for PC1-PC8, in the PCA performed in Section 3.3.3.2 Spearwood Sands [page 167 to 172]

All Spearwood samples					
sample ref	Site	PC-1	PC-2	PC-3	PC-4
11AMBER	11AMB	-18.8149	-7.7809	-5.0016	-1.8160
11AMBERR	11AMB	-33.7428	-10.8956	-6.7257	1.7607
11AMB01	11AMB	-14.8462	-6.2507	-3.5369	2.0359
11AMB02	11AMB	0.7387	-5.3778	-6.4545	-0.1505
11AMB03	11AMB	-16.2170	-12.9207	-9.2603	-1.5663
11AMB04	11AMB	-7.5870	-5.4205	-5.9296	1.1917
11AMB05	11AMB	1.1119	-4.6341	-4.0613	-0.4446
11AMB06	11AMB	-9.8505	-8.2008	-4.4627	-0.5954
11AMB07	11AMB	-1.1700	-6.6878	-6.4978	0.7628
11AMB08	11AMB	5.6716	-6.1327	-6.6596	1.7445
RC130401	Karnup	-26.1534	-17.5274	8.9697	7.3000
RC130402	Karnup	-11.2267	-20.5844	1.6978	-0.1685
GNAN20UM	GNAN	-6.0490	24.9000	0.3412	9.4217
GN20UMR	GNAN	-34.4836	9.0291	-3.6578	7.2048
NA120UM	NA1	6.4702	-12.1613	5.9159	-0.6206
NA220UM	NA2	-9.6681	8.3723	-0.5701	6.9331
NA420UM	NA4	-0.6671	9.6215	1.0882	1.9675
NAB120UM	NAB1	1.0291	25.1334	0.3538	1.7527
NAB220UM	NAB2	-11.7652	6.6561	-1.9490	-3.6964
NAB320UM	NAB3	6.3304	-4.3809	-3.4727	2.8830
NAB420UM	NAB4	4.8415	3.9130	-7.7134	-1.4303
NB120UM	NB1	3.5925	-13.6282	7.0536	-5.7579
NB220UM	NB2	10.0838	1.1667	1.6422	-1.9014
NB320UM	NB3	-7.3083	-0.2995	-7.0119	-3.6658
NB420UM	NB4	9.7142	-13.5180	-2.5397	-7.9957
NBC120UM	NBC1	-0.9132	-4.8960	-2.8686	-1.9042
NBC220UM	NBC2	-21.1258	4.0623	4.0535	-3.6721
NBC320UM	NBC3	-23.7241	5.6952	-2.5285	-5.1373
NC120UM	NC1	2.3624	36.4180	3.9695	10.9378
NC220UM	NC2	-17.7337	-3.4720	6.9845	-0.8889
NC320UM	NC3	-9.7713	-8.1150	1.2788	-0.8968
NC420UM	NC4	16.8354	-6.5165	2.2450	-1.9676
NC520UM	NC5	-19.3019	-1.0275	-2.2574	-3.6559

ND120UM	ND1	16.9936	2.8344	-7.0502	1.2681
ND220UM	ND2	10.8566	1.2133	-6.0228	-0.9132
ND320UM	ND3	0.5774	3.8833	-0.4470	0.2393
ND420UM	ND4	18.0999	-2.5180	-6.6789	0.6441
ND520UM	ND5	19.3522	15.0361	-5.9311	0.3415
ND620UM	ND6	-8.5296	7.2536	5.5826	-3.3670
NE120UM	NE1	6.0774	18.5232	-1.0951	9.8204
NE220UM	NE2	-20.2446	25.9213	2.6291	6.9581
NE2A20UM	NE2A	-28.8386	32.9398	7.1780	10.2397
NS1B20UM	NS1B	-37.5476	5.2884	10.2571	-0.7259
NS220UM	NS2	24.3860	-0.9596	-4.6569	-2.2129
NS220UMY	NS2	26.6710	1.3845	-2.0831	0.0973
NS220UMZ	NS2	28.1081	0.6602	-2.6652	0.3991
NS320UM	NS3	-15.3429	-9.3955	-11.7943	2.8322
NS420UM	NS4	-3.9029	9.2223	-5.4688	0.6259
SA220UM	SA2	20.3342	-24.9737	48.4988	7.5642
SA420UM	SA4	5.1247	11.6512	0.8241	1.4261
SA520UM	SA5	-11.1920	2.9031	6.6210	-1.6523
SA620UM	SA6	-5.6224	5.8206	5.9065	-3.0012
SB220UM	SB2	26.1328	-1.4614	-5.5134	-2.8011
SB220UMR	SB2	-0.2352	1.7958	-0.4260	-2.3576
SB320UM	SB3	-6.9216	-17.0273	-8.6983	7.2319
SB420UM	SB4	10.6170	-13.0257	1.4557	6.1178
SB720UM	SB7	13.0864	1.3261	1.3943	4.7525
SC120UM	SC1	16.0012	-16.6993	4.1576	6.2862
SC220UM	SC2	-9.4560	-10.9411	2.7849	1.9907
SC320UM	SC3	10.9130	-2.5012	-5.9451	1.4394
SC420UM	SC4	14.9921	-14.2636	0.1872	2.5187
SC520UM	SC5	-9.2590	-0.9785	13.7433	-2.9596
SC620UM	SC6	13.9441	-5.2404	-2.5707	-0.7582
SC6B20UM	SC6B	4.4160	1.1310	-0.9419	2.6914
SD220UM	SD2	-2.0329	-6.6821	-4.1915	0.4658
LEDA20UM	SDE1	-2.3420	-14.4885	2.6248	-2.3589
PARM20UM	SDE2	-24.0693	-12.2118	1.6989	-8.7845
BALD20UM	SE1	17.9055	-0.9703	-3.7019	2.2696
SE320UM	SE3	9.4838	-1.6701	-3.7446	0.2729
SEF120UM	SEF1	28.4607	-8.0713	-2.7090	4.1964
KARN20UM	SF1	-33.3273	-10.9751	2.0408	-3.0525
SF220UM	SF2	25.9490	11.1859	-0.7412	2.9336
SF320UM	SF3	3.5951	-6.5014	-0.2036	0.2721
SG120UM	SG1	18.5157	-10.9848	3.8901	0.8366
SG220UM	SG2	18.2130	7.2934	-0.2799	-2.8063
SG320UM	SG3	22.6415	11.1304	3.5381	-3.1128
WEMB100	WEMB	-12.6240	15.3884	4.4968	-25.2284

WEMB1850	WEMB	17.4239	25.8918	9.0016	-12.6890
WEMB925	WEMB	15.0401	26.1453	8.7762	-13.1543
XTALCAVE	YAN	0.9139	-7.8215	-6.1611	-2.7599
Spearwood samples with outlier SA2 removed					
sample ref	**Site**	**PC-1**	**PC-2**	**PC-3**	**PC-4**
11AMBER	11AMB	-18.6755	-7.8446	-1.0120	-4.5514
11AMBERR	11AMB	-33.6579	-10.4747	-5.1528	-4.5455
11AMB01	11AMB	-14.7419	-6.2426	-3.3863	-1.2495
11AMB02	11AMB	1.0075	-6.4397	-2.8571	-4.1116
11AMB03	11AMB	-16.1229	-13.5937	-3.2278	-7.2347
11AMB04	11AMB	-7.3351	-6.0469	-3.8821	-3.3640
11AMB05	11AMB	1.2996	-5.4136	-1.3026	-2.3350
11AMB06	11AMB	-9.7885	-8.5441	-1.4746	-2.9488
11AMB07	11AMB	-0.9633	-7.6511	-3.5982	-3.5573
11AMB08	11AMB	5.8897	-7.3912	-4.3623	-2.8400
RC130401	Karnup	-27.2259	-15.2372	-0.3616	12.7779
RC130402	Karnup	-12.0703	-19.9490	2.3316	3.7985
GNAN20UM	GNAN	-4.6969	24.8632	-8.9424	3.0320
GN20UMR	GNAN	-33.6192	9.7737	-9.1402	-1.3110
NA120UM	NA1	5.7822	-11.7938	4.9434	6.5804
NA220UM	NA2	-9.0504	8.4930	-6.5618	2.2880
NA420UM	NA4	-0.0575	9.4908	-1.3458	1.3338
NAB120UM	NAB1	2.4282	24.6802	-2.4032	-0.8079
NAB220UM	NAB2	-11.0799	6.5268	1.5937	-4.2810
NAB320UM	NAB3	6.4643	-5.2490	-3.6466	0.0077
NAB420UM	NAB4	5.6269	2.3998	-2.8748	-6.3362
NB120UM	NB1	2.8198	-13.0610	9.8627	4.7556
NB220UM	NB2	10.2588	0.6744	2.9879	1.3959
NB320UM	NB3	-6.7182	-1.2089	-0.7085	-7.2687
NB420UM	NB4	9.4242	-14.4873	6.5017	-4.1122
NBC120UM	NBC1	-0.7829	-5.4558	0.5225	-2.3608
NBC220UM	NBC2	-20.8431	5.1290	4.8232	0.3461
NBC320UM	NBC3	-23.0185	5.9767	2.1980	-6.2065
NC120UM	NC1	4.0606	36.4202	-8.6587	5.9256
NC220UM	NC2	-17.9893	-2.0518	4.6945	5.3868
NC320UM	NC3	-9.9880	-7.7232	1.9869	1.6076
NC420UM	NC4	16.5886	-7.1332	3.9521	2.8001
NC520UM	NC5	-18.9551	-0.8119	1.6710	-3.9200
ND120UM	ND1	17.6420	0.9615	-4.4373	-3.9379
ND220UM	ND2	11.4055	-0.2899	-2.1139	-4.4421
ND320UM	ND3	0.9965	3.5228	-0.3527	0.0719
ND420UM	ND4	18.4711	-4.3462	-3.3840	-3.4154
ND520UM	ND5	20.5397	13.0759	-3.6700	-4.5952
ND620UM	ND6	-8.2019	7.9717	5.5303	1.9176

NE120UM	NE1	7.1577	17.8651	-9.4201	3.2623
NE220UM	NE2	-18.9068	26.7277	-6.0749	2.4986
NE2A20UM	NE2A	-27.3875	34.6782	-6.8750	6.8792
NS1B20UM	NS1B	-37.4942	7.8786	5.3630	6.1355
NS220UM	NS2	24.7366	-2.8462	0.1792	-3.1951
NS220UMY	NS2	26.9855	-0.2480	-0.3844	0.0423
NS220UMZ	NS2	28.4108	-1.0961	-0.8813	-0.1238
NS320UM	NS3	-14.9818	-10.4037	-8.4343	-7.0196
NS420UM	NS4	-2.9670	8.3519	-3.9128	-4.7209
SA420UM	SA4	5.8384	11.2114	-0.9672	1.1671
SA520UM	SA5	-11.1308	3.9314	4.9177	4.3394
SA620UM	SA6	-5.3865	6.4715	5.6472	3.2347
SB220UM	SB2	26.5018	-3.5372	0.2668	-4.0664
SB220UMR	SB2	0.0998	1.4546	1.8792	-1.3750
SB320UM	SB3	-7.1382	-17.8370	-9.7353	-0.9989
SB420UM	SB4	10.0544	-13.3012	-2.9350	7.1984
SB720UM	SB7	13.2278	0.7804	-2.6090	4.9592
SC120UM	SC1	15.1119	-16.8107	-1.2099	10.2154
SC220UM	SC2	-9.9069	-10.2916	0.5866	4.6762
SC320UM	SC3	11.2616	-3.9253	-3.7909	-2.5865
SC420UM	SC4	14.4473	-14.9317	-0.4701	4.5431
SC520UM	SC5	-9.7354	0.9097	10.2689	10.0797
SC620UM	SC6	13.9970	-6.3545	0.0970	-0.8959
SC6B20UM	SC6B	4.6984	0.6142	-2.4328	1.3461
SD220UM	SD2	-1.9361	-7.3154	-2.0800	-1.8391
LEDA20UM	SDE1	-2.9439	-14.1911	4.4989	2.9407
PARM20UM	SDE2	-24.4157	-11.2566	8.6612	-2.5303
BALD20UM	SE1	18.1942	-2.3957	-3.1412	-0.1165
SE320UM	SE3	9.7755	-2.7764	-1.6620	-1.4463
SEF120UM	SEF1	28.3155	-9.7074	-3.5152	3.0175
KARN20UM	SF1	-33.6477	-9.5122	3.7913	0.2749
SF220UM	SF2	26.6579	9.7020	-2.5213	1.9130
SF320UM	SF3	3.4900	-6.8557	0.4472	1.6861
SG120UM	SG1	17.9478	-11.3736	2.8696	6.3822
SG220UM	SG2	18.7681	6.1392	2.5282	-0.8046
SG320UM	SG3	23.1833	10.2488	4.7855	1.9097
WEMB100	WEMB	-11.6910	15.7255	22.3811	-12.6609
WEMB1850	WEMB	18.4851	25.6558	14.6860	-1.3748
WEMB925	WEMB	16.1343	25.9685	14.8772	-1.9427
XTALCAVE	YAN	1.0656	-8.8668	-0.4212	-5.2969

Spearwood scores_ with outlier SA2 and WEMB samples removed

sample ref	Site	PC-1	PC-2	PC-3	PC-4
11AMBER	11AMB	-17.8025	-8.2153	-3.9697	-3.3086
11AMBERR	11AMB	-32.5104	-11.4541	-8.3809	1.9754

11AMB01	11AMB	-13.9857	-6.0216	-3.7542	1.1638
11AMB02	11AMB	1.7460	-5.1971	-4.5766	-2.3333
11AMB03	11AMB	-14.8045	-13.5494	-8.1261	-2.2635
11AMB04	11AMB	-6.5955	-5.2587	-5.1055	-0.8157
11AMB05	11AMB	1.9375	-4.3030	-2.0772	-2.3484
11AMB06	11AMB	-8.8920	-8.2022	-3.2878	-1.5585
11AMB07	11AMB	-0.1286	-6.4278	-4.9073	-1.4856
11AMB08	11AMB	6.6897	-5.5489	-4.6559	-1.4214
RC130401	Karnup	-25.9118	-15.7267	7.3800	7.7384
RC130402	Karnup	-10.4341	-19.8808	3.5035	0.4949
GNAN20UM	GNAN	-6.1517	26.2994	-2.3048	3.7715
GN20UMR	GNAN	-33.8881	9.1273	-8.0343	5.9803
NA120UM	NA1	6.7585	-11.0956	6.4006	6.2959
NA220UM	NA2	-9.3411	9.3007	-3.5853	7.3729
NA420UM	NA4	-0.4929	10.2993	0.4190	2.3301
NAB120UM	NAB1	0.9227	25.7302	0.4583	-2.9772
NAB220UM	NAB2	-11.2783	6.2433	-0.3948	-6.1350
NAB320UM	NAB3	7.0962	-3.6044	-3.4759	4.6404
NAB420UM	NAB4	5.7292	4.0272	-3.8216	-9.3179
NB120UM	NB1	3.8539	-13.1783	9.0241	1.8595
NB220UM	NB2	10.3767	1.9073	4.2122	-2.4158
NB320UM	NB3	-6.3389	-0.7946	-3.9700	-8.4329
NB420UM	NB4	10.6290	-13.9632	0.5071	-1.6915
NBC120UM	NBC1	-0.1482	-4.8303	-1.5766	-0.4665
NBC220UM	NBC2	-20.9696	3.7836	3.9735	-1.7155
NBC320UM	NBC3	-23.1350	4.6258	-2.3111	-4.6316
NC120UM	NC1	1.7389	38.3813	0.8597	4.6145
NC220UM	NC2	-17.6411	-2.9265	6.9951	1.1776
NC320UM	NC3	-9.2073	-7.7421	2.1510	0.4893
NC420UM	NC4	17.2332	-5.6308	4.2516	2.1044
NC520UM	NC5	-18.6149	-1.4862	-0.3105	-6.8603
ND120UM	ND1	17.8277	3.4386	-5.1220	-0.9826
ND220UM	ND2	11.6777	1.4421	-4.0661	-1.7969
ND320UM	ND3	0.9769	4.4640	0.8883	-1.7501
ND420UM	ND4	19.0228	-1.9475	-4.9162	1.0173
ND520UM	ND5	19.8462	15.6377	-3.1249	-5.5575
ND620UM	ND6	-8.5762	7.3318	5.3138	0.8532
NE120UM	NE1	6.1766	20.1667	-3.4935	6.6100
NE220UM	NE2	-20.4763	26.6205	-1.7150	5.6417
NE2A20UM	NE2A	-29.5202	34.1346	1.2281	7.7002
NS1B20UM	NS1B	-37.8143	5.4481	8.2898	1.0664
NS220UM	NS2	25.1282	-0.4774	-1.9157	-0.6575
NS220UMY	NS2	27.1714	2.4071	0.0888	1.2622
NS220UMZ	NS2	28.6601	1.7162	-0.5083	1.7195

NS320UM	NS3	-13.8473	-9.5124	-10.6715	-2.8736
NS420UM	NS4	-3.2554	9.2563	-4.8529	-2.6966
SA420UM	SA4	5.2551	12.5475	2.1173	-2.3964
SA520UM	SA5	-11.2283	3.4685	7.5286	-1.8901
SA620UM	SA6	-5.6909	6.4691	9.1313	-8.2220
SB220UM	SB2	26.9435	-1.0661	-2.4561	-1.0966
SB220UMR	SB2	0.2234	1.8745	0.2827	0.2231
SB320UM	SB3	-5.5107	-16.1678	-9.2604	5.9027
SB420UM	SB4	11.1959	-11.1029	2.0699	6.7370
SB720UM	SB7	13.3669	2.9815	2.1962	3.3830
SC120UM	SC1	16.4559	-14.3553	5.1826	8.0599
SC220UM	SC2	-8.9471	-10.0825	2.5736	4.3838
SC320UM	SC3	11.7961	-1.8508	-3.9861	-0.8620
SC420UM	SC4	15.6855	-12.7891	2.0887	4.0345
SC520UM	SC5	-9.7096	0.1001	15.4089	-1.5203
SC620UM	SC6	14.6583	-4.7433	-1.7289	3.8834
SC6B20UM	SC6B	4.8953	2.0081	-0.8996	3.3028
SD220UM	SD2	-1.1486	-6.2937	-2.5203	-1.4920
LEDA20UM	SDE1	-1.7542	-13.9621	4.3675	0.9885
PARM20UM	SDE2	-23.3963	-13.0775	4.7751	-8.2352
BALD20UM	SE1	18.5828	0.1094	-1.7983	0.8858
SE320UM	SE3	10.1960	-0.9458	-0.7064	-4.3619
SEF120UM	SEF1	29.1861	-6.3476	-0.7925	4.8411
KARN20UM	SF1	-32.6929	-11.3421	2.6637	-2.9972
SF220UM	SF2	26.1384	12.7742	2.0265	-2.2133
SF320UM	SF3	4.1789	-5.6116	2.4291	-2.6921
SG120UM	SG1	18.8796	-9.4506	5.8281	4.2064
SG220UM	SG2	18.4827	8.0289	3.9750	-7.6482
SG320UM	SG3	22.5529	12.1655	7.7859	-7.3270
XTALCAVE	YAN	1.9681	-8.1526	-5.2143	0.7366

Appendix E Maximum counts and percentage intensities for the 38 samples from Section 4.3.3, analysed using the Synchrotron PD beamline, treated as per Chapter 3.

sample ref	V1	K1	G1	K2	SUBTOTAL	M1	Q1	F1	TOTAL	%V1	%K1	%G1	%K2	%M1	%Q1	%F1
SC7	1361	7797	16295	8810	34263	260	186967	1035	222525	4.0	22.8	47.6	25.7	0.1	84.0	0.5
SC6B	1176	7489	1955	8344	18964	205	104935	7487	131591	6.2	39.5	10.3	44.0	0.2	79.7	5.7
SC5	1359	8632	6192	7690	23873	-53	345430	8821	378071	5.7	36.2	25.9	32.2	0.0	91.4	2.3
SC4	881	3349	2061	5025	11316	231	92321	4353	108221	7.8	29.6	18.2	44.4	0.2	85.3	4.0
SC3	1007	5221	1448	7043	14719	214	135731	9355	160019	6.8	35.5	9.8	47.8	0.1	84.8	5.8
SC2	1013	3802	1842	5437	12094	103	170488	8242	190927	8.4	31.4	15.2	45.0	0.1	89.3	4.3
SC1	905	3174	3002	4576	11657	-62	89268	4725	105588	7.8	27.2	25.8	39.3	-0.1	84.5	4.5
SB7	893	3907	1849	5571	12220	113	209582	26703	248618	7.3	32.0	15.1	45.6	0.0	84.3	10.7
SB6	636	1994	5304	2142	10076	-197	548827	445	559151	6.3	19.8	52.6	21.3	0.0	98.2	0.1
SB5	462	452	180	585	1679	54	938174	471	940378	27.5	26.9	10.7	34.8	0.0	99.8	0.1
SB4	1092	3819	2422	4961	12294	33	117689	3402	133418	8.9	31.1	19.7	40.4	0.0	88.2	2.5
SB3	1005	4309	1418	6275	13007	109	62410	2633	78159	7.7	33.1	10.9	48.2	0.1	79.9	3.4
SB2	886	5571	1968	8366	16791	65	81800	7198	105854	5.3	33.2	11.7	49.8	0.1	77.3	6.8
SB1	513	2093	3356	1799	7761	-17	658745	542	667031	6.6	27.0	43.2	23.2	0.0	98.8	0.1
SA6B	566	693	109	594	1962	73	738974	1336	742345	28.8	35.3	5.6	30.3	0.0	99.5	0.2
SA5	985	6373	2727	7946	18031	48	103371	5119	126569	5.5	35.3	15.1	44.1	0.0	81.7	4.0
SA4	1317	6369	1515	6669	15870	33	97941	4005	117849	8.3	40.1	9.5	42.0	0.0	83.1	3.4
SA3	821	3694	7100	3976	15591	-36	357064	486	373105	5.3	23.7	45.5	25.5	0.0	95.7	0.1
SA2	984	2326	16593	6141	26044	157	20154	2372	48727	3.8	8.9	63.7	23.6	0.3	41.4	4.9

ND8A	605	492	189	727	2013	-136	926228	167	928272	30.1	24.4	9.4	36.1	0.0	99.8	0.0
ND8	511	463	598	1011	2583	180	384317	91	387171	19.8	17.9	23.2	39.1	0.0	99.3	0.0
ND7	1087	5354	6304	5054	17799	39	434983	1662	454483	6.1	30.1	35.4	28.4	0.0	95.7	0.4
ND6	919	10161	2990	8758	22828	-2	121506	3331	147663	4.0	44.5	13.1	38.4	0.0	82.3	2.3
ND5	828	7527	368	6848	15571	45	180008	8388	204012	5.3	48.3	2.4	44.0	0.0	88.2	4.1
ND4	1036	7410	974	8489	17909	-120	197281	6652	221722	5.8	41.4	5.4	47.4	-0.1	89.0	3.0
ND3	1168	8931	1117	10952	22168	107	102724	4605	129604	5.3	40.3	5.0	49.4	0.1	79.3	3.6
ND2	1172	5830	923	7541	15466	-97	96471	3528	115368	7.6	37.7	6.0	48.8	-0.1	83.6	3.1
ND1	590	1833	496	1404	4323	-25	285912	5806	296016	13.6	42.4	11.5	32.5	0.0	96.6	2.0
NC6	1002	5732	773	6826	14333	-34	204646	5164	224109	7.0	40.0	5.4	47.6	0.0	91.3	2.3
NC5	1065	3460	1770	6183	12478	74	115100	5211	132863	8.5	27.7	14.2	49.6	0.1	86.6	3.9
NC4	1217	8438	3898	9626	23179	67	90872	2247	116365	5.3	36.4	16.8	41.5	0.1	78.1	1.9
NC3	826	9876	3837	8318	22857	122	243151	3671	269801	3.6	43.2	16.8	36.4	0.0	90.1	1.4
NC2	621	3734	647	11289	16291	216	94801	6053	117361	3.8	22.9	4.0	69.3	0.2	80.8	5.2
NC1	434	933	245	500	2112	200	893811	404	896527	20.5	44.2	11.6	23.7	0.0	99.7	0.0
NA5	1150	8154	1260	10708	21272	128	86628	4738	112766	5.4	38.3	5.9	50.3	0.1	76.8	4.2
NA4	507	4874	17675	7169	30225	71	249998	997	281291	1.7	16.1	58.5	23.7	0.0	88.9	0.4
NA3	646	5648	873	11607	18774	222	87384	4886	111266	3.4	30.1	4.7	61.8	0.2	78.5	4.4
NA2	1380	3534	2177	5937	13028	92	154146	5199	172465	10.6	27.1	16.7	45.6	0.1	89.4	3.0

Appendix F Raw counts and percentage intensities for dataset and Case Study 1 in Section 5.2.[page 175 to 186]

XRD FILE	Group for ALL	Site	V1	K1	Gibb1	K2	goe1	SUB TOTAL	M1	Q1	F1	Trad. TOTAL	%V1	%K1	%Gibb1	%K2	%goe1	%M1	%Q1	%F1
0F25082R	Alluvial/ Lateritic	D2 AUGEN GNEISS	586	4715	1109	986	561	7957	2096	30637	5267	45957	7.4	59.3	13.9	12.4	7.1	4.6	66.7	11.5
0F25083R	Alluvial/ Lateritic	D3 QTZ-FELD-BIOTITE GNEISS	446	6870	8006	870	1028	17220	2653	6254	326	26453	2.6	39.9	46.5	5.1	6.0	10.0	23.6	1.2
0F25084R	Alluvial/ Lateritic	D4 DONNYBROOK SST	554	3148	501	425	270	4898	5518	5628	1330	17374	11.3	64.3	10.2	8.7	5.5	31.8	32.4	7.7
0F25085R	Alluvial/ Lateritic	D5 DONNYBROOK SST	2090	9557	3086	983	749	16465	320	5403	664	22852	12.7	58.0	18.7	6.0	4.5	1.4	23.6	2.9
HELENA1	Alluvial/ Lateritic	Helena Valley	88	2192	202	1236	877	4595	510	5012	840	10957	1.9	47.7	4.4	26.9	19.1	4.7	45.7	7.7
HELENA2	Alluvial/ Lateritic	Helena Valley	207	5401	270	2416	1505	9799	949	9622	1456	21826	2.1	55.1	2.8	24.7	15.4	4.3	44.1	6.7
HELENA3	Alluvial/ Lateritic	Helena Valley	133	6053	230	1881	1165	9462	2245	13543	6176	31426	1.4	64.0	2.4	19.9	12.3	7.1	43.1	19.7
HELENA4	Alluvial/ Lateritic	Helena Valley	128	7485	429	2299	2055	12396	642	11957	2192	27187	1.0	60.4	3.5	18.5	16.6	2.4	44.0	8.1
HELENA5	Alluvial/ Lateritic	Helena Valley	165	12324	260	2964	3086	18799	2062	24800	4043	49704	0.9	65.6	1.4	15.8	16.4	4.1	49.9	8.1
HELENA6	Alluvial/ Lateritic	Helena Valley	452	19975	3222	2212	2998	28859	463	17550	3341	50213	1.6	69.2	11.2	7.7	10.4	0.9	35.0	6.7
HELENA7	Alluvial/ Lateritic	Helena Valley	0	21173	489	2238	1846	25746	1387	12034	2296	41463	0.0	82.2	1.9	8.7	7.2	3.3	29.0	5.5
HELENA8	Alluvial/ Lateritic	Helena Valley	0	8409	338	3184	2859	14790	1436	8881	1275	26382	0.0	56.9	2.3	21.5	19.3	5.4	33.7	4.8
2F135406	Alluvial/ Lateritic	Southern Cross	144	15779	0	2438	1988	20349	103	18250	935	39637	0.7	77.5	0.0	12.0	9.8	0.3	46.0	2.4

2F135412	Alluvial/ Lateritic	Wongan Hills	0	10736	0	2039	1640	14415	0	4031	952	19398	0.0	74.5	0.0	14.1	11.4	0.0	20.8	4.9
2F135403	Alluvial/ Lateritic	Wongan Hills	0	23674	0	2176	2498	28348	0	6677	1907	36932	0.0	83.5	0.0	7.7	8.8	0.0	18.1	5.2
2F135409	Alluvial/ Lateritic	Wubin	117	19701	0	2023	1971	23812	191	15326	786	40115	0.5	82.7	0.0	8.5	8.3	0.5	38.2	2.0
NA320UM	Bassendean System	NA3	103	3411	3544	1081	1153	9292	87	24469	5865	39713	1.1	36.7	38.1	11.6	12.4	0.2	61.6	14.8
NA520UM	Bassendean System	NA5	45	308	0	0	0	353	0	19251	245	19849	12.7	87.3	0.0	0.0	0.0	0.0	97.0	1.2
NA520UMX	Bassendean System	NA5	198	464	0	0	0	662	0	102781	1139	104582	29.9	70.1	0.0	0.0	0.0	0.0	98.3	1.1
NB520UM	Bassendean System	NB5	112	660	1576	449	405	3202	0	21590	522	25314	3.5	20.6	49.2	14.0	12.6	0.0	85.3	2.1
NBC420UM	Bassendean System	NBC4	164	1024	458	376	418	2440	87	30775	1946	35248	6.7	42.0	18.8	15.4	17.1	0.2	87.3	5.5
NC620UM	Bassendean System	NC6	0	380	0	74	76	530	129	36706	1694	39059	0.0	71.7	0.0	14.0	14.3	0.3	94.0	4.3
NC620UMX	Bassendean System	NC6	0	626	0	0	0	626	0	77236	1632	79494	0.0	100.0	0.0	0.0	0.0	0.0	97.2	2.1
ND720UM	Bassendean System	ND7	87	867	784	450	574	2762	0	14860	2962	20584	3.1	31.4	28.4	16.3	20.8	0.0	72.2	14.4
ND820UM	Bassendean System	ND8	0	196	85	117	0	398	0	35155	291	35844	0.0	49.2	21.4	29.4	0.0	0.0	98.1	0.8
ND820UMR	Bassendean System	ND8	0	393	243	352	455	1443	0	42095	428	43966	0.0	27.2	16.8	24.4	31.5	0.0	95.7	1.0
ND8A20UM	Bassendean System	ND8A	0	87	0	0	0	87	0	67790	494	68371	0.0	100.0	0.0	0.0	0.0	0.0	99.2	0.7
ND8A20UR	Bassendean System	ND8A	0	146	0	0	0	146	0	145733	728	146607	0.0	100.0	0.0	0.0	0.0	0.0	99.4	0.5
NE320UM	Bassendean System	NE3	0	93	0	0	0	93	0	39530	678	40301	0.0	100.0	0.0	0.0	0.0	0.0	98.1	1.7
NE320URX	Bassendean System	NE3	132	203	0	0	0	335	0	197995	2414	200744	39.4	60.6	0.0	0.0	0.0	0.0	98.6	1.2
NE420UM	Bassendean System	NE4	0	0	0	0	0	0	0	56986	2510	59496	0.0	0.0	0.0	0.0	0.0	0.0	95.8	4.2
NE420URR	Bassendean System	NE4	0	0	0	0	0	0	0	61122	430	61552	0.0	0.0	0.0	0.0	0.0	0.0	99.3	0.7

SA320UM	Bassendean System	SA3	51	456	298	190	226	1221	77	31313	2353	34964	4.2	37.3	24.4	15.6	18.5	0.2	89.6	6.7
SA6B20UM	Bassendean System	SA6B	0	114	0	0	0	114	0	20704	1088	21906	0.0	100.0	0.0	0.0	0.0	0.0	94.5	5.0
SA6B20UX	Bassendean System	SA6B	170	503	0	0	0	673	0	71480	4651	76804	25.3	74.7	0.0	0.0	0.0	0.0	93.1	6.1
SB120UM	Bassendean System	SB1	0	313	404	178	894	1789	0	54657	358	56804	0.0	17.5	22.6	9.9	50.0	0.0	96.2	0.6
SB120UMR	Bassendean System	SB1	0	276	255	129	524	1184	0	35560	919	37663	0.0	23.3	21.5	10.9	44.3	0.0	94.4	2.4
SB120UKX	Bassendean System	SB1	202	1432	1567	759	3421	7381	0	162706	1265	171352	2.7	19.4	21.2	10.3	46.3	0.0	95.0	0.7
SB520UM	Bassendean System	SB5	0	81	0	0	0	81	0	20029	372	20482	0.0	100.0	0.0	0.0	0.0	0.0	97.8	1.8
SB520KR	Bassendean System	SB5	183	282	0	0	0	465	134	171615	1085	173299	39.4	60.6	0.0	0.0	0.0	0.1	99.0	0.6
SB620UM	Bassendean System	SB6	88	427	616	241	692	2064	0	26509	1222	29795	4.3	20.7	29.8	11.7	33.5	0.0	89.0	4.1
SC720UM	Bassendean System	SC7	130	977	1386	350	558	3401	0	14097	1625	19123	3.8	28.7	40.8	10.3	16.4	0.0	73.7	8.5
CASU20UM	Bassendean System	SD1	0	57	0	0	0	57	0	28755	177	28989	0.0	100.0	0.0	0.0	0.0	0.0	99.2	0.6
SD120KR	Bassendean System	SD1	185	339	0	204	187	915	246	265344	2358	268863	20.2	37.0	0.0	22.3	20.4	0.1	98.7	0.9
WELL20UM	Bassendean System	SDE3	99	777	1340	457	905	3578	0	32913	550	37041	2.8	21.7	37.5	12.8	25.3	0.0	88.9	1.5
SE220UM	Bassendean System	SE2	312	2205	130	524	708	3879	93	22857	20830	47659	8.0	56.8	3.4	13.5	18.3	0.2	48.0	43.7
SF420UM	Bassendean System	SF4	169	787	704	211	0	1871	58	26140	7561	35630	9.0	42.1	37.6	11.3	0.0	0.2	73.4	21.2
RH73SLOW	body disposal site	body location	519	1975	428	598	729	4249	144	12225	23699	40317	12.2	46.5	10.1	14.1	17.2	0.4	30.3	58.8
3F116022	body disposal site	E grid A4	521	1535	294	332	529	3211	0	9989	4347	17547	16.2	47.8	9.2	10.3	16.5	0.0	56.9	24.8
3F116039	body disposal site	E grid B2	172	616	138	235	357	1518	0	8371	4948	14837	11.3	40.6	9.1	15.5	23.5	0.0	56.4	33.3
3F116038	body disposal site	E grid B3	277	916	235	173	207	1808	196	4929	3614	10547	15.3	50.7	13.0	9.6	11.4	1.9	46.7	34.3

3F116037	body disposal site	E grid B4	323	717	246	167	224	1677	47	3273	4519	9516	19.3	42.8	14.7	10.0	13.4	0.5	34.4	47.5
3F116042	body disposal site	E grid B6	367	892	290	163	279	1991	65	3379	1629	7064	18.4	44.8	14.6	8.2	14.0	0.9	47.8	23.1
C1VSLOW	body disposal site	E grid C1	507	2931	804	549	1000	5791	247	34746	12257	53041	8.8	50.6	13.9	9.5	17.3	0.5	65.5	23.1
3F116024	body disposal site	E grid C2	369	1975	444	451	608	3847	195	23014	20012	47068	9.6	51.3	11.5	11.7	15.8	0.4	48.9	42.5
3F116025	body disposal site	E grid C2F	167	606	146	133	242	1294	490	10764	33347	45895	12.9	46.8	11.3	10.3	18.7	1.1	23.5	72.7
3F116026	body disposal site	E grid C3	600	2267	531	413	630	4441	114	13057	19092	36704	13.5	51.0	12.0	9.3	14.2	0.3	35.6	52.0
3F116027	body disposal site	E grid C4	468	2103	311	427	632	3941	209	10331	5528	20009	11.9	53.4	7.9	10.8	16.0	1.0	51.6	27.6
3F116040	body disposal site	E grid C6	351	981	320	347	487	2486	199	10607	6366	19658	14.1	39.5	12.9	14.0	19.6	1.0	54.0	32.4
3F116028	body disposal site	E grid D1	302	1015	319	158	288	2082	0	11616	6114	19812	14.5	48.8	15.3	7.6	13.8	0.0	58.6	30.9
3F116029	body disposal site	E grid D2	559	2238	559	375	651	4382	303	12050	15594	32329	12.8	51.1	12.8	8.6	14.9	0.9	37.3	48.2
3F116030	body disposal site	E grid D2F	363	923	314	229	315	2144	0	11400	16261	29805	16.9	43.1	14.6	10.7	14.7	0.0	38.2	54.6
3F116031	body disposal site	E grid D3	560	2715	729	806	1014	5824	0	15857	12847	34528	9.6	46.6	12.5	13.8	17.4	0.0	45.9	37.2
3F116032	body disposal site	E grid D4	403	1519	282	490	573	3267	211	9405	8388	21271	12.3	46.5	8.6	15.0	17.5	1.0	44.2	39.4
3F116033	body disposal site	E grid D5	393	2036	513	734	919	4595	147	13762	7161	25665	8.6	44.3	11.2	16.0	20.0	0.6	53.6	27.9
3F116034	body disposal site	E grid D5A	447	1858	530	732	904	4471	371	19172	15041	39055	10.0	41.6	11.9	16.4	20.2	0.9	49.1	38.5
3F116041	body disposal site	E grid D6	319	848	275	298	319	2059	20	8684	5791	16554	15.5	41.2	13.4	14.5	15.5	0.1	52.5	35.0
3F116018	body disposal site	E grid Z5	265	1569	300	250	411	2795	166	14981	8213	26155	9.5	56.1	10.7	8.9	14.7	0.6	57.3	31.4
RH71SLOW	body disposal site	track	372	1506	208	166	303	2555	277	8884	5025	16741	14.6	58.9	8.1	6.5	11.9	1.7	53.1	30.0
RH72SLOW	body disposal site	track	352	930	181	186	307	1956	0	11276	6672	19904	18.0	47.5	9.3	9.5	15.7	0.0	56.7	33.5

3116043R	near body disposal site	21m elevation carpark end Pipidinny Road	62	587	0	147	80	876	1041	5581	6253	13751	7.1	67.0	0.0	16.8	9.1	7.6	40.6	45.5
116007SS	near body disposal site	E 10M W body	680	2407	441	185	299	4012	0	7936	8525	20473	16.9	60.0	11.0	4.6	7.5	0.0	38.8	41.6
116006SS	near body disposal site	E 10M W body	415	2099	586	618	875	4593	0	13857	5004	23454	9.0	45.7	12.8	13.5	19.1	0.0	59.1	21.3
3F116006	near body disposal site	E 10M W body	148	598	157	152	205	1260	61	3368	2244	6933	11.7	47.5	12.5	12.1	16.3	0.9	48.6	32.4
3F116007	near body disposal site	E 10M W body	189	653	99	47	101	1089	51	1899	1854	4893	17.4	60.0	9.1	4.3	9.3	1.0	38.8	37.9
116008SS	near body disposal site	E 20M W body	242	1020	210	161	261	1894	0	2393	2530	6817	12.8	53.9	11.1	8.5	13.8	0.0	35.1	37.1
3F116008	near body disposal site	E 20M W body	107	288	0	66	85	546	0	960	428	1934	19.6	52.7	0.0	12.1	15.6	0.0	49.6	22.1
116004SS	near body disposal site	E 2M E of body	551	2236	444	559	570	4360	300	13814	15837	34311	12.6	51.3	10.2	12.8	13.1	0.9	40.3	46.2
3F116004	near body disposal site	E 2M E of body	164	602	123	121	135	1145	74	3001	5137	9357	14.3	52.6	10.7	10.6	11.8	0.8	32.1	54.9
116002SS	near body disposal site	E 2M N of body	574	2514	717	852	1032	5689	0	15105	3009	23803	10.1	44.2	12.6	15.0	18.1	0.0	63.5	12.6
3F116002	near body disposal site	E 2M N of body	181	763	181	213	282	1620	0	5170	507	7297	11.2	47.1	11.2	13.1	17.4	0.0	70.9	6.9
116003SS	near body disposal site	E 2M S of body	300	1617	343	541	730	3531	0	25745	20416	49692	8.5	45.8	9.7	15.3	20.7	0.0	51.8	41.1
3F116003	near body disposal site	E 2M S of body	89	478	109	134	199	1009	0	4941	3885	9835	8.8	47.4	10.8	13.3	19.7	0.0	50.2	39.5
116005SS	near body disposal site	E 2M W of body	465	2421	488	536	572	4482	0	9799	21607	35888	10.4	54.0	10.9	12.0	12.8	0.0	27.3	60.2
3F116005	near body disposal site	E 2M W of body	163	649	150	152	188	1302	0	1650	4120	7072	12.5	49.8	11.5	11.7	14.4	0.0	23.3	58.3
3F116009	near body disposal site	E 30M W body	163	427	93	0	0	683	0	9102	2572	12357	23.9	62.5	13.6	0.0	0.0	0.0	73.7	20.8
116009SS	near body disposal site	E 30M W of body	523	1717	282	137	295	2954	115	14425	10762	28256	17.7	58.1	9.5	4.6	10.0	0.4	51.1	38.1
3116048X	near body disposal site	Gibson Park Pinnaroo Valley	299	2860	475	534	0	4168	949	30665	10840	46622	7.2	68.6	11.4	12.8	0.0	2.0	65.8	23.3
3116044R	near body disposal site	Pipidinny Rd	0	555	91	169	0	815	198	4203	4227	9443	0.0	68.1	11.2	20.7	0.0	2.1	44.5	44.8

3F116010	near body disposal site	Pipidinny Rd cutting	109	258	72	37	43	519	101	393	938	1951	21.0	49.7	13.9	7.1	8.3	5.2	20.1	48.1
116010SS	near body disposal site	Pipidinny Rd cutting	290	871	163	251	0	1575	158	1238	4212	7183	18.4	55.3	10.3	15.9	0.0	2.2	17.2	58.6
91M5781	Coastal limestone	CORONATION	0	4931	0	1967	3221	10119	158	8707	3556	22540	0.0	48.7	0.0	19.4	31.8	0.7	38.6	15.8
91M5788	Coastal limestone	CORONATION	339	11618	225	1479	3406	17067	138	4308	1302	22815	2.0	68.1	1.3	8.7	20.0	0.6	18.9	5.7
91M5785	Coastal limestone	CORONATION	227	12693	206	2494	5009	20629	110	9357	4573	34669	1.1	61.5	1.0	12.1	24.3	0.3	27.0	13.2
9KARRDGB	Coastal limestone	GOODE BEACH	233	764	1736	0	411	3144	0	3762	824	7730	7.4	24.3	55.2	0.0	13.1	0.0	48.7	10.7
SHELLY01	Coastal limestone	WEST CAPE HOWE	233	331	403	111	289	1367	0	6087	1273	8727	17.0	24.2	29.5	8.1	21.1	0.0	69.7	14.6
MEH1	House-Quindalup	Melon Hill	0	1223	337	180	0	1740	395	35321	12770	50226	0.0	70.3	19.4	10.3	0.0	0.8	70.3	25.4
MEH2	House-Quindalup	Melon Hill	182	665	178	260	95	1380	152	9855	2049	13436	13.2	48.2	12.9	18.8	6.9	1.1	73.3	15.3
SWB1	House-Quindalup	Swanbourne	0	1177	428	225	126	1956	542	22495	12380	37373	0.0	60.2	21.9	11.5	6.4	1.5	60.2	33.1
SWB2	House-Quindalup	Swanbourne	0	2659	371	209	172	3411	727	56057	21011	81206	0.0	78.0	10.9	6.1	5.0	0.9	69.0	25.9
SWB3	House-Quindalup	Swanbourne	121	2440	311	151	66	3089	770	30925	19053	53837	3.9	79.0	10.1	4.9	2.1	1.4	57.4	35.4
SWB4	House-Quindalup	Swanbourne	244	2943	485	358	255	4285	1494	33495	23068	62342	5.7	68.7	11.3	8.4	6.0	2.4	53.7	37.0
11AMB501	Mixed Origin	11AMB	112	519	0	52	79	762	104	21162	24714	46742	14.7	68.1	0.0	6.8	10.4	0.2	45.3	52.9
NC720KR	Mixed Origin	11AMB	327	1942	119	531	651	3570	170	136729	48050	188519	9.2	54.4	3.3	14.9	18.2	0.1	72.5	25.5
11AMB50S	Mixed Origin	50m 11AMB	62	248	0	142	159	611	63	13299	14872	28845	10.1	40.6	0.0	23.2	26.0	0.2	46.1	51.6
11AMB50SC	Mixed Origin	50m 11AMB	269	1327	0	557	517	2670	221	56236	26324	85451	10.1	49.7	0.0	20.9	19.4	0.3	65.8	30.8
HWYC20UM	Mixed Origin	high wycombe	0	8123	0	1275	994	10392	642	5627	69691	86352	0.0	78.2	0.0	12.3	9.6	0.7	6.5	80.7
HWYCRPT	Mixed Origin	high wycombe	0	14959	0	1852	1414	18225	939	12613	29897	61674	0.0	82.1	0.0	10.2	7.8	1.5	20.5	48.5
RC130403	Mixed Origin	mixed karnup	179	801	71	141	0	1192	63	32933	13790	47978	15.0	67.2	6.0	11.8	0.0	0.1	68.6	28.7
RC130404	Mixed Origin	mixed karnup	0	209	0	120	108	437	71	11996	8545	21049	0.0	47.8	0.0	27.5	24.7	0.3	57.0	40.6

RC13044R	Mixed Origin	mixed karnup	205	1071	0	548	265	2089	0	71677	23742	97508	9.8	51.3	0.0	26.2	12.7	0.0	73.5	24.3
LtMAR	Mixed Origin	POI house	863	7482	9259	505	953	19062	4657	50104	65914	139737	4.5	39.3	48.6	2.6	5.0	3.3	35.9	47.2
RC021204	Mixed Origin	SAB1	0	6766	151	339	0	7256	0	6523	4080	17859	0.0	93.2	2.1	4.7	0.0	0.0	36.5	22.8
RC021205	Mixed Origin	SAB1	205	4912	0	1823	5720	12660	0	9284	2467	24411	1.6	38.8	0.0	14.4	45.2	0.0	38.0	10.1
SE420UM	Mixed Origin	SE4	618	12097	752	2670	0	16137	861	53851	24717	95566	3.8	75.0	4.7	16.5	0.0	0.9	56.3	25.9
SE4B0213	Mixed Origin	SE4	758	15193	1705	6502	4320	28478	7724	117839	76658	230699	2.7	53.3	6.0	22.8	15.2	3.3	51.1	33.2
3F116035	Quindalup System	100m W Pipidinny Rd	155	873	248	168	232	1676	75	20114	6484	28349	9.2	52.1	14.8	10.0	13.8	0.3	71.0	22.9
3F116036	Quindalup System	20m S Pipidinny Rd	669	2174	642	415	632	4532	231	29720	38819	73302	14.8	48.0	14.2	9.2	13.9	0.3	40.5	53.0
3F116047	Quindalup System	burns beach	148	937	50	199	70	1404	491	15373	2947	20215	10.5	66.7	3.6	14.2	5.0	2.4	76.0	14.6
PINNACLE	Quindalup System	pinnacle	1329	12210	458	1833	2640	18470	244	9920	14006	42640	7.2	66.1	2.5	9.9	14.3	0.6	23.3	32.8
3F116045	Quindalup System	Pinnaroo	0	2409	197	105	46	2757	1151	4210	6220	14338	0.0	87.4	7.1	3.8	1.7	8.0	29.4	43.4
3F116046	Quindalup System	yanchep-two rocks	221	1643	21	67	575	2527	240	11904	10373	25044	8.7	65.0	0.8	2.7	22.8	1.0	47.5	41.4
V1.1	Recovered	vehicle	85	362	162	0	0	609	84	895	488	2076	14.0	59.4	26.6	0.0	0.0	4.0	43.1	23.5
V3.1	Recovered	vehicle	0	283	132	41	56	512	78	1762	32	2384	0.0	55.3	25.8	8.0	10.9	3.3	73.9	1.3
V4.1	Recovered	vehicle	101	725	215	71	80	1192	118	421	631	2362	8.5	60.8	18.0	6.0	6.7	5.0	17.8	26.7
V1.2	Recovered	vehicle	109	1333	480	130	151	2203	420	3920	3328	9871	4.9	60.5	21.8	5.9	6.9	4.3	39.7	33.7
V3.2	Recovered	vehicle	179	1017	353	144	158	1851	220	2679	426	5176	9.7	54.9	19.1	7.8	8.5	4.3	51.8	8.2
V1.3	Recovered	vehicle	205	1192	445	120	157	2119	528	2766	2661	8074	9.7	56.3	21.0	5.7	7.4	6.5	34.3	33.0
V2.1	Recovered	vehicle	480	5044	1176	358	465	7523	410	12466	3976	24375	6.4	67.0	15.6	4.8	6.2	1.7	51.1	16.3
V4.2	Recovered	vehicle	292	2351	837	196	209	3885	341	1167	1269	6662	7.5	60.5	21.5	5.0	5.4	5.1	17.5	19.0
V4.3	Recovered	vehicle	262	2108	682	161	171	3384	380	1614	1703	7081	7.7	62.3	20.2	4.8	5.1	5.4	22.8	24.1
11AMBER	Spearwood System	11AMB	212	828	138	455	648	2281	169	7129	5331	14910	9.3	36.3	6.0	19.9	28.4	1.1	47.8	35.8
11AMBERR	Spearwood System	11AMB	314	1785	277	1091	1622	5089	172	9991	3942	19194	6.2	35.1	5.4	21.4	31.9	0.9	52.1	20.5

11AMB01	Spearwood System	11AMB	420	2112	435	1082	1603	5652	294	12054	10567	28567	7.4	37.4	7.7	19.1	28.4	1.0	42.2	37.0
11AMB02	Spearwood System	11AMB	254	1900	343	1078	1474	5049	1847	24626	35007	66529	5.0	37.6	6.8	21.4	29.2	2.8	37.0	52.6
11AMB03	Spearwood System	11AMB	203	1526	265	1128	1548	4670	282	16170	13113	34235	4.3	32.7	5.7	24.2	33.1	0.8	47.2	38.3
11AMB04	Spearwood System	11AMB	229	2090	376	1119	1616	5430	933	17444	19432	43239	4.2	38.5	6.9	20.6	29.8	2.2	40.3	44.9
11AMB05	Spearwood System	11AMB	326	1778	376	939	1282	4701	776	18945	27202	51624	6.9	37.8	8.0	20.0	27.3	1.5	36.7	52.7
11AMB06	Spearwood System	11AMB	380	1850	408	1073	1497	5208	494	16503	16689	38894	7.3	35.5	7.8	20.6	28.7	1.3	42.4	42.9
11AMB07	Spearwood System	11AMB	333	1859	342	1063	1527	5124	418	16075	21754	43371	6.5	36.3	6.7	20.7	29.8	1.0	37.1	50.2
11AMB08	Spearwood System	11AMB	319	1800	346	996	1495	4956	1013	18468	31092	55529	6.4	36.3	7.0	20.1	30.2	1.8	33.3	56.0
GNAN20UM	Spearwood System	GNAN	45	945	53	161	268	1472	51	1588	2347	5458	3.1	64.2	3.6	10.9	18.2	0.9	29.1	43.0
GN20UMR	Spearwood System	GNAN	0	1222	85	399	587	2293	0	2973	1188	6454	0.0	53.3	3.7	17.4	25.6	0.0	46.1	18.4
RC130401	Spearwood System	Karnup	237	1086	765	433	1091	3612	0	7124	3853	14589	6.6	30.1	21.2	12.0	30.2	0.0	48.8	26.4
RC130402	Spearwood System	Karnup	99	531	347	387	641	2005	46	9621	8765	20437	4.9	26.5	17.3	19.3	32.0	0.2	47.1	42.9
NA120UM	Spearwood System	NA1	383	1852	1153	1427	1413	6228	232	13048	22261	41769	6.1	29.7	18.5	22.9	22.7	0.6	31.2	53.3
NA220UM	Spearwood System	NA2	295	3564	503	1286	1609	7257	684	8289	9870	26100	4.1	49.1	6.9	17.7	22.2	2.6	31.8	37.8
NA420UM	Spearwood System	NA4	431	3212	499	1173	1222	6537	487	10396	16040	33460	6.6	49.1	7.6	17.9	18.7	1.5	31.1	47.9
NAB120UM	Spearwood System	NAB1	287	4084	208	887	953	6419	205	12690	21366	40680	4.5	63.6	3.2	13.8	14.8	0.5	31.2	52.5
NAB220UM	Spearwood System	NAB2	409	2667	276	992	1150	5494	162	20405	20040	46101	7.4	48.5	5.0	18.1	20.9	0.4	44.3	43.5
NAB320UM	Spearwood System	NAB3	258	1893	472	1163	1365	5151	68	7903	14819	27941	5.0	36.8	9.2	22.6	26.5	0.2	28.3	53.0
NAB420UM	Spearwood System	NAB4	127	952	66	350	566	2061	95	35272	55628	93056	6.2	46.2	3.2	17.0	27.5	0.1	37.9	59.8

NB120UM	Spearwood System	NB1	204	1141	765	945	830	3885	272	19329	27556	51042	5.3	29.4	19.7	24.3	21.4	0.5	37.9	54.0
NB220UM	Spearwood System	NB2	132	1502	429	673	770	3506	146	22652	42059	68363	3.8	42.8	12.2	19.2	22.0	0.2	33.1	61.5
NB320UM	Spearwood System	NB3	148	1110	103	502	702	2565	0	19389	21172	43126	5.8	43.3	4.0	19.6	27.4	0.0	45.0	49.1
NB420UM	Spearwood System	NB4	226	814	336	847	706	2929	201	16961	29164	49255	7.7	27.8	11.5	28.9	24.1	0.4	34.4	59.2
NBC120UM	Spearwood System	NBC1	236	1985	489	1211	1347	5268	207	16405	22149	44029	4.5	37.7	9.3	23.0	25.6	0.5	37.3	50.3
NBC220UM	Spearwood System	NBC2	215	2836	647	1127	1128	5953	0	17386	12327	35666	3.6	47.6	10.9	18.9	18.9	0.0	48.7	34.6
NBC320UM	Spearwood System	NBC3	233	2577	240	1127	1098	5275	74	15895	10408	31652	4.4	48.9	4.5	21.4	20.8	0.2	50.2	32.9
NC120UM	Spearwood System	NC1	75	5561	320	628	958	7542	1190	7176	15935	31843	1.0	73.7	4.2	8.3	12.7	3.7	22.5	50.0
NC220UM	Spearwood System	NC2	103	2263	893	942	1208	5409	0	17076	13323	35808	1.9	41.8	16.5	17.4	22.3	0.0	47.7	37.2
NC320UM	Spearwood System	NC3	244	2793	1030	1547	2008	7622	0	25272	25333	58227	3.2	36.6	13.5	20.3	26.3	0.0	43.4	43.5
NC420UM	Spearwood System	NC4	280	1293	549	880	843	3845	435	11887	28281	44448	7.3	33.6	14.3	22.9	21.9	1.0	26.7	63.6
NC520UM	Spearwood System	NC5	106	1158	201	473	678	2616	219	16313	12298	31446	4.1	44.3	7.7	18.1	25.9	0.7	51.9	39.1
ND120UM	Spearwood System	ND1	371	2591	284	1318	1561	6125	405	14720	38699	59949	6.1	42.3	4.6	21.5	25.5	0.7	24.6	64.6
ND220UM	Spearwood System	ND2	323	2654	359	1443	1588	6367	119	18798	38291	63575	5.1	41.7	5.6	22.7	24.9	0.2	29.6	60.2
ND320UM	Spearwood System	ND3	347	3771	745	1469	1893	8225	110	26146	38242	72723	4.2	45.8	9.1	17.9	23.0	0.2	36.0	52.6
ND420UM	Spearwood System	ND4	349	2530	455	1636	1792	6762	265	14928	40172	62127	5.2	37.4	6.7	24.2	26.5	0.4	24.0	64.7
ND520UM	Spearwood System	ND5	239	2303	98	763	911	4314	137	17699	49714	71864	5.5	53.4	2.3	17.7	21.1	0.2	24.6	69.2
ND620UM	Spearwood System	ND6	239	3173	775	1341	1021	6549	0	15047	16554	38150	3.6	48.5	11.8	20.5	15.6	0.0	39.4	43.4
NE120UM	Spearwood System	NE1	221	1780	128	442	614	3185	68	2260	5602	11115	6.9	55.9	4.0	13.9	19.3	0.6	20.3	50.4

NE220UM	Spearwood System	NE2	217	5784	342	1194	1291	8828	187	9178	7706	25899	2.5	65.5	3.9	13.5	14.6	0.7	35.4	29.8
NE2A20UM	Spearwood System	NE2A	275	6535	441	748	1031	9030	0	8100	4673	21803	3.0	72.4	4.9	8.3	11.4	0.0	37.2	21.4
NS1B20UM	Spearwood System	NS1B	217	2617	749	708	900	5191	0	11954	4222	21367	4.2	50.4	14.4	13.6	17.3	0.0	55.9	19.8
NS220UM	Spearwood System	NS2	295	1882	393	1239	1155	4964	84	16230	51668	72946	5.9	37.9	7.9	25.0	23.3	0.1	22.2	70.8
NS220UMY	Spearwood System	NS2	231	1193	277	677	657	3035	179	6241	23651	33106	7.6	39.3	9.1	22.3	21.6	0.5	18.9	71.4
NS220UMZ	Spearwood System	NS2	453	2431	573	1440	1403	6300	266	12055	48940	67561	7.2	38.6	9.1	22.9	22.3	0.4	17.8	72.4
NS320UM	Spearwood System	NS3	164	1767	163	966	1753	4813	0	15117	13084	33014	3.4	36.7	3.4	20.1	36.4	0.0	45.8	39.6
NS420UM	Spearwood System	NS4	321	3459	199	1299	1600	6878	124	16128	21510	44640	4.7	50.3	2.9	18.9	23.3	0.3	36.1	48.2
SA220UM	Spearwood System	SA2	360	1020	3143	326	546	5395	691	9697	25065	40848	6.7	18.9	58.3	6.0	10.1	1.7	23.7	61.4
SA420UM	Spearwood System	SA4	405	3038	438	866	1150	5897	202	15428	27335	48862	6.9	51.5	7.4	14.7	19.5	0.4	31.6	55.9
SA520UM	Spearwood System	SA5	562	3191	922	1039	1324	7038	66	21986	21628	50718	8.0	45.3	13.1	14.8	18.8	0.1	43.3	42.6
SA620UM	Spearwood System	SA6	135	613	148	138	242	1276	182	13306	15217	29981	10.6	48.0	11.6	10.8	19.0	0.6	44.4	50.8
SB220UM	Spearwood System	SB2	95	1125	243	778	715	2956	78	15923	51832	70789	3.2	38.1	8.2	26.3	24.2	0.1	22.5	73.2
SB220UMR	Spearwood System	SB2	103	1567	346	825	771	3612	0	9440	13403	26455	2.9	43.4	9.6	22.8	21.3	0.0	35.7	50.7
SB320UM	Spearwood System	SB3	238	1489	450	1142	1983	5302	94	8717	10094	24207	4.5	28.1	8.5	21.5	37.4	0.4	36.0	41.7
SB420UM	Spearwood System	SB4	265	1636	900	1008	1629	5438	264	10511	21538	37751	4.9	30.1	16.6	18.5	30.0	0.7	27.8	57.1
SB720UM	Spearwood System	SB7	120	1180	346	471	674	2791	46	5388	12589	20814	4.3	42.3	12.4	16.9	24.1	0.2	25.9	60.5
SC120UM	Spearwood System	SC1	136	1094	838	757	1229	4054	184	9117	21616	34971	3.4	27.0	20.7	18.7	30.3	0.5	26.1	61.8
SC220UM	Spearwood System	SC2	295	1373	612	795	1107	4182	83	8602	8824	21691	7.1	32.8	14.6	19.0	26.5	0.4	39.7	40.7

SC320UM	Spearwood System	SC3	247	1482	258	793	1061	3841	133	10601	21691	36266	6.4	38.6	6.7	20.6	27.6	0.4	29.2	59.8
SC420UM	Spearwood System	SC4	142	1092	616	810	1121	3781	0	11768	25873	41422	3.8	28.9	16.3	21.4	29.6	0.0	28.4	62.5
SC520UM	Spearwood System	SC5	161	1299	630	402	521	3013	58	17562	17605	38238	5.3	43.1	20.9	13.3	17.3	0.2	45.9	46.0
SC620UM	Spearwood System	SC6	307	1883	552	1406	1290	5438	207	9577	22462	37684	5.6	34.6	10.2	25.9	23.7	0.5	25.4	59.6
SC6B20UM	Spearwood System	SC6B	252	2404	549	1142	1355	5702	0	9693	17035	32430	4.4	42.2	9.6	20.0	23.8	0.0	29.9	52.5
SD220UM	Spearwood System	SD2	246	1453	340	786	1143	3968	228	13505	17595	35296	6.2	36.6	8.6	19.8	28.8	0.6	38.3	49.8
LEDA20UM	Spearwood System	SDE1	165	857	468	628	764	2882	146	11902	14485	29415	5.7	29.7	16.2	21.8	26.5	0.5	40.5	49.2
PARM20UM	Spearwood System	SDE2	191	739	268	432	547	2177	0	21082	12839	36098	8.8	33.9	12.3	19.8	25.1	0.0	58.4	35.6
BALD20UM	Spearwood System	SE1	303	2972	689	1548	1966	7478	146	19891	52194	79709	4.1	39.7	9.2	20.7	26.3	0.2	25.0	65.5
SE320UM	Spearwood System	SE3	486	1487	253	633	990	3849	149	14332	26999	45329	12.6	38.6	6.6	16.4	25.7	0.3	31.6	59.6
SEF120UM	Spearwood System	SEF1	310	2181	866	1495	1914	6766	210	12760	51587	71323	4.6	32.2	12.8	22.1	28.3	0.3	17.9	72.3
KARN20UM	Spearwood System	SF1	235	1661	583	812	1249	4540	0	17728	7666	29934	5.2	36.6	12.8	17.9	27.5	0.0	59.2	25.6
SF220UM	Spearwood System	SF2	167	1661	281	510	707	3326	0	13065	46499	62890	5.0	49.9	8.4	15.3	21.3	0.0	20.8	73.9
SF320UM	Spearwood System	SF3	270	939	292	427	695	2623	367	12294	18651	33935	10.3	35.8	11.1	16.3	26.5	1.1	36.2	55.0
SG120UM	Spearwood System	SG1	334	1582	918	1096	1286	5216	145	14633	36678	56672	6.4	30.3	17.6	21.0	24.7	0.3	25.8	64.7
SG220UM	Spearwood System	SG2	231	845	132	282	358	1848	0	22033	52864	76745	12.5	45.7	7.1	15.3	19.4	0.0	28.7	68.9
SG320UM	Spearwood System	SG3	379	1014	170	278	311	2152	146	13607	39435	55340	17.6	47.1	7.9	12.9	14.5	0.3	24.6	71.3
WEMB100	Spearwood System	WEMB	249	1668	163	1105	0	3185	282	22166	19783	45416	7.8	52.4	5.1	34.7	0.0	0.6	48.8	43.6
WEMB1850	Spearwood System	WEMB	703	5080	736	1967	0	8486	1932	42693	107067	160178	8.3	59.9	8.7	23.2	0.0	1.2	26.7	66.8

WEMB925	Spearwood System	WEMB	836	6175	845	2371	0	10227	1100	49649	114152	175128	8.2	60.4	8.3	23.2	0.0	0.6	28.4	65.2
XTALCAVE	Spearwood System	YAN	649	2543	484	2024	1988	7688	274	16185	23606	47753	8.4	33.1	6.3	26.3	25.9	0.6	33.9	49.4

Appendix G Scores for samples in Case 1 for PCA analysis as presented in Figure 39 in Section 5.2.6.1. [page 187 to 191]

sample ref	Group for ALL	Site description	PC-1	PC-2	PC-3	PC-4
0F25082R	Alluvial/Lateritic	D2 AUGEN GNEISS	31.0606	-2.1735	-4.0659	3.4068
0F25083R	Alluvial/Lateritic	D3 QTZ-FELD-BIOTITE GNEISS	4.5284	6.6227	-52.9795	21.0396
0F25084R	Alluvial/Lateritic	D4 DONNYBROOK SST	12.1554	-20.7326	-27.9866	-0.0294
0F25085R	Alluvial/Lateritic	D5 DONNYBROOK SST	8.2351	-15.8518	-37.6583	4.9402
HELENA1	Alluvial/Lateritic	Helena Valley	12.8692	3.6284	-16.9790	-18.2837
HELENA2	Alluvial/Lateritic	Helena Valley	15.0713	-4.9591	-17.3448	-17.2261
HELENA3	Alluvial/Lateritic	Helena Valley	9.0661	-15.0947	-8.8862	-11.2522
HELENA4	Alluvial/Lateritic	Helena Valley	15.9751	-9.5520	-16.6433	-15.5511
HELENA5	Alluvial/Lateritic	Helena Valley	21.6324	-12.7981	-12.0415	-15.5433
HELENA6	Alluvial/Lateritic	Helena Valley	15.1723	-21.2499	-25.5838	-4.8552
HELENA7	Alluvial/Lateritic	Helena Valley	15.4782	-37.4582	-25.4985	-11.2540
HELENA8	Alluvial/Lateritic	Helena Valley	9.4161	-9.1499	-25.3117	-20.7458
2F135406	Alluvial/Lateritic	Southern Cross	27.2449	-26.6540	-16.3687	-13.9894
2F135412	Alluvial/Lateritic	Wongan Hills	7.0568	-32.1769	-30.4657	-17.3913
2F135403	Alluvial/Lateritic	Wongan Hills	8.4779	-42.2615	-31.4697	-14.3635
2F135409	Alluvial/Lateritic	Wubin	24.1070	-34.5782	-21.2085	-13.1091
NA320UM	Bassendean System	NA3	18.9856	22.7150	-16.7519	16.5375
NA520UM	Bassendean System	NA5	68.1481	-21.7190	16.0488	2.3944
NA520UMX	Bassendean System	NA5	64.9527	-7.0302	17.1240	7.0976
NB520UM	Bassendean System	NB5	39.1418	48.1981	-15.9090	23.0499
NBC420UM	Bassendean System	NBC4	42.9016	24.6855	1.4524	0.8324
NC620UM	Bassendean System	NC6	56.2713	-3.6035	13.8305	-12.0143
NC620UMX	Bassendean System	NC6	70.8241	-32.2769	16.4216	-0.8016
ND720UM	Bassendean System	ND7	23.3928	31.5838	-6.9824	5.4057
ND820UM	Bassendean System	ND8	55.8328	19.4330	5.3036	5.4491
ND820UMR	Bassendean System	ND8	44.7509	45.3966	2.3879	-12.8498
ND8A20UM	Bassendean System	ND8A	73.0605	-31.5182	16.7579	-0.9654
ND8A20UR	Bassendean System	ND8A	73.3827	-31.4185	16.7631	-1.0013
NE320UM	Bassendean System	NE3	71.7014	-31.9367	16.7448	-0.8115
NE320URX	Bassendean System	NE3	62.8106	0.9604	17.6258	9.7165
NE420UM	Bassendean System	NE4	43.6328	48.9900	5.4464	3.2031
NE420URR	Bassendean System	NE4	62.9541	19.6042	8.6591	7.5529
SA320UM	Bassendean System	SA3	42.2257	31.1727	0.7639	3.8978
SA6B20UM	Bassendean System	SA6B	67.0950	-33.3464	16.7395	-0.2789
SA6B20UX	Bassendean System	SA6B	59.2498	-12.9512	17.1336	6.6705
SB120UM	Bassendean System	SB1	42.0010	59.3974	-2.1142	-14.2239

SB120UMR	Bassendean System	SB1	41.7350	51.8282	-0.8507	-11.9561
SB120UKX	Bassendean System	SB1	42.0446	55.8761	-1.6910	-12.7470
SB520UM	Bassendean System	SB5	71.4093	-32.0470	16.6504	-0.8045
SB520KR	Bassendean System	SB5	63.4741	1.0862	17.4775	9.5895
SB620UM	Bassendean System	SB6	37.7062	50.7864	-5.6227	0.3206
SC720UM	Bassendean System	SC7	28.9894	35.6827	-15.0950	16.9069
CASU20UM	Bassendean System	SD1	73.1634	-31.4975	16.7093	-0.9911
SD120KR	Bassendean System	SD1	51.3368	29.9895	13.9171	-12.6459
WELL20UM	Bassendean System	SDE3	40.6157	49.4587	-10.0824	8.5338
SE220UM	Bassendean System	SE2	-5.2880	-7.1761	9.9577	-3.3105
SF420UM	Bassendean System	SF4	25.9616	17.7545	-3.2592	27.7052
RH73SLOW	body disposal site	body location	-29.7746	-4.0161	6.2049	5.2861
3F116022	body disposal site	E grid A4	11.7529	4.9725	0.5909	0.6435
3F116039	body disposal site	E grid B2	2.2545	13.2621	4.9341	-3.6433
3F116038	body disposal site	E grid B3	0.0414	-2.2211	-0.6995	7.5347
3F116037	body disposal site	E grid B4	-19.3838	0.5223	-0.2822	10.9820
3F116042	body disposal site	E grid B6	6.5445	4.7218	-8.3738	5.6497
C1VSLOW	body disposal site	E grid C1	19.3310	7.0699	2.2552	2.1918
3F116024	body disposal site	E grid C2	-4.6890	-1.1148	6.2435	4.4509
3F116025	body disposal site	E grid C2F	-43.2835	-7.0894	10.5481	9.6810
3F116026	body disposal site	E grid C3	-19.5612	-6.7015	4.5535	8.5985
3F116027	body disposal site	E grid C4	7.6209	-2.0628	-0.3138	-1.0620
3F116040	body disposal site	E grid C6	1.6895	12.8714	1.4850	1.7858
3F116028	body disposal site	E grid D1	9.8196	4.8555	3.1631	8.4875
3F116029	body disposal site	E grid D2	-15.9119	-5.6175	2.5624	7.9954
3F116030	body disposal site	E grid D2F	-21.6451	1.7696	6.6363	11.6765
3F116031	body disposal site	E grid D3	-4.8878	3.1126	0.1902	1.9869
3F116032	body disposal site	E grid D4	-7.6842	1.6468	2.3809	0.0234
3F116033	body disposal site	E grid D5	5.2895	8.9244	-1.1013	-2.9517
3F116034	body disposal site	E grid D5A	-5.5693	9.3674	2.8362	0.0934
3F116041	body disposal site	E grid D6	-0.0864	9.6614	2.6662	5.0076
3F116018	body disposal site	E grid Z5	10.0740	-2.5292	4.5430	3.0788
RH71SLOW	body disposal site	track	9.5757	-8.1828	2.6815	4.0576
RH72SLOW	body disposal site	track	5.9528	4.2944	6.3785	4.1396
3116043R	near body disposal site	21m elevation carpark end Pipidinny Road	-8.0415	-21.9259	8.5306	-2.2377
116007SS	near body disposal site	E 10M W body	-6.7204	-15.4995	1.0887	11.2455
116006SS	near body disposal site	E 10M W body	14.1447	9.8162	-2.6343	-1.7077
3F116006	near body disposal site	E 10M W body	0.7288	2.9523	-1.2275	2.6126
3F116007	near body disposal site	E 10M W body	-4.4357	-15.2256	-0.7901	8.1794
116008SS	near body disposal site	E 20M W body	-9.1852	-8.8508	-5.2048	4.2111
3F116008	near body disposal site	E 20M W body	9.7321	-3.9756	-1.2133	-6.3454
116004SS	near body disposal site	E 2M E of body	-12.7150	-5.3734	4.3304	5.5647
3F116004	near body disposal site	E 2M E of body	-23.2760	-10.2916	5.1310	9.2791
116002SS	near body disposal site	E 2M N of body	22.4417	12.8932	-5.5841	-3.4003

3F116002	near body disposal site	E 2M N of body	32.3168	12.4981	-4.0013	-4.0123
116003SS	near body disposal site	E 2M S of body	-4.2887	6.1441	7.2616	-0.8228
3F116003	near body disposal site	E 2M S of body	-3.5310	4.0945	4.9024	0.5494
116005SS	near body disposal site	E 2M W of body	-30.0124	-12.8626	5.5004	8.3502
3F116005	near body disposal site	E 2M W of body	-32.6713	-9.9949	1.3040	7.6849
3F116009	near body disposal site	E 30M W body	33.1468	-6.7527	8.6040	17.9691
116009SS	near body disposal site	E 30M W of body	3.1843	-9.0688	6.6309	9.3429
3116048X	near body disposal site	Gibson Park Pinnaroo Valley	25.9787	-13.7155	5.5304	8.1124
3116044R	near body disposal site	Pipidinny Rd	-3.8971	-20.8539	6.5478	7.4055
3F116010	near body disposal site	Pipidinny Rd cutting	-26.6639	-12.5661	-7.9661	13.2338
116010SS	near body disposal site	Pipidinny Rd cutting	-34.1343	-21.2164	-0.0598	14.2696
91M5781	Coastal limestone	CORONATION	2.0274	2.1049	-14.9152	-24.9486
91M5788	Coastal limestone	CORONATION	3.0939	-25.1094	-32.6302	-18.7479
91M5785	Coastal limestone	CORONATION	0.9967	-15.5108	-23.1013	-19.6933
9KARRDGB	Coastal limestone	GOODE BEACH	11.0951	31.9850	-35.1200	30.9803
SHELLY01	Coastal limestone	WEST CAPE HOWE	20.8610	36.0693	-8.3878	11.9305
MEH1	House-Quindalup	Melon Hill	28.2925	-11.8312	6.0498	13.5121
MEH2	House-Quindalup	Melon Hill	29.6177	9.6954	3.3472	4.0314
SWB1	House-Quindalup	Swanbourne	12.6887	-4.4654	2.8973	12.6921
SWB2	House-Quindalup	Swanbourne	28.8663	-19.7541	9.0413	6.1301
SWB3	House-Quindalup	Swanbourne	15.5379	-26.4571	9.0751	9.9214
SWB4	House-Quindalup	Swanbourne	8.3903	-17.2992	6.6714	8.3812
11AMB501	Mixed Origin	11AMB	-8.3322	-22.2230	17.2971	4.3490
NC720KR	Mixed Origin	11AMB	22.7287	4.4757	12.9148	-5.9141
11AMB50S	Mixed Origin	50m 11AMB	-18.1007	8.1274	14.4747	-10.0682
11AMB50SC	Mixed Origin	50m 11AMB	12.5721	6.0064	13.6091	-9.5726
HWYC20UM	Mixed Origin	high wycombe	-51.2995	-45.0402	11.6188	2.9368
HWYCRPT	Mixed Origin	high wycombe	-19.0157	-42.6352	-1.1343	-2.7459
RC130403	Mixed Origin	mixed karnup	24.1542	-13.3222	13.8959	8.3739
RC130404	Mixed Origin	mixed karnup	-2.0363	6.5619	13.6617	-15.2234
RC13044R	Mixed Origin	mixed karnup	22.7652	6.1989	14.7199	-8.7247
LtMAR	Mixed Origin	POI house	-17.1793	9.0689	-14.9203	37.5085
RC021204	Mixed Origin	SAB1	13.4524	-47.6143	-8.1184	-0.9634
RC021205	Mixed Origin	SAB1	1.6060	14.2020	-20.4689	-31.5660
SE420UM	Mixed Origin	SE4	18.9494	-23.6354	4.5730	1.1460
SE4B0213	Mixed Origin	SE4	2.1142	-1.9003	3.3618	-6.4452
3F116035	Quindalup System	100m W Pipidinny Rd	23.9931	6.9310	5.4504	5.0455
3F116036	Quindalup System	20m S Pipidinny Rd	-17.5085	-2.0011	7.2630	11.3866
3F116047	Quindalup System	burns beach	37.4120	-8.3996	9.1434	-0.8134
PINNACLE	Quindalup System	pinnacle	-11.6386	-24.7987	-11.5649	-6.3012
3F116045	Quindalup System	Pinnaroo	-6.6148	-44.7941	-2.0768	6.9329
3F116046	Quindalup System	yanchep-two rocks	-1.3039	-14.5384	9.0451	-4.7107
V1.1	Recovered	vehicle	9.6386	-11.6360	-15.0934	22.3294
V3.1	Recovered	vehicle	41.5801	8.0290	-12.3510	7.0063

V4.1	Recovered	vehicle	-11.0959	-21.0186	-25.6696	8.0418
V1.2	Recovered	vehicle	-0.9153	-12.5229	-9.3101	13.6266
V3.2	Recovered	vehicle	22.3036	-2.3150	-17.7986	5.9245
V1.3	Recovered	vehicle	-5.2157	-10.9609	-12.9619	13.4444
V2.1	Recovered	vehicle	20.2812	-14.9633	-10.6333	6.7625
V4.2	Recovered	vehicle	-6.0365	-20.1001	-32.4788	9.1462
V4.3	Recovered	vehicle	-5.2052	-20.5301	-25.2016	10.3224
11AMBER	Spearwood System	11AMB	-7.5359	15.0379	1.8128	-10.3408
11AMBERR	Spearwood System	11AMB	4.3942	19.4948	-5.9729	-17.4967
11AMB01	Spearwood System	11AMB	-11.8298	12.4626	-1.5999	-9.6335
11AMB02	Spearwood System	11AMB	-26.0243	9.8815	5.7136	-8.2907
11AMB03	Spearwood System	11AMB	-11.7572	19.6927	2.5611	-15.0091
11AMB04	Spearwood System	11AMB	-18.4648	10.8733	2.5564	-10.2339
11AMB05	Spearwood System	11AMB	-25.7851	9.1622	5.4260	-5.5636
11AMB06	Spearwood System	11AMB	-16.2765	14.0952	2.3254	-8.5929
11AMB07	Spearwood System	11AMB	-24.7040	11.2968	4.2890	-8.8050
11AMB08	Spearwood System	11AMB	-31.1158	9.7317	5.5966	-7.3992
GNAN20UM	Spearwood System	GNAN	-15.5624	-20.0509	-2.3450	-5.6837
GN20UMR	Spearwood System	GNAN	7.6374	-0.5538	-9.4474	-17.1024
RC130401	Spearwood System	Karnup	-1.5738	24.6377	-10.8959	-1.4363
RC130402	Spearwood System	Karnup	-15.7060	26.5973	0.3916	-3.4272
NA120UM	Spearwood System	NA1	-31.6841	15.5873	-1.9382	2.7849
NA220UM	Spearwood System	NA2	-15.5154	-3.3810	-6.5334	-8.1949
NA420UM	Spearwood System	NA4	-22.1749	-5.0691	0.0539	-2.6688
NAB120UM	Spearwood System	NAB1	-20.4251	-20.1767	5.8822	-1.9210
NAB220UM	Spearwood System	NAB2	-10.6918	0.3176	6.2581	-5.4247
NAB320UM	Spearwood System	NAB3	-32.2511	7.5380	0.0200	-6.3569
NAB420UM	Spearwood System	NAB4	-27.1884	0.7420	13.3278	-6.4051
NB120UM	Spearwood System	NB1	-27.7061	18.1973	2.1568	4.4691
NB220UM	Spearwood System	NB2	-31.9702	2.6090	7.8515	1.5439
NB320UM	Spearwood System	NB3	-16.3652	6.6734	10.0882	-8.8156
NB420UM	Spearwood System	NB4	-34.8078	17.3686	7.0117	-2.3658
NBC120UM	Spearwood System	NBC1	-24.0145	9.7844	3.7348	-5.9146
NBC220UM	Spearwood System	NBC2	-1.8513	4.0864	0.4785	-3.5089
NBC320UM	Spearwood System	NBC3	0.0238	2.9352	2.9411	-9.7291
NC120UM	Spearwood System	NC1	-21.2056	-32.6448	-1.5298	-0.8615
NC220UM	Spearwood System	NC2	-6.1004	10.7843	-1.4728	-0.7055
NC320UM	Spearwood System	NC3	-15.3956	14.1661	0.9719	-4.1259
NC420UM	Spearwood System	NC4	-40.4617	8.8861	4.2758	2.8379
NC520UM	Spearwood System	NC5	-4.4392	9.0484	6.0640	-7.4869
ND120UM	Spearwood System	ND1	-40.7088	-0.6262	7.6898	-5.7117
ND220UM	Spearwood System	ND2	-34.6635	2.0897	7.4722	-6.0019
ND320UM	Spearwood System	ND3	-23.3646	0.9142	5.0332	-2.8453
ND420UM	Spearwood System	ND4	-42.8540	4.4584	6.2587	-5.8116

ND520UM	Spearwood System	ND5	-39.8305	-12.5474	12.6088	-2.9015
ND620UM	Spearwood System	ND6	-13.5404	-0.9263	0.5654	-0.0615
NE120UM	Spearwood System	NE1	-28.9975	-15.7433	-3.0876	-4.6321
NE220UM	Spearwood System	NE2	-1.9737	-19.0236	-7.0496	-7.4692
NE2A20UM	Spearwood System	NE2A	7.5152	-25.0881	-11.4220	-5.4716
NS1B20UM	Spearwood System	NS1B	14.4072	4.8037	-6.3073	-1.7197
NS220UM	Spearwood System	NS2	-47.6468	2.4591	9.1460	-1.8386
NS220UMY	Spearwood System	NS2	-49.4489	-0.4622	7.1605	0.9241
NS220UMZ	Spearwood System	NS2	-51.1366	0.0025	7.1344	0.4710
NS320UM	Spearwood System	NS3	-12.5671	15.7675	3.4011	-17.1878
NS420UM	Spearwood System	NS4	-19.3650	-3.8804	5.0448	-8.6518
SA220UM	Spearwood System	SA2	-41.0802	25.6775	-17.9814	43.8518
SA420UM	Spearwood System	SA4	-26.2264	-7.4585	5.8995	-0.0501
SA520UM	Spearwood System	SA5	-10.8829	3.7154	1.7198	2.1657
SA620UM	Spearwood System	SA6	-14.3652	0.5540	8.5870	5.1447
SB220UM	Spearwood System	SB2	-49.3432	2.8459	10.5419	-2.5737
SB220UMR	Spearwood System	SB2	-23.2885	3.1808	3.3892	-3.9697
SB320UM	Spearwood System	SB3	-23.0969	21.2576	-3.8102	-14.6151
SB420UM	Spearwood System	SB4	-36.8920	15.2440	-1.4028	-0.7672
SB720UM	Spearwood System	SB7	-36.3907	1.0941	2.4251	0.3695
SC120UM	Spearwood System	SC1	-42.1128	18.1644	-1.3205	2.5973
SC220UM	Spearwood System	SC2	-16.8734	16.3463	-3.6808	-3.0937
SC320UM	Spearwood System	SC3	-35.5199	5.4700	6.2180	-5.8225
SC420UM	Spearwood System	SC4	-40.6991	16.3628	2.6798	-0.4497
SC520UM	Spearwood System	SC5	-11.5766	7.6362	2.0638	9.3177
SC620UM	Spearwood System	SC6	-39.0872	7.7048	2.4159	-3.5190
SC6B20UM	Spearwood System	SC6B	-28.7639	2.5478	0.8607	-4.0087
SD220UM	Spearwood System	SD2	-23.3485	11.5088	4.0970	-6.7330
LEDA20UM	Spearwood System	SDE1	-23.1187	19.5107	1.6633	-0.7898
PARM20UM	Spearwood System	SDE2	-0.3207	21.2413	5.7499	-3.3880
BALD20UM	Spearwood System	SE1	-41.7326	2.9566	6.3236	-2.9283
SE320UM	Spearwood System	SE3	-32.8755	5.0858	8.0744	-1.8824
SEF120UM	Spearwood System	SEF1	-53.4209	8.1392	4.5829	-0.5527
KARN20UM	Spearwood System	SF1	7.3486	20.5399	-0.9668	-7.2246
SF220UM	Spearwood System	SF2	-46.2172	-9.9042	10.5595	2.8223
SF320UM	Spearwood System	SF3	-27.5261	10.6752	5.4823	-0.4195
SG120UM	Spearwood System	SG1	-42.8138	12.7943	2.6351	4.2588
SG220UM	Spearwood System	SG2	-38.1844	-4.3638	13.0783	4.3290
SG320UM	Spearwood System	SG3	-41.1869	-8.7830	12.5264	9.7220
WEMB100	Spearwood System	WEMB	-5.7640	-6.0577	11.1623	1.2399
WEMB1850	Spearwood System	WEMB	-32.9505	-21.6875	11.6803	11.3196
WEMB925	Spearwood System	WEMB	-30.5671	-21.5301	11.8569	10.7081
XTALCAVE	Spearwood System	YAN	-27.3049	12.2119	2.4388	-8.6304

Appendix H Raw counts and percentage intensities for samples projected onto PCA model for Case 2 in Section 5.3.

XRD FILE	sample ref	Description	group for all	V1	K1	G1	K2	g1	SUBTOTAL	M1	Q1	F1	TOTAL	%V1	%K1	%G1	%K2	%g1	%M1	%Q1	%F1
3F225901	(03F2259001 brownish-yellow sand)	from garden bed	Case Control	248	3632	1476	1371	1392	8119	141	18751	4896	31907	3.1	44.7	18.2	16.9	17.1	0.4	58.8	15.3
3F225904	(03F2259004 brownish-yellow sand)	from plastic bag1	recovered	239	3552	1125	742	755	6413	209	17847	4903	29372	3.7	55.4	17.5	11.6	11.8	0.7	60.8	16.7
3F225905	(03F2259005 brownish-yellow sand)	from plastic bag2	recovered	259	2852	963	700	751	5525	181	12644	4221	22571	4.7	51.6	17.4	12.7	13.6	0.8	56.0	18.7
3F225902	(03F2259002 brownish-yellow sand)	from garden bed	Case Control	264	4314	1247	1425	1055	8305	165	16454	5104	30028	3.2	51.9	15.0	17.2	12.7	0.5	54.8	17.0
3F225903	(03F2259003 brownish-yellow sand)	from garden bed	Case Control	221	3581	1178	908	874	6762	214	16877	4844	28697	3.3	53.0	17.4	13.4	12.9	0.7	58.8	16.9

Appendix I Scores for PCA projection of samples from Case 2, as presented in Figure 44 in Section 5.3.3.[page 195 to 199]

XRD sample	location	PC-1	PC-2	PC-3	SUM
3F225901	from garden bed	17.8224	-10.7568	-9.6961	-2.6305
3F225904	from plastic bag1	22.3951	-0.0146	-5.3839	16.9965
3F225905	from plastic bag2	16.5067	-2.1201	-7.3020	7.0846
3F225902	from garden bed	16.5184	-0.8977	-9.2489	6.3718
3F225903	from garden bed	19.9284	-1.9122	-6.9891	11.0271
0F25082R	D2 AUGEN GNEISS	31.4453	3.4472	-3.4906	31.4019
0F25083R	D3 QTZ-FELD-BIOTITE GNEISS	5.0074	-7.4573	-44.9370	-47.3869
0F25084R	D4 DONNYBROOK SST	12.5726	21.3797	-27.4364	6.5159
0F25085R	D5 DONNYBROOK SST	8.6805	15.9971	-35.1335	-10.4559
116002SS	E 2M N of body	22.8463	-11.3928	-6.4909	4.9626
116003SS	E 2M S of body	-3.8900	-4.4137	6.4884	-1.8153
116004SS	E 2M E of body	-12.3045	6.7416	5.3528	-0.2101
116005SS	E 2M W of body	-29.6013	14.1140	7.1688	-8.3186
116006SS	E 10M W of body	14.5518	-8.3049	-3.1704	3.0765
116007SS	E 10M W body -30cm-	-6.2866	16.5720	3.9294	14.2148
116008SS	E 20M W of body	-8.7583	9.9921	-4.0681	-2.8342
116009SS	E 30M W body	3.6152	10.4172	8.8266	22.8590
116010SS	E scene Pipidinny Rd cutting	-33.7228	22.0340	3.1916	-8.4972
11AMB01	11AMB-1	-11.4271	-10.6805	-4.3961	-26.5037
11AMB02	11AMB-2	-25.6334	-7.9654	2.8812	-30.7176
11AMB03	11AMB-3	-11.3733	-17.5854	-1.9578	-30.9164
11AMB04	11AMB-4	-18.0743	-8.9644	-0.6719	-27.7105
11AMB05	11AMB-5	-25.3863	-7.3529	3.4097	-29.3295
11AMB06	11AMB-6	-15.8773	-12.2401	-0.3512	-28.4686
11AMB07	11AMB-7	-24.3065	-9.3975	1.4404	-32.2636
11AMB08	11AMB-8	-30.7147	-7.8552	3.1066	-35.4633
11AMBER	11AMB	-7.1355	-13.1137	-1.2966	-21.5458
11AMBERR	11AMB rep	4.7869	-17.5175	-10.7742	-23.5049
2F135403	7.5K NNE WONGAN HILLS	8.8512	43.2071	-35.2979	16.7604
2F135406	45K SW SOUTHERN CROSS	27.5980	28.1047	-20.6412	35.0615
2F135409	66K NNW WUBIN	24.4684	35.8345	-25.0572	35.2458
2F135412	7.2K NNE WONGAN HILLS	7.4200	33.2670	-35.2021	5.4850
3116043R	21m elevation carpark end Pipidinny Road	-7.6832	23.6522	6.6132	22.5823
3116044R	Pipidinny Road toward carpark	-3.5625	22.1413	7.0820	25.6609
3116048X	QP ref soil from Gibson Park Pinnaroo Valley	26.3430	15.0537	6.7246	48.1213
3F116002	E scene 2M N of body	32.7209	-10.9047	-5.1133	16.7028

3F116003	E scene 2M S of body	-3.1253	-2.4827	4.6420	-0.9661
3F116004	E scene 2M E of body	-22.8538	11.5253	7.1950	-4.1334
3F116005	E scene 2M W of body	-32.2464	11.1518	3.0824	-18.0123
3F116006	E scene 10M W of body	1.1458	-1.5924	-0.6370	-1.0836
3F116007	E scene sc. 10M W of body (30 cm)	-4.0003	16.3625	1.3050	13.6672
3F116008	E scene 20M W of body	10.1466	5.6607	-3.1980	12.6093
3F116009	E scene scene 30M W of body (track)	33.5878	7.9162	13.2236	54.7275
3F116010	E scene Pipidinny Rd cutting	-26.2051	13.2689	-4.0866	-17.0227
3F116018	E grid Z5	10.4793	4.0553	4.9537	19.4883
3F116022	E grid A4	12.1768	-3.4526	0.6770	9.4012
3F116024	E grid C2	-4.2825	2.6115	6.9531	5.2821
3F116025	E grid C2F	-42.8506	8.4552	12.6857	-21.7097
3F116026	E grid C3	-19.1339	7.9653	6.5659	-4.6027
3F116027	E grid C4	8.0298	3.5862	-0.8638	10.7522
3F116028	E grid D1	10.2504	-3.5400	5.3928	12.1032
3F116029	E grid D2	-15.4828	6.8563	4.5232	-4.1034
3F116030	E grid D2F	-21.2056	-0.5368	9.5876	-12.1549
3F116031	E grid D3	-4.4781	-1.7047	0.4845	-5.6983
3F116032	E grid D4	-7.2759	-0.1111	2.0104	-5.3766
3F116033	E grid D5	5.6904	-7.3475	-2.1261	-3.7832
3F116034	E grid D5A	-5.1622	-7.7990	2.5496	-10.4116
3F116035	Eca 100m W of Pipidinny Rd/ Beonaddy Rd intersection	24.3963	-5.4040	6.4519	25.4442
3F116036	E20m S of Pipidinny Rd at E end of long straight where it veers S	-17.0759	3.2636	10.0420	-3.7703
3F116037	Grid square B4, 14m NW body location Egl	-18.9344	0.5306	2.7809	-15.6230
3F116038	Grid square B3, E scene	0.4683	3.4107	1.2434	5.1224
3F116039	Grid square B2, E scene	2.6637	-11.4635	3.6415	-5.1583
3F116040	Grid square C6, E scene	2.1133	-11.3713	1.9076	-7.3503
3F116041	Grid square D6, E scene	0.3352	-8.2615	3.8431	-4.0832
3F116042	Grid square B6, E scene	6.9924	-3.6559	-6.4087	-3.0722
3F116045	1m elevation, Pinnaroo Point	-6.2427	45.8410	-1.1025	38.4958
3F116046	QP ref soil from Yanchep-Two Rocks	-0.8921	16.4628	7.2010	22.7717
3F116047	QP ref soil from Burns Beach-Quinns blow	37.7712	10.2093	7.7917	55.7722
91M5781	CORONATION 0-10CM	2.4021	-0.1781	-21.7517	-19.5276
91M5785	CORONATION 60-90CM	1.3859	16.9674	-28.2390	-9.8857
91M5788	CORONATION 160-195CM	3.4921	26.2294	-37.1929	-7.4713
9KARRDGB	GOODE BEACH, Albany -9 Karrakatta Rd	11.6120	-32.5419	-24.2876	-45.2176
BALD20UM	SE1	-41.3388	-1.2688	4.8683	-37.7394
C1VSLOW	E grid C1 v slow	19.7407	-5.5376	2.6598	16.8629
CASU20UM	SD1	73.4919	33.5755	14.7612	121.8287
GN20UMR	GNAN rep	8.0089	2.3629	-14.3764	-4.0047
GNAN20UM	GNAN	-15.1759	21.5851	-4.4606	1.9486
HELENA1	All1	13.2209	-2.0182	-22.2433	-11.0406

HELENA2	All2	15.4195	6.5033	-22.4193	-0.4965
HELENA3	All3	9.4145	16.6574	-12.6771	13.3947
HELENA4	All4	16.3352	11.0660	-21.1475	6.2538
HELENA5	All5	21.9898	14.4646	-16.7176	19.7367
HELENA6	All6	15.5669	22.1036	-26.5886	11.0818
HELENA7	All7	15.8449	38.4964	-28.6921	25.6492
HELENA8	All8	9.7761	10.5759	-30.9651	-10.6130
KARN20UM	SF1	7.7486	-18.7696	-3.0220	-14.0430
LEDA20UM	SDE1	-22.7126	-17.9647	1.2366	-39.4408
MEH1	MelonHill1	28.6537	13.0005	8.7560	50.4102
MEH2	MelonHill2	30.0000	-8.2147	3.8446	25.6299
NA120UM	NA1	-31.2760	-14.3140	-1.3305	-46.9205
NA220UM	NA2	-15.1260	4.9089	-9.0557	-19.2728
NA320UM	NA3	19.4148	-22.2542	-11.4601	-14.2995
NA420UM	NA4	-21.7841	6.5747	-1.2208	-16.4302
NA520UM	NA5	68.5166	23.6826	15.4455	107.6447
NA520UMX	NA5 rep	65.3727	8.9044	18.3052	92.5824
NAB120UM	NAB1	-20.0492	21.8000	4.3640	6.1147
NAB220UM	NAB2	-10.3073	1.5116	4.0397	-4.7560
NAB320UM	NAB3	-31.8576	-5.8932	-2.1288	-39.8796
NAB420UM	NAB4	-26.7980	1.3195	10.6878	-14.7907
NB120UM	NB1	-27.3071	-16.8547	3.0209	-41.1408
NB220UM	NB2	-31.5790	-1.0208	7.5518	-25.0481
NB320UM	NB3	-15.9817	-4.5974	6.8836	-13.6954
NB420UM	NB4	-34.4222	-15.6584	5.6560	-44.4247
NB520UM	NB5	39.5861	-47.8489	-8.4733	-16.7360
NBC120UM	NBC1	-23.6293	-8.0254	1.5356	-30.1191
NBC220UM	NBC2	-1.4722	-2.4844	-1.0214	-4.9780
NBC320UM	NBC3	0.3897	-1.0392	-0.4925	-1.1420
NBC420UM	NBC4	43.2942	-23.0623	1.5146	21.7465
NC120UM	NC1	-20.8251	33.9898	-2.5303	10.6343
NC220UM	NC2	-5.7058	-9.3233	-1.8972	-16.9262
NC320UM	NC3	-15.0010	-12.5189	-0.4669	-27.9868
NC420UM	NC4	-40.0595	-7.4602	4.5477	-42.9720
NC520UM	NC5	-4.0547	-7.1112	3.4244	-7.7415
NC620UM	NC6	56.5983	6.0078	9.1310	71.7371
NC620UMX	NC6 rep	71.1534	34.3331	14.5320	120.0186
ND120UM	ND1	-40.3211	2.4461	5.3153	-32.5596
ND220UM	ND2	-34.2820	-0.2542	4.9949	-29.5413
ND320UM	ND3	-22.9745	0.7646	3.6286	-18.5813
ND420UM	ND4	-42.4680	-2.6775	3.9193	-41.2263
ND520UM	ND5	-39.4500	14.3904	10.6752	-14.3843
ND620UM	ND6	-13.1639	2.3617	-0.1177	-10.9200
ND720UM	ND7	23.8061	-30.3980	-5.1296	-11.7215
ND820UM	ND8	56.1488	-17.9315	5.5754	43.7927

ND820UMR	ND8 rep	45.1209	-43.2101	-1.3114	0.5994
ND8A20UM	ND8A	73.3890	33.5965	14.8150	121.8004
ND8A20UR	ND8A rep	73.7111	33.4991	14.8106	122.0208
NE120UM	NE1	-28.5987	17.1983	-4.7973	-16.1977
NE220UM	NE2	-1.6008	20.4921	-9.6324	9.2589
NE2A20UM	NE2A	7.8975	26.3668	-13.2393	21.0251
NE320UM	NE3	72.0303	34.0055	14.8422	120.8780
NE320URX	NE3 rep	63.2593	0.8599	19.8017	83.9210
NE420UM	NE4	44.6468	-48.8016	7.1531	2.9983
NE420URR	NE4 rep	49.3709	-50.1770	6.8176	6.0116
NS1B20UM	NS1B	14.8020	-3.4231	-6.8745	4.5044
NS220UM	NS2	-47.2629	-0.7555	7.7244	-40.2940
NS220UMY	NS2 rep	-49.0529	2.0043	6.6516	-40.3970
NS220UMZ	NS2 rep2	-50.7416	1.5518	6.4945	-42.6953
NS320UM	NS3	-12.1768	-13.5509	-1.6643	-27.3920
NS420UM	NS4	-18.9874	5.7607	1.8810	-11.3458
PARM20UM	SDE2	0.0800	-19.4259	4.4749	-14.8711
PINNACLE	PINNACLE	-11.2413	26.0720	-13.5137	1.3169
RC130401	97F-036	-1.1299	-23.3550	-10.5400	-35.0249
RC130402	97F-037	-15.2888	-24.9466	-0.4756	-40.7110
RH71SLOW	RH71 E scene track	9.9939	9.6117	3.4701	23.0757
RH72SLOW	RH72 E scene track	6.3813	-2.7348	7.2514	10.8980
RH73SLOW	RH73 E scene body location	-29.3580	5.4243	7.1423	-16.7914
SA220UM	SA2	-40.5706	-26.3156	-4.4720	-71.3582
SA320UM	SA3	42.6230	-29.6654	1.8126	14.7702
SA420UM	SA4	-25.8292	9.0439	5.2098	-11.5755
SA520UM	SA5	-10.4760	-2.2794	1.9899	-10.7654
SA620UM	SA6	-13.9474	0.9844	9.5346	-3.4284
SA6B20UM	SA6B	67.4253	35.3838	14.9754	117.7846
SA6B20UX	SA6B rep	59.6578	14.8112	18.0417	92.5107
SB120UKX	SB1 rep2	42.4854	-53.7192	-4.2770	-15.5108
SB120UM	SB1	42.4423	-57.1865	-5.0166	-19.7608
SB120UMR	SB1 rep	42.1635	-49.6933	-3.4057	-10.9355
SB220UM	SB2	-48.9687	-1.0814	8.7917	-41.2584
SB220UMR	SB2 rep	-22.9136	-1.5264	1.5632	-22.8768
SB320UM	SB3	-22.6886	-19.3581	-7.7404	-49.7871
SB420UM	SB4	-36.4699	-13.8114	-1.5831	-51.8644
SB520KR	SB5 rep	63.9226	0.7359	19.6237	84.2821
SB520UM	SB5	71.7384	34.1119	14.7527	120.6030
SB620UM	SB6	38.1487	-49.2633	-4.6253	-15.7399
SB720UM	SB7	-35.9850	0.3724	2.1275	-33.4851
SC120UM	SC1	-41.6861	-16.8538	-0.5112	-59.0511
SC220UM	SC2	-16.4593	-14.8651	-4.4877	-35.8121
SC320UM	SC3	-35.1232	-3.6587	4.0300	-34.7519

SC420UM	SC4	-40.2885	-14.8349	2.3245	-52.7990
SC520UM	SC5	-11.1630	-6.4377	4.4000	-13.2007
SC620UM	SC6	-38.7003	-6.1165	0.8465	-43.9702
SC6B20UM	SC6B	-28.3715	-0.9650	-0.7138	-30.0503
SC720UM	SC7	29.4358	-35.1201	-9.4347	-15.1190
SD120KR	SD1 rep	51.7168	-27.4832	9.7064	33.9400
SD220UM	SD2	-22.9483	-9.6858	1.8562	-30.7780
SE220UM	SE2	-4.9028	9.0431	8.1633	12.3036
SE320UM	SE3	-32.4564	-3.3395	7.1119	-28.6841
SEF120UM	SEF1	-53.0145	-6.5983	3.9795	-55.6333
SF220UM	SF2	-45.8189	11.4824	10.4677	-23.8688
SF320UM	SF3	-27.1045	-9.0345	5.1102	-31.0288
SF420UM	SF4	26.3860	-17.3000	4.4632	13.5492
SG120UM	SG1	-42.3988	-11.4541	3.5400	-50.3130
SG220UM	SG2	-37.7727	5.9968	13.4607	-18.3152
SG320UM	SG3	-40.7597	10.1934	14.4735	-16.0927
SHELLY01	WEST CAPE HOWE -cliff above Shelly Beach	21.3371	-35.1127	-4.0678	-17.8434
SWB1	Swanbourne1	13.0680	5.5669	5.7223	24.3572
SWB2	Swanbourne2	29.2269	21.2823	9.6096	60.1188
SWB3	Swanbourne3	15.9113	27.8120	10.6913	54.4146
SWB4	Swanbourne4	8.7731	18.6448	8.0902	35.5081
WELL20UM	SDE3	41.0544	-48.3818	-6.7748	-14.1022
WEMB100	WEMB100	-5.4485	7.6975	9.6464	11.8954
WEMB1850	WEMB1850	-32.5947	22.9312	13.1941	3.5306
WEMB925	WEMB925	-30.2132	22.8049	13.1846	5.7762
XTALCAVE	XTALCAVE	-26.9180	-10.4016	-0.4768	-37.7965